arXiv:hep-ph/0305076v3 18 May 2003

Soft Gluon Exponentiation and Resummation

A Dissertation Presented

by

Carola Friederike Berger

to

The Graduate School

in Partial Fulfillment of the Requirements

for the Degree of

Doctor of Philosophy

in

Physics

State University of New York
at
Stony Brook

May 2003

Copyright © by
Carola Friederike Berger
2003

State University of New York
at Stony Brook

The Graduate School

Carola Friederike Berger

We, the dissertation committee for the above candidate for the Doctor of Philosophy degree, hereby recommend acceptance of the dissertation.

Dr. George Sterman
Advisor
Professor, C. N. Yang Institute for Theoretical Physics

Dr. John Smith
Professor, C. N. Yang Institute for Theoretical Physics

Dr. Barbara Jacak
Professor, Department of Physics and Astronomy

Dr. Sally Dawson
Senior Scientist, High Energy Theory Division,
Brookhaven National Laboratory

This dissertation is accepted by the Graduate School.

Graduate School

Abstract of the Dissertation
Soft Gluon Exponentiation and Resummation

by

Carola Friederike Berger

Doctor of Philosophy

in

Physics

State University of New York at Stony Brook

2003

In calculations of (semi-) inclusive events within perturbative Quantum Chromodynamics, large logarithmic corrections arise from certain kinematic regions of interest which need to be resummed. When resumming soft gluon effects one encounters quantities built out of eikonal or Wilson lines (path ordered exponentials). In this thesis we develop a simplified method to calculate higher orders of the singular coefficients of parton distribution functions which is based on the exponentiation of cross sections built out of eikonal lines. As an illustration of the method we determine the previously uncalculated fermionic contribution to the three-loop coefficient $A^{(3)}$.

The knowledge of these coefficients is not only important for the study of the parton distribution functions themselves, but also for the resummation of large logarithmic effects due to soft radiation in a variety of cross sections.

In the second part of this thesis we study the energy flow pattern of this soft radiation in jet events. We develop the concept of event shape-energy flow correlations that suppress radiation from unobserved "minijets" outside the region of interest and are sensitive primarily to radiation from the highest-energy jets. We give analytical and numerical results at next-to-leading logarithmic order for shape/flow correlations in e^+e^- dijet events. We conclude by illustrating the application of our formalism to events with hadrons in the initial state, where the shape/flow correlations can be described via matrices in the space of color exchanges.

[...] *δῆλον ὁτι καὶ τῆς περὶ φύσεως επιστήμης πειρατέον διορίσασθαι πρῶτον τὰ περὶ τὰς αρχάς.* Π*έφυκε δὲ εκ τῶν γνωριμωτέρων ημῖν η οδὸς καὶ σαφεστέρων επὶ τὰ σαφέστερα τῆ φύσει καὶ γνωριμώτερα ου γὰρ ταυτὰ ημῖν τε γνώριμα καὶ απλῶς.*

ΑΡΙΣΤΟΤΕΛΟΥΣ ΦΥΣΙΚΗΣ ΑΚΡΟΑΣΕΩΣ Α (1), 184 a 14.

[...] systematic knowledge of nature must start with an attempt to settle questions about principles. The natural course is to proceed from what is clearer and more knowable to us, to what is more knowable and clear by nature.

Aristotle, *Physics*, Book I (1), 184 a 14.

Contents

List of Figures . . . . . **xviii**

List of Tables . . . . . **xix**

Acknowledgements . . . . . **xx**

1 Prologue: Perturbative Quantum Chromodynamics **1**

1.1 Perturbative QCD - Basic Concepts 2

1.1.1 Asymptotic Freedom 2

1.1.2 Assumptions of Perturbative QCD 3

1.1.3 Infrared Safety 5

1.1.4 Nonperturbative Effects and Power Corrections 6

1.2 Motivation for Further Exploration 8

1.3 Outline of the Thesis 10

2 Factorization, Evolution, and Resummation **14**

2.1 Identification of Infrared Enhancements 14

2.1.1 Landau Equations 15

2.1.2 Power Counting 19

2.2 Factorization 23
2.2.1 Ward Identities 23
2.2.2 Glauber/Coulomb Gluons and Infrared Safety 25
2.2.3 Summary 32
2.3 Refactorization of Nonsinglet Partonic Splitting Functions . . 32
2.3.1 Definition of Parton-in-Parton Distribution Functions . 32
2.3.2 Power Counting as $x \to 1$ 34
2.3.3 Refactorization 39
2.4 Factorization of the Thrust Cross Section in e^+e^- Annihilation 44
2.4.1 Jet Event Shapes 44
2.4.2 Leading Regions and Factorization for the Thrust . . . 46
2.5 Evolution and Resummation at the Example of the Thrust . . 49
2.5.1 Resummation of Single Logarithms 51
2.5.2 Resummation of Sudakov Double Logarithms 52
2.5.3 The Resummed Thrust 57

3 Nonabelian Eikonal Exponentiation 59
3.1 Proof of Exponentiation for Cross Sections with Two Eikonal Lines 60
3.1.1 Some Terminology 60
3.1.2 An Example 64
3.1.3 Exponentiation 65
3.2 Cancellation of Subdivergences in the Exponent 67
3.3 Exponentiation for Quantities with Three Eikonal Lines 69

3.4 Implications for Physical Observables 71
3.4.1 Properties of Webs 71
3.4.2 Leading Logarithms of the Thrust from Eikonal Exponentiation 72
3.4.3 Power Corrections 74

4 Higher Orders in $A(\alpha_s)/[1-x]_+$ of Non-Singlet Partonic Splitting Functions 77

4.1 Renormalization of Parton Distribution Functions and of Webs 79
4.1.1 Renormalization of Parton Distribution Functions . . . 79
4.1.2 Renormalization of Webs 79
4.2 Summary of the Method in LCOPT 81
4.2.1 Remark About Eikonal Integrals 83
4.3 Calculation of the 1- and 2-loop Coefficients $A_f^{(1)}$, $A_f^{(2)}$ 84
4.4 Higher Loops 89
4.4.1 N_f^{n-1}-Terms in $A^{(n)}$ 89
4.4.2 Towards the Three-Loop Coefficient $A_f^{(3)}$ 89
4.5 Summary and Outlook 96

5 Dijet Event Shapes 97

5.1 A Generalized Event Shape 97
5.2 Factorization of the Cross Section 102
5.2.1 Leading Regions Near the Two-Jet Limit 102
5.2.2 The Factorization in Convolution Form 103
5.2.3 Recoil Effects 106

5.2.4 The Short-Distance Function 109
5.2.5 The Jet Functions 110
5.2.6 The Soft Function 112
5.3 Resummation 115
5.3.1 Evolution 116
5.3.2 The Resummed Event Shape 119
5.4 Results at NLL in Transform Space 119
5.4.1 Analytical Results at NLL 120
5.4.2 Independence of the Vectors ξ_c 122
5.4.3 The Inclusive Event Shape at NLL in Transform Space 123
5.5 Inverse Transform 128
5.5.1 Double and Leading Logarithmic Approximation 129
5.6 Numerical Results 129
5.6.1 Matching with Fixed Order Calculations 129
5.6.2 Matched Results at NLL 131
5.7 Power Corrections 133
5.8 Summary and Outlook 135

6 Interjet Energy Flow/Event Shape Correlations 137
6.1 Non-global Logarithms 138
6.2 Shape/Flow Correlations in e^+e^- Dijet Events 140
6.2.1 Shape/Flow Correlations 140
6.2.2 Low Order Example 142
6.3 Factorization of the Cross Section for e^+e^- 147

6.3.1 The Soft Function 148
6.4 Resummation for e^+e^- Shape/Flow Correlations 149
6.4.1 Energy Flow Dependence 149
6.4.2 The Resummed Correlation 151
6.5 Analytical Results for e^+e^- Shape/Flow Correlations 153
6.5.1 Results for the Soft Function 153
6.5.2 Closed Expressions for the Correlation 154
6.6 Numerical Results for e^+e^- Shape/Flow Correlations 156
6.7 Extension to Hadronic Cross Sections 160
6.7.1 Refactorization of the Cross Section 160
6.7.2 The Soft Function 162
6.7.3 Resummation in Color Space 164
6.7.4 Renormalization and Color Mixing 166
6.7.5 Results for Lowest Order Momentum Parts 169
6.7.6 Results for Hadronic Shape/Flow Correlations 171
6.8 Summary and Outlook 171

7 Epilogue: Conclusions and Perspectives 173

A QCD Conventions and Eikonal Feynman Rules 175

A.1 The Running Coupling 175
A.2 Eikonal Feynman Rules 178

B Multiloop Techniques **179**

B.1 Feynman Parametrization 179

B.2 Reduction of Loop Integrals 179

B.2.1 Integration by Parts 181

B.2.2 Numerators 182

B.2.3 Collection of a Few Integrals 183

B.3 Rules for LCOPT 184

C Color Space Decomposition **187**

C.1 Color Bases 187

C.1.1 Basis for $q\bar{q} \to q\bar{q}$ 187

C.1.2 Basis for $qq \to qq$ 187

C.1.3 Basis for $qg \to qg$ 187

C.1.4 Basis for $gg \to q\bar{q}$ and $q\bar{q} \to gg$ 188

C.1.5 Bases for $gg \to gg$ 188

C.2 Hard Scattering Matrices 190

C.2.1 Hard Matrices for $q\bar{q} \to q\bar{q}$ 190

C.2.2 Hard Matrix for $qq \to qq$ 191

C.2.3 Hard Matrices for $qg \to qg$ 191

C.2.4 Hard Matrices for $gg \to q\bar{q}$ and $q\bar{q} \to gg$ 192

C.2.5 Hard Matrix for $gg \to gg$ 192

C.3 Soft Functions for $2 \to 2$ Scattering 193

C.3.1 Soft Matrices for $qq \to qq$ 193

C.3.2 Soft Matrix for $qg \to qg$ and $\bar{q}g \to \bar{q}g$ 193

C.3.3 Soft Matrices for $gg \to q\bar{q}$ and $q\bar{q} \to gg$ 194

C.3.4 Soft Matrix for $gg \to gg$ 195

Bibliography **196**

List of Figures

1.1 Outline of the thesis. 11

2.1 The electromagnetic form factor: a) 1-loop correction, b) graphical representation of the solutions to the Landau equations, Eqs. (2.4), in Feynman gauge, c) general reduced diagram. . . 18

2.2 a) Ward identity for a scalar polarized gluon. b) Identity for a single longitudinally polarized gluon attaching to an eikonal line. c) Resulting identity after iterative application of Figs. a) and b). 25

2.3 Illustration of momentum flow for two jet-configurations: a) a final-state jet in e^+e^- annihilation, b) a jet which radiates into initial and final states in the Drell-Yan process. The reduced diagrams in cut-diagram notation for the two processes are shown on the left, the jet-configurations which we study as examples are shown in the boxes. 28

2.4 Pole structure of configuration Fig. 2.3 b) in the complex plane, according to Eq. (2.37) for small and larger k^+. The scale is arbitrary. 29

2.5 a) Graphical representation of a parton-in-parton distribution function, Eq. (2.46), and b) its factorized form for arbitrary momentum fraction x, drawn as a reduced diagram. c) The reduced diagram for the PDF in the limit $x \to 1$. 36

2.6 Parton distribution function for $x \to 1$ with the jet functions factorized from the hard part, graphical representation of Eq. (2.65). 41

2.7 Parton distribution function for $x \to 1$, factorized into hard scatterings, an eikonal cross section, and purely virtual jet-remainders, as derived in Eq. (2.75). 44

2.8 Factorized cross section (2.83) after the application of Ward identities. The vertical line denotes the final state cut. 49

2.9 Graphical illustration of the variation of the gluon propagator with respect to the gauge fixing vector ξ, Eq. (2.104). 53

2.10 a) Graphical illustration of the variation of the jet function with respect to the gauge fixing vector ξ. b) Factorization of the variation into a soft and an ultraviolet part, Eq. (2.105). . . . 54

3.1 Graphical representations of the commutation relations between a) T^a_{ij}s, and b) $i\, f_{ijk}$s (Jacobi identity), Eq. (3.2). 61

3.2 Examples of a) a web (order 2), b) a c-web (web of order 3), and c) a diagram which is not a web (consisting of a product of an order-1 web and of an order-2 web). 62

3.3 a) Eikonal identity for 2 gluons, and b) an illustration of the generalized eikonal identity Eq. (3.5) for two webs. 63

3.4 Diagrams contributing at $\mathcal{O}(\alpha_s^2)$ (excluding self-energies). . . . 64

3.5 a) Rearrangement of the first two terms of Fig. 3.4 using Eq. (3.4), and b) Eq. (3.3). 65

3.6 Graphical expression of the exponentiation up to webs of order 2 in Feynman gauge. The color weights are given for (anti)quark eikonal lines. 66

3.7 Factorization of jet-like collinear configurations, represented by the grey oval, from the eikonal cross section with the help of the soft approximation. 68

3.8 a) Factorization of contributions at order 2 into webs of order 1.

b) Diagram with color weight 0, and decomposition into diagrams of Fig. 3.8 a) using Fig. 3.1. 70

4.1 Webs contributing to $A_f^{(2)}$ (compare to Fig. 3.6): a) web of order 1 with 1-loop gluon self-energy inserted, b) the "crossed ladder", c) and d) graphs with a triple gluon vertex. 85

4.2 LCOPT diagrams obtained from Fig. 4.1 b)-d). 87

4.3 QCD counterterm for the triple-gluon vertex, where PP denotes the pole part (omitting scheme-dependent constants). 88

5.1 Illustration of the effect of the parameter a in the weight (5.4) on the shape of the event: a) shape for $a = 1$, b) shape for $a = 0$, c) shape for $a = -1$. 100

5.2 Spherical limit of the shape (5.2) as a function of a, Eq. (5.6). 101

5.3 Comparison of fixed order and resummed cross sections for $a = -0.5$ at c.m. energy $\sqrt{s} = 91$ GeV as a function of $\bar{\varepsilon}$. Shown are the leading order (LO), matched leading logarithmic (LL), next-to-leading order (NLO) and matched next-to-leading logarithmic (NLL) results. 131

5.4 Comparison of matched NLL resummed cross sections for $a = -1$ and $a = 0$ to the corresponding cross sections calculated by PYTHIA with string hadronization (SF) at $\sqrt{s} = 91$ GeV. The data for $a = 0$ ($\bar{\varepsilon} = 1 - T$) are taken from [165] (SLD) and [166] (DELPHI). 133

5.5 Shifts of the peaks $\Delta\bar{\varepsilon}_p(a, Q = \sqrt{s} = 91 \text{ GeV})$ of the distributions $\frac{1}{\sigma}\frac{d\sigma}{d\bar{\varepsilon}}$ between NLL partonic resummed predictions and hadronic cross sections computed with PYTHIA with string fragmentation. The result is multiplied by $(1 - a)$. The blue band is the shift of the peak for the thrust determined in [170] between resummed predictions and experimental data. 136

6.1 Sources of global and non-global logarithms in dijet events. Configuration 1, a primary emission, is the source of global logarithms. Configuration 2 can give non-global logarithms. . 140

6.2 A kinematic configuration that gives rise to the non-global logarithms. A soft gluon with momentum k is radiated into the region Ω, and an energetic gluon with momentum l is radiated into $\bar{\Omega}$. Four-vectors β_1 and β_2, define the directions of jet 1 and jet 2, respectively. 142

6.3 The relevant two-loop cut diagrams corresponding to the emission of two real gluons in the final state contributing to the eikonal cross section. 143

6.4 $C(\Delta\eta)$, as defined in (6.17), as a function of rapidity width $\Delta\eta$ of the region Ω. The dashed line is its limiting value, $C(\Delta\eta \to \infty) = \pi^2/6$. 146

6.5 Differential cross section $\frac{\varepsilon d\sigma/(d\varepsilon d\hat{n}_1)}{d\sigma_0/d\hat{n}_1}$, normalized by the Born cross section, at $Q = 100$ GeV, as a function of ε and a at fixed ν: a) $\nu = 10$, b) $\nu = 50$. Ω is a ring (slice) centered around the jets, with a width of $\Delta\eta = 2$. 157

6.6 Differential cross section $\frac{\varepsilon d\sigma/(d\varepsilon d\hat{n}_1)}{d\sigma_0/d\hat{n}_1}$, normalized by the Born cross section, at $Q = 100$ GeV, as a function of a at fixed $\nu = 20$ and $\varepsilon = 0.05$. Ω is chosen as in Fig. 6.5. Solid line: $c_1 = e^{-\gamma_E}$, $c_2 = 2$, as in Eq. (3.34), dashed line: $c_1 = c_2 = 1$, dotted line: $c_1 = c_2 = 2$. 158

6.7 Ratios of differential cross sections for quark to gluon jets at $Q = 100$ GeV as a function of ε and a at fixed ν: a) $\nu = 10$, b) $\nu = 50$. 159

6.8 Diagrams for the calculation of the anomalous dimension matrix. 167

6.9 Color identity corresponding to Eq. (6.68). 168

A.1 One-loop (solid line) and three-loop (dashed red line) strong coupling as a function of scale μ (in GeV). 177

A.2 Feynman rules for eikonal lines in the fundamental representation with velocities β^μ, represented by the double lines. 178

List of Tables

4.1 $\alpha_s(\mu^2)^n N_f^{n-1} \left[\frac{1}{1-x}\right]_+$-contributions to the anomalous dimension P_{ff}. The expansion of A_f is performed in terms of α_s/π (cf. Eq. (4.4)). 90

4.2 Webs contributing to the N_f-term of the three-loop coefficient $A^{(3)}$ and their counterterms (c.t.s). 95

Acknowledgements

First and foremost, I would like to thank my Ph.D. advisor George Sterman, for his advice, support, and valuable insights during my graduate studies at Stony Brook. I acknowledge a fruitful collaboration with Tibor Kúcs, on which part of this thesis is based. Furthermore, I owe deep gratitude to Maria Elena Tejeda-Yeomans for many helpful discussions and her support in multi-loop and other matters. I also thank my Master's advisor Wolfgang Schweiger for raising my interest in particle physics, and for ongoing fruitful collaborations. I am indebted to Anton Chuvakin and Chi Ming Hung for their rescue-attempts when computers tried to erase my work. I acknowledge very useful exchanges with Lilia Anguelova, Rob Appleby, John Collins, Sally Dawson, Barbara Jacak, Edward Shuryak, Jack Smith, Peter van Nieuwenhuizen, Jos Vermaseren, and Andreas Vogt.

Next, I want to thank all my friends, too numerous to list on this page, except the physics-related ones who are among the people listed above. I thank my family, especially my parents and my sister Petra, for their support in my attempt to learn more about the smallest building blocks of the Universe, despite their initial viewpoint that "quark" is some sort of cheese.

Last, but not least, I acknowledge financial support by the Austrian Ministry of Science (Österreichisches Bundesministerium für Wissenschaft), the Department of Physics and Astronomy, SUNY at Stony Brook, and the U.S. National Science Foundation, grants PHY9722101 and PHY0098527.

Chapter 1

Prologue: Perturbative Quantum Chromodynamics

> Divergent series are the invention of the devil, and it is shameful to base on them any demonstration whatsoever.
>
> N. H. Abel, 1828.

The coefficients of a perturbation series in Quantum Chromodynamics (QCD) exhibit factorial growth, in other words, the series diverges. Nevertheless it is possible to construct meaningful physical observables that are calculable within perturbation theory, if the perturbative QCD series is asymptotic[1]. In the following we will illustrate this for (semi-)inclusive processes [1, 2]. We will not discuss exclusive processes where all hadrons in the final state are observed [3, 4, 5]. For exclusive processes currently experimentally accessible energies may not be high enough to make them amenable to a purely perturbative treatment, and non-perturbative effects have to be included, for example via additional parameters in effective models [6, 7, 8]. In the following we will denote processes where no hadronic final states are observed by inclusive or semi-inclusive. The latter denote cross sections with some additional restrictions that do not distinguish different hadronic decompositions of the events, for example event shapes in jet cross sections.

In this introduction we will start with an overview of the basic concepts of perturbative QCD (pQCD), and the main assumptions that allow us to

[1] Mr. Abel's statement may need to be modified to: Non-asymptotic series are the invention of the devil.

compare perturbative calculations with experiment. After giving a brief motivation for the work presented in this thesis we outline its contents which are based on our publications Refs. [9, 10, 11, 12].

1.1 Perturbative QCD - Basic Concepts

We refrain here from listing the QCD Lagrangian, and other generalities of non-abelian quantum field theories. In this thesis we follow the conventions for the QCD Feynman rules listed, for example, in [13], where also a variety of useful relations regarding SU(N) and Dirac algebra can be found.

Throughout this thesis we will use dimensional regularization [14], in $n = 4 - 2\varepsilon$ dimensions, and give explicit results in the $\overline{\rm MS}$ scheme [15]. We use Feynman gauge, unless explicitly stated otherwise.

1.1.1 Asymptotic Freedom

Here we want to point out the main feature of unbroken non-abelian, renormalizable field theories that makes them amenable to a perturbative treatment: asymptotic freedom [16, 17]. The running coupling in asymptotically free theories vanishes at large momentum scales, as illustrated in Fig. A.1 for the strong coupling in QCD, $\alpha_s(\mu)$. This is due to the sign of the first coefficient of the beta-function (see Appendix A.1 for the conventions used here), which, for QCD (SU(3)), is positive if the number of flavors is less than $33/2 = 16.5$. At large scales, or equivalently, short distances, the theory is then treatable perturbatively, if long-distance effects are incoherent to short-distance effects. At long distances > 1 fm, which correspond to low momentum transfer of order 1 GeV or less[2], confinement effects become dominant, and perturbation theory fails.

Furthermore, if short- and long-distance effects are incoherent, we may neglect masses in the computation of short-distance effects, since masses exhibit the same asymptotic behavior as the running coupling,

$$\begin{aligned} m(\mu^2) &= m(\mu_0^2)\exp\left\{-\frac{1}{2}\int_{\mu_0^2}^{\mu^2}\frac{d\lambda^2}{\lambda^2}\left[1+\gamma_m(\alpha_s(\lambda^2))\right]\right\}, \\ \lim_{\mu^2\to\infty}\frac{m(\mu^2)}{\mu^2} &= 0. \end{aligned} \tag{1.1}$$

[2]In the following we use natural units, for example, we set the speed of light c, or $\hbar$ to 1.

Here, γ_m is the mass anomalous dimension, the analog of the beta-function of the running coupling.

1.1.2 Assumptions of Perturbative QCD

There are two main assumptions that go into any calculation within perturbative QCD. These assumptions have not been proven yet, but the remarkable success of pQCD seems to confirm their validity.

The pQCD Series is Asymptotic

The first of these assumptions has already been mentioned above, namely, that pQCD is an asymptotic series, despite being divergent, in the mathematical sense: In perturbation theory a physical quantity is computed as a power series in terms of the small coupling

$$f(\alpha_s) \sim \sum_{n=0}^{\infty} f_n \alpha_s^n, \tag{1.2}$$

where in field theory, and thus in QCD, one finds $n!$ growth with the order of the coefficients f_n [18]. Only at $\alpha_s = 0$ the series would equal the function, being simply a Taylor expansion. For $\alpha_s \to 0$ the series can at best be asymptotic to $f(\alpha_s)$, but does not necessarily uniquely define $f(\alpha_s)$, even if summed to all orders, irrespective of the convergence or divergence of the series.

A series $\sum_{n=0}^{\infty} f_n \alpha_s^n$ is called *asymptotic* to $f(\alpha_s)$ for $\alpha_s \to 0$ on a set S if the remainder R_{N+1} obeys

$$|R_{N+1}| = \left| f(\alpha_s) - \sum_{n=0}^{N} f_n \alpha_s^n \right| \leq C_{N+1} \left|\alpha_s\right|^{N+1} \tag{1.3}$$

for all positive integer N and for all α_s in S. As stated above the asymptotic series does not define a unique function $f(\alpha_s)$ in general. Only under additional restrictions the series might give only one $f(\alpha_s)$.

If the truncation error C_N follows the same pattern as the coefficients f_N, in field theory

$$C_N \sim N! a^N N^b \tag{1.4}$$

(this follows from $\frac{C_{N+1}}{C_N} \sim \frac{1}{f_N} \sim N \Rightarrow C_N \sim N!$) the error decreases as a function of the order N until order $N_* \sim \frac{1}{|a|z}$ as a short calculation of the

minimum of the remainder (1.3) with the behavior (1.4) with respect to N shows, using Stirling's formula

$$\lim_{n\to\infty} n! = \sqrt{2\pi n} n^n e^{-n} \left[1 + \mathcal{O}\left(\frac{1}{n}\right)\right]. \tag{1.5}$$

If we truncate the series at its minimal term N_* then we get the best approximation to $f(\alpha_s)$ with an accuracy of $C_{N_*}\alpha_s^{N_*} \sim e^{-\frac{1}{|a|\,\alpha_s}}$. This means that the series $\sum f_n \alpha_s^n$ is not only asymptotic to $f(\alpha_s)$ but also to

$$f'(\alpha_s) = f(\alpha_s) + Ce^{-\frac{1}{|a|\,\alpha_s}}, \qquad C \text{ real.} \tag{1.6}$$

For $f'(\alpha_s)$ Eq. (1.3) still holds, that is, the expansions in powers of α_s of $f(\alpha_s)$ and $f'(\alpha_s)$, respectively, are the same even though $f(\alpha_s)$ and $f'(\alpha_s)$ are clearly two different functions. However, if α_s is sufficiently small, the difference between $f(\alpha_s)$ and $f'(\alpha_s)$ may be numerically small, and perturbation theory may give a well-approximated answer, up to power corrections as we will briefly mention in Sec. 1.1.4.

Incoherence of Long- and Short-Distance Effects

The second assumption is that properties that hold order-by-order for the asymptotic series up to power corrections in the regulated theory also hold in the full theory up to power corrections. Factorization can be proven in a sufficiently rigorous way for certain partonic quantities to any order in a regulated perturbation theory at leading power [1, 2], assuming only that this regulated theory has bound states whose formation decouples from short-distance physics, and that this factorization continues to hold when the unphysical, regulator-dependent states become physical upon removing the regulator.

However, the mechanisms that confine partons in hadrons are far from fully understood and have to be parameterized in an appropriate way in perturbative calculations. More or less heuristic argumentation, based on the parton model, suggests that these long-distance effects decouple. Colliding hadrons in the center-of-mass frame are highly Lorentz contracted, and internal interactions are time dilated. At sufficiently high energies, the interacting hadrons are in virtual states with a definite number of partons which are well separated in transverse directions. One parton in each colliding hadron then interacts incoherently at the hard scattering, interactions among partons within a hadron cannot interfere with this hard scattering because they take place at time-dilated scales. Therefore, an inclusive hadronic cross section

σ_{AB} for the process $A + B \to X$ with two hadrons in the initial state can then schematically be factorized at leading power in the hard scale, Q,

$$\sigma_{AB} = \sum_{a,b} f_{a/A}(\mu) \otimes f_{b/B}(\mu) \otimes \hat{\sigma}_{ab}(\mu). \tag{1.7}$$

Here the $f_{h/H}(x)$ are parton-in-hadron distribution functions, which describe the distribution of a parton h with momentum fraction x in hadron H. These distribution functions are convoluted in terms of the momentum fractions x with the partonic cross section $\hat{\sigma}_{ab}$, denoted by the symbol $\otimes$:

$$(f \otimes g)(x) = \int_0^1 dx_1 \int_0^1 dx_2 \, \delta(x - x_1 \, x_2) \, f(x_1) g(x_2). \tag{1.8}$$

Long distance effects of hadronic distribution functions are separated from the short distance scattering by the factorization scale μ. The physical cross section is of course independent of this scale. For the determination of the distribution functions experimental and/or nonperturbative input is needed, whereas the hard scattering is calculable in perturbation theory if it is infrared safe. The calculability of $\hat{\sigma}_{ab}$ follows from analyzing the partonic counterpart of Eq. (1.7):

$$\sigma_{a'b'} = \sum_{a,b} f_{a/a'}(\mu) \otimes f_{b/b'}(\mu) \otimes \hat{\sigma}_{ab}(\mu). \tag{1.9}$$

From this factorization $\hat{\sigma}_{ab}$ is calculable for infrared safe observables, as well as the parton-in-parton distribution functions, and the evolution of all these functions with the factorization scale μ. Furthermore, due to the incoherence of long- and short-distance effects, parton distribution functions are universal, that is, the same functions occur in a variety of infrared safe (semi-)inclusive cross sections.

Similarly, for (semi-)inclusive cross sections without hadrons in the initial state, we assume that the observed spectra of hadrons should be mathematically similar to the calculated spectra of partons. For example in jet cross sections we assume that the distribution of experimentally observed energy deposits in the detector is calculable by studying the corresponding distribution of more or less collimated, energetic partons.

All these assumptions reduce to the assertion that power corrections in the regulated theory remain small in transition to the full theory.

1.1.3 Infrared Safety

Quantities that are dominated by the short-distance behavior of the theory are *infrared (IR) safe*. For such quantities perturbation theory is applica-

ble. In order to be IR safe a physical quantity τ in QCD has to behave in the limit of the renormalization scale $\mu \to \infty$ as

$$\tau\left(\frac{Q^2}{\mu^2}, \alpha_s(\mu^2), \frac{m^2(\mu^2)}{\mu^2}\right) \underset{\mu \to \infty}{\longrightarrow} \hat{\tau}\left(\frac{Q^2}{\mu^2}, \alpha_s(\mu^2)\right) + \mathcal{O}\left(\left(\frac{m^2}{\mu^2}\right)^a\right),\ a > 0. \tag{1.10}$$

Thus τ should approach a limit as $\frac{m}{\mu} \to 0$ (m represents light quark and vanishing gluon masses, Q "large" invariants, $Q \gg \Lambda$) with $\frac{Q}{\mu}$ held fixed. In Chapter 2 we will show how to identify infrared safe observables.

Although infrared safe quantities are free of IR divergences as powers, large logarithmic corrections occur at the edge of phase space in all but fully inclusive observables, due to soft (with vanishing four-momentum) and/or collinear (parallel to primary, energetic quanta) radiation. These logarithmic corrections need to be resummed in order to provide reliable quantitative predictions. The remainder of this thesis deals with resummation of large logarithms. Another source of uncertainty in perturbative calculations are power corrections. These, however, are in the majority of cases incalculable within perturbation theory.

1.1.4 Nonperturbative Effects and Power Corrections

Above we have noted that Eqs. (1.7)-(1.10) are valid up to power corrections in the hard scale $Q \gg \Lambda_{\rm QCD}$. In only a few cases factorization theorems can also be proven beyond leading power. In addition, due to the at best asymptotic nature of QCD, Eq. (1.6), there will always be exponential ambiguities. These ambiguities correspond to power corrections proportional to

$$e^{-\frac{1}{|a|\,\alpha_s(Q^2)}} \sim \left(\frac{\Lambda^2_{\rm QCD}}{Q^2}\right)^{\frac{\beta_0}{4\pi|a|}}, \tag{1.11}$$

using the one-loop running coupling (A.6).

Nevertheless, perturbation theory itself encodes some information about the form of these power corrections. As we have mentioned above, in field theoretic expansions one often finds factorial growth of the coefficients. This suggests to attempt summation of the series via Borel transformation, which is defined as [19]

$$B(t) = \sum_{n=0}^{\infty} f_n \frac{t^n}{n!}. \tag{1.12}$$

If an asymptotic series is *Borel summable*, then the inverse transform, the so-called *Borel integral*

$$\tilde{f}(\alpha_s) = \frac{1}{\alpha_s}\int_0^\infty dt\, e^{-\frac{t}{\alpha_s}} B(t) \tag{1.13}$$

uniquely determines the function $f(\alpha_s) \equiv \tilde{f}(\alpha_s)$ to which the series is asymptotic. $\tilde{f}(\alpha_s)$ is a Laplace transform (the conventional variable for a Laplace transform is $s = 1/\alpha_s$). Thus the theory of Borel summability is essentially the theory of Laplace transforms.

If the Borel transform $B(t)$ of a pQCD series has singularities on the real positive axis then the series is not uniquely Borel summable. Nevertheless, we can still define the Borel integral by moving the integration contour above or below the singularities of $B(t)$ if they are on the positive real axis. For example, consider

$$B(t) = \frac{1}{1-at}, \tag{1.14}$$

where a determines the position of the singularity. Larger a means smaller radius of convergence of the series. We can define the Borel integral to be the principal value which introduces an ambiguity

$$\sim e^{-1/(|a|\,\alpha_s)}.$$

This ambiguity leads according to Eq. (1.11) to a power correction proportional to $1/Q^{\beta_0/(2\pi|a|)}$.

Although the power of the correction can be deduced from perturbation theory, the magnitude and functional form of these power corrections cannot be inferred without additional, nonperturbative or experimental information. In QCD one finds $n!$ growth of perturbative coefficients, which lead to singularities of the Borel transform on the positive and negative real axis.

One source of $n!$ growth is the factorial growth of the number of Feynman graphs with the order, which is connected to the occurrence of *instantons* [18, 20, 21]. Thus the study of instantons [22], which are solutions to the classical field equations, may provide the necessary additional information to determine the ambiguity in Eq. (1.6) stemming from instanton singularities in the Borel plane. Instantons in QCD produce singularities on the positive real axis, however, far away from the origin.

Another source of $n!$ growth at nth order in the perturbative expansion is called *renormalons* [23, 24], classified into UV and IR renormalons, connected to the large and small loop momentum behavior, respectively. UV renormalons in QCD produce singularities in the Borel plane on the negative

real axis and thus do not spoil the Borel summability. Furthermore, they are although theory-specific, process independent, analogous to UV counterterms in renormalizable field theories. IR renormalons, on the other hand, are located on the positive real axis for asymptotically free theories, in general much closer to the origin than instanton-singularities. IR renormalons therefore give rise to ambiguities of the aforementioned form (1.11), which are much less suppressed than instanton ambiguities. The location of IR renormalon poles is process-dependent. Renormalons are found in graphs that grow as $n!$ themselves, for example diagrams with loop insertions in the form of one or more "bubble chains" [20, 25].

1.2 Motivation for Further Exploration

From the above it may almost seem hopeless to attempt any calculation within perturbation theory. Nevertheless, nature itself seems to almost invite us to do perturbative calculations in QCD - the series seems asymptotic, with power corrections that are numerically small compared to the leading perturbative terms; the incoherence of long- and short-distance effects allows factorization with parton distribution functions that are universal for broad classes of observables. Thus, determined once experimentally for one observable in a class, all other observables within that class are then predictable in principle from perturbative calculations, up to power corrections.

Moreover, although much progress has been made in the development of non-perturbative techniques, or in the attempt of deriving the Standard Model from a more general theory, perturbative calculation is still the most complete and precise way to obtain quantitative predictions that can be compared to experiment. QCD processes need to be calculated as precisely as possible, in order not only to "test" the theory of strong interactions itself, but also to understand the background for other observables within the Standard Model and beyond, in the search for "new physics".

For precise quantitative predictions, it is necessary to sum the series to as high orders as possible, for the following reasons:

- Eq. (1.7) is in principle independent of the factorization scale μ, in practice, however, fixed order calculations up to order m introduce an error proportional to α_s^{m+1}:

$$\mu\frac{d}{d\mu}\sigma_{AB} = \mu\frac{d}{d\mu}\sum_{n=0}^{\infty} f_n(\mu)\alpha_s(\mu) = 0 \qquad \Rightarrow$$

$$\mu\frac{d}{d\mu}\sum_{n=0}^{m} f_n(\mu)\alpha_s^n(\mu) = -\mu\frac{d}{d\mu}\sum_{n=m+1}^{\infty} f_n(\mu)\alpha_s^n(\mu). \tag{1.15}$$

Calculations to as high order as possible reduce the factorization scale uncertainty.

- Power corrections, since they are incalculable within perturbation theory, are usually determined by experimental fits. However, numerically, at the presently calculated accuracy, power corrections are not distinguishable from higher order contributions. For example, the mean value of the thrust[3] T has the following perturbative expansion (see for example [26] or [27][4])

$$\langle 1 - T\rangle \approx 0.33\,\alpha_s(Q) + 1.0\,\alpha_s^2(Q) + c\,\alpha_s^3(Q) + \frac{\lambda}{Q} + \ldots. \tag{1.16}$$

The dependence on the scale Q of Eq. (1.16) with $\lambda = 1$ GeV and $c = 0$ (higher order corrections are vanishingly small) is numerically indistinguishable from $\lambda = 0.6$ GeV and $c = 3$ using the scale-dependence of the running coupling as shown in Fig. A.1.

- As already mentioned above, large logarithmic corrections arise that need to be resummed. In the case of the thrust, from Eq. (1.16), the average is at small values of $(1 - T)$, such that the corresponding logarithms of $\ln(1-T)$ are quite substantial. Resummation to high levels of logarithms also requires the calculation of the configurations that give rise to these logarithms at high orders.

As we have already emphasized, QCD processes are present as background in the searches for new physics. A thorough understanding of this background is therefore absolutely necessary, especially the distribution of energy between energetic jets. Interjet radiation is emitted from a variety of sources, from fragments of hadrons that do not participate in the primary hard scattering which produces the jets, from multiple parton scattering, and by soft bremsstrahlung from the primary scattering partons. All of these sources of interjet radiation are far from fully understood.

Although an enormous amount of valuable insights has been obtained in the past thirty years of perturbative calculations within QCD, there still

[3] A definition and discussion can be found in Chapter 2.

[4] Resummed results can be found, for example in [27] which contains a collection of the results of [28, 29, 30].

remains a wealth of open problems - the short list above contains only those directly connected with the content of this thesis; it would be beyond its scope to list further topics.

1.3 Outline of the Thesis

In this thesis we discuss two main topics - the higher order calculation of singular coefficients of partonic splitting functions, and jet event shapes, including their correlations with interjet energy flow (shape/flow correlations). The singularities in the splitting functions are due to simultaneously soft and collinear configurations. Similar configurations can be found in any quantity that contains collimated beams of particles (jets) which is not completely inclusive in the final state. It is therefore not surprising that the same coefficients appear in jet events whose discussion comprises the second part of the thesis.

The outline of this thesis which follows the successive steps in factorization and resummation procedures is illustrated schematically in Figure 1.1. The starting point is in all cases the definition of a cross section or other physical observable, denoted collectively by σ in the figure. Here σ is either a parton distribution function, a jet event shape, or a shape/flow correlation. σ contains in general singularities, or, in the case of IR safe observables (such as event shapes and correlations) logarithmic enhancements that need to be resummed. Resummation follows from factorization, that is, from the procedure of separating short-distance (in Fig. 1.1 denoted by the hard function $f_{\rm H}$) from long-distance effects. In the figure we distinguish between collinear configurations, $f_{\rm CO}$, which include soft/collinear radiation and soft configurations, $f_{\rm S}$. These configurations have typical momentum scales Q_i, $i = {\rm H,S,CO}, Q_{\rm H} = Q$.To obtain a factorized form is highly non-trivial, but once an observable is factorized, resummation is almost automatic.

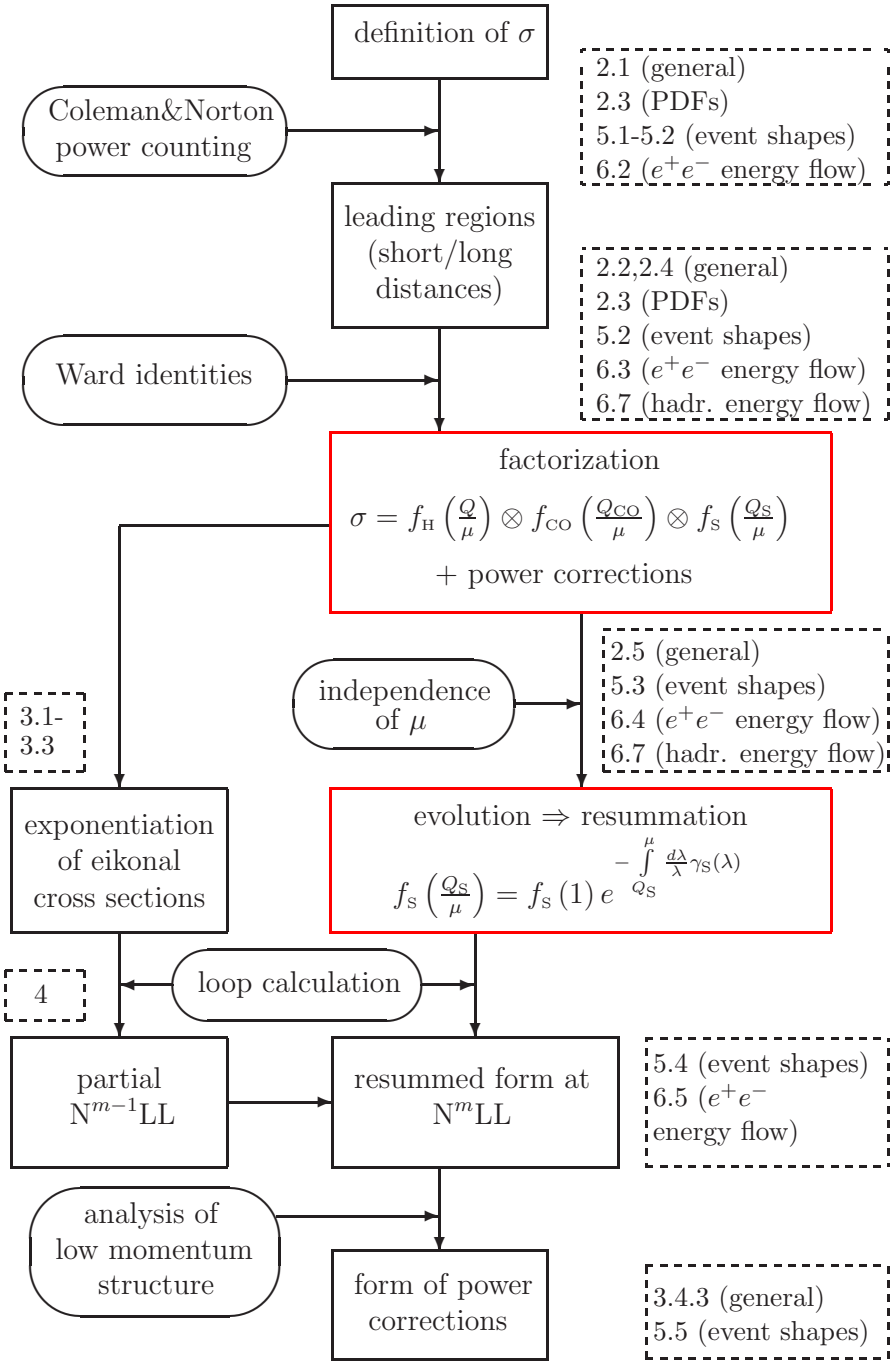

Figure 1.1: Outline of the thesis. The boxes denote various intermediate stages in factorization and resummation procedures, the ovals describe the necessary tools. The items in the dashed boxes correspond to the sections of this thesis where corresponding descriptions and examples can be found.

These leading regions in momentum space are in general linked by a convolution in terms of one or more variables, depending on the observable under consideration, denoted by the symbol $\otimes$. We can disentangle this convolution (see below, Chapter 2.5 for details) by taking for example Mellin moments, if the convolution is in terms of the variable x, Eq. (1.8),

$$\begin{aligned} \tilde{\sigma}(N) &= \int_0^1 dx\, x^{N-1} \sigma(x), \\ \tilde{\sigma}(N) &= \tilde{f}_{\rm H}\left(\frac{Q}{\mu}, N\right) \tilde{f}_{\rm CO}\left(\frac{Q_{\rm CO}}{\mu}, N\right) \tilde{f}_{\rm S}\left(\frac{Q_{\rm S}}{\mu}, N\right), \end{aligned} \tag{1.17}$$

where quantities in moment space are denoted by $\tilde{}$. The convolution is now a product in moment space. Eq. (1.17) contains potentially large ratios of the various scales intrinsic to the functions f_i, $i = $ H,S,CO to the factorization scale which give rise to the large logarithms mentioned above. These need to be resummed.

From the independence of the physical quantity σ of the factorization scale (here in moment space)

$$\mu \frac{d}{d\mu} \tilde{\sigma} = 0 \tag{1.18}$$

follow the evolution equations:

$$\begin{aligned} \mu \frac{d}{d\mu} \ln \tilde{f}_{\rm H}\left(\frac{Q}{\mu}\right) &= -\gamma_{\rm H}(\mu) \\ \mu \frac{d}{d\mu} \ln \tilde{f}_{\rm CO}\left(\frac{Q_{\rm CO}}{\mu}\right) &= -\gamma_{\rm CO}(\mu) \\ \mu \frac{d}{d\mu} \ln \tilde{f}_{\rm S}\left(\frac{Q_{\rm S}}{\mu}\right) &= -\gamma_{\rm S}(\mu) \end{aligned} \tag{1.19}$$

with

$$\gamma_{\rm H} + \gamma_{\rm CO} + \gamma_{\rm S} = 0. \tag{1.20}$$

The anomalous dimensions γ_i follow from separation of variables. The set of Eqs. (1.19) can be solved to resum large logarithmic corrections in exponents:

$$\tilde{f}_{\rm S}\left(\frac{Q_{\rm S}}{\mu}\right) = \tilde{f}_{\rm S}\left(1\right) e^{-\int_{Q_{\rm S}}^{\mu} \frac{d\lambda}{\lambda} \gamma_{\rm S}(\lambda)}. \tag{1.21}$$

We have evolved the soft function from its natural scale $Q_{\rm S}$, where no large logarithms arise, to the factorization scale with the help of Eq. (1.19). Calculation of the functions $f_i(1)$ and γ_i to a specific order resums large logarithms

at the $\mathrm{N}^m\mathrm{LL}$ level, that is $m = 0$ denotes leading logarithmic level (LL), $m = 1$ next-to-leading logarithmic (NLL), $m = 2$ next-to-next-to-leading logarithmic, etc. On the other hand, as we will see in Chapter 3 certain quantities exponentiate directly, not just via resummation as in (1.21). These quantities, when calculated to order m give the soft/collinear contribution to cross sections with jets at the $\mathrm{N}^{m-1}\mathrm{LL}$ level.

The sections where the above is discussed in detail for parton distribution functions [12], for jet shapes [10, 11], and shape/flow correlations [9, 10, 11] are indicated in the dashed boxes in Figure 1.1.

Chapter 2

Factorization, Evolution, and Resummation

In order to factorize infrared safe, perturbatively calculable quantities from long-distance dependence it is necessary to develop means to systematically identify the latter. This chapter describes how to analyze and classify long-distance behavior, and how to separate it from short-distance contributions. For the general discussion below we follow Refs. [2, 13, 31] and the cited references.

These methods were applied in our studies of the singular behavior of parton distribution functions [12], and of dijet events [9, 10, 11], which will be discussed in Sections 2.3 and 2.4.

2.1 Identification of Infrared Enhancements

In Minkowski space there are two basic types of divergences remaining after ultraviolet divergences have been removed by a suitable renormalization procedure, which does not introduce new infrared singularities: *soft divergences* that arise from vanishing four-momenta and *collinear* ones that are associated with parallel-moving on-shell lines of finite energy.

However, as consequences of the famous Bloch-Nordsieck [32, 33, 34] (which only holds in QCD for quantities without initial-state hadrons) and Kinoshita-Lee-Nauenberg theorems [35, 36], which follow from unitarity, these infrared divergences cancel between real and virtual emissions in suitably defined quantities[1]. In some important cases this cancellation is incomplete at the edge of phase space. For example for cross sections at threshold, that is, in the limit of soft and/or collinear radiation, fixed order perturbation theory is insufficient. In such cases, although no infrared divergences occur as powers, large logarithmic corrections arise that need to be resummed.

[1]For pedagogical reviews of these theorems see, for example, Refs. [13] and [37].

While the Bloch-Nordsieck and Kinoshita-Lee-Nauenberg theorems give general arguments, it is imperative for the resummation of logarithmic corrections to identify infrared singularities at the levels of the expressions corresponding to the Feynman diagrams at arbitrarily high, but fixed, order. This section, which is based on Refs. [38, 39], deals with the identification of infrared enhancements, while the remainder of this Chapter describe the factorization and resummation of large logarithmic corrections.

2.1.1 Landau Equations

To see where the aforementioned singularities may come from we consider an arbitrary Feynman diagram $G\left(\{p_s^\mu\}\right)$ with external momenta $\{p_s^\mu\}$ which is given by the following expression after Feynman parametrization, Eq. (B.2),

$$G\left(\{p_s^\mu\}\right) = \prod_{\text{lines } i} \int_0^1 d\alpha_i \delta\left(\sum_i \alpha_i - 1\right) \prod_{\text{loops } r} \int d^n k_r D(\alpha_i, k_r, p_s)^{-N} F(\alpha_i, k_r, p_s) \tag{2.1}$$

$$D(\alpha_i, k_r, p_s) \;\; = \sum_j \alpha_j \left[l_j^2(p,k) - m_j^2\right] + i\epsilon, \tag{2.2}$$

where F denotes all numerator and constant factors, and D denotes the denominator. We work in n dimensions, using dimensional regularization. α_j is the Feynman parameter of the jth line and l_j^μ its momentum, which is a linear function of loop momenta $\{k_r\}$ and external momenta $\{p_s\}$. Singularities arise in the integral 2.1 if isolated poles cannot be avoided by contour deformation. This can happen if the pole is at one of the end-points of the integral (*end-point singularity*) or if the contour is trapped between two poles (*pinch singularity*). The so-called *Landau equations* summarize the conditions for the existence of pinch surfaces, which are surfaces in (k, α) space where D vanishes [40, 41].

If the poles of D coalesce and therefore the contour cannot be deformed we encounter a pinch. The condition for this to occur is

$$\frac{\partial}{\partial k_j^\mu} D(\alpha_i, k_r, p_s) = 0 \tag{2.3}$$

at $D = 0$, because D is quadratic in momenta. Considering the α_i we see that D is only linear in each α_i, so there are never two poles to pinch, but a pole may migrate to an end-point $\alpha_i = 0$. Or alternatively, D may be independent of α_i at $D = 0$ if $l_i^2 - m_i^2 = 0$.

In summarizing these conditions we arrive at the Landau equations which state that a pinch surface exists only if the following conditions hold for each point $\{k_r^\mu, \alpha_i\}$ on the surface:

$$\begin{aligned} &\text{either} \quad l_i^2 = m_i^2, \quad \text{or} \quad \alpha_i = 0, \\ &\text{and} \quad \sum_{\text{line i in loop j}} \eta_{ij} \alpha_i l_i^\mu = 0, \end{aligned} \tag{2.4}$$

where η_{ij} is an "incidence matrix" which is ± 1 if the momentum l_i of line i flows in the same or opposite direction, respectively, as loop momentum k_r.

These equations can be given a physical interpretation, following Coleman and Norton [42]. We can identify α_i as the Lorentz-invariant ratio of the time of propagation to the energy for particle i which is represented by the on-shell line l_i. So the space-time separation between the starting point and the endpoint of line i is given by

$$\begin{aligned} \Delta x_i^\mu &\equiv \alpha_i l_i^\mu \\ &= \Delta x_i^0 v_i^\mu \end{aligned} \tag{2.5}$$

with

$$v_i^\mu = \left(1, \frac{\vec{l}_i}{l_i^0}\right) \tag{2.6}$$

the four-velocity of the particle. The Landau equations can then be illustrated in form of a *reduced diagram* where all off-shell lines are contracted to a point.

Here a comment about masses is in order: The contributions of momenta near pinch surfaces are sensitive to infrared cut-offs such as quark masses, hadronic binding energies and other long-distance scales. We want to identify precisely these momentum regions, to separate them from perturbatively calculable parts which we evaluate at a large scale, Q. The above considerations are most relevant when Q becomes very large, $Q \to \infty$. In this limit, due to Eq. (1.1), we can neglect masses since they become vanishingly small. Up and down quarks have masses of a few MeV at scales of the order of $\Lambda_{\rm QCD}$, where we do not expect perturbation theory to be reliable anyway. Thus, studying the theory with all masses at their physical values is equivalent to studying the corresponding massless theory with external particles on shell. Corrections to the so identified leading behavior for infrared safe quantities, Eq. (1.10), will be proportional to powers of m/Q, where m denotes any long-distance scale, including quark masses.

An Example

To illustrate the above, let us consider the one-loop vertex graph shown in Fig. 2.1 a). As discussed above, it suffices to consider the massless limit. Its momentum structure in $n = 4 - 2\varepsilon$ dimensional regularization in Feynman gauge is given by

$$V_\mu\left(p_1, p_2\right) = \int \frac{d^n k}{(2\pi)^n} \frac{\bar{u}(p_1)\gamma^\alpha \left(\not{p}_1 + \not{k}\right) \gamma_\mu \left(-\not{p}_2 + \not{k}\right) \gamma_\alpha v(p_2)}{\left[(p_1+k)^2 + i\epsilon\right]\left[(p_2-k)^2 + i\epsilon\right]\left(k^2 + i\epsilon\right)}, \tag{2.7}$$

where we omitted all prefactors unnecessary for the argument that follows. The Landau equation for this expression is

$$\alpha_1(p_1 + k)^\mu + \alpha_2(p_2 - k)^\mu + \alpha_3 k^\mu = 0, \tag{2.8}$$

which is not modified by the numerator. The solutions to this equation and the second condition of Eqs. (2.4) which give non-vanishing contributions when taking the numerator into account, are

$$k^\mu = 0,\ \alpha_1 = \alpha_2 = 0, \tag{2.9}$$

$$\alpha_1(p_1 - k)^\mu + \alpha_3 k^\mu = 0,\ \alpha_2 = 0,\ k^2 = p_1 \cdot k = 0, \tag{2.10}$$

$$\alpha_2(p_2 + k)^\mu + \alpha_3 k^\mu = 0,\ \alpha_1 = 0,\ k^2 = p_2 \cdot k = 0. \tag{2.11}$$

These solutions are depicted graphically in Fig. 2.1 b). In the first solution the radiated gluon k is soft, in the other two solutions it is collinear to either of the outgoing quarks.

As one can see by inspection of Eq. (2.7), this scaling behavior is not changed by making the following approximations as $k^\mu \to 0$:

- We neglect k^μ compared to p^μ in numerator factors, and
- we neglect k^2 compared to $p_1 \cdot k$ and $p_2 \cdot k$ in denominators.

The resulting expression for (2.7) is

$$V_\mu\left(p_1, p_2\right) \approx -p_1 \cdot p_2 \bar{u}(p_1)\gamma_\mu v(p_2) \int \frac{d^n k}{(2\pi)^n} \frac{1}{\left(p_1 \cdot k + i\epsilon\right)\left(-p_2 \cdot k + i\epsilon\right)\left(k^2 + i\epsilon\right)}. \tag{2.12}$$

We observe that this integral is logarithmically divergent as $k^\mu \to 0$. Furthermore, for $p_1 \cdot p_2 \to \infty$ it approaches a constant value, in other words, the composite vertex exhibits the same asymptotic behavior as the elementary (Born) vertex. This behavior is characteristic of theories with vector particles, as we will show explicitly by infrared power counting in the next section. The

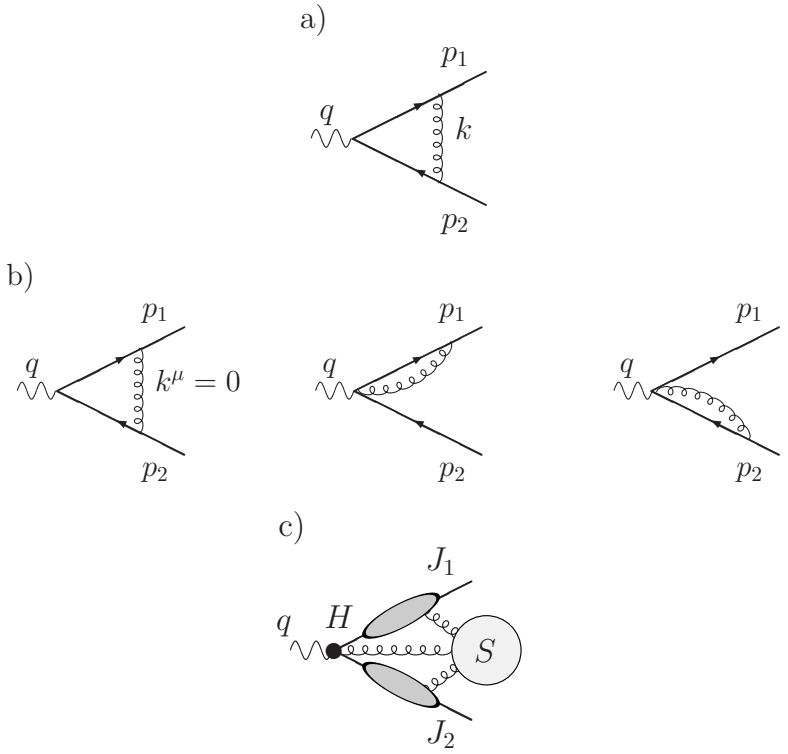

Figure 2.1: The electromagnetic form factor: a) 1-loop correction, b) graphical representation of the solutions to the Landau equations, Eqs. (2.4), in Feynman gauge, c) general reduced diagram.

set of approximations above is called *eikonal approximation*, closely connected to path-ordered exponentials, also called Wilson lines. We will have to say more about this connection below. The eikonal approximation leads to the eikonal Feynman rules listed in Appendix A.2. Especially the second approximation, the neglect of k^2 compared to $p \cdot k$ in denominators, is nontrivial in Minkowski space. In Section 2.2.2 we will study this issue in more detail.

Following Coleman and Norton, we can generalize the above to arbitrarily high, but fixed orders. The resulting pinch surfaces for the electromagnetic form factor are shown in Fig. 2.1 c) in reduced diagram notation. Only short-distance effects contribute to the hard scattering, H, where the two primary outgoing partons are produced. H is therefore contracted to a (slightly extended) point in the reduced diagram. Once the primary partons are produced, only collinear and/or soft radiation can be emitted, since they travel away from the hard scattering at the speed of light, if massless. They can

never meet again at a point in space-time. We label the soft radiation S in the reduced diagram, and the collinear configurations, the "jets" are labelled J_i, $i = 1, 2$.

2.1.2 Power Counting

Eqs. (2.4) are only necessary conditions for infrared divergences. In many cases, integration contours in perturbative integrals may pass through pinch surfaces without producing significant contributions in the limit of large momentum transfer. In such cases infrared safety (1.10) is not violated. Infrared power counting [38] gives the potential degree of divergence of the pinch surfaces under consideration. Before becoming more explicit, let us just remark that in Feynman gauge individual diagrams in general have much worse scaling behavior than the gauge invariant contribution after summing over all diagrams, since in the sum unphysical contributions cancel.

In the following we use light-cone coordinates, our conventions are given in Eq. (B.29). The following momentum configurations, scaled relative to the large momentum scale in the problem, Q, are possible:

- Soft momenta that scale as $k^\mu \sim \lambda\, Q$, $\lambda \ll 1$, in all components.
- Soft momenta with components that scale in the strongly ordered form $k^+ \sim \sigma\, Q, k^- \sim \lambda\, Q, k_\perp^2 \sim \lambda\, (Q)^2$, or $k^- \sim \sigma\, Q, k^+ \sim \lambda\, Q, k_\perp^2 \sim \lambda\, (Q)^2$, respectively, where $\sigma \ll \lambda \ll 1$. These are the so-called Glauber or Coulomb momenta [43, 44]. Glauber momenta have to be considered separately.
- Momenta collinear to the momenta of initial or final state particles. Momenta collinear to particles moving in the plus direction scale as $k^+ \sim Q, k^- \sim \lambda\, Q, k_\perp^2 \sim \lambda\, (Q)^2$, whereas momenta collinear to the minus direction behave as $k^- \sim Q, k^+ \sim \lambda\, Q, k_\perp^2 \sim \lambda\, (Q)^2$.
- Hard momenta that are far off-shell, and thus scale as $\sim Q$ in all components.

Real momenta contributing to the final state have the same scaling behavior as purely virtual momenta since

- for a jet momentum crossing the cut we obtain

$$\int dk^+ dk^- dk_\perp^2 \delta_+ \left(2k^+k^- - k_\perp^2\right) = \int \frac{dk^+}{2k^+} dk_\perp^2 \sim \lambda Q^2,$$

which is the same scaling behavior found for a virtual jet line

$$\int dk^+ dk^- dk_\perp^2 \frac{1}{k^2} \sim \frac{\lambda^2 Q^4}{\lambda Q^2} = \lambda Q^2.$$

- Similarly, we find for real soft momenta

$$\int dk^+ dk^- dk_\perp^2 \delta_+ \left(2k^+k^- - k_\perp^2\right) \sim \lambda^2 Q^2,$$

which coincides with the behavior of virtual soft momenta.

In the remainder of this section we scale all momenta implicitly by Q which we drop from here on, that is

$$k^\mu \to k^\mu / Q. \tag{2.13}$$

Vertex Suppression Factors

Let us now study how numerator factors change the scaling behavior of momentum lines and loops. These numerator suppression factors are different in covariant and physical gauges. Let us consider a fermion-gluon-fermion vertex in Feynman and in axial gauge as representative examples. This vertex is given by

$$(\not{p} + \not{k})\, \gamma^\mu\, \not{p} = -\gamma^\mu\, (\not{p} + \not{k})\, \not{p} + 2\,(p+k)_\mu\, \not{p}. \tag{2.14}$$

The first term in Eq. (2.14) scales as $\sim \lambda^{1/2}$ if k is part of the jet. The contribution of the second term, however, is different in covariant and physical gauges, respectively. In physical gauges, this term does not contribute, due to

$$\lim_{k^2 \to 0} k^2 k^\mu D_{\mu\nu}(k, \xi, \kappa) = 0, \tag{2.15}$$

where $D_{\mu\nu}(k, \xi, \kappa)$ is the gluon propagator from a Lagrangian with gauge fixing term $[-1/2\kappa(\xi \cdot \mathcal{A})^2]$, $\mathcal{A}$ being the gauge potential, modulo color factors,

$$D_{\mu\nu}(k, \xi, \kappa) = \left[-g_{\mu\nu} + \frac{\xi_\mu k_\nu + k_\mu \xi_\nu}{\xi \cdot k} - \xi^2 \left(1 + \frac{k^2}{\kappa \xi^2}\right) \frac{k_\mu k_\nu}{(\xi \cdot k)^2}\right] \frac{1}{k^2 + i\epsilon}. \tag{2.16}$$

Eq. (2.15), however, does not hold in covariant gauges with gauge fixing $[-1/2\kappa(\partial \cdot \mathcal{A})^2]$. *Scalar polarized* gluons, that is, gluons that are contracted into their own momenta at jet-vertices, are then unsuppressed. Analogous considerations apply to other three-point vertices in jets.

All jet three-point vertices contribute a numerator suppression factor of $\lambda^{1/2}$, unless one of the attached gluons is scalar polarized and attaches to a

hard part, in a covariant gauge, or soft. This is due to the above observation, and because we obtain a numerator suppression-factor proportional to λ in any gauge when analyzing purely soft three-point gluon-gluon or ghost-gluon vertices in a similar manner. Four-point vertices do not suppress the scaling behavior.

Contracted vertices have the same scaling behavior as the elementary vertices analyzed above. In contracted vertices in reduced diagrams internal lines which are off-shell by ~ 1 have been shrunk to a point, following (2.6) and (2.6). The behavior of contracted vertices can be analyzed by decomposing each vertex into its most general Lorentz structure, and by using Ward identities.

For example, the most general decompositions in Feynman and physical gauges for the gluon two-point one-particle irreducible Green function are

$$\Pi_{\mu\nu}^{\text{Feynman}}(p) = p^2 g_{\mu\nu} f_1 + p_\mu p_\nu f_2, \tag{2.17}$$

$$\Pi_{\mu\nu}^{\text{physical}}(p,\xi) = \frac{(p\cdot\xi)^2}{\xi^2} g_{\mu\nu} f_1' + p_\mu p_\nu f_2' + \\ +(p_\mu \xi_\nu + \xi_\mu p_\nu)\frac{(p\cdot\xi)}{\xi^2} f_3' + \frac{\xi_\mu \xi_\nu}{\xi^2}\frac{(p\cdot\xi)^2}{\xi^2} f_4', \tag{2.18}$$

where the f_i, f_i' are dimensionless functions of contracted momenta with scaling behavior ~ 1. Upon insertion of these composite propagators into a diagram they are contracted with elementary gluon propagators. For the Feynman gauge expression it is immediately obvious that the combination (gluon jet line-Π^{Feynman}-gluon jet line) has the same scaling behavior as an elementary gluon jet line. In the physical gauge we observe that the terms proportional to f_3' and f_4' drop out, using Eq. (2.15). The term with f_2' gives at least one factor p^2 upon contraction with a gluon jet line, and thus the same scaling contribution arises as for elementary propagators. The term with f_1', however, seems to spoil this behavior. It can be shown using the techniques of [38, 45] that this term is absent in Π^{physical}. Therefore, the composite gluon jet line has also in a physical gauge the same scaling behavior as an elementary jet line. Similar considerations apply to all other propagators and vertices in QCD, further details can be found in Refs. [38, 45].

Summary

- Every internal jet line scales as $\sim \lambda^{-1}$. Every bosonic soft momentum contributes as $\sim \lambda^{-2}$, fermionic soft momenta are proportional to $\sim \lambda^{-1}$. Jet loops scale as $\sim \lambda^2$, whereas soft loops behave proportional to

$\sim \lambda^4$. This leads to the following superficial degrees ω of infrared (IR) divergence

$$\omega_S = 4L_S - 2N_S^b - N_S^f + t_S, \tag{2.19}$$
$$\omega_J = 2L_J - N_J + t_J, \tag{2.20}$$

where the subscripts denote soft (S) or jet (J) pinch surfaces. L_i are the number of loops in $i = S$, J, N_i are the number of lines therein, where the superscripts b and f label bosonic and fermionic lines, respectively,

$$N = N^b + N^f. \tag{2.21}$$

We can count the degree of IR divergence separately for each pinch surface, if we carefully take into account momenta which link the surfaces in order to avoid double counting. t_i denote numerator suppression factors which are summarized below.

- Soft three-point vertices suppress the scaling by λ. Therefore the soft suppression factor is given by

$$t_S = v_S^{(3)}, \tag{2.22}$$

where $v_S^{(3)}$ is the number of soft three-point vertices.

- On the other hand, jet three-point vertices give a suppression of $\lambda^{1/2}$, unless the gluons involved are scalar polarized in covariant gauges. This leads to a suppression factor t_J for jets in physical gauges:

$$t_J \geq \max\left\{\frac{1}{2}\left[v_J^{(3)} - s_J\right], 0\right\}, \tag{2.23}$$

where $v_J^{(3)}$ is the number of jet 3-point vertices, and s_J denotes the number of soft lines attached to the jet. In covariant gauges this is modified to

$$t_J \geq \max\left\{\frac{1}{2}\left[v_J^{(3)} - s_J - l_J\right], 0\right\}, \tag{2.24}$$

due to scalar polarized gluons l_J, linking jet lines and the hard scattering.

Furthermore, we will need the following useful identities: the relation between the number of i-point vertices $v^{(i)}$, the number of internal momentum lines N, and the number of external lines E,

$$2N + E = \sum_i i v^{(i)}, \tag{2.25}$$

and the Euler identity

$$L = N - \sum_i v^{(i)} + 1, \tag{2.26}$$

where L is the number of loops. We will use these rules below.

In this section we have described how to identify regions in momentum space that give leading contributions, and how to determine the degree of infrared divergence by counting powers in each of these regions. Before going on to actually apply the techniques developed above, we will first explain how to factorize the leading regions which we expect to be linked by soft and/or scalar polarized gluons because of the numerator suppression factors Eqs. (2.23) and (2.24), respectively.

2.2 Factorization

We are now going to show how to factorize infrared safe quantities from long-distance behavior, and how to refactorize these leading regions, which will allow us to resum large logarithmic corrections. In the following we will denote both procedures by factorization. The final results can in many cases be rewritten in terms of gauge-independent functions which reproduce the leading behavior in any gauge.

2.2.1 Ward Identities

The factorization of scalar polarized gluons from hard contributions is a matter of straightforward application of the Ward identity shown in Fig. 2.2 c) for scalar polarized gluons. The grey blob denotes a hard part.

Fig. 2.2 c) follows from the Ward identity shown in Fig. 2.2 a), and the identity for scalar polarized gluons attaching to an eikonal line in Fig. 2.2 b). Fig. 2.2 a) is the graphical representation (in momentum space) of the following equation [46, 47]

$$\left\langle N \left| \kappa \, \partial \cdot A^b(x) \right| M \right\rangle = 0, \tag{2.27}$$

where M and N are physical states, and A^b_μ is a nonabelian gauge field carrying color b. By physical states we denote states involving on-shell fermions and gauge particles with physical polarizations; ghosts are not included. Throughout this thesis, gluons with arrows are scalar polarized. Eq. (2.27) can be proven, for example, by taking the BRST variation [48, 49, 50] of the Green function $\left\langle 0 \left| T\, b^b(x) \prod_i \Psi(y_i) \prod_j \bar{\Psi}(z_j) \right| 0 \right\rangle$. The sum of BRST variations of all

of the fields is 0, since the QCD Lagrangian is BRST invariant. Then we use the reduction formula to relate the truncated Green function to the transition matrix element above. All variations of the quark and antiquark fields Ψ and $\bar{\Psi}$ vanish due to truncation, and since

$$\bar{u}(p)(\not{p} - m) = 0, \quad (\not{p} - m)u(p) = 0\,. \tag{2.28}$$

In the following we set all masses to zero. The remaining variation of the antighost b^b gives Eq. (2.27), where now the fields Ψ and $\bar{\Psi}$ are on-shell, denoted by M and N. Similar considerations apply to gluons. Eq. (2.27) says that the sum of all possible attachments of a scalar polarized gluon to a matrix element vanishes. From this follows Fig. 2.2 a), since, by definition, we do not include the graph into the hard function where the gluon attaches to the physically polarized parton (quark or gluon), shown on the right-hand side of Fig. 2.2 a).

The eikonal identity in Fig. 2.2 b) follows from the eikonal Feynman rules in Fig. A.2. The attachment of the unphysical gluon to the fermion line is equivalent to its attachment to an eikonal or Wilson line, or path-ordered exponential Φ, in direction β opposite to the fermion line's momentum:

$$\begin{aligned}\Phi_\beta^{(\mathrm{f})}(0,\eta;0) &\equiv P e^{ig_s\int_0^\eta d\xi\beta\cdot\mathcal{A}^{(\mathrm{f})}(\xi\beta^\mu)} \\ &= 1 + P\sum_{m=1}^{\infty}\prod_{i=1}^{m}\int\frac{d^nk_i}{(2\pi)^n}g_s\beta\cdot\mathcal{A}^{(\mathrm{f})}(k_i^\mu)\frac{1}{\beta\cdot\sum\limits_{j=1}^{i}k_j + i\varepsilon}.\end{aligned} \tag{2.29}$$

The exponent is the resulting phase rotation on a particle of flavor (f) due to unphysical, scalar polarized, gluons. Here P denotes path ordering, g_s is the strong coupling, and $\mathcal{A}^{(\mathrm{f})}$ is the vector potential in representation (f). In the second line of (2.29) we have expanded the ordered exponential in momentum space. The resulting Feynman rules are precisely the ones mentioned above, of the eikonal approximation, listed in Appendix A.2. The eikonal propagators are the result of the path ordering, because

$$\int\limits_{-\infty}^{\infty} dz\, e^{ikz}\theta(z) = \frac{i}{k + i\epsilon}. \tag{2.30}$$

We will represent eikonal lines graphically as double lines. Fig. 2.2 b) displays the following equality for $p^2 = k^2 = 0$, k collinear to p,

$$\begin{aligned}-g_sT^b\bar{u}(p)\frac{\beta^\mu k_\mu}{-\beta\cdot k} &= g_sT^b\bar{u}(p)\gamma^\mu\frac{1}{\not{p}+\not{k}}k_\mu \\ &= g_sT^b\bar{u}(p)\frac{\not{k}+\not{p}-\not{p}}{\not{p}+\not{k}} = g_sT^b\bar{u}(p).\end{aligned} \tag{2.31}$$

where we have used Eq. (2.28) in the last equality on the right-hand side. p is the quark momentum which flows into the final state, and k the gluon's momentum. T^b is a SU(N) generator in the fundamental representation. Since the right-hand sides of Figures 2.2 a) and b) are the same (the "empty" eikonal line carries no momentum), the left-hand sides are the same. Repeated application of this identity results in Fig. 2.2 c) [51, 52]. Note that the color factors are included in the Ward identity, resulting in the appropriate color factor for the attachments of the gluons as shown in Fig. c). We have succeeded in decoupling unphysical gluons from physical processes, their only effect being phase rotations on the factorized physical momentum lines. In completely inclusive cross sections these phase rotations cancel due to the unitarity of Wilson lines [44]:

$$\Phi_\beta^{(\mathrm{f})\,\dagger}\Phi_\beta^{(\mathrm{f})} = \mathbf{1}. \tag{2.32}$$

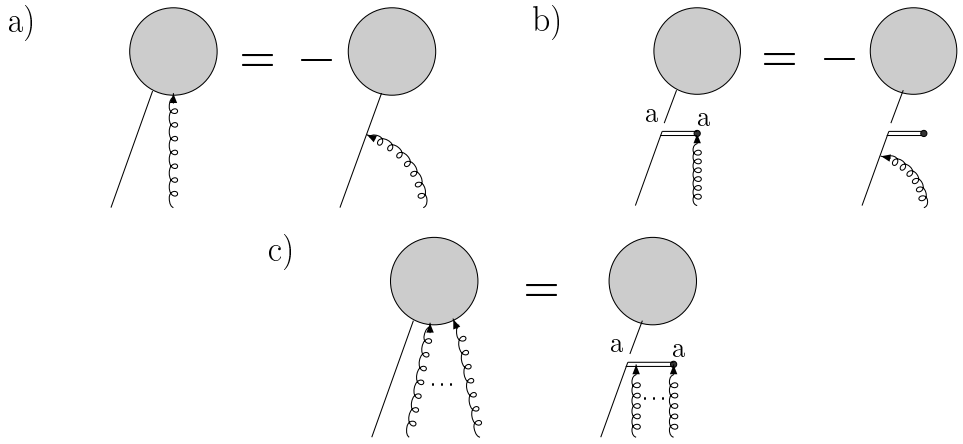

Figure 2.2: a) Ward identity for a scalar polarized gluon. b) Identity for a single longitudinally polarized gluon attaching to an eikonal line. c) Resulting identity after iterative application of Figs. a) and b). Repeated gauge-group indices are summed over.

2.2.2 Glauber/Coulomb Gluons and Infrared Safety

The factorization of soft gluons, which are not necessarily scalar polarized, from jet lines does not follow immediately from the Ward identity Fig. 2.2. To achieve factorization in this case, we have to make the following two approximations: the neglect of non-scalar gluon polarizations, and the eikonal approximation discussed above in Sec. 2.1.1, which consists of neglecting soft momenta k^μ in the numerator compared to jet-momenta p^μ and k^2 compared

to $p \cdot k$ in the denominator. After making these approximations, which are referred to by the term *soft approximation*, we can factor soft momenta from collinear jet momenta with the help of Fig. 2.2 c).

We start by decomposing each soft gluon propagator $D_{\mu\nu}$ with momentum k^μ into a scalar-polarized contribution and a remainder [34, 53]:

$$D_{\mu\nu}(k) \;=\; G_{\mu\nu}(k,\beta) + K_{\mu\nu}(k,\beta)\,, \tag{2.33}$$

where we define

$$\begin{aligned} K_{\mu\nu}(k) &\equiv D_{\mu\rho}(k)\,\frac{\beta^\rho\, k_\nu}{\beta\cdot k + i\epsilon}, \\ G_{\mu\nu}(k,\beta) &\equiv D_{\mu\nu}(k) - D_{\mu\rho}(k)\,\frac{\beta^\rho\, k_\nu}{\beta\cdot k + i\epsilon}. \end{aligned} \tag{2.34}$$

β is chosen to flow in the direction opposite to p, that is, if the jet flows into the plus-direction, β points into the minus-direction, and vice versa. The sign of the $i\epsilon$-prescription is chosen in such a way as to not introduce new pinch singularities near the ones produced by the soft gluons under consideration. For momenta to the right of the cut in initial-state jets we also have $+i\epsilon$, since the sign of the momentum flow to the right of the cut is reversed relative to the jet momentum p. That is, we have for momenta to the left of the cut $(p+k)^2 + i\epsilon \approx 2p\cdot k + i\epsilon$, whereas to the right of the cut we obtain $(p-k)^2 - i\epsilon \approx -2p\cdot k - i\epsilon$.

From Eq. (2.34) we see, that for the scalar polarized K-gluons the identity shown in Fig. 2.2 c) is immediately applicable, leading to the desired factorized form. So it remains to be shown that the G-gluons do not give leading contributions. Power-counting, as we have demonstrated in the previous section, shows that only 3-point vertices are relevant for the coupling of soft gluons to jets.

First, let us consider a 3-point vertex in a purely initial or purely final state jet, as shown in Fig. 2.3 a). Such jets, as indicated in the left part of Fig. 2.3 a) occur for example in e^+e^- annihilation, as we have seen in Sec. 2.1.1 above. The soft G-gluon with propagator $G_{\mu\nu}(k,\beta)$ couples to a fermion jet-line with momentum p^μ in a jet moving in the plus-direction:

$$\frac{\not{k}+\not{p}}{(k+p)^2+i\epsilon}\gamma^\nu\frac{\not{p}}{p^2+i\epsilon}G_{\mu\nu}(k,\beta) \approx 2\frac{\not{p}}{((k+p)^2+i\epsilon)\,(p^2+i\epsilon)}p^\nu G_{\mu\nu}(k,\beta) \approx 0, \tag{2.35}$$

because $p^\nu \approx p^+\beta^\nu$. Corrections are proportional to $\lambda Q, \lambda \ll 1$, as follows from the power counting described in Sect. 2.1.2 when neglecting k, and because $G_{\mu\nu}(k,\beta)\,\beta^\nu = 0$. An analogous observation holds for the coupling of G-gluons

to jet-lines via triple-gluon vertices. In (2.35) we neglect all terms of order λQ in the numerator, including the momentum k, because we assume that the denominator also scales as $\sim \lambda Q$. This approximation is only valid for soft gluons not in the Glauber or Coulomb region, where the denominator behaves as $\sim \lambda^2 Q$. If the soft momenta are not pinched in this Glauber/Coulomb region we can deform the integration contours over these momenta away from this dangerous region, into a purely soft region where the above approximations are applicable. This is straightforward to show for purely virtual initial or final state jet configurations, as displayed in Fig. 2.3 a)[2].

Consider again the 3-point vertex in Eq. (2.35), where now the gluon with momentum k is in the Glauber/Coulomb region. If $|p^+k^-|$ is not dominant over $|2p_\perp \cdot k_\perp + k_\perp^2|$ in the denominator our approximation fails. The poles of the participating denominators are in the k^- complex plane at

$$\begin{aligned} k^- &= \frac{k_\perp^2 - i\epsilon}{2k^+}, \\ k^- &= \frac{(k_\perp + p_\perp)^2 - i\epsilon}{2(k^+ + p^+)} - p^-. \end{aligned} \tag{2.36}$$

As long as the jet-line p carries positive plus momentum, we see that the k^--poles are not pinched in the Glauber region. In this case we can deform the contour away from this region into the purely soft region, where $|p^+k^-| \gg |2k_\perp \cdot p_\perp + k_\perp^2|$. In a reduced diagram, which represents a physical process, there must be at every vertex at least one line whose plus momentum flows into the vertex, and at least one line whose plus momentum flows out of the vertex. Thus, at every vertex, we can always find a momentum p for which the above observation holds, and we can always choose the flow of k through the jet along such lines. If the soft gluon momenta k, which we want to decouple, connect only to a purely virtual or final state jet, this observation remains true throughout the jet. An analogous argument applies to the right of the cut.

For other jet configurations, where the jet appears in both initial and final states, the situation is significantly more complicated. Here pinches in the Glauber/Coulomb region occur on a diagram by diagram basis, and cancel only in sufficiently inclusive cross sections. Let us illustrate this at the example of the inclusive Drell-Yan cross section shown in Fig. 2.3 b) in cut-diagram notation, $A + B \to X$, where A and B are hadrons, and X is all radiation into the final state. In a cut diagram, the amplitude is displayed to the left of the cut (the vertical line), the complex conjugate amplitude is shown to the right.

[2]Initial and final states are defined with respect to the hard scattering.

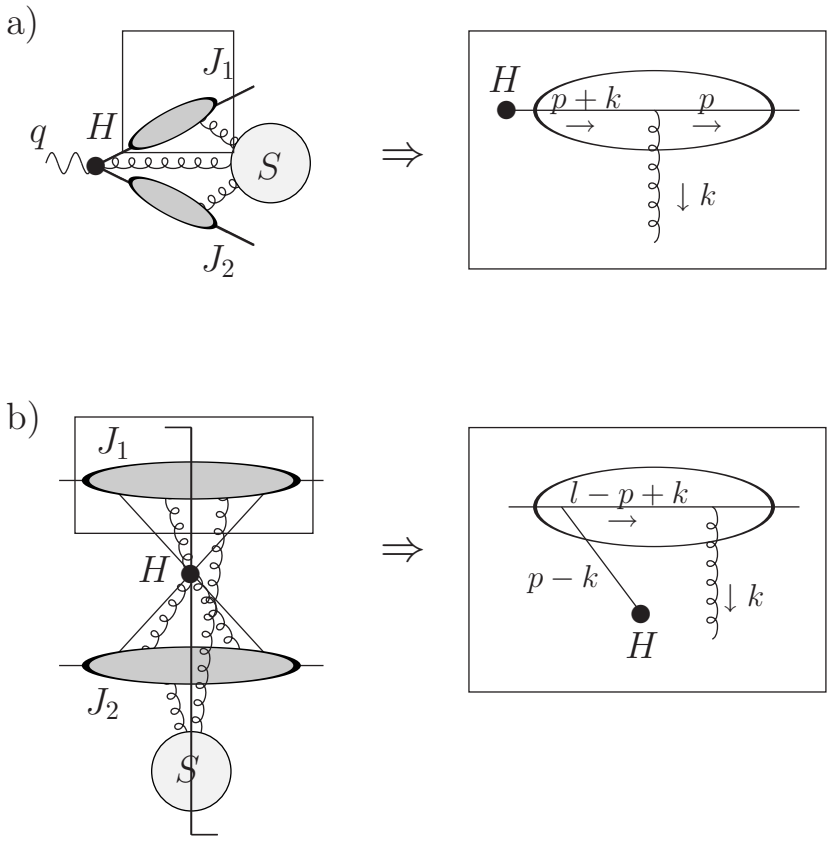

Figure 2.3: Illustration of momentum flow for two jet-configurations: a) a final-state jet in e^+e^- annihilation, b) a jet which radiates into initial and final states in the Drell-Yan process. The reduced diagrams in cut-diagram notation for the two processes are shown on the left, the jet-configurations which we study as examples are shown in the boxes. The vertical line (cut) represents the final state.

In Fig. 2.3 b), a soft gluon with momentum k connects the active jet line $p-k$ which participates in the hard scattering, and the spectator jet line $l-p+k$ which flows into the final state after emitting the soft gluon. The relevant denominators have poles in the k^- complex plane at

$$\begin{aligned} k^- &= \frac{k_\perp^2 - i\epsilon}{2k^+}, \\ k^- &= \frac{-(p_\perp - k_\perp)^2 + i\epsilon}{2(p^+ - k^+)} + p^-, \\ k^- &= \frac{(l_\perp - p_\perp + k_\perp)^2 - i\epsilon}{2(l^+ - p^+ + k^+)} + p^- - l^-. \end{aligned} \tag{2.37}$$

The pole-structure for k^- in the complex plane is shown in Fig. 2.4. For fixed, small k^+ the contour is pinched between the poles of lines $p-k$ and $l-p+k$ which are in the Glauber/Coulomb region. This is the case for the pole-configuration shown as filled circles in the figure. If k^+ is not pinched, however, then its contour can be deformed such that the two poles move away from each other, as illustrated by the poles drawn as squares. Then the k^- contour is not trapped near the Glauber/Coulomb region, and the soft approximation is applicable. On the other hand, if also k^+ is pinched by a configuration similar to Fig. 2.3 b) in the other jet, then the contour cannot be deformed, and the soft approximation fails. This occurs in general if there are at least two initial state hadrons or jets whose spectator fragments proceed into the final state.

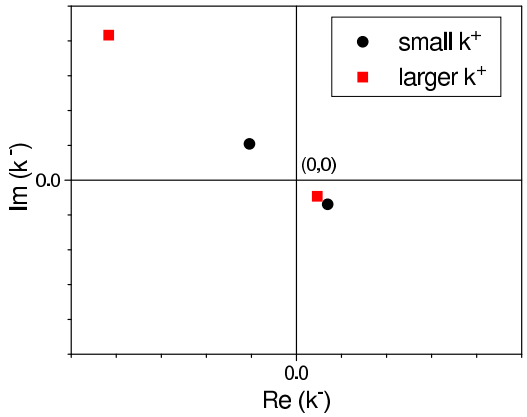

Figure 2.4: Pole structure of configuration Fig. 2.3 b) in the complex plane, according to Eq. (2.37) for small and larger k^+. The scale is arbitrary.

A careful analysis [51, 52, 54, 55] shows that these pinches in the Glauber/Coulomb region cancel in the sum over states for the inclusive Drell-Yan cross section, and in general, in sufficiently inclusive cross sections. Let us sketch the proof of cancellation to all orders, following [52].

Cancellation of Pinches in the Glauber/Coulomb Region

The cancellation is best seen in light-cone ordered perturbation theory (LCOPT). The rules for LCOPT can be found in Appendix B.3 [56, 57, 58], they can be derived by performing the minus integrals. LCOPT is similar to old-fashioned, or time-ordered, perturbation theory, but ordered along the light-cone, x^+, rather than in x^0. In a LCOPT diagram all internal lines are on-shell, in contrast to a covariant Feynman diagram. A covariant Feynman diagram is comprised of one or more LCOPT diagrams.

In LCOPT the jet shown in Fig. 2.3 b) at a specific cut (C) can be written schematically as a sum over x^+-orderings T of its vertices:

$$J^{(C)} = \sum_T I'_T\left(k_l^\alpha\right)^* \otimes F_T^{(C)}\left(k_l^\alpha\right) \otimes I_T\left(k_l^\alpha\right). \tag{2.38}$$

The factor I_T collects all initial state interactions to the left of the cut, ${I'_T}^*$ contains all initial state interactions to the right of the cut, and $F_T^{(C)}$ collects all final state interactions consistent with cut (C). The functions are linked by soft gluons $\{k_l^\alpha\}$, as indicated by the symbol $\otimes$. Following the rules in Appendix B.3, the factors $I_T, {I'_T}^*$ and $F_T^{(C)}$ are given by

$$I_T\left(k_l^\alpha\right) = \prod_{\text{states } \xi<H}\left[\sum_{\text{vertices } l<\xi}\left(k_l^- + i\epsilon\right) - \sum_{\text{lines } j\in\xi}\frac{q_{j,\perp}^2}{2q_j^+}\right]^{-1}, \tag{2.39}$$

$$I'_T\left(k_l^\alpha\right)^* = \prod_{\text{states } H'<\xi}\left[-\sum_{\text{vertices } \xi<l}\left(k_l^- + i\epsilon\right) - \sum_{\text{lines } j\in\xi}\frac{q_{j,\perp}^2}{2q_j^+}\right]^{-1}, \tag{2.40}$$

$$\begin{aligned} F_T^{(C)}\left(k_l^\alpha\right) = {} & \int_{-\infty}^{\infty}\frac{dp_J^-}{2\pi}\prod_{\text{states } C<\xi<H'}\left[-p_J^- + \sum_{\text{vertices } l<\xi}\left(k_l^- - i\epsilon\right) - \sum_{\text{lines } j\in\xi}\frac{q_{j,\perp}^2}{2q_j^+}\right]^{-1} \\ & \times 2\pi\delta\left(-p_J^- + \sum_{\text{vertices } l<C}k_l^- - \sum_{\text{lines } j\in\xi}\frac{q_{j,\perp}^2}{2q_j^+}\right) \\ & \times \prod_{\text{states } H<\xi<C}\left[-p_J^- + \sum_{\text{vertices } l<\xi}\left(k_l^- + i\epsilon\right) - \sum_{\text{lines } j\in\xi}\frac{q_{j,\perp}^2}{2q_j^+}\right]^{-1} \end{aligned} \tag{2.41}$$

The vertices and lines are ordered with respect to x^+. p_J^- is the minus momentum leaving the jet J at the hard vertex H, and $p_J^- - \sum k_l^-$ flows back into the vertex at H'. Eqs. (2.39)-(2.41) exhibit the same pinching of poles as the simple example, Eq. (2.37).

For a given x^+-ordering of vertices we can sum over all cuts (C), if the remainder of the factorized cross section (that is, the other jet or jets) is independent of the choice of which of the vertices where soft gluons join the jet J are to the left or to the right of the cut (C). Let us assume this independence for the moment. Then the cancellation of final state interactions, $F_T^{(C)}$, is a matter of straightforward application of the unitarity relation:

$$\sum_{c=1}^{N} \left\{ \prod_{n=c+1}^{N} \frac{1}{-p_J^- - D_n - i\epsilon}\, 2\pi\, \delta\left(-p_J^- - D_c\right) \prod_{n=1}^{c-1} \frac{1}{-p_J^- - D_n + i\epsilon} \right\} = i \prod_{n=1}^{N} \frac{1}{-p_J^- - D_n + i\epsilon} - i \prod_{n=1}^{N} \frac{1}{-p_J^- - D_n - i\epsilon}, \quad (2.42)$$

and the fact that the p_J^- integral vanishes for any $N > 1$. Applying Eq. (2.42) to (2.38), we obtain

$$\sum_C J^{(C)} = \sum_C \sum_T I'_T\left(k_l^\alpha\right)^* \otimes I_T\left(k_l^\alpha\right), \quad (2.43)$$

where now only initial states are kept.

Thus the Glauber/Coulomb pinches disappear, and the soft approximation is applicable. Two subtleties remain to be discussed for a complete proof: why the remainder of the graph is independent of the choice of which of the soft gluon fields are to the left or to the right of the final state cut, and why all transverse components of soft momenta can safely be neglected in Eq. (2.43).

The independence of the remainder of the graph of soft gluon arrangements can be proven in exactly the same way as the above cancellation of Glauber/Coulomb pinches, by using LCOPT in the form (2.38) for the remainder, and applying (2.42). Details can be found in [52].

The neglect of transverse components may not seem obvious from the LCOPT-forms (2.39) and (2.40), since it can happen that $\sum_l k_l^- = 0$, that is, no minus-momentum flows into a specific set of vertices. As stated above, the sum of all LCOPT-expressions of a given graph and performing all internal minus-integrals of this graph give equivalent expressions, however, the two forms differ by partial fraction manipulations. In the latter form these apparent divergences as $\sum_j q_{j,\perp}^2 \to 0$ when $\sum_l k_l^- = 0$, are absent. Therefore, the transverse components can be neglected, and our overview of the proof of cancellation of Glauber/Coulomb pinches is complete. For further information and a nontrivial example we refer to Refs. [52, 55].

2.2.3 Summary

We have succeeded in identifying and disentangling the regions in momentum space that give leading contributions by means of power counting and application of Ward identities. This results in a product of hard scattering, jet, and soft functions. These functions, although separated in momentum space by a factorization scale, are still at least additionally linked by eikonal lines. The eikonal lines replace in each of the functions the momenta of the partons that do not give leading contributions to the particular region. In most cases, we can construct operators for each of the functions which reproduce exactly their leading behavior. Examples will be given below.

The above arguments are valid at arbitrary orders in the perturbative expansion. In Refs. [45, 59] a recursive algorithm, the so-called "tulip-garden formalism", was developed to systematically disentangle the leading contributions of any given diagram. This algorithm is similar to Zimmermann's forest formula for ultraviolet divergences [60]. The result of applying the tulip-garden formalism to all diagrams up to a given order in perturbative QCD is of course equivalent to the result of the approach described above. We refer the interested reader to the literature [45, 59] for further information.

We emphasize that a careful treatment of Glauber/Coulomb gluons is necessary for a complete proof of factorization in processes where two or more initial-state jets contribute to the final state.

2.3 Refactorization of Nonsinglet Partonic Splitting Functions

Let us now apply the above to determine the leading behavior of parton-in-parton distribution functions in the limit $x \to 1$, that is, in the limit that the emerging parton carries nearly all the momentum of the original parton. In the introduction, Sec. 1.1.2, we have introduced parton distribution functions (PDFs) $f_{a/A}(x)$ which describe the distribution of parton a in hadron A.

2.3.1 Definition of Parton-in-Parton Distribution Functions

Hadronic distribution functions $f_{a/A}(x)$ are incalculable within perturbation theory. However, their evolution is perturbatively calculable from the

renormalization group equation [61, 62, 63, 64]

$$\mu\frac{d}{d\mu}f_{a/A}(x,\mu)=\sum_b\int_x^1\frac{d\zeta}{\zeta}P_{ab}\left(\zeta,\alpha_s(\mu)\right)f_{b/A}\left(\frac{x}{\zeta},\mu\right), \tag{2.44}$$

where P_{ab} is the evolution kernel or splitting function, and μ denotes the factorization scale, usually taken equal to the renormalization scale. This follows from the factorization assumption, Eq. (1.7), which enables us to write a large class of physical cross sections as convolutions of these PDFs with perturbatively calculable short-distance functions. Eq. (2.44) follows from the independence of the physical cross section of the factorization scale μ, as seen in Eq. (1.19). Similar considerations apply to partonic cross sections. There the parton-in-parton distribution functions f_{f_i/f_j} describe the probability of finding parton f_i in parton f_j. The evolutionary behavior of the partonic PDFs obeys the same equation, (2.44), as for the hadronic PDFs. Thus the splitting functions can be computed in perturbation theory.

Up to non-leading corrections which vanish as $x\to 1$ we can neglect flavor mixing, that is, we deal with non-singlet distributions:

$$f_{NS}^{\pm}=f_{q_a/q}^{\pm}-f_{q_b/q}^{\pm},\quad f_{q_i/q}^{\pm}=f_{q_i/q}\pm f_{\bar{q}_i/q}. \tag{2.45}$$

Factorization allows us to define PDFs in terms of nonlocal operators. At leading power one can define [2, 65] the following function[3]

$$\begin{aligned} f_{q_i/q}(x) &= \frac{1}{4\pi}\int dy^- e^{-ixp^+y^-}\left\langle p\left|\bar{\psi}_i(0,y^-,0_\perp)\gamma^+\right.\right. \\ &\qquad\qquad \left.\left.\times\ Pe^{ig_s\int_0^{y^-}dz^-\mathcal{A}^{(q)+}(0,z^-,0_\perp)}\psi_i(0)\right|p\right\rangle \\ &= \frac{1}{4\pi}\int dy^- e^{-ixp^+y^-}\sum_n\left\langle p\left|\bar{\Psi}_i(0,y^-,0_\perp)\right|n\right\rangle\gamma^+\left\langle n\left|\Psi_i(0)\right|p\right\rangle, \end{aligned} \tag{2.46}$$

which describes the distribution of a quark q_i, created by the operator $\bar{\psi}_i$, in a quark q with momentum p. We use light-cone coordinates where our conventions are as in (B.29). The operators are separated by a light-like distance, and are joined with a path-ordered exponential, denoted by P, to achieve

[3]Recently there has been some discussion about the correct behavior of transverse-momentum dependent PDFs in some noncovariant gauges [66, 67]. This question does not arise in this thesis since we will work in Feynman gauge and consider only distribution functions where all transverse-momentum dependence has been integrated out.

gauge-invariance. This exponential describes the emission of arbitrarily many gluons of polarization in the plus-direction. $\mathcal{A}^{(q)}$ is the vector potential in the fundamental representation. In the second line we have inserted a complete set of states, have used the identity

$$Pe^{ig_s\int_0^\eta d\xi\beta\cdot\mathcal{A}(\xi n^\mu)} = \left[Pe^{ig_s\int_0^\infty d\xi\beta\cdot\mathcal{A}((\xi+\eta)\beta^\mu)}\right]^\dagger \left[Pe^{ig_s\int_0^\infty d\xi\beta\cdot\mathcal{A}(\xi\beta^\mu)}\right], \qquad (2.47)$$

and have defined

$$\Psi_i(y) = Pe^{ig_s\int_0^\infty d\xi\beta\cdot\mathcal{A}(y+\xi\beta^\mu)}\psi_i(y), \qquad (2.48)$$

with the light-like vector β^μ chosen in the minus-direction, $\beta^+ = \beta_\perp = 0$. As we have seen in the previous section, the occurrence of the path-ordered exponential follows from the factorization of unphysical gluons from the physical, short-distance, cross section. Gluon parton distribution functions can be constructed analogously [2, 65], with the vector potentials in the adjoint representation, and appropriate operators for the creation of gluons.

In the following we will be interested in the limit $x \to 1$, since there large logarithmic corrections arise due to soft-gluon radiation. We will show below that the factorized form of a perturbative non-singlet parton-in-parton distribution function contains a cross section built out only of eikonal lines that absorbs all collinear and infrared singular behavior as $x \to 1$. An equivalent observation was made by Korchemsky [68], who related the flavor-diagonal splitting function P_{ff} to the cusp anomalous dimension of a Wilson loop.

2.3.2 Power Counting as $x \to 1$

We start with the definition Eq. (2.46) of a perturbative parton-in-parton distribution function, which is shown in Fig. 2.5 a) in cut-diagram notation. We pick the incoming momentum to flow in the plus direction,

$$p^\mu = (p^+, 0, 0_\perp). \qquad (2.49)$$

Because the minus and transverse momenta in (2.46) are integrated over, they can flow freely through the eikonal line, whereas no plus momentum flows across the cut in the eikonal line.

The regions that can give leading contributions are shown in Fig. 2.5 b) in form of a reduced diagram, following the discussion in Sec. 2.1.1. We can have a jet J_p collinear to the incoming momentum p^+, as well as an arbitrary number of jets J_i emerging from the hard scattering. Furthermore, we can have momenta collinear to the eikonal moving in the minus direction, β^-, represented by J_β in the figure. The jets can be connected by arbitrarily many

soft gluons, S. Here and below, unless explicitly stated otherwise, we use the term "soft" for both soft and Glauber momenta.

A further simplification of the leading behavior occurs when we perform the limit to $x \to 1$, in which we are interested here. Jet lines having a finite amount of plus momentum in the final state become soft, and only virtual contributions can have large plus momenta. This does not affect the jet collinear to the eikonal, since it is moving in the minus direction. Thus we arrive at the leading regions depicted in Fig. 2.5 c), with hard scatterings H_L and H_R, which are the only vertices where finite amounts of momentum can be transferred, virtual jets $J_{p,\,L}$ and $J_{p,\,R}$ collinear to the incoming momentum p^+, a jet J_β collinear to the eikonal β^-, connected via soft momenta, S. Here and below the subscripts L and R, respectively, indicate that the momenta and functions are purely virtual, located to the left or to the right of the cut.

Let us now determine the degree of infrared divergence $\omega(f)$ of Fig. 2.5 c) using the tools developed in Sec. 2.1.2. The degree of divergence of the various regions is additive,

$$\omega(f) = \omega_{J_{p,\,L}} + \omega_{J_{p,\,R}} + \omega_{J_\beta} + \omega_S. \tag{2.50}$$

The degree of divergence of the soft function is given by

$$\omega_S = 4(E^b + E^f - 1) - 2E^b - E^f + \omega'_S, \tag{2.51}$$

where ω'_S denotes the degree of divergence of the internal part of the soft function only, without the lines attaching to the jets, which are denoted by E^b and E^f, for bosonic and fermionic lines, respectively. The first term in Eq. (2.51) comes from $E-1$ loop integrations over these attachments, the second and third term stem from the denominators of these loops. ω'_S is found from Eqs. (2.19) with (2.22), (2.25), and (2.26):

$$\omega'_S = 4 - E^b - \frac{3}{2}E^f. \tag{2.52}$$

Putting everything together, we arrive at

$$\omega_S = E^b + \frac{3}{2}E^f. \tag{2.53}$$

This result can also be obtained by simple dimensional analysis of the soft function since soft momenta have the same scaling behavior in all components.

The degree of divergences of the jet functions can be found similarly, using Eqs. (2.20), (2.23) or (2.24), (2.26), and slight modifications of (2.25) for jet $J_{p,\,L/R}$:

$$2N_{J_{p,\,L/R}} + E_{J_{p,\,L/R}} + 1 = \sum_i i v^{(i)}_{J_{p,\,L/R}} + l_{J_{p,\,L/R}} + p_{J_{p,\,L/R}}, \tag{2.54}$$

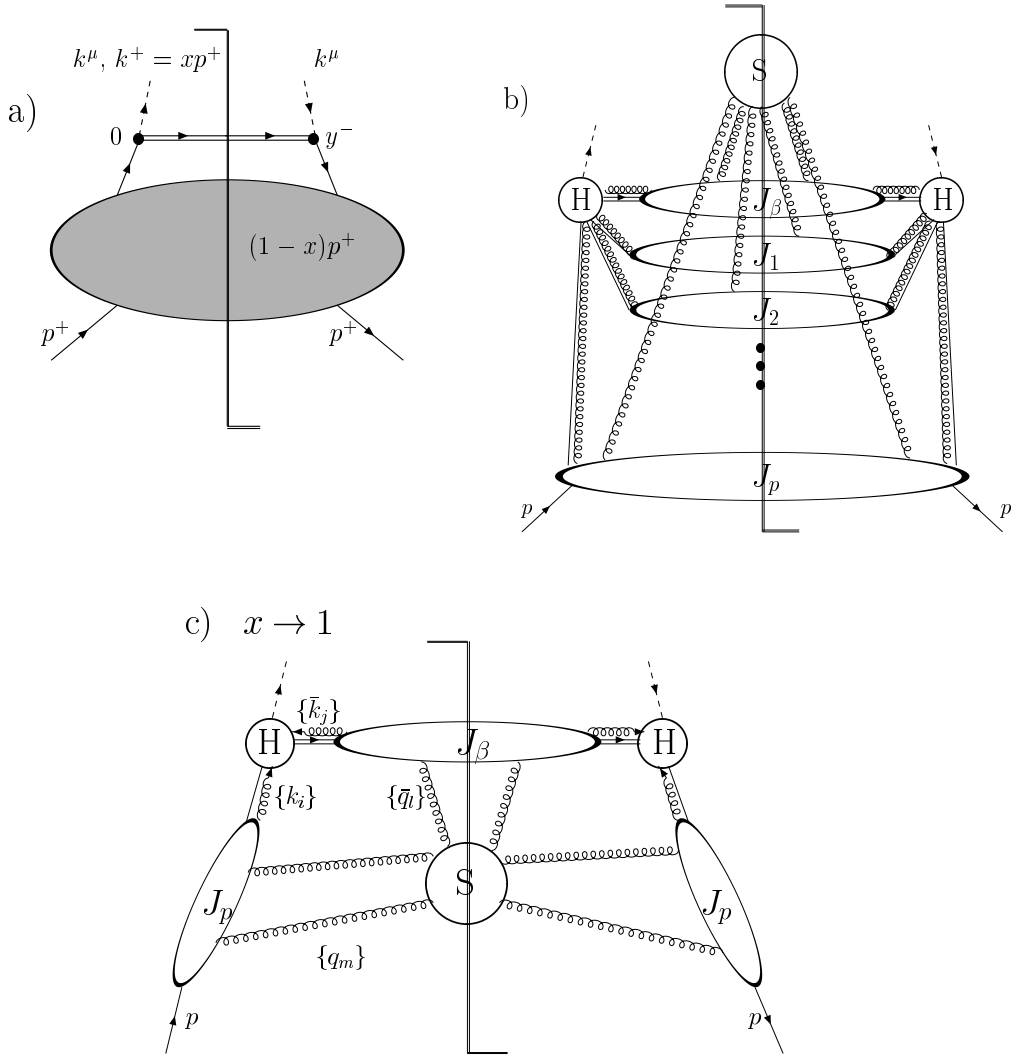

Figure 2.5: a) Graphical representation of a parton-in-parton distribution function, Eq. (2.46), and b) its factorized form for arbitrary momentum fraction x, drawn as a reduced diagram. c) The reduced diagram for the PDF in the limit $x \to 1$. Here we have suppressed the labels L and R for purely virtual contributions to the left and to the right of the cut, respectively, compared to the notation in the text. The cut represents the final state.

where the number of external lines counts only attachments to the soft function, but not to the hard scattering. These have to be added separately, where $l_{J_{p,\,L/R}}$ and $p_{J_{p,\,L/R}}$ denote scalar polarized gluons and physical lines (scalars, fermions, physically polarized gluons), respectively, which connect the jet (to the left or to the right of the cut) and the hard part. Similarly, the modifications for jet J_β result in

$$2N_{J_\beta} + E_{J_\beta} = \sum_i i v^{(i)}_{J_\beta} + l_{J_\beta} + p_{J_\beta}. \tag{2.55}$$

After a bit of algebra we find in Feynman gauge:

$$\begin{aligned}
\omega_{J_{p,\,L/R}} &\geq \frac{1}{2}\Big[-1 - E^f_{J_{p,\,L/R}} - E^b_{J_{p,\,L/R}} + p_{J_{p,\,L/R}} - s_{J_{p,\,L/R}} \\
&\quad + \left(s_{J_{p,\,L/R}} + l_{J_{p,\,L/R}} - v^{(3)}_{J_{p,\,L/R}}\right)\theta\left(s_{J_{p,\,L/R}} + l_{J_{p,\,L/R}} - v^{(3)}_{J_{p,\,L/R}}\right)\Big], \qquad (2.56)\\
\omega_{J_\beta} &\geq -2 - \frac{1}{2}E^f_{J_\beta} - \frac{1}{2}E^b_{J_\beta} + \frac{1}{2}p_{J_\beta} - \frac{1}{2}s_{J_\beta} \\
&\quad + \left(s_{J_\beta} + l_{J_\beta} - v^{(3)}_{J_\beta}\right)\theta\left(s_{J_\beta} + l_{J_\beta} - v^{(3)}_{J_\beta}\right). \qquad (2.57)
\end{aligned}$$

Adding Eqs. (2.53), (2.56), and (2.57), we arrive at

$$\begin{aligned}
\omega(f) \;\geq\; & \Big\{\frac{1}{2}\left(E^b_{J_{p,\,L}} + E^b_{J_{p,\,R}}\right) + E^f_{J_{p,\,L}} + E^f_{J_{p,\,R}} \\
& + \frac{1}{2}\left(p_{J_{p,\,L}} + p_{J_{p,\,R}} - s_{J_{p,\,L}} - s_{J_{p,\,R}}\right) - 1 \\
& + \frac{1}{2}\Big[\left(s_{J_{p,\,L}} + l_{J_{p,\,L}} - v^{(3)}_{J_{p,\,L}}\right)\theta\left(s_{J_{p,\,L}} + l_{J_{p,\,L}} - v^{(3)}_{J_{p,\,L}}\right) \\
& \quad + \left(s_{J_{p,\,R}} + l_{J_{p,\,R}} - v^{(3)}_{J_{p,\,R}}\right)\theta\left(s_{J_{p,\,R}} + l_{J_{p,\,R}} - v^{(3)}_{J_{p,\,R}}\right)\Big]\Big\} \\
& + \Big\{E^f_{J_\beta} + \frac{1}{2}E^b_{J_\beta} - 2 + \frac{1}{2}p_{J_\beta} - \frac{1}{2}s_{J_\beta} \\
& + \left(s_{J_\beta} + l_{J_\beta} - v^{(3)}_{J_\beta}\right)\theta\left(s_{J_\beta} + l_{J_\beta} - v^{(3)}_{J_\beta}\right)\Big\}. \qquad (2.58)
\end{aligned}$$

From this lengthy expression we see that the maximum degree of divergence is

$$\omega(f) \geq -1. \tag{2.59}$$

$\omega(f) = -1$ corresponds to a divergence proportional to $1/(1-x)$.

To get this maximum degree of IR divergence the following conditions have to be fulfilled (compare to Fig. 2.5 c)):

- No soft vectors directly attach H_L or H_R with S.

- The jets and the soft part can only be connected through soft gluons, denoted by the sets $\{q_{L,\,m_L}\}$, $\{q_{R,\,m_R}\}$, and $\{\bar{q}_l\}$.

- Arbitrarily many scalar-polarized gluons, $\{k_{L,\,i_L}\}$, $\{k_{R,\,i_R}\}$, $\{\bar{k}_{L,\,j_L}\}$ and $\{\bar{k}_{R,\,j_R}\}$, attach the jets with H_L and H_R, respectively. The barred momenta are associated with J_β, the unbarred with the J_p's.

- Exactly one scalar, fermion, or physically polarized gluon with momentum $k_L^\mu - \sum\limits_{i_L} k_{L,\,i_L}^\mu$, $k_R^\mu - \sum\limits_{i_R} k_{R,\,i_R}^\mu$, $\bar{k}_L^\mu - \sum\limits_{j_L} \bar{k}_{L,\,j_L}^\mu$ or $\bar{k}_R^\mu - \sum\limits_{j_R} \bar{k}_{R,\,j_R}^\mu$, respectively, connects each of the jets with the hard parts. The momenta $k_L^{\nu_L}$ ($k_R^{\nu_R}$) and $\bar{k}_L^{\rho_L}$ ($\bar{k}_R^{\rho_R}$) denote the *total* momenta flowing into H_L (H_R) from $J_{p,\,L}$ ($J_{p,\,R}$) and J_β, respectively, that is, they are the sum of the scalar, fermion or physically polarized gluon momenta, and the scalar-polarized gluon momenta.

  In an individual diagram we can have only scalar-polarized gluons connecting the jets with the hard parts, and no scalar, fermion or physically polarized gluon. However, the sum of these configurations vanishes after application of the Ward identity shown in Fig. 2.2 a).

- The number of soft and scalar-polarized vector lines emerging from a particular jet is less or equal to the number of 3-point vertices in that jet.

In summary, we have found that the regions in momentum space which give leading contributions may in Feynman gauge be represented as:

$$
\begin{aligned}
f_f^{x\to 1}(x) = \sum_{C_\beta, C_S} & \int \frac{d^n k_L}{(2\pi)^n} \int \frac{d^n k_R}{(2\pi)^n} \int \frac{d^n \bar{k}_L}{(2\pi)^n} \int \frac{d^n \bar{k}_R}{(2\pi)^n} \\
& \prod_{i_L, i_R, j_L, j_R} \int \frac{d^n k_{L,\,i_L}}{(2\pi)^n} \frac{d^n k_{R,\,i_R}}{(2\pi)^n} \frac{d^n \bar{k}_{L,\,j_L}}{(2\pi)^n} \frac{d^n \bar{k}_{R,\,j_R}}{(2\pi)^n} \\
& \prod_{m_L, m_R, l} \int \frac{d^n q_{L,\,m_L}}{(2\pi)^n} \frac{d^n q_{R,\,m_R}}{(2\pi)^n} \frac{d^n \bar{q}_l}{(2\pi)^n} \; S^{(C_S)}\left(\{q_{L,\,m_L}^{\gamma_{k_L}}\}; \{q_{R,\,m_R}^{\gamma_{k_R}}\}; \{\bar{q}_l^{\delta_l}\}\right) \\
& \times H_L\left(k_L^{\nu_L}, \{k_{L,\,i_L}^{\alpha_{i_L}}\}; \bar{k}_L^{\rho_L}, \{\bar{k}_{L,\,j_L}^{\eta_{j_L}}\}\right) \; H_R\left(k_R^{\nu_R}, \{k_{R,\,i_R}^{\alpha_{i_R}}\}; \bar{k}_R^{\rho_R}, \{\bar{k}_{R,\,j_R}^{\eta_{j_R}}\}\right) \\
& \times J_{p,\,L}\left(k_L^{\nu_L}, \{k_{L,\,i_L}^{\alpha_{i_L}}\}; \{q_{L,\,m_L}^{\gamma_{m_L}}\}\right) \; J_{p,\,R}\left(k_R^{\nu_R}, \{k_{R,\,i_R}^{\alpha_{i_R}}\}; \{q_{R,\,m_R}^{\gamma_{m_R}}\}\right) \\
& \times J_\beta^{(C_\beta)}\left(\bar{k}_L^{\rho_L}, \{\bar{k}_{L,\,j_L}^{\eta_{j_L}}\}; \bar{k}_R^{\rho_R}, \{\bar{k}_{R,\,j_R}^{\eta_{j_R}}\}; \{\bar{q}_l^{\delta_l}\}\right) \\
& \times \delta^n\left(\sum_{m_L} q_{L,\,m_L}^\mu + \sum_{m_R} q_{R,\,m_R}^\mu + \sum_l \bar{q}_l^\mu\right) \; \delta^n\left(k_L^\mu + \bar{k}_L^\mu - x p^\mu\right)
\end{aligned}
$$

$$\times\, \delta^n\left(k_R^\tau + \bar{k}_R^\tau - x p^\tau\right)$$
$$\times\, \delta^n\left(k_L^\mu - \sum_{m_L} q_{L,\,m_L}^\mu - p^\mu\right)\; \delta^n\left(k_R^\tau - \sum_{m_R} q_{R,\,m_R}^\tau - p^\tau\right)\,. \qquad (2.60)$$

The sum in Eq. (2.60) runs over all cuts of jet J_β, C_β, and of the soft function S, C_S, which are consistent with the constraints from the delta-functions due to momentum conservation. The functions in (2.60) are still connected with each other by scalar polarized or soft gluons. This obscures the independent evolution of the functions. In the next subsection we will show how to simplify this result.

2.3.3 Refactorization

We will show here that the scalar polarized gluons decouple via the help of the Ward identity, Fig. 2.2 c), and that we can disentangle the jets and the soft part, which are connected by soft gluon exchanges, via the soft approximation as described in Sec. 2.2. In the following we will work in Feynman gauge throughout.

Decoupling of the Hard Part

Starting from Eq. (2.60), we use the fact that the leading contributions come from regions where the gluons carrying momenta $\{k_{L,\,i_L}\}$, $\{k_{R,\,i_R}\}$, $\{\bar{k}_{L,\,j_L}\}$ and $\{\bar{k}_{R,\,j_R}\}$ are scalar polarized. Thus H_L, H_R, $J_{p,\,L}$, $J_{p,\,R}$, and J_β have the following structure:

$$H_L \;=\; \left(\prod_{i_L} \xi^{\nu_{i_L}}\right)\left(\prod_{j_L} \beta^{\rho_{j_L}}\right)$$
$$\times\, H_{L,\,\{\nu_{i_L}\},\{\rho_{j_L}\}}\left(k_L^+\;\xi^{\nu_L}, \left\{k_{L,\,i_L}^+ \xi^{\alpha_{i_L}}\right\}; \bar{k}_L^-\;\beta^{\rho_L}, \{\bar{k}_{L,\,i_L}^- \beta^{\eta_{j_L}}\}\right), \qquad (2.61)$$

$$J_{p,\,L} \;=\; \left(\prod_{i_L} \beta^{\nu_{i_L}}\right) J_{p,\,L\,\{\nu_{i_L}\}}\left(k_L^{\nu_L}, \{k_{L,\,i_L}^{\alpha_{i_L}}\}; \{q_{L,\,k_L}^{\gamma_{m_L}}\}\right); \qquad (2.62)$$

$$J_\beta \;=\; \left(\prod_{j_L} \xi^{\rho_{j_L}}\right)\left(\prod_{j_R} \xi^{\rho_{j_R}}\right)$$
$$\times\, J_{\beta\,\{\rho_{j_L}\},\,\{\rho_{j_R}\}}\left(\bar{k}_L^{\rho_L}, \{\bar{k}_{L,\,j_L}^{\eta_{j_L}}\}; \bar{k}_R^{\rho_R}, \{\bar{k}_{R,\,j_R}^{\eta_{j_R}}\}; \{\bar{q}_l^{\delta_l}\}\right), \qquad (2.63)$$

where, as above, for the functions to the right of the cut, we replace the subscripts L with R. In these relations the vectors

$$\xi^\mu \;=\; \delta_+^\mu\,,$$

$$\beta^\mu \;=\; \delta^\mu_- \tag{2.64}$$

are the light-like vectors parallel to p^μ and parallel to the direction of the eikonal, respectively.

We now use the identity depicted in Fig. 2.2 c) as described above for all scalar polarized gluons in the sets $\{k_{L,\,i_L}\}$, $\{k_{R,\,i_R}\}$, $\{\bar{k}_{L,\,j_L}\}$ and $\{\bar{k}_{R,\,j_R}\}$, to decouple the jet functions from the hard function. This decoupling occurs in Feynman gauge only after summation over the full gauge-invariant set of graphs which contribute to the reduced diagram Fig. 2.5 c). The result is shown in Fig. 2.6. The products over the vectors β and ξ are replaced by eikonal factors $\mathcal{E}$, which we can group with the jets. Furthermore, the hard scatterings, by definition far off-shell, become independent of x up to corrections which vanish for $x \to 1$. Eq. (2.60) then becomes

$$\begin{aligned}
f_f^{x\to 1}\,(x) \;=\; & H_L(p,\mu;\beta,\xi)\; H_R(p,\mu;\beta,\xi) \sum_{C_\beta, C_S} \prod_{m_L, m_R, l} \int \frac{d^n q_{L,\,m_L}}{(2\pi)^n} \frac{d^n q_{R,\,m_R}}{(2\pi)^n} \frac{d^n \bar{q}_l}{(2\pi)^n} \\
& \times \quad \tilde{J}_{p,\,L}(p,\mu;\beta;\{q_{L,\,m_L}^{\gamma_{m_L}}\})\; \tilde{J}_{p,\,R}(p,\mu;\beta;\{q_{R,\,m_R}^{\gamma_{m_R}}\}) \\
& \times \quad \int dy \int dz\; S^{(C_S)}\left(yp,\mu;\{q_{L,\,m_L}^{\gamma_{m_L}}\};\{q_{R,\,m_R}^{\gamma_{m_R}}\};\{\bar{q}_l^{\delta_l}\}\right) \\
& \qquad \times\; \tilde{J}_\beta^{(C_\beta)}(zp,\mu;\xi;\{\bar{q}_l^{\delta_l}\}) \\
& \times \quad \delta^n\left(\sum_{m_L} q^\mu_{L,\,m_L} + \sum_{m_R} q^\mu_{R,\,m_R} + \sum_l \bar{q}^\mu_l\right)\; \delta(1-x-y-z)\;, \qquad (2.65)
\end{aligned}$$

where μ denotes the renormalization scale, which we set equal to the factorization scale, for simplicity. Corrections are subleading by a power of $1-x$. We define the functions $\tilde{J}_{p,\,L}$, $\tilde{J}_{p,\,R}$, and $\tilde{J}_\beta$ as follows:

$$\begin{aligned}
\tilde{J}_{p,\,L} \;=\; & \int \frac{d^n k_L}{(2\pi)^n} \prod_{i_L} \int \frac{d^n k_{L,\,i_L}}{(2\pi)^n}\; \mathcal{E}\left(\beta,\{k^+_{L,\,i_L}\}\right)^{\{\nu_{i_L}\}} \\
& \times\; J_{p,\,L\,\{\nu_{i_L}\}}\left(k_L^{\nu_L},\{k_{L,\,i_L}^{\alpha_{i_L}}\};\{q_{L,\,k_L}^{\gamma_{m_L}}\}\right)\; \delta^n\left(k_L^\mu - \sum_{m_K} q^\mu_{L,\,m_L} - p^\mu\right), \qquad (2.66) \\
\tilde{J}_\beta^{(C_\beta)} \;=\; & \int \frac{d^n \bar{k}_L}{(2\pi)^n} \int \frac{d^n \bar{k}_R}{(2\pi)^n} \prod_{j_L, j_R} \int \frac{d^n \bar{k}_{L,\,j_L}}{(2\pi)^n} \frac{d^n \bar{k}_{R,\,j_R}}{(2\pi)^n} \\
& \times\; \mathcal{E}\left(\xi,\{\bar{k}^-_{L,\,j_L}\}\right)^{\{\rho_{j_L}\}}\; \mathcal{E}^*\left(\xi,\{\bar{k}^-_{R,\,j_R}\}\right)^{\{\rho_{j_R}\}} \\
& \times\; J^{(C_\beta)}_{\beta\,\{\rho_{j_L}\},\{\rho_{j_R}\}}\left(zp;\bar{k}_L^{\rho_L},\{\bar{k}_{L,\,j_L}^{\eta_{j_L}}\};\bar{k}_R^{\rho_R},\{\bar{k}_{R,\,j_R}^{\eta_{j_R}}\};\{\bar{q}_l^{\delta_l}\}\right)\;, \qquad (2.67)
\end{aligned}$$

and $\tilde{J}_{p,\,R}$ is defined analogously to $\tilde{J}_{p,\,L}$, with the subscripts L replaced by R, and with a complex conjugate eikonal line, since it is to the right of the cut.

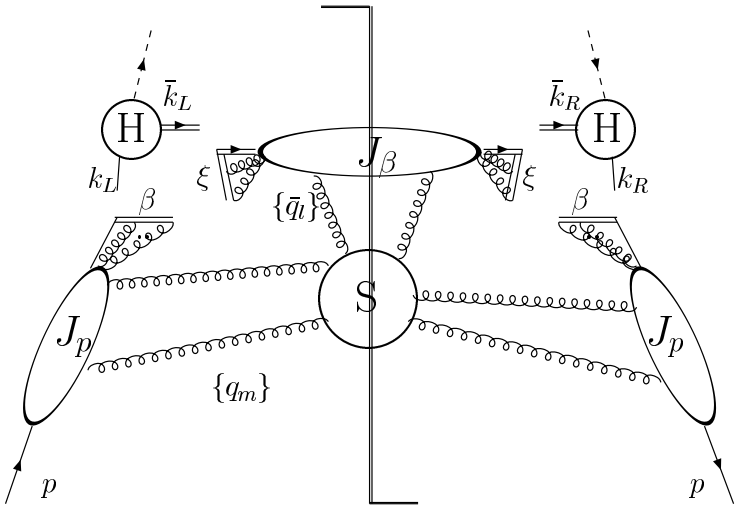

Figure 2.6: Parton distribution function for $x \to 1$ with the jet functions factorized from the hard part, graphical representation of Eq. (2.65).

In (2.65) the total plus momentum flowing across the cut is restricted to be $(1-x)p^+$, and flows through the soft function and/or the eikonal jet. The plus momenta flowing across the cuts C_S and C_β, denoted by yp^+ and zp^+, respectively, are therefore restricted to be $(1-x)p^+$ via the delta-function in Eq. (2.65). Above we have factorized the hard part from the remaining functions, which are still linked via soft momenta.

Fully Factorized Form

Here we will use the soft approximation to factorize the jets J_p from the soft function, which, by power counting, are connected only through soft gluons. We could factorize the eikonal jet J_β from S in an analogous way, but we choose not to do so here because eventually we will combine all soft and eikonal functions to form an eikonal cross section. From the arguments given in Sec. 2.2.2, we see that in our case Glauber gluons do not pose a problem, since there is only one initial-state jet, which in addition, does not proceed into the final state due to the restriction that $x \to 1$.

The application of the soft approximation is therefore straightforward, and we arrive arrive at the factorized form of the parton distribution function

as $x \to 1$:

$$\begin{aligned} f_f^{x\to 1}(x) &= H_L(p,\mu;\beta,\xi)\, H_R(p,\mu;\beta,\xi)\bar{J}_{p,\,L}(p,\mu;\beta;\xi)\, \bar{J}_{p,\,R}(p,\mu;\beta;\xi) \\ &\times \sum_{C_\beta,C_S} \prod_{m_L,m_R,l} \int \frac{d^n q_{L,\,m_L}}{(2\pi)^n} \frac{d^n q_{R,\,m_R}}{(2\pi)^n} \frac{d^n \bar{q}_l}{(2\pi)^n} \\ &\times \mathcal{E}\left(\xi, \{q^-_{L,\,m_L}\}\right)^{\{\gamma_{m_L}\}} \mathcal{E}^*\left(\xi, \{q^-_{R,\,m_R}\}\right)^{\{\gamma_{m_R}\}} \\ &\times \int dy \int dz\; S^{(C_S)}\left(yp,\mu;\{q^{\gamma_{m_L}}_{L,\,m_L}\};\{q^{\gamma_{m_R}}_{R,\,m_R}\};\{\bar{q}_l^{\delta_l}\}\right) \\ &\times \tilde{J}_\beta^{(C_\beta)}(zp,\mu;\xi;\{\bar{q}_l^{\delta_l}\}) \\ &\times \delta^n\left(\sum_{m_L} q^\mu_{L,\,m_L} + \sum_{m_R} q^\mu_{R,\,m_R} + \sum_l \bar{q}^\mu_l\right)\, \delta(1-x-y-z)\;, \end{aligned} \tag{2.68}$$

where we have grouped the eikonal factors stemming from the soft approximation with the soft function and the eikonal jet. We define

$$\tilde{J}_{p,\,L}(p,\mu;\beta;\{q^{\gamma_{m_L}}_{L,\,m_L}\}) = \mathcal{E}\left(\xi,\{q^-_{L,\,m_L}\}\right)^{\{\gamma_{m_L}\}}\; \bar{J}_{p,\,L}(p,\mu;\beta;\xi), \tag{2.69}$$

and analogously for the jet to the right of the cut, $J_{p,\,R}$, with a complex conjugate eikonal.

Fully Factorized Form with an Eikonal Cross Section

Although in Eq. (2.68) the various functions are clearly separated in their momentum dependence, the parton distribution function is not quite in the desired form yet. We want to write the PDF in terms of a color singlet eikonal cross section, built from ordered exponentials:

$$\begin{aligned} \sigma^{(\mathrm{eik})}_{aa}\left(\frac{(1-x)p^+}{\mu},\alpha_s(\mu),\varepsilon\right) &= \frac{p^+}{\mathrm{Tr}\;\mathbf{1}} \int \frac{dy^-}{2\pi} e^{i(1-x)p^+y^-} \\ &\times \mathrm{Tr}\;\left\langle 0\left|\bar{\mathrm{T}}\left[\mathcal{W}^{(aa)}(0,y^-,0_\perp)^\dagger\right]\;\mathrm{T}\left[\mathcal{W}^{(aa)}(0)\right]\right|0\right\rangle, \end{aligned} \tag{2.70}$$

where the product of two non-Abelian phase operators (Wilson lines) in the representation a, for quarks, is defined as follows:

$$\mathcal{W}^{(aa)}(x) = \Phi^{(a)}_\beta(\infty,0;x)\;\Phi^{(a)}_\xi(0,-\infty;x), \tag{2.71}$$

$$\Phi^{(f)}_\beta(\lambda_2,\lambda_1;x) = P e^{-ig\int_{\lambda_1}^{\lambda_2} d\lambda\beta\cdot\mathcal{A}^{(f)}(\lambda\beta+x)}, \tag{2.72}$$

where the light-like velocities ξ and β are defined in (2.64), and where $\mathcal{A}^{(f)}$ is the vector potential in the representation of a parton with flavor f. The trace

in (2.70) is over color indices. The lowest order of the eikonal cross section is normalized to $\delta(1-x)$. This eikonal cross section has ultraviolet divergences which have to be renormalized, as indicated by the renormalization scale μ. Furthermore, the delta-function for the soft momenta in Eq. (2.68) constrains the momentum of the final state in $\sigma^{(\mathrm{eik})}$ to be $(1-x)p^+$.

We can factorize the eikonal cross section (2.70) in a manner analogous to the full parton distribution function, and obtain

$$\begin{aligned}
\sigma_{aa}^{(\mathrm{eik})}(1-x) &= \sum_{C_\beta, C_S} \prod_{m_L, m_R, l} \int \frac{d^n q_{L,\,m_L}}{(2\pi)^n} \frac{d^n q_{R,\,m_R}}{(2\pi)^n} \frac{d^n \bar{q}_l}{(2\pi)^n} \\
&\times \quad \tilde{J}_{p,\,L}^{(\mathrm{eik})}(\xi, \mu; \beta; \{q_{L,\,m_L}^{\gamma_{m_L}}\})\ \tilde{J}_{p,\,R}^{(\mathrm{eik})}(\xi, \mu; \beta; \{q_{R,\,m_R}^{\gamma_{m_R}}\}) \\
&\times \quad \int dy \int dz\ S^{(C_S)}\left(yp, \mu; \{q_{L,\,m_L}^{\gamma_{m_L}}\}; \{q_{R,\,m_R}^{\gamma_{m_R}}\}; \{\bar{q}_l^{\delta_l}\}\right) \\
&\times \quad \tilde{J}_{\beta}^{(C_\beta)}(zp, \mu; \xi; \{\bar{q}_l^{\delta_l}\}) \\
&\times \quad \delta^n\left(\sum_{m_L} q_{L,\,m_L}^{\mu} + \sum_{m_R} q_{R,\,m_R}^{\mu} + \sum_{l} \bar{q}_l^{\mu}\right)\ \delta(1-x-y-z).
\end{aligned} \tag{2.73}$$

The eikonal jets $\tilde{J}_{p,\,L}^{(\mathrm{eik})}$, $\tilde{J}_{p,\,R}^{(\mathrm{eik})}$ moving collinear to the momentum p, are defined analogously to Eq. (2.66), with the fermion line carrying momentum p replaced by an eikonal line in representation a with velocity β. We can define analogous to Eq. (2.69)

$$\tilde{J}_{p,\,L}^{(\mathrm{eik})}(\xi, \mu; \beta; \{q_{L,\,m_L}^{\gamma_{m_L}}\}) = \mathcal{E}\left(\xi, \{q_{L,\,m_L}^{-}\}\right)^{\{\gamma_{m_L}\}}\ \bar{J}_{p,\,L}^{(\mathrm{eik})}(\mu; \beta; \xi), \tag{2.74}$$

and similarly for the jet to the right of the cut, $J_{p,\,R}^{(\mathrm{eik})}$, with a complex conjugate eikonal. In the following we suppress the index a for better readability.

Combining Eqs. (2.68), (2.73), and (2.74), we arrive at the final form of the factorized parton distribution function, shown in Fig. 2.7,

$$f_f^{x\to 1}(x) = H_L(p,\mu)\ H_R(p,\mu)\ J_{p,\,L}^R(p,\mu)\ J_{p,\,R}^R(p,\mu)\ \sigma^{(\mathrm{eik})}((1-x)p,\mu)\,, \tag{2.75}$$

suppressing the dependence on the lightlike vectors (2.64). The purely virtual jet-remainders are defined by

$$J_{p,\,L}^R(p,\mu) = \frac{\bar{J}_{p,\,L}(p,\mu;\beta;\xi)}{\bar{J}_{p,\,L}^{(\mathrm{eik})}(\mu;\beta;\xi)}\,. \tag{2.76}$$

In Chapter 3 we will show that the eikonal cross section exponentiates, where the resulting exponent can be given a simple, recursive definition. We

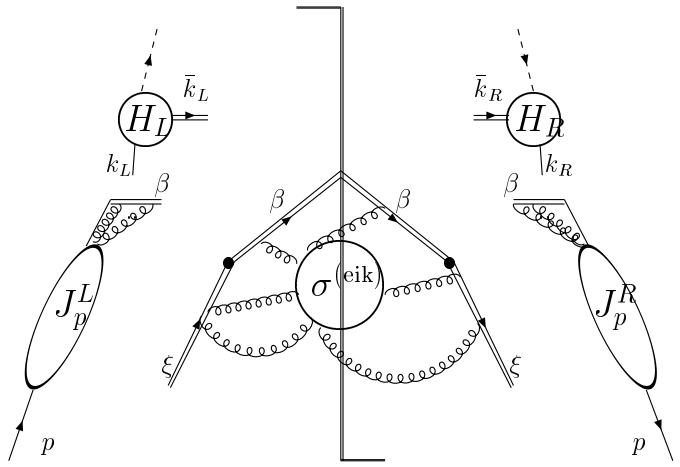

Figure 2.7: Parton distribution function for $x \to 1$, factorized into hard scatterings, an eikonal cross section, and purely virtual jet-remainders, as derived in Eq. (2.75). The virtual jet functions are normalized by their eikonal analogs, as in Eq. (2.76).

will use this exponentiation in Chapter 4 to study the renormalization properties of eikonal cross sections. These studies lead to a powerful method for the calculation of the singular contribution to the splitting functions as introduced in Eq. (2.44). We will illustrate this method with the calculation of the fermionic contribution proportional to $1/(1-x)$ at three loops.

Let us now turn to the second topic of this thesis, resummation of large logarithmic corrections to dijet event shapes. These topics are linked by the exponentiation of soft gluon radiation, as will become apparent shortly.

2.4 Factorization of the Thrust Cross Section in e^+e^- Annihilation

2.4.1 Jet Event Shapes

Jet cross sections measure the probability of producing jet-like final states, where most of the radiation is collimated. Jet cross sections are infrared safe [69]. In the following we will study the characteristics of hadronic final states

in e^+e^- annihilation more generally by weighting the final states with *shape variables* $S(p_1, \ldots, p_n)$. These shape variables are functions of the final state momenta p_i, $i = 1, \ldots, n$, and characterize the shape of an event, whether it is pencil-like, spherical, etc.. They provide information about the distribution of radiation, information which is complementary to the information obtained by computing inclusive or threshold jet cross sections. Event shapes also provide important tests of perturbative QCD. The shape of the distributions is a direct test of the QCD matrix elements, and the strong coupling α_s can be determined very precisely through the normalization of the cross sections.

A weighted cross section $d\sigma/d\mathcal{S}$ at fixed shape variable $\mathcal{S}$ is given by

$$\frac{d\sigma}{d\mathcal{S}} = \frac{1}{2Q^2} \sum_n \int\limits_{\mathrm{PS}_n} |M(p_1, \ldots, p_n)|^2 \, \delta\left(S(p_1, \ldots, p_n) - \mathcal{S}\right), \tag{2.77}$$

where Q is the center-of-mass (c.m.) energy, and M are the matrix elements integrated over the n-particle phase space PS_n available for radiation to the momenta p_i. Such cross sections are infrared safe if the weight is insensitive to collinear and/or soft radiation,

$$S\left(p_1, \ldots, p_i, \ldots, p_{n-1}, \alpha\, p_i\right) = S\left(p_1, \ldots, p_i + \alpha\, p_i, \ldots, p_{n-1}\right). \tag{2.78}$$

A prominent example of an infrared safe shape function is the *thrust* T in e^+e^- annihilation [70]:

$$T = \max_{\hat{n}} \frac{\sum_i |\vec{p}_i \cdot \hat{n}|}{\sum_j |\vec{p}_j|} = \frac{1}{\sqrt{s}} \max_{\hat{n}} \sum_i \omega_i \, |\cos\theta_{i\hat{n}}|, \tag{2.79}$$

where $\hat{n}$ is an arbitrary unit vector, whose direction is called the "thrust axis" when T is maximal. In the second equality we have expressed the thrust in terms of the energies ω_i of radiated particles i and their angles with respect to the thrust axis $\hat{n}$. $\sqrt{s} = Q$ denotes the c.m. energy. The second definition in terms of angles and energies is equivalent to the first definition in terms of three-momenta only at the massless level, which we are considering for the main part of this thesis. The thrust measures how pencil-like a two-jet event is. For two jets perfectly back-to-back, its value is 1, at the three-jet boundary it assumes a value of 2/3, and for completely spherical events it takes a value of 1/2.

Another well-known example of an infrared safe shape observable is the *jet-broadening* B in e^+e^- dijet events [71],

$$B = \sum_{c=1}^{2} \left[\frac{1}{2} \frac{1}{\sqrt{s}} \sum_{i \in \Omega_c} \omega_i \, |\sin\theta_i| \right] = \sum_{c=1}^{2} \left[\frac{1}{2} \frac{1}{\sqrt{s}} \sum_{i \in \Omega_c} |k_{\perp,\,i}| \right], \tag{2.80}$$

where all angles and the transverse components of the final state momenta, $k_{\perp,i}$, are taken relative to the thrust axis. Instead of minimizing the axis as above, the event's thrust axis is found first, and then the phase space is divided into two hemispheres, Ω_1 and Ω_2, by the plane perpendicular to the thrust axis. The jet broadening is again 1 for pencil-like configurations, but $\pi/4$ for spherical ones.

Many other event shape functions can be found in the literature, see for example Refs. [30, 27], and references therein. In the following we will discuss the factorization of the thrust cross section in the two-jet limit. For $T \to 1$, as we will see below, large logarithmic enhancements occur, of the form $\ln(1-T)$, which we will resum in the next section. In general, any weighted, differential cross section $d\sigma/d\mathcal{S}$ has at nth order in perturbation theory logarithmic enhancements proportional to $\alpha_s^n(\ln^m \mathcal{S})/\mathcal{S}$, where $m \leq 2n-1$.

In Chapter 5 we will introduce a generalized shape function that interpolates continuously between the thrust, Eq. (2.79) and the jet broadening, Eq. (2.80) [10, 11].

2.4.2 Leading Regions and Factorization for the Thrust

The role of an event shape at its limiting value with regard to power counting is to constrain the final state radiation to physical configurations which contribute to that value. It is at this edge of phase space that large logarithmic corrections occur which need to be resummed. At other values of the event shape, fixed order perturbation theory suffices. In order to resum these large corrections we need to identify the regions in momentum space where these logarithms originate. The procedure is quite analogous to the previous argumentation on parton distribution functions.

Following Coleman and Norton once more, the leading contributions in momentum space for the thrust cross section as $T \to 1$ are given by the reduced diagram shown in Fig. 2.1 c), for the electromagnetic form factor. Due to the requirement that $T \approx 1$ the final state is restricted to contain exactly two very narrow jets. Thus the discussion of leading regions reduces to the one given in Sec. 2.1.1.

The degree of infrared divergence $\omega(T)$ is, as above, given by the incoherent contributions of jet and soft regions

$$\omega(T) = \sum_{c=1}^{2} \omega_{J_c} + \omega_S. \tag{2.81}$$

The degree of IR divergence of the soft function is the same as in Eq. (2.53) since it can be found by dimensional analysis. The degrees of IR divergence of the jet functions are easily found, using Eqs. (2.20), (2.23) or (2.24), (2.26), and (2.25). The final result is in Feynman gauge

$$\begin{aligned}\omega(T) \;\geq\; \sum_{c=1}^{2}\Big\{&\frac{1}{2}\left(p_{J_c}-1\right)+N_{J_c}^{f}+\frac{1}{2}\left(N_{J_c}^{b}-s_{J_c}\right)\\ &+\frac{1}{2}\left(s_{J_c}+l_{J_c}-v_{J_c}^{(3)}\right)\theta\left(s_{J_c}+l_{J_c}-v_{J_c}^{(3)}\right)\Big\}, \qquad (2.82)\end{aligned}$$

with the same notation as in Sec. 2.1.2.

The maximal degree of divergence in this case is logarithmic in $1-T$, $\omega(T\to 1)=0$, if and only if:

- No soft vectors directly attach the hard scattering with the soft function.
- The jets and the soft part can only be connected through soft gluons.
- Exactly one scalar, fermion, or physically polarized gluon, respectively, connects each of the jets with the hard part.
- Additionally, only scalar polarized gluons can connect the jets with the hard scattering.
- The number of soft and scalar-polarized vector lines emerging from a particular jet is less or equal to the number of 3-point vertices in that jet.

As announced above, the IR behavior of the thrust cross section is proportional to $\ln(1-T)$, more precisely, at order n in the perturbative expansion, maximally proportional to $\alpha_s^n \ln^{2n}(1-T)$. Simultaneously collinear and soft configurations give two logarithms per loop, only collinear or only soft gluons contribute at the level of one logarithm per loop, as one can see in the simple example discussed above in Sec. 2.1.1. Here we will consider the differential cross section, whose behavior is therefore $\alpha_s^n[\ln^m(1-T)]/(1-T)$, where $m\leq 2n-1$. $m=2n-1$ is referred to as leading logarithmic (LL) behavior, $m=2n-2$ is called next-to-leading logarithmic (NLL) and so forth.

The factorization is straightforward, using the Ward identities and the decomposition of gluon propagators discussed ins Section 2.2, Glauber configurations do not pose a problem here, as we have seen in Sec. 2.2.2. The

resulting cross section is linked via a convolution in $1-T$

$$\begin{aligned}\frac{d\sigma(T,s)}{d(1-T)} &= \sigma_0\, H\left(\frac{\sqrt{s}}{\mu}, \frac{p_{J_c}\cdot\hat{\xi}_c}{\mu}, \alpha_s(\mu)\right)\prod_{c=1}^{2}\int d\tau_{J_c} J_c\left(\frac{p_{J_c}\cdot\hat{\xi}_c}{\mu}, \tau_{J_c}\frac{\sqrt{s}}{\mu}, \alpha_s(\mu)\right)\\ &\quad\times\int d\tau_s\, S\left(\tau_s\frac{\sqrt{s}}{\mu}, \hat{\beta}_c\cdot\hat{\xi}_c, \alpha_s(\mu)\right)\delta\left(1-T-\sum_{c=1}^{2}\tau_{J_c}-\tau_s\right), \quad (2.83)\end{aligned}$$

since the leading contributions are incoherent and thus additive to the weight in the elastic limit, up to corrections that vanish as τ^2 for small τ, where

$$\tau \equiv 1-T. \quad (2.84)$$

Eq. (2.83) is illustrated in Fig. 2.8. μ is the factorization scale which we set in the following equal to the renormalization scale. The arguments of the various dimensionless functions in Eq. (2.83) follow from dimensional considerations. σ_0 is the dimensionful Born cross section, which we separated such that the hard scattering H begins at $1+\mathcal{O}(\alpha_s)$. $\hat{\xi}_c^\mu = \xi_c^\mu/|\xi_c|$ are the normalized eikonal vectors that arise in the course of the factorization. The physical cross section on the left hand side is of course independent of the factorization scale and of the $\hat{\xi}_c$. Due to the soft approximation the soft function S cannot depend on the magnitude of the jet momenta p_{J_c}, only on their normalized directions, denoted by $\hat{\beta}_c$, $c=1,2$. Explicit definitions in form of (nonlocal) operators of the various functions above will be discussed in Chapter 5. In Eq. (2.83) we have neglected recoil effects, which, in principle also link the various functions. In Chapter 5 we will provide the justification for this approximation.

Following the power-counting arguments above, the dimensionless jet and soft functions above begin at $1/\tau_i$, $i=s,J_c$, and are multiplied in higher orders by logarithms of their arguments. These logarithms stem from the expansion of kinematic combinations such as $1/\varepsilon\ 1/(\tau_i\sqrt{s})^{1+\varepsilon}$:

$$\frac{1}{\varepsilon}\frac{1}{(\tau_i)^{1+\varepsilon}} = \frac{1}{\varepsilon^2}\delta(\tau_i) + \frac{1}{\varepsilon}\left[\frac{1}{\tau_i}\right]_+ + \left[\frac{\ln(\tau_i)}{\tau_i}\right]_+ + \mathcal{O}(\varepsilon)\,, \quad (2.85)$$

when working in $n=4-2\varepsilon$ dimensions. The plus-distribution above is defined as

$$\int_z^1 dx\, f(x)\,[g(x)]_+ = \int_z^1 dx\, g(x)\,[f(x)-f(1)] - f(1)\int_0^z dx\, g(x). \quad (2.86)$$

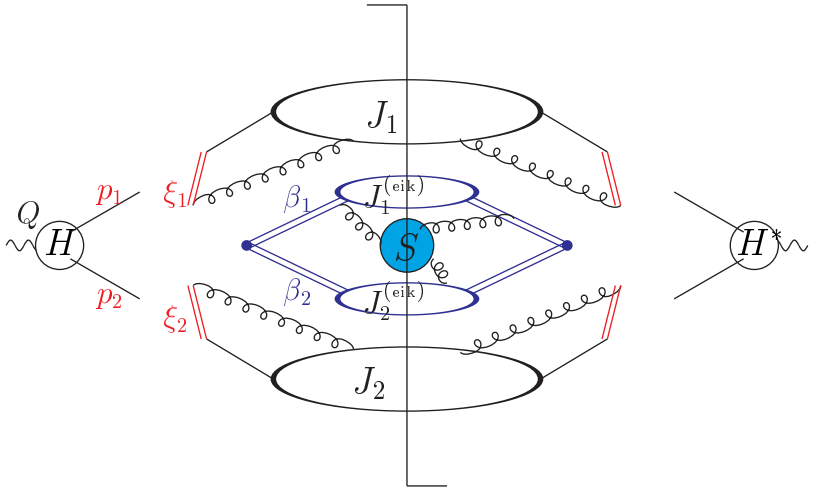

Figure 2.8: Factorized cross section (2.83) after the application of Ward identities. The vertical line denotes the final state cut.

2.5 Evolution and Resummation at the Example of the Thrust

The following discussion of resummation of large logarithms in $1-T$ is based on Refs. [31, 72]. The natural scale for the hard scattering is $\sqrt{s}/2$, such that it contains no large ratios. Setting $\mu = \sqrt{s}/2$ in Eq. (2.83) we obtain

$$\frac{d\sigma(T,s)}{d(1-T)} = \sigma_0 H\left(\frac{2\,p_{J_c}\cdot\hat{\xi}_c}{\sqrt{s}}, \alpha_s\left(\frac{\sqrt{s}}{2}\right)\right) \prod_{c=1}^{2} \int d\tau_{J_c} J_c\left(\frac{2\,p_{J_c}\cdot\hat{\xi}_c}{\sqrt{s}}, 2\tau_{J_c}, \alpha_s\left(\frac{\sqrt{s}}{2}\right)\right) \times \int d\tau_s\, S\left(2\tau_s, \hat{\beta}_c\cdot\hat{\xi}_c, \alpha_s\left(\frac{\sqrt{s}}{2}\right)\right) \delta\left(1-T-\sum_c \tau_{J_c} - \tau_s\right) \quad (2.87)$$

As $T \to 1$, the τ_i are restricted to be very small by the delta-function. In this limit the logarithms of the τ_i in the soft and jet functions become large and fixed-order calculations become inadequate. Resummation of these logarithms is needed to provide reliable predictions.

Since the functions in the factorized thrust are still linked by a convolution in the variables τ_i it is advantageous to take moments to disentangle this

convolution:

$$\tilde{\sigma}(N,s) \equiv \int_0^1 dT\, T^{N-1} \frac{d\sigma(T,s)}{d(1-T)} = \int_0^\infty d\tau e^{-N\tau} \frac{d\sigma(\tau,s)}{d\tau} + \mathcal{O}\left(\frac{1}{N}\right). \quad (2.88)$$

The first definition in (2.88) is the Mellin transform, which is equivalent to the second definition, the Laplace transform, at large N, because then $e^{-N\tau} \approx (1-\tau)^N$ (recall the definition of τ, Eq. (2.84)). Tildes denote quantities in moment space in this chapter.

The factorized thrust becomes a simple product in moment space,

$$\begin{aligned}
\tilde{\sigma}(N,s) &= \sigma_0 H\left(\frac{\sqrt{s}}{\mu}, \frac{p_{J_c}\cdot\hat{\xi}_c}{\mu}, \alpha_s(\mu)\right) \tilde{S}\left(\frac{\sqrt{s}}{\mu N}, \hat{\beta}_c\cdot\hat{\xi}_c, \alpha_s(\mu)\right) \\
&\quad \times \prod_{c=1}^{2} \tilde{J}_c\left(\frac{p_{J_c}\cdot\hat{\xi}_c}{\mu}, \frac{\sqrt{s}}{\mu N}, \alpha_s(\mu)\right) \quad (2.89) \\
&= \sigma_0 H\left(\frac{2\,p_{J_c}\cdot\hat{\xi}_c}{\sqrt{s}}, \alpha_s\left(\frac{\sqrt{s}}{2}\right)\right) \tilde{S}\left(\frac{2}{N}, \hat{\beta}_c\cdot\hat{\xi}_c, \alpha_s\left(\frac{\sqrt{s}}{2}\right)\right) \\
&\quad \times \prod_{c=1}^{2} \tilde{J}_c\left(\frac{2p_{J_c}\cdot\hat{\xi}_c}{\sqrt{s}}, \frac{2}{N}, \alpha_s\left(\frac{\sqrt{s}}{2}\right)\right), \quad (2.90)
\end{aligned}$$

where

$$\tilde{S}\left(\frac{\sqrt{s}}{\mu N}, \alpha_s(\mu)\right) \equiv \int_0^\infty d\tau_s\, e^{-N\tau_s} S\left(\tau_s \frac{\sqrt{s}}{\mu}, \alpha_s(\mu)\right), \quad (2.91)$$

and analogously for the jet functions. In Eq. (2.90) we have set $\mu = \sqrt{s}/2$. The large logarithms of the τ_i are transformed into large logarithms of N in moment space. Specifically, logarithms of the form displayed in Eq. (2.85) transform under moments as

$$\int_0^1 d\tau (1-\tau)^{N-1} \left[\frac{\ln^m(\tau)}{\tau}\right]_+ = \frac{(-1)^{m+1}}{m+1} \ln^{m+1} N + \mathcal{O}\left(\frac{1}{N}\right). \quad (2.92)$$

The factorized cross section (2.87) or (2.88) already provides all the information necessary for the resummation. The physical cross section is independent of the factorization scale

$$\frac{d}{d\ln\mu} \frac{d\sigma(T,s)}{d(1-T)} = \frac{d}{d\ln\mu} \tilde{\sigma}(N,s) = 0, \quad (2.93)$$

and of the choice of the eikonal directions $\hat{\xi}_c$,

$$\frac{\partial}{\partial \ln\left(p_{J_c}\cdot\hat{\xi}_c\right)} \frac{d\sigma(T,s)}{d(1-T)} = \frac{\partial}{\partial \ln\left(p_{J_c}\cdot\hat{\xi}_c\right)} \tilde{\sigma}(N,s) = 0. \quad (2.94)$$

These conditions are exactly fulfilled only if the cross section is calculated to all orders in perturbation theory. Upon truncation at order m, the relations (2.93) and (2.94) are fulfilled only up to the same order, with corrections proportional to α_s^{m+1}. In the remainder of this section we explore the consequences of the renormalization group conditions (2.93) and (2.94) [72].

2.5.1 Resummation of Single Logarithms

The renormalization group equation (2.93) organizes all single logarithms in the soft function, and some of the single logarithms in the jet functions. The jet functions contain, as we will see shortly, double logarithms, due to emissions that are simultaneously soft and collinear. Applying Eq. (2.93) to the factorized thrust, Eq. (2.88), we derive the following consistency conditions since all functions are multiplicatively renormalizable:

$$\frac{d}{d\ln\mu}\ln\tilde{S}\left(\frac{\sqrt{s}}{\mu N},\hat{\beta}_c\cdot\hat{\xi}_c,\alpha_s(\mu)\right) = -\gamma_s(\alpha_s(\mu)), \tag{2.95}$$

$$\frac{d}{d\ln\mu}\ln\tilde{J}_c\left(\frac{p_{J_c}\cdot\hat{\xi}_c}{\mu},\frac{\sqrt{s}}{\mu N},\alpha_s(\mu)\right) = -\gamma_{J_c}(\alpha_s(\mu)), \tag{2.96}$$

$$\frac{d}{d\ln\mu}\ln H\left(\frac{\sqrt{s}}{\mu},\frac{p_{J_c}\cdot\hat{\xi}_c}{\mu},\alpha_s(\mu)\right) = -\gamma_H(\alpha_s(\mu)), \tag{2.97}$$

with

$$\gamma_s+\sum_{c=1}^{2}\gamma_{J_c}+\gamma_H=0. \tag{2.98}$$

The anomalous dimensions γ_d, $d=s,J_c,H$ can depend on variables held in common between at least two of the functions. Because each function is infrared safe, while ultraviolet divergences are present only in virtual diagrams, the anomalous dimensions cannot depend on N. This leaves as arguments of the γ_d only the coupling $\alpha_s(\mu)$ and the dimensionless ratio $(2p_{J_c}\cdot\hat{\xi}_c)/\sqrt{s}$. Since the dependence on $p_{J_c}\cdot\hat{\xi}_c$ will be studied with the help of Eq. (2.94) below, we suppress this argument for now.

The solutions to Eqs. (2.95) and (2.96) are given by

$$\tilde{S}\left(\frac{\sqrt{s}}{\mu N},\hat{\beta}_c\cdot\hat{\xi}_c,\alpha_s(\mu)\right) = \tilde{S}\left(\frac{\sqrt{s}}{\mu_0 N},\hat{\beta}_c\cdot\hat{\xi}_c,\alpha_s(\mu_0)\right)e^{-\int_{\mu_0}^{\mu}\frac{d\lambda}{\lambda}\gamma_s(\alpha_s(\lambda))}, \tag{2.99}$$

$$\tilde{J}_c\left(\frac{p_{J_c}\cdot\hat{\xi}_c}{\mu},\frac{\sqrt{s}}{\mu N},\alpha_s(\mu)\right) = \tilde{J}_c\left(\frac{p_{J_c}\cdot\hat{\xi}_c}{\mu_0},\frac{\sqrt{s}}{\mu_0 N},\alpha_s(\mu_0)\right)e^{-\int_{\mu_0}^{\mu}\frac{d\lambda}{\lambda}\gamma_{J_c}(\alpha_s(\lambda))} \tag{2.100}$$

Setting $\mu_0 = \sqrt{s}/N$, we avoid logarithms of N in the soft function in Eq. (2.90):

$$\begin{aligned}\tilde{\sigma}(N,s) &= \sigma_0 H\left(\frac{2\,p_{J_c}\cdot\hat{\xi}_c}{\sqrt{s}},\alpha_s\left(\frac{\sqrt{s}}{2}\right)\right) \\ &\quad\times\tilde{S}\left(1,\hat{\beta}_c\cdot\hat{\xi}_c,\alpha_s\left(\frac{\sqrt{s}}{N}\right)\right)e^{-\int_{\sqrt{s}/N}^{\sqrt{s}/2}\frac{d\lambda}{\lambda}\gamma_s(\alpha_s(\lambda))} \\ &\quad\times\prod_{c=1}^{2}\tilde{J}_c\left(\frac{2Np_{J_c}\cdot\hat{\xi}_c}{\sqrt{s}},1,\alpha_s\left(\frac{\sqrt{s}}{N}\right)\right)e^{-\int_{\sqrt{s}/N}^{\sqrt{s}/2}\frac{d\lambda}{\lambda}\gamma_{J_c}(\alpha_s(\lambda))} \qquad (2.101)\end{aligned}$$

2.5.2 Resummation of Sudakov Double Logarithms

The remaining unorganized large logarithms of N in Eq. (2.101) reside in the jet functions. $p_{J_c}\cdot\hat{\xi}_c$ is of the order of the hard scale, $\sim\sqrt{s}$. The requirement that the cross section be independent of $p_{J_c}\cdot\hat{\xi}_c$, Eq. (2.94), implies that the jet, soft and hard functions obey equations analogous to (2.95)-(2.97), again in terms of the variables that they hold in common [72]. The same results may be derived following the method of Collins and Soper [59], by defining the jets in an axial gauge, and then studying their variations under boosts. The latter method provides an explicit construction of the functions that control the variation which is needed for explicit calculations. We will discuss both ways below.

$p_{J_c}\cdot\hat{\xi}_c$-Dependence in Axial Gauge

Since the definition of the jets can be made gauge invariant, we can derive the evolution with $\frac{\partial}{\partial\ln\left(p_{J_c}\cdot\hat{\xi}_c\right)}$ in any gauge. The derivation is most easily done in axial gauge with the gauge vector $\hat{\xi}_c$. The variation with respect to $p^\mu_{J_c}$ is equivalent to the variation with respect to $\hat{\xi}^\mu_c$:

$$\frac{\partial}{\partial\ln p^\mu_{J_c}}J_c = \frac{\partial}{\partial\ln\hat{\xi}^\mu_c}J_c. \qquad (2.102)$$

We will derive the effect of the variation with respect to $\xi_1\equiv\xi$ on jet 1, which we choose to move in the plus direction,

$$p^\mu_{J_1} = (p^+,0,0_\perp). \qquad (2.103)$$

The derivation for jet 2 is analogous. The final cross section obeys Eq. (2.94) for each ξ_c, $c = 1, 2$ separately.

The only dependence on the gauge-vector ξ in axial gauge is in the gluon propagator, given by Eq. (2.16) with $\kappa \to \infty$, which allows us to trace out the ξ-dependence relatively easily. We choose as variation a boost in the plus-direction, which leaves ξ^2 invariant, with $\xi_\perp = 0$. A straightforward calculation gives

$$\frac{\delta}{\delta \ln \hat{\xi}^\alpha} D_{\mu\nu} = -\frac{k_\mu}{k \cdot \hat{\xi}} \left(\frac{1}{\hat{\xi} \cdot \bar{v}} \bar{v}^\alpha + v_\perp^\alpha \right) D_{\alpha\nu} + \{\mu \leftrightarrow \nu\} \,, \tag{2.104}$$

where $\bar{v}$ is a unit vector in the minus-direction $\bar{v}^\mu = (0^+, 1, 0_\perp)$, and $v_\perp$ is a unit vector in the perpendicular direction, $v_\perp^\mu = (0^+, 0^-, 1_\perp)$. This variation is shown graphically in Fig. 2.9, where the box denotes $i \left(\frac{\xi^2}{\xi \cdot \bar{v}} \bar{v}^\alpha + v_\perp^\alpha \right)$.

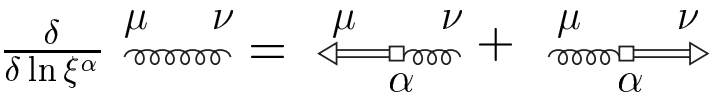

Figure 2.9: Graphical illustration of the variation of the gluon propagator with respect to the gauge fixing vector ξ, Eq. (2.104).

Applying this to the jet function in axial gauge we obtain Fig. 2.10 a). We will provide an explicit construction of the jet function in Chapter 5. Here it suffices to know that the jet can only have one external physical line on each side of the cut, which follows from power-counting. In the axial gauge $\xi \cdot \mathcal{A} = 0$ the eikonal lines from factoring unphysically polarized gluons connecting the jet with the hard part are not present. With the help of power counting, as presented in 2.1.2, we find that the effect of the variation with respect to ξ on J_c can either be far off-shell or soft to give a leading contribution. Collinear configurations are subleading. Only virtual diagrams can contribute to the off-shell part, in the following denoted by G. G is therefore an overall factor. The soft part, denoted by K, can be factored from the jet via the Ward identity 2.2 c), linked only by an overall convolution in the momentum q flowing through the jet and K.

$$\frac{\partial}{\partial \ln \hat{\xi}^\mu} J_1 \left(p_{J_1}^\mu, \tau_{J_1}, \mu \right) = \int \frac{d^n q}{(2\pi)^n} K_1' \left(q^\mu, \tau_{J_1}, \mu', \mu \right) J_1 \left(p_{J_1}^\mu - q^\mu, \tau_{J_1}, \mu \right)$$

$$+G_1\left(\frac{p_{J_1}\cdot\hat{\xi}}{\mu'},\mu'\right)J_1\left(p^\mu_{J_1},\tau_{J_1},\mu\right), \tag{2.105}$$

where μ' is the scale separating hard contributions in G from soft ones in K. The jet, of course, is independent of μ'. Eq. (2.105) is displayed in Fig. 2.10 b). Both K_1' and J_1 on the right-hand-side contribute to the weight τ_{J_1}.

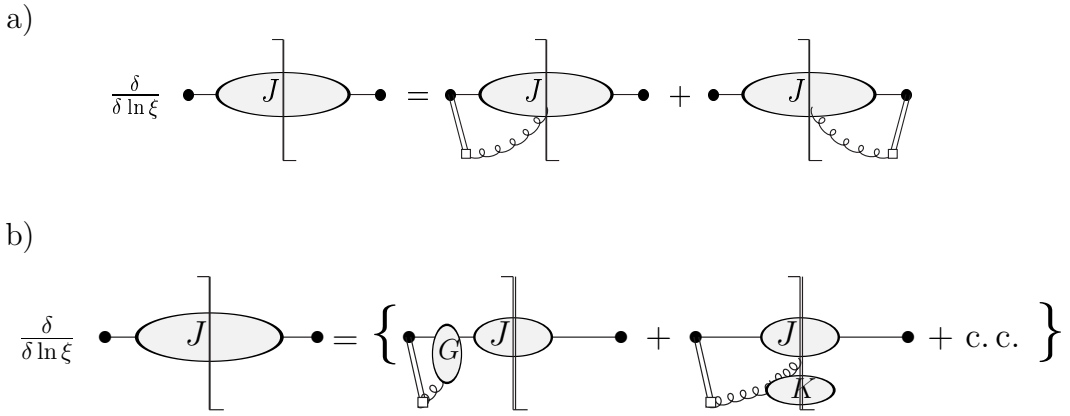

Figure 2.10: a) Graphical illustration of the variation of the jet function with respect to the gauge fixing vector ξ. b) Factorization of the variation into a soft and an ultraviolet part, Eq. (2.105). c. c. denotes the complex conjugate contribution.

We can reduce the convolution in the four-momentum q^μ further, since q^μ is soft,

$$\ln\frac{(p_{J_1}-q)\cdot\hat{\xi}}{\mu'}\sim\ln\frac{p_{J_1}\cdot\hat{\xi}}{\mu'}. \tag{2.106}$$

We can therefore neglect q^μ in J_1 to leading accuracy. But we cannot neglect its contribution to τ_{J_1}. Thus the convolution in (2.105) reduces to a convolution in terms of τ:

$$\begin{aligned}\frac{\partial}{\partial\ln\hat{\xi}}J_1\left(\frac{p_{J_1}\cdot\hat{\xi}}{\mu},\tau_{J_1}\frac{\sqrt{s}}{\mu},\alpha_s(\mu)\right)&=\int d\tau_K\,K_1\left(\tau_K\frac{\sqrt{s}}{\mu},\frac{\mu'}{\mu},\alpha_s(\mu')\right)\\&\quad\times\int d\tau_1'\,J_1\left(\frac{p_{J_1}\cdot\hat{\xi}}{\mu},\tau_1'\frac{\sqrt{s}}{\mu},\alpha_s(\mu)\right)\delta\left(\tau_{J_1}-\tau_1'-\tau_K\right)\\&\quad+G_1\left(\frac{p_{J_1}\cdot\hat{\xi}}{\mu'},\alpha_s(\mu')\right)J_1\left(\frac{p_{J_1}\cdot\hat{\xi}}{\mu},\tau_{J_1}\frac{\sqrt{s}}{\mu},\alpha_s(\mu)\right).\end{aligned} \tag{2.107}$$

Taking moments, and setting $\mu' = \mu$ (corrections are non-leading), we arrive for both jets at

$$\frac{\partial}{\partial \ln\left(p_{J_c}\cdot\hat{\xi}_c\right)} \ln\ \tilde{J}_c\left(\frac{p_{J_c}\cdot\hat{\xi}_c}{\mu}, \frac{\sqrt{s}}{\mu N}, \alpha_s(\mu)\right) = \tilde{K}_c\left(\frac{\sqrt{s}}{\mu\, N}, \alpha_s(\mu)\right) + G_c\left(\frac{p_{J_c}\cdot\hat{\xi}_c}{\mu}, \alpha_s(\mu)\right). \quad (2.108)$$

We note that although the derivation of Eq. (2.108) has been performed in axial gauge, the result is gauge invariant, since the jet function can be given a gauge-invariant definition, as we will show in Chapter 5.

$p_{J_c}\cdot\hat{\xi}_c$-Dependence from General Considerations

Eq. (2.108) can also be derived in a manner similar to the derivation of Eqs. (2.95)-(2.97), by considering the variables held in common by at least two of the functions [72]. Applying Eq. (2.94) to Eq. (2.88) we obtain for jet 1

$$\begin{aligned}\frac{\partial}{\partial \ln\left(p_{J_1}\cdot\hat{\xi}_1\right)} \ln\ \tilde{J}_1\left(\frac{p_{J_1}\cdot\hat{\xi}_1}{\mu}, \frac{\sqrt{s}}{\mu N}, \alpha_s(\mu)\right) &= -\frac{\partial}{\partial \ln\left(p_{J_1}\cdot\hat{\xi}_1\right)} \ln H\left(\frac{\sqrt{s}}{\mu}, \frac{p_{J_1}\cdot\hat{\xi}_1}{\mu}, \frac{p_{J_2}\cdot\hat{\xi}_2}{\mu}, \alpha_s(\mu)\right) \\ &\quad -\frac{\partial}{\partial \ln\left(p_{J_1}\cdot\hat{\xi}_1\right)} \ln \tilde{S}\left(\frac{\sqrt{s}}{\mu N}, \hat{\beta}_1\cdot\hat{\xi}_1, \hat{\beta}_2\cdot\hat{\xi}_2, \alpha_s(\mu)\right). \quad (2.109)\end{aligned}$$

The logarithmic derivative of the jet can depend additively on a function containing the hard scale $p_{J_1}\cdot\hat{\xi}_1 \sim \sqrt{s}/2$, or on a function containing the soft scale $\sqrt{s}/N$. These functions can contain all arguments that the jet and the hard function, or the jet and the soft function hold in common, respectively. Aside from the hard and the soft scales, the only other common variable is the running coupling, $\alpha_s(\mu)$. These considerations result again in Eq. (2.108).

The Resummed Jet Functions

From the above considerations, $\tilde{K}_c + G_c$ are renormalized additively, and satisfy [59]

$$\mu\frac{d}{d\mu}\ \tilde{K}_c\left(\frac{\sqrt{s}}{\mu\, N}, \alpha_s(\mu)\right) \;=\; -\gamma_{K_c}\left(\alpha_s(\mu)\right),$$

$$\mu\frac{d}{d\mu}G_c\left(\frac{p_{J_c}\cdot\hat{\xi}_c}{\mu},\alpha_s(\mu)\right) \;=\; \gamma_{K_c}\left(\alpha_s(\mu)\right)\,. \tag{2.110}$$

γ_{K_c} is the universal Sudakov anomalous dimension [45, 59, 73].

This Sudakov anomalous dimension is the anomalous dimension of the soft-collinear functions $\tilde{K}_c$, which is built out solely of eikonal lines. Therefore, as we will also see by explicit calculation below, the anomalous dimension of $\tilde{K}_c$, and the anomalous dimension of the eikonal cross section in Eq. (2.70) are the same, since the eikonal anomalous dimension for lightlike lines is independent of the directions of the scattering eikonals. The anomalous dimension of (2.70) controls the most singular evolutionary behavior of parton-in-parton distribution functions as $x\to 1$ [12, 68], which is, as in Eq. (2.110), due to simultaneously soft and collinear radiation. By analogous reasoning, the same anomalous dimension appears in a variety of other jet-related processes [74].

With the help of these evolution equations, the terms $\tilde{K}_c$ and G_c in Eq. (2.108) can be reexpressed as [75]

$$\begin{aligned}
&\tilde{K}_c\left(\frac{\sqrt{s}}{\mu\,N},\alpha_s(\mu)\right)+G_c\left(\frac{p_{J_c}\cdot\hat{\xi}_c}{\mu},\alpha_s(\mu)\right)\\
&=\tilde{K}_c\left(\frac{1}{c_1},\alpha_s\left(c_1\,\frac{\sqrt{s}}{N}\right)\right)+G_c\left(\frac{1}{c_2},\alpha_s\left(c_2\,p_{J_c}\cdot\hat{\xi}_c\right)\right)\;-\int\limits_{c_1\sqrt{s}/N}^{c_2\,p_{J_c}\cdot\hat{\xi}_c}\frac{d\lambda'}{\lambda'}\gamma_{K_c}\left(\alpha_s\left(\lambda'\right)\right)\\
&=-B_c\left(c_1,c_2,\alpha_s\left(c_2\,p_{J_c}\cdot\hat{\xi}_c\right)\right)-2\int\limits_{c_1\sqrt{s}/N}^{c_2\,p_{J_c}\cdot\hat{\xi}_c}\frac{d\lambda'}{\lambda'}A_c\left(c_1,\alpha_s\left(\lambda'\right)\right)\,,
\end{aligned}\tag{2.111}$$

where in the second equality we have shifted the argument of the running coupling in $\tilde{K}_c$, and have introduced the notation

$$\begin{aligned}
B_c\left(c_1,c_2,\alpha_s\left(\mu\right)\right) &\equiv -\tilde{K}_c\left(\frac{1}{c_1},\alpha_s\left(\mu\right)\right)-G_c\left(\frac{1}{c_2},\alpha_s\left(\mu\right)\right),\\
2A_c\left(c_1,\alpha_s\left(\mu\right)\right) &\equiv \gamma_{K_c}\left(\alpha_s(\mu)\right)+\beta(g(\mu))\frac{\partial}{\partial g(\mu)}\tilde{K}_c\left(\frac{1}{c_1},\alpha_s(\mu)\right).
\end{aligned}\tag{2.112}$$

The choice of the constants c_1 and c_2 is a matter of convenience. They reflect the freedom in separating soft/collinear (K_c) from collinear (G_c) contributions. If the functions in (2.111) were calculated to all orders the jet evolution would be independent of their choice. Residual dependence on the c_i is due to fixed logarithmic resummation.

The solution to Eq. (2.108) with $\mu = \mu_0$ is

$$\begin{aligned}\tilde{J}_c\left(\frac{p_{J_c}\cdot\hat{\xi}_c}{\mu_0},\frac{\sqrt{s}}{\mu_0 N},\alpha_s(\mu_0)\right) &= \tilde{J}_c\left(\frac{\sqrt{s}}{\mu_0 N},\frac{\sqrt{s}}{\mu_0 N},\alpha_s(\mu_0)\right) \\ \times\exp\left\{-\int_{\sqrt{s}/N}^{p_{J_c}\cdot\hat{\xi}_c}\frac{d\lambda}{\lambda}\left[B_c\left(c_1,c_2,\alpha_s\left(c_2\lambda\right)\right)+2\int_{c_1\frac{s}{2\lambda N}}^{c_2\lambda}\frac{d\lambda'}{\lambda'}A_c\left(c_1,\alpha_s\left(\lambda'\right)\right)\right]\right\}&.\end{aligned} \tag{2.113}$$

After combining Eqs. (2.100) and (2.113), the choice $\mu_0 = \sqrt{s}/N$ allows us to control all large logarithms in the jet functions simultaneously:

$$\begin{aligned}\tilde{J}_c\left(\frac{p_{J_c}\cdot\hat{\xi}_c}{\mu},\frac{\sqrt{s}}{\mu N},\alpha_s(\mu)\right) &= \tilde{J}_c\left(1,1,\alpha_s\left(\frac{\sqrt{s}}{N}\right)\right)\exp\left\{-\int_{\sqrt{s}/N}^{\mu}\frac{d\lambda}{\lambda}\gamma_{J_c}\left(\alpha_s(\lambda)\right)\right\} \\ \times\exp\left\{-\int_{\sqrt{s}/N}^{p_{J_c}\cdot\hat{\xi}_c}\frac{d\lambda}{\lambda}\left[B_c\left(c_1,c_2,\alpha_s\left(c_2\lambda\right)\right)+2\int_{c_1 s/(2\lambda N)}^{c_2\lambda}\frac{d\lambda'}{\lambda'}A_c\left(c_1,\alpha_s\left(\lambda'\right)\right)\right]\right\}&.\end{aligned} \tag{2.114}$$

2.5.3 The Resummed Thrust

Putting everything together, we arrive at the fully resummed form of the thrust,

$$\begin{aligned}\tilde{\sigma}(N,s) &= \sigma_0 H\left(1,\alpha_s\left(\frac{\sqrt{s}}{2}\right)\right) \\ &\times\tilde{S}\left(1,\alpha_s\left(\frac{\sqrt{s}}{N}\right)\right)\exp\left\{-\int_{\sqrt{s}/N}^{\sqrt{s}/2}\frac{d\lambda}{\lambda}\gamma_s(\alpha_s(\lambda))\right\} \\ &\times\prod_{c=1}^{2}\tilde{J}_c\left(1,1,\alpha_s\left(\frac{\sqrt{s}}{N}\right)\right)\exp\left\{-\int_{\sqrt{s}/N}^{\sqrt{s}/2}\frac{d\lambda}{\lambda}\left[\gamma_{J_c}(\alpha_s(\lambda))+B_c\left(c_1,c_2,\alpha_s\left(c_2\lambda\right)\right)\right.\right. \\ &\qquad\left.\left.+2\int_{c_1 s/(2\lambda N)}^{c_2\lambda}\frac{d\lambda'}{\lambda'}A_c\left(c_1,\alpha_s\left(\lambda'\right)\right)\right]\right\}.\end{aligned} \tag{2.115}$$

We have set $\mu = \sqrt{s}/2$ and identified

$$p_{J_c}\cdot\hat{\xi}_c = \frac{\sqrt{s}}{2}, \tag{2.116}$$

since the cross section is independent of the choice of ξ_c. Eq. (2.115) contains double logarithms from the integral with A_c, and single logarithms from the remaining exponents. At NLL it suffices to evaluate A_c at two loops, and the remaining functions at one loop.

In general, since the term with A_c contains one more integral compared to the remaining exponents, this term has to be evaluated to one order higher for consistency. A simplified method to calculate this function at higher orders is therefore desirable. At NNLL the calculation of the Sudakov anomalous dimension is required at three loops. In the next two chapters, Ch.s 3-4, we develop the necessary tools to perform this calculation at higher loops, before returning to the discussion of event shapes. In Chapter 4 the method is illustrated with the fermionic contribution to the three-loop anomalous dimension.

Chapter 3

Nonabelian Eikonal Exponentiation

As we have shown in the previous chapter, soft radiation at wide angles from the hard scattering directions decouples, and is equally well described by radiation from path ordered exponentials. These eikonal lines replace each of the partons involved in the hard scattering. We have shown how to resum large logarithmic corrections in exponentials by solving renormalization group equations. For certain quantities that are built out only of eikonal lines, as we will show here, this exponentiation occurs directly by reordering of diagrams.

This observation, first made by Sterman [76], then proved by Gatheral [77], and Frenkel and Taylor [78], overcomes the following difficulties which one faces in perturbative calculations at higher order: Although perturbative calculations within the eikonal approximation are significantly less complex than calculations within the full theory, we pay the price of introducing new infrared divergences. Of course, these infrared divergences cancel in the infrared safe physical observable under consideration. Also, the number of graphs at each order is in general[1] the same as in the full theory, and can be quite significant at higher orders in the perturbative expansion.

Nonabelian eikonal exponentiation remedies these difficulties. This theorem states that a cross section X with two eikonal lines in a nonabelian theory exponentiates,

$$\sigma^{(\mathrm{eik})} \equiv X = e^{Y}, \tag{3.1}$$

where Y can be given a simple recursive definition. In Section 3.1 we will recall the proof of Eq. (3.1) [77, 78], for the sake of completeness, including a few illustrative examples which will be used in Chapter 4. The exponent Y in (3.1) has the following properties:

[1] Self-energies of light-like eikonal lines vanish in Feynman gauge.

1. Y is a subset of the diagrams contributing to X, which we will call "webs" in the following, since, as we will see below, their lines " [...] are all nested [...] in a spider's web pattern" [76].

2. The color weights of the diagrams in Y are in general different from those in X.

3. For Eq. (3.1) to hold, the phase-space region should be symmetric in the real gluon momenta.

Below we will outline the arguments necessary to prove this theorem. The proof relies on the recursive definition of color-weights and on the iterated application of a well-known eikonal identity. In the exponentiated form, the number of graphs to be calculated at each order is significantly reduced. Furthermore, IR and UV subdivergences cancel in the exponent at each order as we will show in Section 3.2, before extending the proof to three eikonal quantities, and listing a few implications of this exponentiation, including the form of power corrections for the thrust in Sec. 3.4.3. Sections 3.1 and 3.2 were published in [12].

3.1 Proof of Exponentiation for Cross Sections with Two Eikonal Lines

3.1.1 Some Terminology

In order to specify which subset of diagrams of the original perturbation series X contributes to the exponent Y we need to introduce some terminology.

Each diagram will be decomposed into its color part and its Feynman integral in the eikonal approximation. The eikonal Feynman rules can be found in Appendix A.2. The color part can be represented graphically in a diagram which is similar to an ordinary Feynman diagram, but the vertices represent the color part of the Feynman rules, i. e. the vertices are just the T^a_{ij}s and $i\,f_{ijk}$s, for quark or gluon, respectively, and the lines are δ_{ij}s. In addition, all soft lines have to be drawn inside the (cut) eikonal loop for reasons which will become clear shortly. Certain color diagrams are related to each other by use of the commutation relations of the T^a_{ij}s and $i\,f_{ijk}$s (Jacobi identity) which are graphically represented in Fig. 3.1.

$$\begin{aligned} \left[T^a, T^b\right] &= i f_{abc} T^c \\ f_{ilm} f_{mjk} &+ f_{jlm} f_{imk} + f_{klm} f_{ijm} = 0. \end{aligned} \tag{3.2}$$

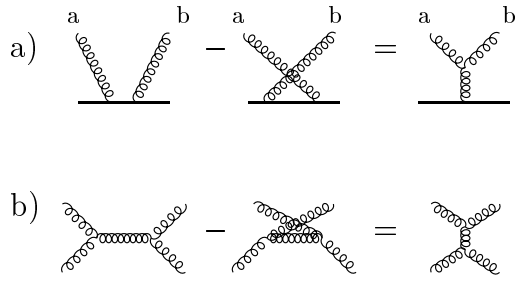

Figure 3.1: Graphical representations of the commutation relations between a) T^a_{ij}s, and b) $i\,f_{ijk}$s (Jacobi identity), Eq. (3.2).

As mentioned above, the diagrams contributing to Y will be called "webs" [76]. Originally [77], a web was defined as a set of gluon lines which cannot be partitioned without cutting at least one of its lines. As already stated above, all soft lines are to be drawn inside the eikonal loop(s). However, at $\mathcal{O}\left(\alpha_s^3\right)$ new types of diagrams arise which Frenkel and Taylor [78] called connected webs ("c-webs"). c-webs are not included in the original definition for the following reason: If one cuts the horizontal gluon line of the c-web drawn in Fig. 3.2 one would get two webs consisting of three-point vertices since real and virtual gluon lines are treated on equal footing in a color-weight diagram. Below we will refer to webs and c-webs just as webs.

The definitions given by Gatheral, and Frenkel and Taylor can be unified by the following *definition*:

A web is a (sub)diagram consisting of soft gluon lines connecting two eikonal lines which cannot be partitioned into webs of lower order by cutting all eikonal lines exactly once. Stated differently, webs are two-eikonal irreducible diagrams. The *order of a web* is defined to be equal to the powers of α_s it contains, e. g. a web of $\mathcal{O}\left(\alpha_s^2\right)$ will be called a web of order 2. Diagrammatic examples are shown in Fig. 3.2. A web has a color factor $\overline{C}$ and a Feynman integral part $\mathcal{F}$. $\mathcal{F}$ contains only those eikonal propagators which are *internal* to the web. The color weight is in general different from the one which one would get from the usual Feynman rules.

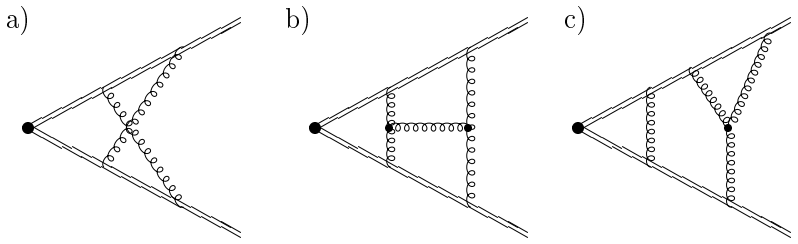

Figure 3.2: Examples of a) a web (order 2), b) a c-web (web of order 3), and c) a diagram which is not a web (consisting of a product of an order-1 web and of an order-2 web).

The color weight of a web of order m is recursively defined as

$$\begin{aligned} \overline{C}(W^{(m)}) &\equiv \frac{1}{\text{Tr } \mathbf{1}} C(W^{(m)}) - \sum_d \prod_{n_i} \overline{C}(W^{(i)}_{n_i}), \\ \overline{C}(W^{(1)}) &\equiv \frac{1}{\text{Tr } \mathbf{1}} C(W^{(1)}), \end{aligned} \tag{3.3}$$

where $C(W^{(m)})$ is the ordinary color factor, $\frac{1}{\text{Tr } \mathbf{1}}$ is the usual normalization of the lowest order, $C^{(0)} = \text{Tr } \mathbf{1}$, $\sum_d$ is the sum over the set of all non-trivial decompositions d of $W^{(m)}$ into webs of order $i < m$, and $\prod_{n_i}$ denotes the product of all webs n_i of order i ($1 \leq i < m$) in a particular decomposition d. The set of all non-trivial *decompositions* of a given web can be obtained by successively disentangling crossed gluon lines in the web by repeated application of the color identities given in Fig. 3.1.

In [77] Gatheral showed that webs in the original definition have what he called "maximally nonabelian" color weights $\sim \alpha_s^m C_F C_A^{m-1}$, where the C_is are the Casimir factors in the fundamental and adjoint representation, respectively. This statement, however, is misleading at orders $\geq \alpha_s^3$ [78]. We will see an example in Ch. 4, in the calculation of the N_f term contributing to the coefficient A at three loops.

In the following subsection we will clarify the above definitions in an example which shows how to factorize eikonal Feynman diagrams into sums of products of webs. This then leads directly to exponentiation. The recursive definition of the color weights of the webs ensures the factorization of the color parts. For the factorization of the Feynman eikonal integrals $\mathcal{F}$ we will make

repeated use of the eikonal identity [79]

$$\frac{1}{p\cdot k_1}\frac{1}{p\cdot(k_1+k_2)}+\frac{1}{p\cdot k_2}\frac{1}{p\cdot(k_1+k_2)}=\frac{1}{p\cdot k_1}\frac{1}{p\cdot k_2}, \tag{3.4}$$

illustrated in Fig. 3.3 a). This identity can be extended to an arbitrary number of soft gluons in a straightforward way by repeated application of Eq. (3.4): For two webs W_1 and W_2 with gluon legs $k_i\,(i=1,\ldots,m)$ and $l_j\,(j=1,\ldots,n)$ attached to an eikonal line with velocity p the generalized identity reads

$$\begin{aligned}\mathcal{F}(W_1)\mathcal{F}(W_2) \;&\sim\; \frac{1}{p\cdot k_1\, p\cdot(k_1+k_2)\ldots p\cdot(k_1+\ldots+k_m)}\\ &\quad\times\frac{1}{p\cdot l_1\, p\cdot(l_1+l_2)\ldots p\cdot(l_1+\ldots+l_n)}\\ &=\sum_{\text{perms}(n,m)} F,\end{aligned} \tag{3.5}$$

where the sum is over all Feynman diagrams F obtained by permuting the $n+m$ gluon lines such that the order of the k_i, and l_j, respectively, *within* each web is not changed. A simple example is shown in Fig. 3.3 b). The extension to more than two webs follows by repeating the above argument:

$$\sum_{F\,\text{in}\,d} F=\prod_{n_i}\mathcal{F}\left(W^{(i)}_{n_i}\right). \tag{3.6}$$

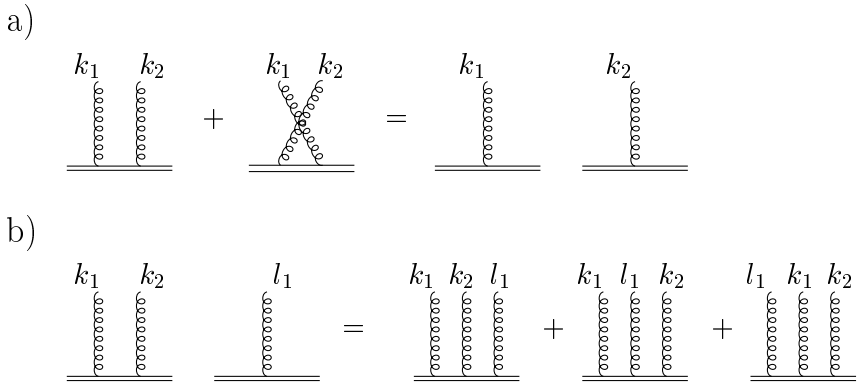

Figure 3.3: a) Eikonal identity for 2 gluons, and b) an illustration of the generalized eikonal identity Eq. (3.5) for two webs.

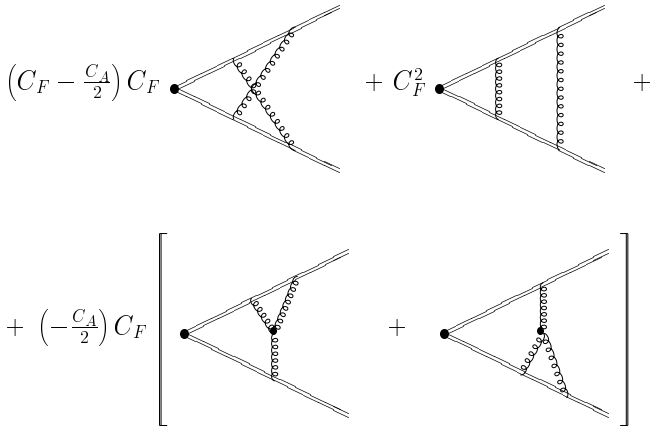

Figure 3.4: Diagrams contributing at $\mathcal{O}(\alpha_s^2)$ (excluding self-energies). The color factors are given for eikonal lines in the fundamental representation, omitting the overall normalization $\frac{1}{\mathrm{Tr}\ \mathbf{1}}$ everywhere.

3.1.2 An Example

We will show by induction that the terms in the perturbation series X in Eq. (3.1), normalized by the zeroth order contribution, can be reorganized into a sum of products of webs which can be rewritten as $\exp(Y)$. Therefore it is necessary and also instructive to start with the first nontrivial example, diagrams of $\mathcal{O}(\alpha_s^2)$. At this order we have the Feynman diagrams shown in Fig. 3.4, for quark or antiquark eikonal lines, excluding eikonal and gluon self-energies. Eikonal self-energies vanish if we work in Feynman gauge. The sum of diagrams at a given order in α_s is gauge invariant, of course. The contribution of the first two terms in Fig. 3.4 can be rearranged by applying Eqs. (3.3) and (3.4) as shown in Fig. 3.5.

Thus we arrive at the following series obtained by rearranging the expansion of X up to $\mathcal{O}(\alpha_s^2)$:

$$\begin{aligned} X &= \mathbf{1} + \sum_{\substack{\text{all webs}\\ \text{of order } 1}} \overline{C}\left(W^{(1)}\right)\mathcal{F}\left(W^{(1)}\right) + \\ &+ \frac{1}{2!}\Big(\sum_{\substack{\text{all webs}\\ \text{of order } 1}} \overline{C}\left(W^{(1)}\right)\mathcal{F}\left(W^{(1)}\right)\Big)^2 + \sum_{\substack{\text{all webs}\\ \text{of order } 2}} \overline{C}\left(W^{(2)}\right)\mathcal{F}\left(W^{(2)}\right) + \ldots, \end{aligned} \tag{3.7}$$

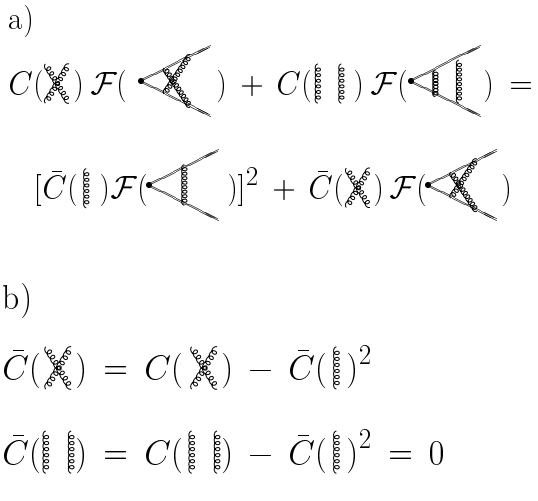

Figure 3.5: a) Rearrangement of the first two terms of Fig. 3.4 using Eq. (3.4), and b) Eq. (3.3).

which is illustrated in Fig. 3.6. The combinatorial factor $\frac{1}{2!}$ is necessary to avoid overcounting since two webs with the same structure are indistinguishable if the integration measure is symmetric in the real gluon momenta.

3.1.3 Exponentiation

Looking at the above example it is now clear that any Feynman diagram with two eikonal lines can be expressed as a sum of products of webs by applying Eqs. (3.3) and (3.6) repeatedly. By induction we arrive at the following equation for the set of Feynman diagrams of $\mathcal{O}(\alpha_s^n)$, $F^{(n)}$:

$$F^{(n)} = \sum_{\{n_i\}} \delta_{n \sum_i i n_i} \prod_i \frac{1}{n_i!} \Big(\sum_{\substack{\text{all webs} \\ \text{of order } i}} \overline{C}(W^{(i)}) \mathcal{F}(W^{(i)}) \Big)^{n_i}, \tag{3.8}$$

where i labels the order of the webs and the sum is over all sets $\{n_i\}$, $0 \leq n_i < \infty$ such that $\sum_i i\, n_i = n$. For example, at $\mathcal{O}(\alpha_s^3)$ we can have $n_1 = 3$ webs of order 1 ($\{3, 0, \ldots\}$), or $n_1 = 1$ webs of order 1 and $n_2 = 1$ webs of order 2 ($\{1, 1, 0, \ldots\}$), or $n_3 = 1$ webs of order 3 ($\{0, 0, 1, 0, \ldots\}$). The combinatorial factor of $\frac{1}{n!}$ is needed to avoid overcounting because of property 3.) of X, stated in the introduction to this section, namely that the

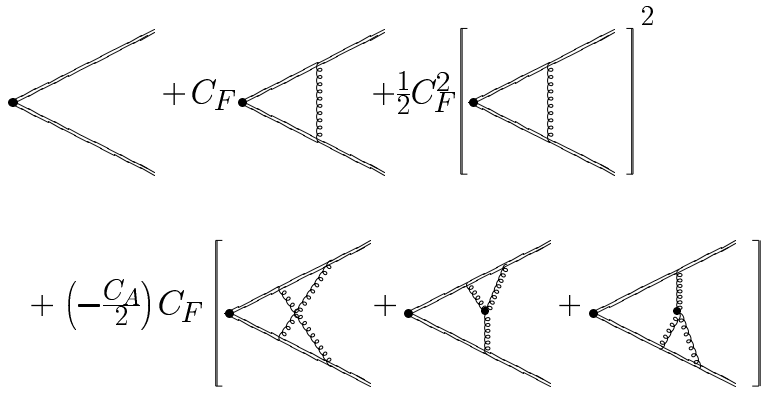

Figure 3.6: Graphical expression of the exponentiation up to webs of order 2 in Feynman gauge. The color weights are given for (anti)quark eikonal lines.

integration measure is symmetric in the real gluon momenta, for example $\mathcal{F}^{(1)}(k_1)\mathcal{F}^{(2)}(k_2,k_3) = \mathcal{F}^{(1)}(k_2)\mathcal{F}^{(2)}(k_1,k_3)$, which means that webs of the same structure are indistinguishable. Were property 3.) not fulfilled, the perturbation series would not exponentiate.

We now rearrange the original perturbation series given in powers of α_s^n

$$X = \sum_{n=0}^{\infty} F^{(n)}, \tag{3.9}$$

$$\begin{aligned}
X &= \sum_{n=0}^{\infty} \sum_{\{n_i\}} \delta_{n \sum_i i n_i} \prod_i \frac{1}{n_i!} \Big(\sum_{\substack{\text{all webs} \\ \text{of order } i}} \overline{C}(W^{(i)}) \mathcal{F}(W^{(i)}) \Big)^{n_i} \\
&= \sum_{\substack{\text{all possible} \\ \{n_i\}}} \prod_i \frac{1}{n_i!} \Big(\sum_{\substack{\text{all webs} \\ \text{of order } i}} \overline{C}(W^{(i)}) \mathcal{F}(W^{(i)}) \Big)^{n_i} \\
&= \prod_i \left\{ \sum_{n_i} \frac{1}{n_i!} \Big(\sum_{\substack{\text{all webs} \\ \text{of order } i}} \overline{C}(W^{(i)}) \mathcal{F}(W^{(i)}) \Big)^{n_i} \right\} \\
&= \prod_i \exp \Big(\sum_{\substack{\text{all webs} \\ \text{of order } i}} \overline{C}(W^{(i)}) \mathcal{F}(W^{(i)}) \Big),
\end{aligned} \tag{3.10}$$

where we have used the fact that for any function $f(n_i, i)$

$$\sum_{\substack{\text{all possible}\\ \{n_i\}}} \prod_i f(n_i, i) = \prod_i \sum_{n_i} f(n_i, i) \tag{3.11}$$

which is easy to see by comparing the expansions of the left and the right hand sides.

So the series exponentiates

$$X = e^Y, \quad Y \equiv \sum_i \Big(\sum_{\substack{\text{all webs}\\ \text{of order } i}} \overline{C}(W^{(i)}) \mathcal{F}(W^{(i)}) \Big). \tag{3.12}$$

This completes the proof that eikonal cross sections with two eikonal lines can be written as an exponent of an infinite sum of webs.

3.2 Cancellation of Subdivergences in the Exponent

Gatheral, Frenkel, and Taylor showed in [80] by explicit fixed-order calculations that infrared/collinear subdivergences cancel in the exponent. Here we will outline the proof of this cancellation, as well as of the cancellation of UV subdivergences involving the eikonal vertex, to all orders with the help of the identities in Fig. 2.2 in the soft approximation. The remaining UV subdivergences are removed via ordinary QCD counterterms, and thus an additional investigation of the renormalizability of the eikonal vertex is unnecessary.

To show the absence of subdivergences, let us rewrite Eq. (3.8) as

$$\sum_{\text{order } n} \bar{C}^{(n)} \mathcal{F}^{(n)} = F^{(n)}_{\text{conv}} + F^{(n)}_{\text{div}} - \sum_{\{n_i\}, i<n} \prod_i \frac{1}{n_i!} \Big(\sum_{\substack{\text{all webs}\\ \text{of order } i<n}} \overline{C}(W^{(i)}) \mathcal{F}(W^{(i)}) \Big)^{n_i}. \tag{3.13}$$

Eq. (3.13) means, that the sum of all webs at order n are given by the original perturbation series at that order where all lower-order webs have been subtracted out. The original perturbation series can be classified into terms without subdivergences, denoted by $F^{(n)}_{\text{conv}}$, and terms which contain subdivergences, $F^{(n)}_{\text{div}}$.

In eikonal cross sections, infrared/collinear divergences stem from the same momentum configuration as UV divergences. Since eikonal cross sections are scaleless, when a line becomes collinear to an eikonal it can carry infinite momentum in a light-like direction. But in this case we can employ the soft

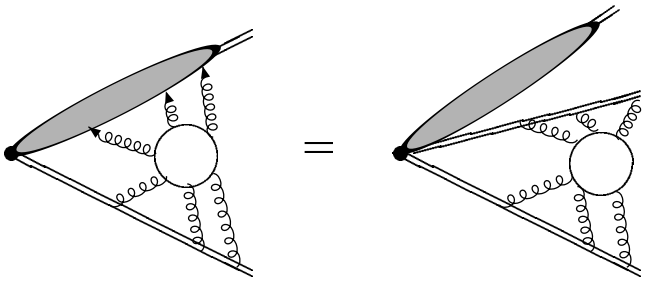

Figure 3.7: Factorization of jet-like collinear configurations, represented by the grey oval, from the eikonal cross section with the help of the soft approximation.

approximation described in Sect. 2.2.2 to factorize these jet-like configurations from the rest of the eikonal cross section. The reasoning follows Section 2.2.2, and we arrive at the equality shown in Fig. 3.7. The grey oval in the figure represents a specific jet-like configuration, collinear to one of the eikonal lines. The displayed equality states that the sum of all webs at a given order, where this jet-like configuration is connected to the rest of the eikonal cross section by soft gluons, can be expressed in the factored form shown on the right-hand side. As in Section 2.2.2, remainders are non-leading. Due to the definition of the color weights (3.3), the right-hand side does not constitute a web of the same order, but rather a product of webs of lower orders. The contribution shown on the left-hand side of Fig. 3.7 is a contribution to $F_{\text{div}}^{(n)}$ of Eq. (3.13). In (3.13), however, we subtract out all products of webs of lower orders, thus cancelling the divergent contributions because of the equality shown in Fig. 3.7. Using the equality in Fig. 3.7 and Eq. (3.13) recursively for every IR/collinear subdivergence, we see that the sum of webs at a given order is free of such subdivergences.

To summarize, the collinear configuration does not contribute at order n after summing over all relevant webs at that order, because this collinear configuration has already been taken into account at a lower order $< n$. The only possible collinear and UV vertex divergence can occur in the final, overall integral. Of course, in the original perturbative expansion X of the eikonal cross section in Eq. (3.9) these collinear and UV subdivergent configurations contribute, but in the exponent Y of Eq. (3.12) they only appear as overall divergences.

3.3 Exponentiation for Quantities with Three Eikonal Lines

Above we have presented the necessary ingredients to show that this exponentiation generalizes to three eikonal lines. The proof is analogous to the proof for two eikonal lines, because the vertex structure is again a singlet in color space - T^a_{ij} for $q(i)\,\bar{q}(j)\,g(a)$ or if_{abc} for $g(a)\,g(b)\,g(c)$, respectively, where q and g denote a quark and a gluon, respectively, the i, j, a, b, c are color indices. Soft gluons do not change this basic color flow. This is not true, however, for more than three eikonal lines.

To be specific, let us consider a process involving a $q(i)$-, a $\bar{q}(j)$-, and a $g(a)$-eikonal line, for example $q\,\bar{q} \to g\,\gamma +$ soft gluons. We want to show that

$$X' = \exp Y'. \tag{3.14}$$

The properties of Y', the recursive definition of the color weights Eq. (3.3), and the application of the eikonal identity (3.4) are exactly analogous to the simpler case of two eikonal lines, with the normalization

$$C(W^{(0)}) = T^a_{ij} T^a_{ji} \tag{3.15}$$

instead of Tr **1** in Eq. (3.3):

$$\begin{aligned} \overline{C'}(W^{(m)}) &\equiv \frac{1}{C(W^{(0)})} C(W^{(m)}) - \sum_d \prod_{n_i} \overline{C'}(W^{(i)}_{n_i}), \\ \overline{C'}(W^{(1)}) &\equiv \frac{1}{C(W^{(0)})} C(W^{(1)}), \end{aligned} \tag{3.16}$$

The only difference from the 2-eikonal case is the number and complexity of webs contributing at a given order.

The proof of exponentiation resulting in Eq. (3.8) and then in Eq. (3.14) is again by induction on the order. The first web where all three eikonal lines could in principle be connected occurs at order 2. Any contribution at order 2 can be factored into contributions of order 1 with the help of the eikonal identity Eq. (3.4), graphical examples are shown in Fig. 3.8. These terms which factor into order-1 webs connecting only two eikonal lines are exactly the terms that stem from

$$\frac{1}{2!}\Big(\sum_{\substack{\text{all webs} \\ \text{of order } 1}} \overline{C'}(W^{(1)}) \mathcal{F}(W^{(1)}) \Big)^2 .$$

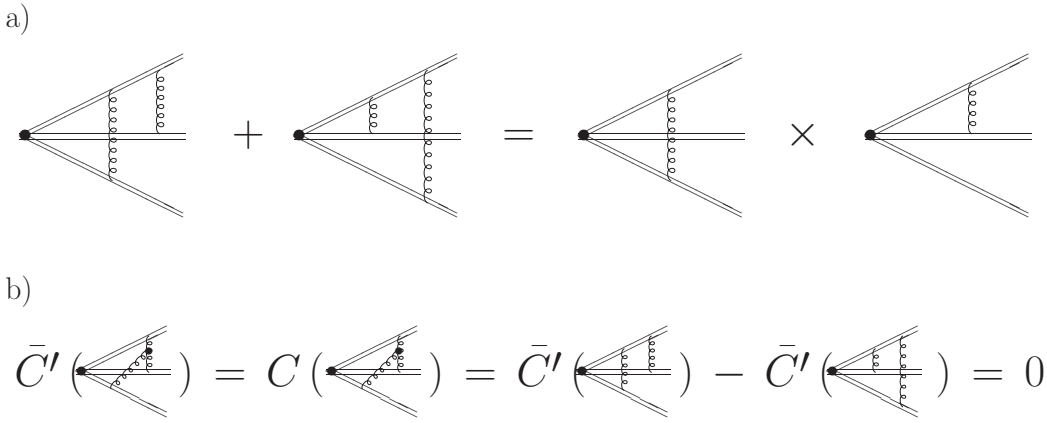

Figure 3.8: a) Factorization of contributions at order 2 into webs of order 1. b) Diagram with color weight 0, and decomposition into diagrams of Fig. 3.8 a) using Fig. 3.1.

There are no webs at order 2 that connect all three lines, since the color weight $\overline{C'}$ of all the diagrams in Fig. 3.8 b) is 0. This also applies to the case when all lines are gluon lines. In that case we apply the Jacobi identity Fig. 3.1 b) instead of 3.1 a) to arrive at a color weight $\overline{C'} = 0$.

At order 3 or higher, this observation does not remain true. Then all three eikonal lines can be connected. Nevertheless, the combinatorics remains the same, since the definition of the color weights is not modified for color singlet configurations except for the overall normalization (3.15).

By induction we arrive at Eq. (3.8) with webs of a slightly more complicated structure. Summation of Eq. (3.8) over all powers of α_s^n results again in exponentiation, and the full cross section consisting of three eikonal lines can be written as

$$X' = e^{Y'}, \quad Y' \equiv \sum_i \Big(\sum_{\substack{\text{all webs} \\ \text{of order } i}} \overline{C'}(W^{(i)}) \mathcal{F}(W^{(i)}) \Big). \tag{3.17}$$

The case of three gluon eikonal lines, $g(a)\, g(b)\, g(c)$, is analogous to the one considered above, with

$$C(W^{(0)}) = i f_{abc} i f_{cba} \tag{3.18}$$

instead of (3.15).

This completes the proof of exponentiation for three eikonal cross sections which are free of subdivergences, following the same argumentation as for two eikonal cross sections, given in Sec. 3.2.

3.4 Implications for Physical Observables

As we have seen in Chapter 2, eikonal cross sections contain all information about soft radiation, and their anomalous dimensions control double logarithms that arise from soft-collinear emission. The exponentiation of webs directly implies this exponentiation of double logarithmic behavior. In addition, important consequences on the behavior of power corrections arise, as was also observed, for example, in Refs. [81, 82].

3.4.1 Properties of Webs

The properties proved in the Section 3.2, and the invariance under rescalings of the light-like eikonal momenta give the following constraints on the possible dependence of webs on the web-momentum k and the eikonal momenta, denoted in the following by β_i, $i = 1, 2$ or $i = 1, 2, 3$:

- Invariance under rescalings requires that each eikonal momentum appears with the same power in the numerator as in the denominator of the argument.
- After regulating the one overall UV divergence the webs obey

$$\mu \frac{d}{d\mu} W(k, \beta_i, \mu, \alpha_s(\mu), \varepsilon) = 0. \tag{3.19}$$

  Here μ is the renormalization scale, and ε the dimensional regulator.
- The fact that they have at most one overall IR divergence, coupled with a single overall collinear divergence requires that the factors $k \cdot \beta_i$ occur only once for each β_i.

From the above properties we deduce for $n = 2$ eikonal lines

$$W\left(k, \beta_1, \beta_2, \mu, \alpha_s(\mu), \varepsilon\right) = W\left(k^2, \frac{(k \cdot \beta_1)(k \cdot \beta_2)}{\beta_1 \cdot \beta_2}, \mu^2, \alpha_s(\mu), \varepsilon\right). \tag{3.20}$$

The last property allows us to rewrite this as

$$W\left(k^2, \frac{(k \cdot \beta_1)(k \cdot \beta_2)}{\beta_1 \cdot \beta_2}, \mu^2, \alpha_s(\mu), \varepsilon\right) = W\left(k^2, k^2 + k_\perp^2, \mu^2, \alpha_s(\mu), \varepsilon\right), \tag{3.21}$$

where $k_\perp$ is the momentum transverse to the plane spanned by β_1 and β_2. It is easy to derive this form using a Sudakov parametrization for k,

$$k^\mu = x\beta_1^\mu + \frac{k^2 + k_\perp^2}{2x}\beta_2^\mu + k_\perp^\mu. \tag{3.22}$$

We have reduced the maximum number of independent parameters from four, k^μ, to two, k^2 and $k_\perp^2$.

These observations do not remain true for the case of three eikonal lines. Nevertheless, our argumentation on two-eikonal webs also applies to a subset of three-eikonal cross sections, which we will call in the following "degenerate". In degenerate webs only two out of the three eikonals are connected. As we have seen in Sec. 3.3, these are the only contributions up to, and including, next-to-leading order. Nondegeneracy begins at order 3. For degenerate webs, the dependence splits into the sum

$$W = W_{ab} + W_{ac} + W_{bc}, \tag{3.23}$$

where a, b, c are the colors carried by the three eikonal lines, in the fundamental or adjoint representation, respectively.

3.4.2 Leading Logarithms of the Thrust from Eikonal Exponentiation

We now return to the study of the thrust cross section to illustrate the consequences of the above observations. In the previous chapter we have exponentiated large logarithms by solving renormalization group equations. The final result for the thrust cross section in moment space is given in Eq. (2.115). However, as we have seen in this chapter, eikonal cross sections exponentiate directly. Here we will demonstrate how the exponentiation of eikonal cross sections and the properties listed in Section 3.4.1 lead to the same form as Eq. (2.115).

The thrust is related to the minus momentum, from Eq. (2.79),

$$\tau = 1 - T = \frac{\sqrt{2}}{Q} \sum_i k_i^-. \tag{3.24}$$

The factorized thrust contains also an eikonal cross section, as displayed in Fig. 2.8. This eikonal cross section exponentiates. Taking moments with respect to $\tau = 1 - T$, we obtain with Eq. (3.21),

$$\begin{aligned} \tilde{\sigma}_T^{(\mathrm{eik})}(N) \;=\; \exp\Bigg\{ 2 \int_0^{Q^2} \frac{d^{2-2\varepsilon} k_\perp}{\Omega_{1-2\varepsilon}} \int_0^{Q^2-k_\perp^2} dk^2 \int_{k_\perp^2/(\sqrt{2}Q)}^{|k_\perp|/\sqrt{2}} \frac{dk^-}{2k^-} \left(e^{-N/Q\sqrt{2}k^-} - 1 \right) \\ \times W\left(k^2, k^2 + k_\perp^2, \mu^2, \alpha_s(\mu), \varepsilon\right) \Bigg\}. \end{aligned} \tag{3.25}$$

The factor of 2 is due to adding the complex conjugate contributions. Here $\Omega_{1-2\varepsilon} = 2\pi^{1-\varepsilon}/\Gamma(1-\varepsilon)$ is the dimensionally continued transverse angular volume, and the limits of the integrals correspond to the one-particle phase space [30]. We have normalized the virtual contributions to 1 for $N = 0$, and the single-gluon emission in $\overline{\text{MS}}$ scheme to

$$W^{(1),\,\text{real}}(k) = \frac{2C_F\alpha_s}{\pi}\mu^{2\varepsilon}\frac{1}{k_\perp^2}\delta_+(k^2). \tag{3.26}$$

Using the equivalence of the minus momentum to τ, Eq. (3.24) we obtain

$$\begin{aligned}\tilde{\sigma}_T^{(\text{eik})}(N) &= \exp\left\{\int_0^{Q^2}\frac{dk_\perp^2}{k_\perp^{2\varepsilon}}\int_{k_\perp^2/Q^2}^{k_\perp/Q}\frac{d\tau}{\tau}\left(e^{-N\tau}-1\right)\right. \\ &\qquad\left.\times\int_0^{Q^2-k_\perp^2}dk^2\,W\left(k^2,k^2+k_\perp^2,\mu^2,\alpha_s(\mu),\varepsilon\right)\right\},\end{aligned} \tag{3.27}$$

where we have used the azimuthal symmetry of the webs, Eq. (3.21).

From the considerations in the previous two sections we know that there are no internal divergences. Moreover, for fixed $k_\perp$ the webs do not require overall UV regularization, and the convergence occurs on a scale set by $k_\perp$, independent of N or Q. Thus we can formally expand the integral over k^2 in inverse powers of Q^2 [81]

$$\int_0^{Q^2-k_\perp^2}dk^2\,W\left(k^2,k^2+k_\perp^2,\mu^2,\alpha_s(\mu),\varepsilon\right) = \frac{2A\left(\alpha_s(k_\perp^2)\right)}{(k_\perp^2)^{1-2\varepsilon}} + \mathcal{O}\left(\frac{k_\perp^{2\varepsilon}}{Q^2}\right). \tag{3.28}$$

We have used the independence of the webs of the renormalization scale, Eq. (3.19), to set the scale of the running coupling to $k_\perp^2$. We will confirm the form (3.28) by explicit calculation in Chapter 4 below.

Eq. (3.27) can then be written as

$$\tilde{\sigma}_T^{(\text{eik})}(N) = \exp\left\{2\int_0^{Q^2}\frac{dk_\perp^2}{k_\perp^2}A\left(\alpha_s(k_\perp^2)\right)\int_{k_\perp^2/Q^2}^{k_\perp/Q}\frac{d\tau}{\tau}\left(e^{-N\tau}-1\right)\right\}. \tag{3.29}$$

We have neglected all terms that vanish as $k_\perp \to 0$.

The form (3.29), obtained directly from the exponentiation of webs, is identical to the term with A_c in Eq. (2.115) [83]. To see this, we use the relation

$$e^{-x/y} - 1 \approx -\theta\left(x - ye^{-\gamma_E}\right), \tag{3.30}$$

which is valid to next-to-leading logarithmic order. Upon relabelling $k_\perp \to \lambda'$ we obtain

$$\tilde{\sigma}_T^{(\mathrm{eik})}(N) = \exp\left\{-2\int_0^Q \frac{d\lambda'}{\lambda'} A\left(\alpha_s(\lambda')\right) \int_{\lambda'^2/Q^2}^{\lambda'/Q} \frac{d\tau}{\tau}\theta\left(e^{\gamma_E} N\tau - 1\right)\right\}. \tag{3.31}$$

Then we change variables,

$$\lambda = \frac{\tau Q^2}{2\lambda'}, \tag{3.32}$$

and exchange orders of integration. We arrive at

$$\tilde{\sigma}_T^{(\mathrm{eik})}(N) = \exp\left\{-2\int_{Q/(2N)}^{Q/2} \frac{d\lambda}{\lambda} \int_{e^{-\gamma_E} Q^2/(2N\lambda)}^{2\lambda} \frac{d\lambda'}{\lambda'} A\left(\alpha_s(\lambda')\right)\right\}. \tag{3.33}$$

We have reproduced the term in Eq. (2.115) with the double integral, with

$$\begin{aligned} c_1 &= e^{-\gamma_E}, \\ c_2 &= 2. \end{aligned} \tag{3.34}$$

The remaining terms in (2.115) with a single integral, on the other hand, account for the difference between the eikonal cross section and the full partonic cross section for the thrust [81]. This is analogous to the jet-remainders in Eq. (2.75) that match the eikonal cross section to the full parton distribution function as $x \to 1$.

3.4.3 Power Corrections

As we have seen in the introduction, due to the asymptotic nature of the perturbation series, pQCD calculations can only be accurate up to power corrections $\sim 1/Q^p$, where Q is the hard scale in the problem. In general, mean values $\langle\mathcal{O}\rangle$ or integrated cross sections depend on hadronization corrections and other non-perturbative effects in a more trivial way than differential observables $d\sigma/(d\mathcal{O})$:

$$\frac{1}{\sigma_{\mathrm{tot}}}\frac{d\sigma}{d\mathcal{O}} = \frac{d\sigma_{\mathrm{PT}}}{d\mathcal{O}} + f_{\mathrm{hadr}}(Q^{-p}, \mathcal{O}), \tag{3.35}$$

$$\langle\mathcal{O}\rangle = \langle\mathcal{O}\rangle_{\mathrm{PT}} + \frac{\lambda_p}{Q^p}. \tag{3.36}$$

Here the subscript PT is the perturbatively calculable part, and f_{hadr} is a non-perturbative function, related to the nonperturbative parameter λ_p, $\lambda_p/Q^p =$

$\int d\mathcal{O}\,\mathcal{O} f_{\rm hadr}$. The power p is a measure of the sensitivity of the observable $\mathcal{O}$ to confinement physics.

However, perturbation theory itself contains information about the form of these non-perturbative corrections. Sensitivity of an observable to long-distance behavior is adjustable by studying its Laplace transform, Eq. (2.88). The value of N controls the influence of long-distance effects. For large N, non-perturbative corrections become important.

The form for the double logarithmic terms derived from eikonal exponentiation, Eq. (3.29), allows us to deduce the form of power corrections. Using (3.29) with the one-loop running coupling at scale $k_\perp^2$ reexpressed in terms of the running coupling at the hard scale Q^2 via Eq. (A.10), we arrive at

$$\begin{aligned}\tilde{\sigma}_T^{(\rm eik)}(N) &= \exp\left\{2\int\limits_0^{Q^2}\frac{dk_\perp^2}{k_\perp^2}A\left(\frac{\alpha_s(Q^2)}{1+\frac{\beta_0}{4\pi}\alpha_s(Q^2)\ln\frac{k_\perp^2}{Q^2}}\right)\right.\\ &\left.\times\int\limits_{k_\perp^2/Q^2}^{k_\perp/Q}\frac{d\tau}{\tau}\left(e^{-N\tau}-1\right)\right\}. \qquad (3.37)\end{aligned}$$

Since N is conjugate to τ, and since we are interested in the infrared region for small $k_\perp^2$, we can expand the exponential in the exponent. This results in

$$\begin{aligned}\tilde{\sigma}_T^{(\rm eik)}(N) &= \exp\left\{2\sum_{n=1}^{\infty}\frac{1}{n\,n!}(-N)^n\int\limits_0^{Q^2}\frac{dk_\perp^2}{k_\perp^2}A\left(\frac{\alpha_s(Q^2)}{1+\frac{\beta_0}{4\pi}\alpha_s(Q^2)\ln\frac{k_\perp^2}{Q^2}}\right)\right.\\ &\left.\times\left(\frac{k_\perp}{Q}\right)^n\left[1-\left(\frac{k_\perp}{Q}\right)^n\right]\right\}, \qquad (3.38)\end{aligned}$$

after performing the integration over τ. We now change variables

$$t_n \equiv n\,t = \frac{n}{2}\alpha_s(Q^2)\ln\frac{Q^2}{k_\perp^2}, \qquad (3.39)$$

and obtain

$$\begin{aligned}\tilde{\sigma}_T^{(\rm eik)}(N) &= \exp\left\{2\sum_{n=1}^{\infty}\frac{1}{n^2\,n!}\frac{1}{\alpha_s(Q^2)}(-N)^n\int\limits_0^{\infty}dt_n\,A\left(\frac{\alpha_s(Q^2)}{1-\frac{\beta_0}{2\pi\,n}t_n}\right)e^{-\frac{t_n}{\alpha_s(Q^2)}}\right.\\ &\left.\times\left[1-e^{-\frac{t_n}{\alpha_s(Q^2)}}\right]\right\}. \qquad (3.40)\end{aligned}$$

The integral over t has the form of the Borel integral introduced in the introduction, Eq. (1.13). The Borel integral (3.40) has singularities at

$$t_n = \frac{2\pi\, n}{\beta_0}, \quad \text{or equivalently,} \quad t = \frac{2\pi}{\beta_0}, \tag{3.41}$$

leading with Eq. (1.11) to an ambiguity proportional to

$$e^{-\frac{2\pi\, n}{\beta_0\, \alpha_s(Q^2)}} \sim \left(\frac{\Lambda_{\rm QCD}}{Q}\right)^n. \tag{3.42}$$

The crucial factor in the exponent that results in power corrections proportional to $\sim 1/Q$ comes from the upper limit in (3.40), and is therefore due to radiation at wide angles. In summary, the thrust behaves as

$$\ln \tilde{\sigma}_T(N,Q) = \ln \tilde{\sigma}_{T,\,\rm PT}(N,Q) + \ln \tilde{\sigma}_T^{\rm power}\left(\frac{N}{Q}\right) + \mathcal{O}\left(\frac{N}{Q^2}\right). \tag{3.43}$$

The last term is power-suppressed by $1/Q$ relative to the leading non-perturbative corrections. This term comes from the lower limit of the integral in (3.37), as can be seen in (3.40), corresponding to radiation close to the jets.

In the above arguments we have used the one-loop running coupling. But the occurrence of poles in the Borel integral is not connected to the specific form of the one-loop coupling. That is, the ambiguity above is not connected to the Landau pole. Above we have only used the relation between the coupling evaluated at two different scales, independent of $\Lambda_{\rm QCD}$. Although this relation is nonlinear at higher orders (see Eq. (A.7)), conclusions similar to the above are reached in studies of couplings without a simple Landau pole [84, 85, 86], as also the derivation of the result (3.43) for the thrust with a variety of methods shows [83, 87, 88, 89, 90, 91, 92, 93, 94].

Above, we have shown that eikonal cross sections exponentiate, and have illustrated the consequences of this exponentiation. The exponentiation simplifies the explicit calculation of the term A significantly at higher orders. We now turn to the calculation of A, that is, the anomalous dimension of an eikonal cross section, also called the cusp anomalous dimension of a Wilson loop.

Chapter 4

Higher Orders in $A(\alpha_s)/[1-x]_+$ of Non-Singlet Partonic Splitting Functions

In the previous chapters we have developed the tools necessary for the computation of eikonal diagrams at higher orders. We have seen in Chapters 2 and 3 that soft-collinear emission is controlled by the anomalous dimensions of eikonal cross sections. In this Chapter we will develop a simplified method to calculate this anomalous dimension at higher orders which is equivalent to the singular part of the partonic splitting functions, P_{ff} (see Eq. (2.44)).

To leading power in N the moments of the partonic splitting functions,

$$\gamma_{ff}(N) = \int_0^1 dx x^{N-1} P_{ff}(x), \tag{4.1}$$

take the simple form [68, 95]

$$\gamma_{ff}(N, \alpha_s) = A_f(\alpha_s) \ln N + B_f(\alpha_s) + \mathcal{O}\left(\frac{1}{N}\right), \tag{4.2}$$

or in x-space,

$$P_{ff}(x, \alpha_s) = A_f(\alpha_s) \left[\frac{1}{1-x}\right]_+ + B_f(\alpha_s)\delta(1-x) + \mathcal{O}\left([1-x]^0\right), \tag{4.3}$$

with the plus distribution as defined in Eq. (2.86). The term with the plus distribution represents the cancellation of a single overall infrared divergence. The coefficient of $\ln N$ in Eq. (4.2) can be expanded in the strong coupling,

$$A_f(\alpha_s) = \sum_n \left(\frac{\alpha_s}{\pi}\right)^n A_f^{(n)}. \tag{4.4}$$

As we have seen above, the exact knowledge of the terms $A^{(n)}$ is important for $x \to 1$ (large N), since there large logarithmic corrections arise due to soft-gluon radiation. These corrections need to be resummed in order to be able

to make reliable predictions within perturbation theory. The knowledge of the coefficients $A^{(3)}$ and $B^{(2)}$ is required at the next-to-next-to-leading logarithmic (NNLL) level [96] (compare to Eq. (2.115)).

The anomalous dimensions $\gamma_{ff}(N)$ are currently known to two loops [17, 97, 98, 99, 100, 101, 102], and a general formula for the $\alpha_s^n N_f^{n-1}$-terms of $\gamma_{ff}(N)$ was computed by Gracey [103]. From the known exact values for some specific moments and the behavior at small x [104, 105, 106, 107] a numerical parametrization for the coefficient $A^{(3)}$ was obtained in [96, 108, 109], although, for the above reasons, the exact knowledge of this term is desirable. A calculation at the three-loop level by Moch, Vermaseren, and Vogt of the splitting functions via the operator product expansion (OPE) in moment space will be completed in the near future [110]. Their results for the fermionic contributions are now available [111]. However, the method presented here, although only applicable for the calculation of the coefficients A, not of the complete x-dependence, is complementary to the OPE method in two ways: we calculate only virtual diagrams, and furthermore, it is much less computationally intensive, thus a computation of the four- or even higher loop coefficients may be feasible. The work presented in this chapter was published in [12].

In Chapter 2 we have related the anomalous dimension of PDFs to the anomalous dimension of an eikonal cross section which exponentiates. A similar observation was made by Korchemsky [68], who related the anomalous dimension of PDFs, Eq. (4.3), with the cusp anomalous dimension of a Wilson loop. His work was performed in a noncovariant axial gauge, whereas here we will use Feynman gauge throughout. Korchemsky's observation was used in [112] for the calculation of the two-loop coefficient $A^{(2)}$, which was done in Feynman gauge. The work of Ref. [112] was also based on the renormalization properties and exponentiation of Wilson loops (see [73, 113, 114, 115, 116, 117, 118] and references therein). This approach is related to ours. However, the additional observations we make result in several advantages. The number of diagrams contributing at each order is decreased by working with light-like eikonals. Furthermore, we can restrict ourselves only to virtual graphs. With the help of Ward identities we have shown explicitly the absence of infrared (IR) subdivergences and the cancellation of ultraviolet (UV) subdivergences at the eikonal vertex, leaving only the usual QCD UV divergences.

Below we first relate the renormalization properties of PDFs with those of webs, then summarize the method in light-cone ordered perturbation theory. We rederive as examples the one- and two-loop coefficients $A^{(1)}$ and $A^{(2)}$. In Section 4.4 we derive a formula for the coefficients of $A^{(n)}$ proportional to

N_f^{n-1}, which agrees with the corresponding contribution computed by Gracey [103] using an effective theory. We end by illustrating the steps necessary for the complete calculation of the 3-loop coefficient $A^{(3)}$. The IR structure of $A^{(3)}$ is explored for the graphs contributing at $\alpha_s^3 N_f$, which we calculate exactly.

4.1 Renormalization of Parton Distribution Functions and of Webs

4.1.1 Renormalization of Parton Distribution Functions

As was shown in [65], the parton distribution functions, defined in their unrenormalized form in terms of nonlocal operators (2.46), obey the evolution equation (2.44), where the kernel P_{ab} is found from the usual relation [13, 31, 65]

$$P_{ff}(\alpha_s, x) = A_f(\alpha_s) \left[\frac{1}{1-x}\right]_+ + \ldots = -\frac{1}{2} g_s \frac{\partial}{\partial g_s} \ln Z_1^A \left[\frac{1}{1-x}\right]_+ + \ldots, \quad (4.5)$$

where $\ln Z_1^A$ denotes the $\frac{1}{\varepsilon}$-pole of the counterterm which multiplies the plus-distribution, plus scheme dependent constants, if we work in a minimal subtraction scheme with dimensional regularization. Above we only exhibit the term that is singular as $x \to 1$, since it is this term which we want to extract from the renormalization of our factorized form, Eq. (2.75).

From Eq. (2.75) we observe that only the eikonal cross section can contribute to the A-term proportional to a plus-distribution. This is because the hard functions are off-shell by $\mathcal{O}(xp^+)$, and the jet-remainders are purely virtual, thus cannot contain plus-distributions. Therefore, their renormalization has to be proportional to $B_f\, \delta(1-x)$, as was observed in [81].

It is thus the renormalization of a color singlet eikonal vertex which we have to study, in order to compute the coefficients $A^{(n)}$ in (4.4).

4.1.2 Renormalization of Webs

For definiteness, we pick the incoming line ξ moving in the plus direction, and the outgoing eikonal β in the minus direction, and since quantities built from eikonal lines are scaleless, we can scale the eikonal velocities to 1.

$$\begin{aligned} \xi &= (1, 0, 0_\perp) \\ \beta &= (0, 1, 0_\perp) \end{aligned} \quad (4.6)$$

in light-cone coordinates. This choice will simplify the calculations considerably, as we will see below.

With the considerations in Sec. 3.4.1, we can write the contributions from virtual webs of order n to the eikonal cross section as

$$2\int \frac{d^{2-2\varepsilon}k_\perp}{(2\pi)^{1-2\varepsilon}} \int_0^\infty \frac{dk^+}{2k^+} \int dk^2 W_{aa}^{(n)}\left(k^2, k^2+k_\perp^2, \alpha_s(\mu^2), \varepsilon\right)$$
$$= 2\,\bar{C}_a^{(n)} \left(\frac{\alpha_s(\mu^2)}{\pi}\right)^n \left(\mu^2\right)^{l\varepsilon} (4\pi)^{l\varepsilon}\, K(\varepsilon) \int \frac{d^{2-2\varepsilon}k_\perp}{(k_\perp^2)^{1+(l-1)\varepsilon}} \int_0^\infty \frac{dk^+}{k^+}, \quad (4.7)$$

where l is an integer $\leq n$, and K contains numerical factors (including factors of π) and is, in general, a function of ε due to the regulation of infrared and UV (sub)divergences. Above, on the left hand side, all internal momenta have been integrated over, as well as k^-, and internal UV divergences have been renormalized. The integration over k^2 results in terms $\sim \frac{1}{(k_\perp^2)^{(l-1)\varepsilon}}$. For graphs including (local) counterterms $l < n$, whereas for graphs with n loops $l = n$. Both virtual webs and their complex conjugates contribute to the overall factor of 2. The structure of the integral over k^+ follows from boost invariance. In Eq. (4.7), this integral is divergent, but these divergences cancel against the corresponding real contributions, and therefore do not affect the anomalous dimension of the eikonal vertex. The k^+-integral plays the role of $\frac{dx}{1-x}$ for the full parton-in-parton distribution functions (cf. Eq. (2.70)), after combining real and virtual graphs. It suffices to consider only virtual graphs, since real and virtual graphs built out of eikonal lines have the same IR singularity structure, which, due to the scalelessness of virtual graphs, is equivalent to the UV structure:

$$\frac{1}{\varepsilon} + \frac{1}{(-\varepsilon)} = 0. \quad (4.8)$$

In other words, the coefficients of the UV poles are equal to those of the IR poles.

The final scaleless $k_\perp$ integral provides the n-loop UV counterterm which contributes to the anomalous dimension P_{ff}, Eq. (4.3). To isolate the UV pole we temporarily introduce a mass

$$\int \frac{d^{2-2\varepsilon}k_\perp}{(k_\perp^2+m^2)^{1+(l-1)\varepsilon}} = \pi^{1-\varepsilon} \frac{\Gamma(l\varepsilon)}{\Gamma(1+(l-1)\varepsilon)} \left(m^2\right)^{-l\varepsilon}. \quad (4.9)$$

The counterterm is then given, as usual, by minus the pole terms after expanding in ε. After summing over the contributions of all webs at a given order and their counterterms for subdivergences, all nonlocal terms ($\sim \ln \frac{\mu^2}{m^2}$) cancel as

well as UV vertex counterterms and IR divergences, and we obtain the n-loop counterterm contributing at $x \to 1$, which can be written as a series in ε:

$$Z^{(n)\,A} = \sum_{m=1}^{n} \frac{1}{\varepsilon^m} \left(\frac{\alpha_s(\mu^2)}{\pi} \right)^n a_m^{(n)} \int_0^\infty \frac{dk^+}{k^+}, \tag{4.10}$$

with purely numerical coefficients $a_m^{(n)}$. Because webs exponentiate, the counterterm for UV divergences in the perturbative expansion of a non-singlet parton distribution is given by

$$Z^A = \exp\left\{ \sum_{m=1}^{\infty} \sum_{n=1}^{m} \frac{1}{\varepsilon^m} \left(\frac{\alpha_s(\mu^2)}{\pi} \right)^n a_m^{(n)} \int_0^\infty \frac{dk^+}{k^+} \right\} \tag{4.11}$$

in the limit $x \to 1$, as indicated by the superscript A. As noted above, the notation $\int_0^\infty dk^+/k^+$ is equivalent to $[1/(1-x)]_+$. Now it is trivial to extract the contribution to P_{ff}. From (4.5) and (4.11) we get

$$A_f^{(n)} = -n a_1^{(n)}. \tag{4.12}$$

As emphasized above, internal UV divergences, including the usual QCD divergences and divergences at the eikonal vertex, have to be renormalized. Further complications arise because collinear/IR divergences cancel only after summing over all diagrams at a given order, so an individual diagram has in general UV singularities multiplying IR/collinear singularities. Our method to resolve these technical problems is most transparent in light-cone ordered perturbation theory [56, 57, 58] (see Appendix B.3), which is equivalent to performing all minus integrals of all loops, because it allows us to identify UV divergent loops in eikonal diagrams more easily.

4.2 Summary of the Method in LCOPT

The method can be summarized as follows, details will be given below:

1. We start with the expressions in LCOPT, as introduced in Section 2.2.2 and Appendix B.3, for the set of webs at a given order with a fixed coupling. The number of web-diagrams is much less than the number of all possible diagrams at a given order. Moreover, since we work in Feynman gauge, the number of possible webs is further reduced. For example, at order 2, as we will see below, only three diagrams contribute, aside from gluon self-energies.

2. Ultraviolet divergent internal $k_{\perp,i}$-integrals are regularized via dimensional regularization, with $\varepsilon > 0$. At this stage we do not yet encounter IR/collinear singularities since all integrals over transverse momenta are performed at fixed plus momenta.

3. We add the necessary QCD counterterms and the counterterms for the eikonal vertex which has to be renormalized as a composite operator. As we showed in Section 3.2, the sum of the latter cancels because of the recursive definition of webs and a Ward identity. However, in the intermediate stages the vertex counterterms are necessary to make individual diagrams UV finite.

4. After elimination of the UV singularities we dimensionally continue to $\varepsilon < 0$ to regulate the IR/collinear plus-integrals. It follows from the rules for LCOPT that all internal plus momenta are bounded by the total k^+ flowing into the minus eikonal. Therefore, the integrals over these internal plus momenta give no UV subdivergences.

5. When we sum over the set of diagrams at a given order the IR divergent parts cancel, as well as the UV counterterms for the vertex, thus also the internally UV divergent vertex parts cancel.

6. The final scaleless $k_\perp$ integral provides the UV counterterm contributing to the anomalous dimension (see Eqs. (4.7)-(4.12)).

We start by writing down all light-cone ordered diagrams of a given covariant Feynman diagram. All momenta in crossed gluon ladders have to be chosen independent of each other, such that they all flow through the eikonal vertex, since we seek the anomalous dimension for this vertex. Because ξ has no minus-component (cf. Eq. (4.6)), we have $q^- = 0$ in Eq. (B.32) of the appendix when applying the Feynman rules for LCOPT in our case. This can be depicted graphically by contracting all propagators on the minus-eikonal (here β) to a point, which coincides with the eikonal vertex. Two-loop examples can be found in Fig. 4.2. Sometimes, numerators stemming from triple-gluon vertices or quark propagators cancel the corresponding propagators on the plus-eikonal ($\xi \cdot k = k^-$). Graphically, this can again be described by contracting these propagators to a point. Then we can read off easily from the various light-cone ordered diagrams the analytical expressions, whose $k_{\perp,i}$-integrals we perform, and renormalize.

We need QCD counterterms and counterterms for the effective vertex. More specifically, by QCD counterterms we mean the usual gluon self-energy

counterterms, as well as the counterterms for triple-gluon vertices and eikonal-gluon-eikonal vertices. The latter are UV divergent in any covariant diagram, however, this is not necessarily the case for all LCOPT diagrams found from a covariant diagram. Examples will be given below. Self-energies of the light-like eikonal lines vanish in Feynman gauge. Both types of counterterms are found via the (recursive) BPHZ-formalism [60, 119, 120], and the subdivergences are identified with the help of naive power-counting on a graph-by-graph basis.

4.2.1 Remark About Eikonal Integrals

The usual methods for treating loop-integrals (see, for example, Appendix B and [121]) aim at reducing combinations of propagators to complete squares. This is not possible in the eikonal approximation where the propagator-denominators have been linearized to give Fig. A.2.

The linear occurrence of loop-momenta in eikonal propagators suggests a different strategy. It is advantageous to perform the first integrations by contour methods. In the case of two light-like eikonal lines, in a frame where these momenta are back-to-back, contour integration over either minus- or plus-momenta in all internal eikonal propagators simplifies the expressions significantly. As mentioned before, the integration over all minus-momenta is equivalent to the expressions obtained via LCOPT (see Appendix B.3), up to partial fraction manipulations. The $n-2$ dimensional perpendicular integrals can then be performed via Feynman parametrization, Eq. (B.2). This results in integrals from 0 to 1 over Feynman parameters and ratios of plus-momenta, which can be expressed in closed form in terms of Beta- and generalized hypergeometric functions. For more than two eikonal lines, or when the eikonals are not light-like, it is best to perform all internal energy (k^0) integrals via contour integration, and then proceed as above.

The discussion in the previous paragraph applies only to loops with eikonal propagators. Loops that involve no eikonal propagators and thus contain no linearized momenta, are best treated with the methods described in the previous two sections. This also avoids potential difficulties with so-called "z-graphs", where fermions flow backwards [58]. For example, the integrals over all loop momenta in the fermion bubbles and triangles in Table 4.2 are performed first by usual n-dimensional integration, then the results are inserted into the remainder of the graph which is then treated via contour integration.

We will now illustrate our method by the rederivation of the 1- and 2-loop A-coefficients.

4.3 Calculation of the 1- and 2-loop Coefficients $A_f^{(1)}$, $A_f^{(2)}$

The well-known [17, 97, 98, 99, 100, 101, 102] coefficients of the collinear parts of the splitting functions to one and two-loop order are given by

$$A_a^{(1)} = C_a, \tag{4.13}$$

$$A_a^{(2)} = \frac{1}{2} C_a K \equiv \frac{1}{2} C_a \left[C_A \left(\frac{67}{18} - \frac{\pi^2}{6} \right) - \frac{10}{9} T_F N_f \right], \tag{4.14}$$

where $C_q = C_F$, $C_g = C_A$, N_f is the number of fermions, and T_F determines the normalization of the generators of the fundamental fermion representation, $T_F = \frac{1}{2}$. We will now apply our method to the recalculation of these coefficients.

The only web at order 1 in Feynman gauge is a single gluon exchanged between the two eikonal lines. The color weight is $\overline{C}^{(1)} = C_a$ by definition (3.3), and the web has no internal momenta. Straightforwardly we obtain

$$2 \int \frac{d^n k}{(2\pi)^n} W_{aa}^{(1)} = \overline{C}^{(1)} \left(\frac{\alpha_s(\mu^2)}{\pi} \right) \left(\frac{\mu^2}{m^2} \right)^{\varepsilon} (4\pi)^{\varepsilon} \, \Gamma(\varepsilon) \int_0^\infty \frac{dk^+}{k^+}. \tag{4.15}$$

So at lowest order we get from Eq. (4.12) $A_a^{(1)} = \overline{C}^{(1)} = C_a$, as in (4.13).

At order 2 we have the webs shown in Fig. 4.1, where we rotated the eikonal lines in the figure compared to the diagrams shown in Section 3.1.2, to make the connection to Figs. 2.5 a) and 2.7 more evident. The original color factors are (compare to Fig. 3.4)

$$\begin{aligned} C(W_b) &= \left(C_F - \frac{C_A}{2} \right) C_a, \\ C(W_c) &= C(W_d) = -\frac{C_A}{2} C_a \end{aligned} \tag{4.16}$$

for eikonal lines in the a-representation. The respective color weights of the webs c) and d) are the same as the original color factors, since they do not have decompositions (these diagrams are "maximally nonabelian"). The decomposition of diagram b) was shown as an example in Section 3.1.2, which resulted in a color weight

$$\bar{C}(W_b) = -\frac{C_A}{2} C_a. \tag{4.17}$$

The contribution of Fig. 4.1 a) is easily found from Eq. (4.15) and the well-known finite terms (see e. g. [13, 31]) after renormalization of the of the gluon-self energy in the $\overline{\rm MS}$ scheme, which is an example of what we called a QCD renormalization in the previous subsection:

$$A_a^{(2),\,a)} = \frac{29}{36}C_A C_a + \frac{1}{18}C_A C_a - \frac{5}{9}T_F N_f C_a = \left(\frac{31}{36}C_A - \frac{5}{9}T_F N_f\right) C_a. \quad (4.18)$$

The first term in the first equality in Eq. (4.18) stems from the gluon loop, the second term from the ghost loop. The last term is obviously the fermion loop contribution found from the expression for the graph,

$$\begin{aligned} 2\int \frac{d^n k}{(2\pi)^n} W^{(2)}_{aa,\,a)N_f} &= -T_F N_f C_a \left(\frac{\alpha_s(\mu^2)}{\pi}\right)^2 \left(\frac{\mu^2}{m^2}\right)^{2\varepsilon} (4\pi)^{2\varepsilon} \frac{\Gamma(2\varepsilon)}{\varepsilon} \\ &\quad \times 2B(2-\varepsilon, 2-\varepsilon) \int_0^\infty \frac{dk^+}{k^+}, \end{aligned} \quad (4.19)$$

and its counterterm.

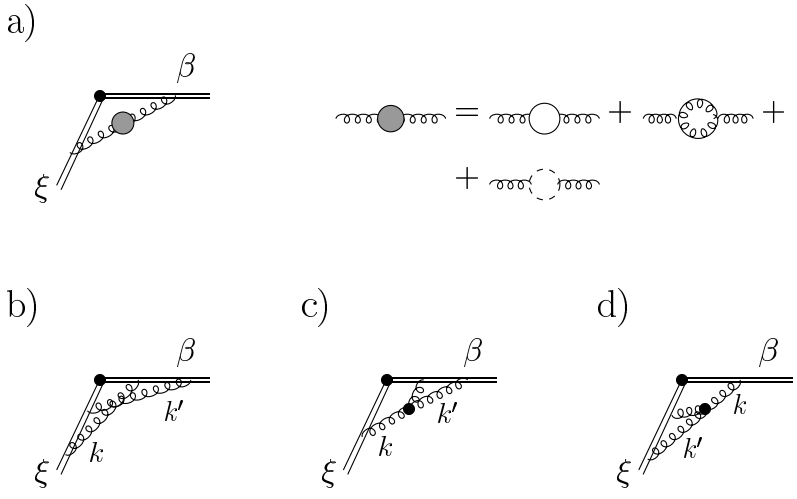

Figure 4.1: Webs contributing to $A_f^{(2)}$ (compare to Fig. 3.6): a) web of order 1 with 1-loop gluon self-energy inserted, b) the "crossed ladder", c) and d) graphs with a triple gluon vertex.

The LCOPT diagrams obtained from the webs 4.1 b)-d) are shown in Fig. 4.2. We see that due to the numerator $(2k'^- - k^-)$ in the triple-gluon vertex, web d) contains two orderings on the light-cone; the factors of 2 and (-1) next to the eikonal vertices in the figure come from this numerator. Furthermore, for web b) it is important to route the momenta in the crossed ladder independently of each other, such that both of them flow through the vertex, to separate the subdivergence associated with the upper loop (k') from the overall UV divergence.

Now we determine the divergent 1-loop subgraphs for each web by naively counting the powers of transverse momentum components in numerators and denominators. The UV divergent subgraphs are marked with boxes in Fig. 4.2. We see that for web c) and the first term of web d) we need a QCD counterterm for the triple-gluon vertex, whereas for the webs a) and d)(ii) we require vertex counterterms, as shown in the second column of Fig. 4.2. Web d)(ii) is an example for a LCOPT graph with a triple-gluon vertex which does not need QCD renormalization, in contrast to loop-corrections to 3-gluon-vertices in every covariant diagram. Due to the factor of (-1) in web d)(ii) the two vertex counterterms cancel each other, as announced above. The QCD counterterm, as shown in Fig. 4.3, is in the $\overline{\rm MS}$ scheme for quark eikonal lines β given by

$$Z^{a\,\mu}_{\text{3-g},\,ij} = -\frac{C_A}{2} T^a_{ij} \frac{\alpha_s}{\pi}\, g\, \beta^\mu \frac{1}{2} \left(\frac{1}{\varepsilon} - \ln \frac{e^{\gamma_E}}{4\pi} \right), \tag{4.20}$$

where g is the QCD coupling, $\alpha_s = g^2/(4\pi)$, and $\varepsilon > 0$.

The next step, after adding the appropriate counterterms to the respective graphs, is to perform the plus-momentum integrals. To do so, we dimensionally continue to $\varepsilon < 0$, that is, to $n > 4$ dimensions. The results for the webs b)-d) and the counterterms for UV subdivergences, denoted by Z (omitting the vertex counterterms which cancel each other) are:

$$\begin{aligned} 2\int \frac{d^n k}{(2\pi)^n} W^{(2)}_{aa,\,b)} &= -\overline{C}^{(2)} \left(\frac{\alpha_s(\mu^2)}{\pi} \right)^2 \left(\frac{\mu^2}{m^2} \right)^{2\varepsilon} (4\pi)^{2\varepsilon} \\ &\quad \times \frac{1}{2} \frac{\Gamma(2\varepsilon)}{\varepsilon} B(1+\varepsilon, -\varepsilon) \int_0^\infty \frac{dk^+}{k^+}, \end{aligned} \tag{4.21}$$

$$\begin{aligned} 2\int \frac{d^n k}{(2\pi)^n} W^{(2)}_{aa,\,c)} &= 2\int \frac{d^n k}{(2\pi)^n} W^{(2)}_{aa,\,d)} = \overline{C}^{(2)} \left(\frac{\alpha_s(\mu^2)}{\pi} \right)^2 \left(\frac{\mu^2}{m^2} \right)^{2\varepsilon} (4\pi)^{2\varepsilon} \\ &\quad \times \frac{1}{4} \frac{\Gamma(2\varepsilon)}{\varepsilon} \left\{ B(1-\varepsilon, -\varepsilon) - 2B(1-\varepsilon, 1-\varepsilon) \right\} \int_0^\infty \frac{dk^+}{k^+}, \end{aligned} \tag{4.22}$$

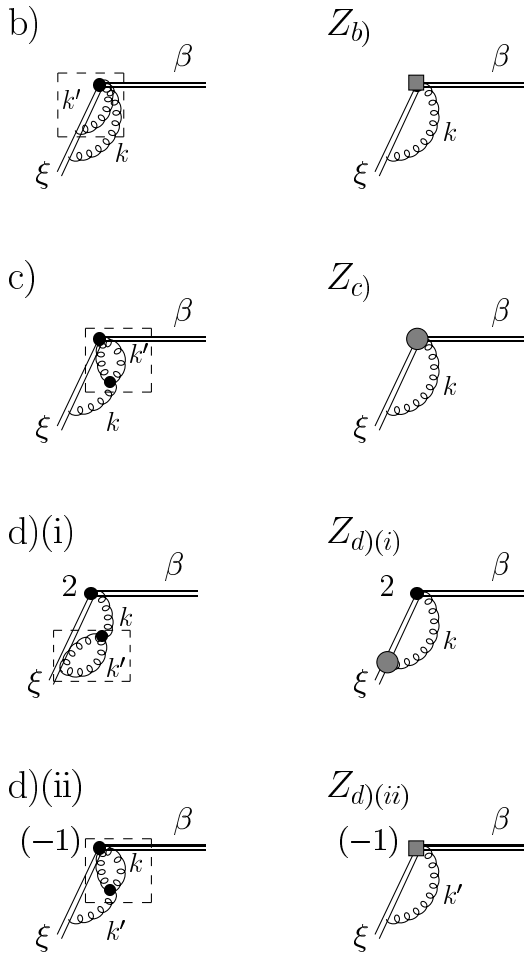

Figure 4.2: LCOPT diagrams obtained from Fig. 4.1 b)-d). The subgraphs in the dashed boxes are UV divergent 1-loop subgraphs, whose counterterms are shown in the second column. The grey boxes denote the eikonal vertex counterterms, whereas the grey blobs are the triple-gluon-vertex counterterms, shown in Fig. 4.3.

$$2\int \frac{d^nk}{(2\pi)^n} Z_{c)} \;=\; 2\int \frac{d^nk}{(2\pi)^n} Z_{d)(i)} = \overline{C}^{(2)} \left(\frac{\alpha_s(\mu^2)}{\pi}\right)^2 \left(\frac{\mu^2}{m^2}\right)^{\varepsilon} (4\pi)^{\varepsilon} \times \frac{1}{2}\,\Gamma(\varepsilon)\left(\frac{1}{\varepsilon} - \ln\frac{e^{\gamma_E}}{4\pi}\right) \int_0^\infty \frac{dk^+}{k^+}. \tag{4.23}$$

The color weight, as stated in Eqs. (4.16) and (4.17), is $\overline{C}^{(2)} = -\frac{C_A}{2} C_a$ for all diagrams. We notice that diagram d) gives the same contribution as its upside-down counterpart c), as expected, but only after adding different types of counterterms.

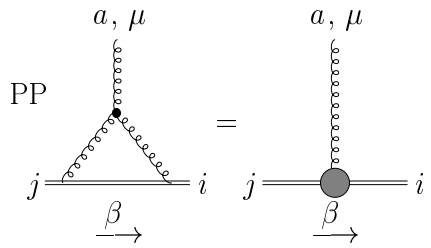

Figure 4.3: QCD counterterm for the triple-gluon vertex, where PP denotes the pole part (omitting scheme-dependent constants).

After summing over the contribution of the webs b)-d) and the counterterms, we see that the infrared poles $1/(-\varepsilon)$ in the Beta-functions cancel, as well as the vertex counterterms, leaving us with

$$A_a^{(2),\,b)-d)} = \frac{C_A}{2} C_a \left(2 - \frac{\pi^2}{6}\right) \tag{4.24}$$

according to Eq. (4.12). The contributions of all diagrams, (4.18) and (4.24), result in the 2-loop coefficient (4.14), as announced.

4.4 Higher Loops

4.4.1 N_f^{n-1}-Terms in $A^{(n)}$

It is relatively straightforward to obtain a general formula for the N_f^{n-1}-contribution to the n-loop coefficient $A^{(n)}$, since the only graphs involved are one-loop webs with $n-m-1$ fermion bubbles and m counterterms for the fermion bubbles inserted into the gluon propagator. It is therefore a matter of simple combinatorics to obtain the $\alpha_s^n N_f^{n-1}$ contribution (compare to the one-loop expression Eq. (4.19)):

$$\begin{aligned} 2\int \frac{d^{4-2\varepsilon}k}{(2\pi)^{4-2\varepsilon}} W^{(n)}_{aa,\,N_f^{n-1}} &= 2\,C_a T_F^{n-1} N_f^{n-1} \left(\frac{\alpha_s(\mu^2)}{\pi}\right)^n \int_0^\infty \frac{dk^+}{k^+} \\ &\times \sum_{m=0}^{n-1} \left(\begin{array}{c} n-1 \\ m \end{array}\right) (-1)^{n-m-1} \left(\frac{\mu^2}{m^2}\right)^{(n-m)\varepsilon} (4\pi)^{(n-m)\varepsilon} \\ &\times 2^{n-m-2} \frac{\Gamma\left((n-m)\varepsilon\right)}{\Gamma\left(1+(n-m-1)\varepsilon\right)} \\ &\times \left[\Gamma(\varepsilon) B(2-\varepsilon, 2-\varepsilon)\right]^{n-m-1} \left[\frac{1}{3}\left(\frac{1}{\varepsilon} - \ln\frac{e^{\gamma_E}}{4\pi}\right)\right]^m . \end{aligned} \tag{4.25}$$

The $\frac{1}{\varepsilon}$-pole in the expansion of the Γ- and Beta-functions in the sum is the contribution to the anomalous dimension (cf. Eq. (4.12)). The contributions up to α_s^6 are given in Table 4.1. They coincide with the corresponding values (the $\ln N$-terms, or equivalently, the $S_1(N)$-terms) calculated by Gracey in [103][1].

4.4.2 Towards the Three-Loop Coefficient $A_f^{(3)}$

Vogt [96, 108, 109] obtained a numerical parametrization of the $A^{(3)}$ from the known integer moments of the splitting function[2]:

$$A_f^{(3)} = \left[(13.81 \pm 0.14) - (4.31 \pm 0.02) T_F N_f - \frac{1}{27} T_F^2 N_f^2\right] C_F. \tag{4.26}$$

[1] Note the different overall normalization of the anomalous dimension there.

[2] Note the expansion in $(\frac{\alpha_s}{4\pi})$ there, whereas we expand in terms of $(\frac{\alpha_s}{\pi})$ in Eq. (4.4).

n	$C_a(T_F N_f)^{n-1}$-term in $A_a^{(n)}$
2	$-\frac{5}{9}$
3	$-\frac{1}{27}$
4	$-\frac{1}{81}+\frac{2}{27}\zeta(3)$
5	$-\frac{1}{243}-\frac{10}{243}\zeta(3)+\frac{\pi^4}{2430}$
6	$-\frac{1}{729}-\frac{2}{729}\zeta(3)-\frac{\pi^4}{4374}+\frac{2}{81}\zeta(5)$

Table 4.1: $\alpha_s(\mu^2)^n N_f^{n-1}\left[\frac{1}{1-x}\right]_+$-contributions to the anomalous dimension P_{ff}. The expansion of A_f is performed in terms of α_s/π (cf. Eq. (4.4)).

We obtained the term proportional to N_f^2 in the previous subsection, as listed in Table 4.1. Now we will go on to compute the term proportional to N_f. All intermediate expressions are simple enough to be handled by the general algebraic computer program *Mathematica* [122]. For the calculation of the full $A^{(3)}$ or even higher loops, however, an implementation of the algorithm into a more specialized computer algebra program such as FORM [123] may be desirable.

The diagrams contributing to this term and their QCD counterterms are listed in Table 4.2, labelled in analogy to the two-loop case. We only have to compute the contributions from the $g_{\mu\nu}$ part of the dressed gluon propagator, since the longitudinal parts $\sim k_\mu k_\nu$ cancel due to the Ward identity shown in Fig. 3.7. This cancellation has been verified explicitly.

The contributions to the set a) are easily computed to be

$$A_f^{(3),\,a)} = \frac{1}{18} C_A T_F N_f C_F. \tag{4.27}$$

The contributions to the N_f-part of the two-loop gluon self-energy inserted into a one-loop web (set g)) give:

$$A_f^{(3),\,g)} = -\left[C_A\left(\frac{509}{864}+\frac{1}{2}\zeta(3)\right) - C_F\left(-\frac{55}{48}+\zeta(3)\right)\right] T_F N_f C_F. \tag{4.28}$$

To compute the two-loop gluon self-energy, the occurring tensor integrals have been reduced to simple scalar one- and two-loop master integrals using the relations discussed in Appendix B.2. We checked our calculations of the set g) against previous computations of the two-loop gluon self-energy in Feynman gauge, see for example [124, 125]. Note that this contribution has a term $\sim C_F^2$, which is not "maximally non-abelian". The results of [124, 125] include

the scalar polarized terms of the gluon propagator, which is dressed with a fermion bubble. Since these terms in the two-loop gluon self-energy, as stated above, cancel against the scalar polarized parts in the remaining webs, Eq. (4.28) does not contain these contributions.

The expressions for the two-loop webs with a one-loop bubble-insertion are found easily from the corresponding two-loop expressions Eqs. (4.21)-(4.23), taking into account the proper multiples of ε in the Gamma- and Beta-functions due to the bubbles. The calculation of the triangles e) and f) is a bit more nontrivial. The resulting contributions can be found in the table. The results for e) and f) have been expanded in terms of ε and Beta-functions using various identities tabulated in [126, 127, 128].

Since the infrared structure of the graphs is modified by the bubbles, which effectively raise the powers of the corresponding gluon propagators by ε to a non-integer value, the upside-down counterparts do not give the same contributions. This asymmetry is not surprising, since we compute the coefficients collinear to the plus eikonal, thus introducing an asymmetry in how we treat the eikonal lines and the gluons attaching to them. However, we find that the sum of graphs in set d) gives the same contribution as the sum of graphs in set c), as can be seen from the tabulated expressions.

The individual diagrams b)-f) have at most three UV (QCD) divergences and one IR/collinear divergence, in addition to the overall scaleless k^+-integral. We observe that the diagrams with a one-loop counterterm for the fermion bubble and the one-loop counterterms for the triangle graphs have the same IR structure as the two-loop webs. Thus their IR divergences cancel separately from the rest of the diagrams. This implies that the collinear divergences have to cancel within the set of remaining diagrams, that is, within the set of webs with bubbles and the triangles. Moreover, we observe that the infrared divergences cancel within certain subsets of these graphs. Namely, they cancel separately between graphs b)(1), c)(1), and d)(1), between graphs b)(2), c)(2), and d)(2), as well as between c)(3), d)(3), e) and f).

Summing over all contributions from graphs b)-f) we arrive at

$$A_f^{(3),\,b)-f)} = -\left(\frac{125}{288} - \frac{5\pi^2}{54} + \frac{2\zeta(3)}{3}\right) T_F N_f C_A C_F. \tag{4.29}$$

We performed several checks of our computations. The infrared structure described above is one check of the results listed in Table 4.2. Another check is the cancellation of non-local logarithms $\sim \log M$. Furthermore, the values of the $1/\varepsilon^3$- and $1/\varepsilon^2$-poles can be predicted from the one- and two-loop calculations performed in Section 4.3 [129]. The sum of all diagrams contributing

at $\alpha_s^3 N_f$ has the following structure:

$$
\begin{aligned}
2\int \frac{d^n k}{(2\pi)^n} W^{(3)}_{aa,\,N_f} &= \left\{ -\frac{11}{54} C_A C_F T_F \frac{1}{\varepsilon^3} + \right. \\
&+ \left[\left(\frac{167}{324} - \frac{\pi^2}{108} \right) C_A + \frac{1}{12} C_F \right] C_F T_F \frac{1}{\varepsilon^2} \\
&+ \left. \frac{1}{3} A^{(3)}_{N_f} \frac{1}{\varepsilon} \right\} N_f \left(\frac{\alpha_s}{\pi} \right)^3 \int\limits_0^\infty \frac{dk^+}{k^+}.
\end{aligned}
\tag{4.30}
$$

The predictions of the higher poles in Eq. (4.30) coincide with the poles obtained from the expansion of the calculated expressions listed in the table.

Adding (4.27), (4.28), and (4.29) we obtain the term proportional to N_f contributing to the three-loop coefficient $A^{(3)}$:

$$
\begin{aligned}
A^{(3)}_{N_f} &= -\left[C_A \left(\frac{209}{216} - \frac{5\pi^2}{54} + \frac{7\zeta(3)}{6} \right) - C_F \left(-\frac{55}{48} + \zeta(3) \right) \right] T_F N_f C_F \\
&= -4.293\, T_F N_f C_F,
\end{aligned}
\tag{4.31}
$$

which agrees with the numerical prediction in Eq. (4.26). The same result was obtained in Ref. [111], which was published simultaneously to our result [12].

Table 4.2:

Web	Factor	Contribution
a) 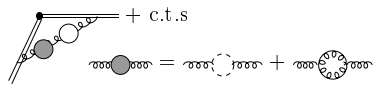	2	see Eq. (4.27)
b)(1) 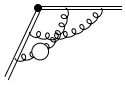	2	$-KM^{3\varepsilon}\frac{\Gamma(3\varepsilon)}{2\varepsilon^2}B(2-\varepsilon,2-\varepsilon)B(1+\varepsilon,-\varepsilon)$
b)(2) 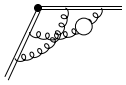	2	$-KM^{3\varepsilon}\frac{\Gamma(3\varepsilon)}{4\varepsilon^2}B(2-\varepsilon,2-\varepsilon)$ $\times B(1+2\varepsilon,-2\varepsilon)$
b)(C1) 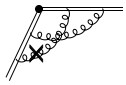	4	$+KM^{2\varepsilon}\frac{\Gamma(2\varepsilon)}{12\varepsilon}N_\varepsilon B(1+\varepsilon,-\varepsilon)$
c)(1) 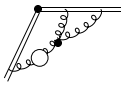	2	$+KM^{3\varepsilon}\frac{1}{4}\frac{\Gamma(3\varepsilon)}{e^2}\frac{(\Gamma(1+\varepsilon))^2}{\Gamma(1+2\varepsilon)}B(2-\varepsilon,2-\varepsilon)$ $\times\{B(1-\varepsilon,-\varepsilon)-2B(1-\varepsilon,1-\varepsilon)\}$
c)(2) 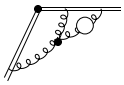	2	$+KM^{3\varepsilon}\frac{1}{4}\frac{\Gamma(3\varepsilon)}{2\varepsilon^2}B(2-\varepsilon,2-\varepsilon)$ $\times\{B(1-\varepsilon,-2\varepsilon)-2B(1-\varepsilon,1-2\varepsilon)\}$
c)(3) 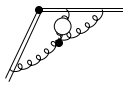	2	$+KM^{3\varepsilon}\frac{1}{4}\frac{\Gamma(3\varepsilon)}{2\varepsilon^2}B(2-\varepsilon,2-\varepsilon)$ $\times\{B(1-2\varepsilon,-\varepsilon)-2B(1-\varepsilon,1-2\varepsilon)\}$

Continuation of Table 4.2:

Web	Factor	Contribution
d)(1) 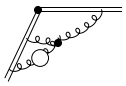	2	$+KM^{3\varepsilon}\frac{1}{4}\frac{\Gamma(3\varepsilon)}{\varepsilon^2}B(2-\varepsilon,2-\varepsilon)$ $\times\left\{\frac{(\Gamma(1+\varepsilon))^2}{\Gamma(1+2\varepsilon)}B(1-\varepsilon,-\varepsilon)-B(1-2\varepsilon,1-\varepsilon)\right\}$
d)(2) 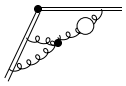	2	$+KM^{3\varepsilon}\frac{1}{4}\frac{\Gamma(3\varepsilon)}{2\varepsilon^2}B(2-\varepsilon,2-\varepsilon)$ $\times\left\{B(1-\varepsilon,-2\varepsilon)-4\frac{(\Gamma(1+\varepsilon))^2}{\Gamma(1+2\varepsilon)}B(1-\varepsilon,1-2\varepsilon)\right\}$
d)(3) 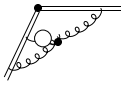	2	$+KM^{3\varepsilon}\frac{1}{4}\frac{\Gamma(3\varepsilon)}{2\varepsilon^2}B(2-\varepsilon,2-\varepsilon)$ $\times\{B(1-2\varepsilon,-\varepsilon)-2B(1-\varepsilon,1-2\varepsilon)\}$
c)d)(C1) 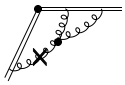	12	$-KM^{2\varepsilon}\frac{1}{24}\frac{\Gamma(2\varepsilon)}{\varepsilon}N_\varepsilon\{B(1-\varepsilon,-\varepsilon)-2B(1-\varepsilon,1-\varepsilon)\}$
c)d)(C2) 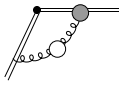	4	$+KM^{2\varepsilon}\frac{\Gamma(2\varepsilon)}{2\varepsilon}N_\varepsilon B(2-\varepsilon,2-\varepsilon)$
c)d)(C3) 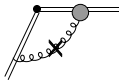	4	$-KM^{\varepsilon}\frac{\Gamma(\varepsilon)}{12}N_\varepsilon^2$
c)d)(C4) 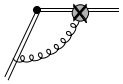	8	$-KM^{\varepsilon}\frac{\Gamma(\varepsilon)}{2}\left[\frac{1}{12}N_\varepsilon^2-\frac{1}{18}N_\varepsilon\right]$
e) 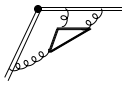	2	$-KM^{3\varepsilon}\frac{\Gamma(3\varepsilon)}{8\varepsilon^2}B(2-\varepsilon,2-\varepsilon)\{B(3-2\varepsilon,-\varepsilon)$ $-B(1-\varepsilon,2-2\varepsilon)+\frac{2\pi^2}{3}\varepsilon+(4\zeta(3)-2)\varepsilon^2\Big\}$
f) 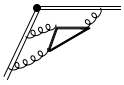	2	$-KM^{3\varepsilon}\frac{\Gamma(3\varepsilon)}{8\varepsilon^2}B(2-\varepsilon,2-\varepsilon)\{B(3-2\varepsilon,-\varepsilon)$ $-B(1-\varepsilon,2-2\varepsilon)-\frac{\pi^2}{3}\varepsilon+(10\zeta(3)-2)\varepsilon^2\Big\}$

Continuation of Table 4.2:

Web	Factor	Contribution
e)f)(C1) 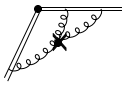	4	$+KM^{2\varepsilon}\frac{1}{24}\frac{\Gamma(2\varepsilon)}{\varepsilon}N_\varepsilon\left\{B(1-\varepsilon,-\varepsilon)\right.$ $\left.-2B(1-\varepsilon,1-\varepsilon)\right\}$
e)f)(C2) 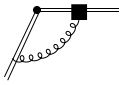	4	$+KM^{\varepsilon}\frac{\Gamma(\varepsilon)}{2}\frac{1}{12}\left(N_\varepsilon^2-\frac{5}{12}N_\varepsilon\right)$
g) 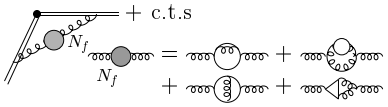	2	see Eq. (4.28)

We introduced the following abbreviations:

$$K \equiv \frac{C_A}{2}T_F N_f C_F\left(\frac{\alpha_s}{\pi}\right)^3\int_0^\infty\frac{dk^+}{k^+}, \tag{4.32}$$

$$M \equiv \left(\frac{\mu^2}{m^2}\right)(4\pi), \tag{4.33}$$

$$N_\varepsilon \equiv \frac{1}{\varepsilon}-\ln\frac{e^{\gamma_E}}{4\pi}. \tag{4.34}$$

Table 4.2: Webs contributing to the N_f-term of the three-loop coefficient $A^{(3)}$ and their counterterms (c.t.s), labelled (C). The cross denotes the counterterm for the fermion bubble. Similarly, the cross in the triple-gluon vertex denotes the counterterm for the fermion triangle. The grey blob represents the counterterm Fig. 4.3, the grey blob with a cross is the 2-loop counterterm for the triple-gluon vertex with a fermion bubble inside. And finally, the black box denotes the fermion part of the 2-loop counterterm for the triple-gluon vertex. We omitted vertex counterterms which cancel. We refrain from drawing all counterterms which give the same contribution. Instead, we indicate multiple contributions in the column "factor". A factor of 2 is due to the two complex conjugate contributions, and has already been taken into account in Eqs. (4.27) and (4.28).

4.5 Summary and Outlook

We have developed and proved a method for the calculation of the coefficients proportional to $\left[\frac{1}{1-x}\right]_+$ of the non-singlet parton splitting functions, whose knowledge, for example, is important for NNLL resummations. The method is based on the factorization properties of the splitting functions, and on the exponentiation of eikonal cross sections.

We have illustrated the method with the rederivation of the 1- and 2-loop coefficients $A^{(1)}$ and $A^{(2)}$, as well as the N_f^{n-1} terms at order n. We have presented the result for the term proportional to N_f at three loops, which coincides with the approximate result obtained by Vogt [96]. The full splitting functions at three loops are currently being computed by Moch, Vermaseren, and Vogt [110] with the help of the operator product expansion. Their results for the N_f-term [111] provide a further check of our calculations.

Although a calculation via the OPE provides the complete N, or equivalently, x-dependence of the splitting functions, it involves a large number of diagrams and complex expressions at higher orders. A computation at three loops is a formidable task, and it seems unlikely that higher loop calculations will be completed in the near future. However, for certain observables, large logarithms due to soft and/or collinear radiation become numerically important, and need to be resummed to as high a level in logarithms as possible. Our method, although limited to only the computation of A, has the advantage that higher-order computations are much less complex than within conventional methods, because the number of graphs is greatly reduced, and the expressions involved are relatively simple in LCOPT. Moreover, a fully computerized implementation of the algorithm should be straightforward. Therefore, the computation of the coefficients A at four or even higher loops may be within reach.

Let us now return to the discussion of event shapes, where the resummation of large logarithmic enhancements has lead to the same anomalous dimension discussed above. This anomalous dimension controls the double logarithmic behavior, due to coherent radiation. Soft radiation, on the other hand, is emitted incoherently at wide angles. In Sec. 2.5 we have reviewed the tools to resum coherent and incoherent radiation to all orders. We will now go on to apply this formalism to a generalized class of event shapes.

Chapter 5

Dijet Event Shapes

The agreement of theoretical predictions with experiment for jet cross sections is often impressive. This is especially so for inclusive jet cross sections at high p_T, using fixed-order factorized perturbation theory and parton distribution functions [130, 131, 132]. A good deal is also known about the substructure of jets, through the theoretical and experimental study of multiplicity distributions and fragmentation functions [133], and of event shapes [70, 134, 135, 136, 137, 138, 139, 140, 141]. We have discussed the example of the thrust in Chapter 2. Event shape distributions [71, 30, 142, 143] in particular offer a bridge between the perturbative, short-distance and the nonperturbative, long-distance dynamics of QCD [82, 83, 90, 94, 144, 145], as we have seen in Section 3.4.3 for the thrust.

In the following we will introduce a general class of inclusive event shapes in e^+e^- dijet events. This chapter is based on our publications [10, 11], and includes some as yet unpublished material. After introducing the general event shape we factorize the corresponding cross section in order to resum large logarithmic corrections. In Sec. 5.4 we give explicit analytical results at next-to-next-to-leading logarithmic order. We conclude this chapter by deriving the form of power corrections to the generalized event shape in Sec. 5.7.

5.1 A Generalized Event Shape

Schematically we consider the following cross section where the final state radiation into all of phase space is weighted with weight functions $\bar{f}$,

$$e^+ + e^- \to J_1(p_{J_1}, \bar{f}_{\bar{\Omega}_1}) + J_2(p_{J_2}, \bar{f}_{\bar{\Omega}_2})\,. \tag{5.1}$$

J_1 and J_2 are two jets with momenta $p_{J_c}, c = 1, 2$ at center of mass (c.m.) energy $Q = \sqrt{s} \gg \Lambda_{\rm QCD}$.

To impose the two-jet condition on the states of Eq. (5.1) we choose weights that suppress states with substantial radiation into $\bar{\Omega}$ away from the jet axes. We now introduce a class of event shapes $\bar{f}$, related to the thrust, that enforce the two-jet condition in a natural way.

These event shapes interpolate between and extend the familiar thrust [70] and jet broadening [71, 143], through an adjustable parameter a. For each state N that defines the process (5.1), we separate $\bar{\Omega}$ into two regions, $\bar{\Omega}_c$, $c = 1, 2$, containing jet axes, $\hat{n}_c(N)$. To be specific, we let $\bar{\Omega}_1$ and $\bar{\Omega}_2$ be two hemispheres that cover the entire space. Region $\bar{\Omega}_1$ is centered on $\hat{n}_1$, and $\bar{\Omega}_2$ is the opposite hemisphere. We will specify the method that determines the jet axes $\hat{n}_1$ and $\hat{n}_2$ momentarily. To identify a meaningful jet, of course, the total energy within $\bar{\Omega}_1$ should be a large fraction of the available energy, of the order of $Q/2$ in dijet events. In e^+e^- annihilation, if there is a well-collimated jet in $\bar{\Omega}_1$ with nearly half the total energy, there will automatically be one in $\bar{\Omega}_2$.

We are now ready to define the contribution from particles in region $\bar{\Omega}_c$ to the a-dependent event shape,

$$\bar{f}_{\bar{\Omega}_c}(N, a) = \frac{1}{\sqrt{s}} \sum_{\hat{n}_i \in \bar{\Omega}_c} k_{i,\perp}^a \, \omega_i^{1-a} \, (1 - \hat{n}_i \cdot \hat{n}_c)^{1-a} \, , \tag{5.2}$$

where a is any real number less than two. The sum is over those particles of state N with direction $\hat{n}_i$ that flow into $\bar{\Omega}_c$, and their transverse momenta $k_{i,\perp}$ are measured relative to $\hat{n}_c$. The jet axis $\hat{n}_1$ for jet 1 is identified as that axis that minimizes the specific thrust-related quantity $\bar{f}_{\bar{\Omega}_1}(N, a = 0)$. When $\bar{\Omega}_c$ in Eq. (5.2) is extended to all of phase space, the case $a = 0$ is then essentially $1 - T$, with T the thrust, while $a = 1$ is related to the jet broadening.

Any choice $a < 2$ in (5.2) specifies an infrared safe event shape variable, because the contribution of any particle i to the event shape behaves as θ_i^{2-a} in the collinear limit, $\theta_i = \cos^{-1}(\hat{n}_i \cdot \hat{n}_c) \to 0$. Negative values of a are clearly permissible, and the limit $a \to -\infty$ corresponds to the total cross section. At the other limit, the factorization and resummation techniques that we discuss below will apply only to $a < 1$. For $a > 1$, contributions to the event shape (5.2) from energetic particles near the jet axis are generically larger than contributions from soft, wide-angle radiation, or equal for $a = 1$. When this is the case, the analysis that we present below must be modified, at least beyond the level of leading logarithm [143].

In summary, once $\hat{n}_1$ is fixed, we have divided the phase space into two regions:

- Region $\bar{\Omega}_1$, the entire hemisphere centered on $\hat{n}_1$, that is, around jet 1.
- Region $\bar{\Omega}_2$, the complementary hemisphere.

In these terms, we define the complete event shape variable $\bar{f}(N, a)$ by

$$\bar{f}(N, a) \;=\; \bar{f}_{\bar{\Omega}_1}(N, a) + \bar{f}_{\bar{\Omega}_2}(N, a)\,, \tag{5.3}$$

with $\bar{f}_{\bar{\Omega}_c}$, $c = 1, 2$ given by (5.2) in terms of the axes $\hat{n}_1$ of jet 1 and $\hat{n}_2$ of jet 2.

In Eq. (5.2), a is a parameter that allows us to study various event shapes within the same formalism; it helps to control the approach to the two-jet limit. As noted above, $a < 2$ for infrared safety, although the factorization that we will discuss below applies beyond leading logarithm only to $1 > a > -\infty$. A similar weight function with a non-integer power has been discussed in a related context for $2 > a > 1$ in [146].

To see how the parameter a affects the shape of the jets, let us reexpress the weight function for jet 1 as

$$\bar{f}_{\bar{\Omega}_1}(N, a) = \frac{1}{\sqrt{s}} \sum_{\hat{n}_i \in \bar{\Omega}_1} \omega_i \sin^a \theta_i \,(1 - \cos\theta_i)^{1-a}\,, \tag{5.4}$$

where θ_i is the angle of the momentum of final state particle i with respect to jet axis $\hat{n}_1$. As $a \to 2$ the weight vanishes only very slowly for $\theta_i \to 0$, and at fixed $\bar{f}_{\bar{\Omega}_1}$, the jet becomes very narrow. On the other hand, as $a \to -\infty$, the event shape vanishes more and more rapidly in the forward direction, and the cross section at fixed $\bar{f}_{\bar{\Omega}_1}$ becomes more and more inclusive in the radiation into $\bar{\Omega}_1$. The effect of a on the shape of the radiation is illustrated in Fig. 5.1. In Fig. 5.1 we compare the phase space available to a particle at fixed $\bar{f}$ for three different values of a. The radial magnitude of each plot is the maximum energy ω found from Eq. (5.4): $r = \bar{f} Q \sin^{-a}\theta (1 - \cos\theta)^{a-1}$. For $a = 1$, as shown in Fig. 5.1 a), the particle is restricted to be close to the jet axes, while for $a = 0$, and $a = -1$, depicted in Figs. 5.1 b) and c), respectively, the particle is allowed to be farther away from the axes.

As an aside, the generalized event shape (5.2) goes to zero for all values of a in the limit of two back-to-back jets. The three-jet limit for the thrust T is $2/3$, as is well-known. On the other hand, the three-jet limit for the generalized shape is given by

$$f^{(3\text{ jets})}(a) = \frac{1}{3}\sqrt{3}^{\,a}, \tag{5.5}$$

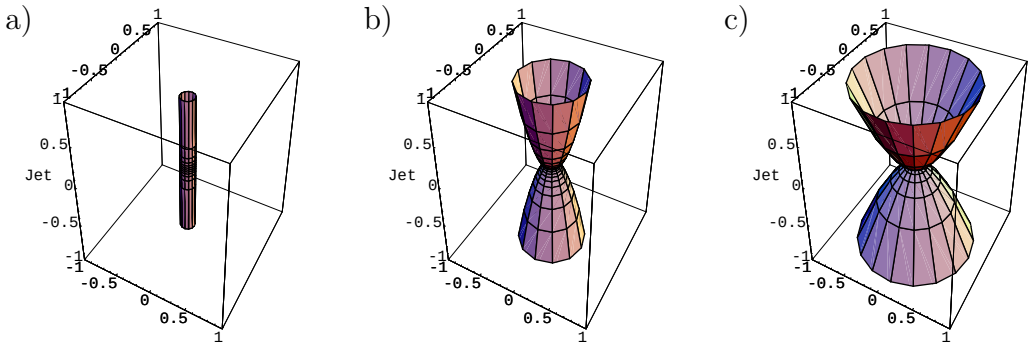

Figure 5.1: Illustration of the effect of the parameter a in the weight (5.4) on the shape of the event: a) shape for $a = 1$, b) shape for $a = 0$, c) shape for $a = -1$. The jet axes are in the vertical direction. The radial normalization $(\bar{f}Q)$ is arbitrary, but the same for all three plots.

which reduces to $1/3$ for $f(a = 0) = 1-T$, and to $1/\sqrt{3}$ for the jet broadening, $f(a = 1)$. We can also compute the limit for infinitely many homogeneously distributed final-state partons for the generalized event shape (5.2). We find

$$f^{(\infty \text{ jets})}(a) = \frac{1}{4}\left[2(1+a) - a(2-a)\left(\Psi\left(\frac{3}{2} - \frac{a}{4}\right) - \Psi\left(1 - \frac{a}{4}\right)\right)\right], \qquad (5.6)$$

where $\Psi(z) = \Gamma'(z)/\Gamma(z)$ is the digamma function, that is, the logarithmic derivative of the gamma function. This reduces to $1/2$ for the thrust-related shape, and to $\pi/4$ for the jet broadening when $a = 1$. Eq. (5.6) is illustrated in Fig. 5.2.

The differential cross section for such dijet events at fixed values of $\bar{f}$ is now

$$\begin{aligned}\frac{d\bar{\sigma}^{\text{incl}}(\bar{\varepsilon}, s, a)}{d\bar{\varepsilon}\, d\hat{n}_1} &= \frac{1}{2s}\sum_N |M(N)|^2\,(2\pi)^4\,\delta^4(p_I - p_N) \\ &\quad \times \delta(\bar{\varepsilon} - \bar{f}(N, a))\,\delta^2(\hat{n}_1 - \hat{n}(N))\,, \qquad (5.7)\end{aligned}$$

where we sum over all final states N that contribute to the weighted event, and where $M(N)$ denotes the corresponding amplitude for $e^+e^- \to N$. The total momentum is p_I, with $p_I^2 = s \equiv Q^2$.

Since we are investigating two-jet cross sections, we fix the constant $\bar{\varepsilon}$ to be much less than unity:

$$0 < \bar{\varepsilon} \ll 1. \qquad (5.8)$$

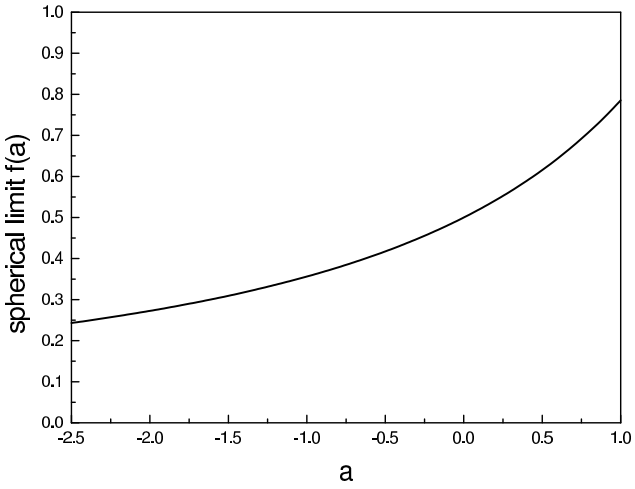

Figure 5.2: Spherical limit of the shape (5.2) as a function of a, Eq. (5.6).

We refer to this as the elastic limit for the two jets. In the elastic limit, the dependence of the directions of the jet axes on soft radiation is weak. We will return to this dependence below. Independent of soft radiation, we can always choose our coordinate system such that the transverse momentum of jet 1 is zero,

$$p_{J_1,\perp} = 0\,, \tag{5.9}$$

with $\vec{p}_{J_1}$ in the x_3 direction. In the limit $\bar{\varepsilon} \to 0$, and in the overall c.m., p_{J_1} and p_{J_2} then approach light-like vectors in the plus and minus directions:

$$\begin{aligned} p_{J_1}^\mu &\to \left(\sqrt{\frac{s}{2}}, 0^-, 0_\perp\right) \\ p_{J_2}^\mu &\to \left(0^+, \sqrt{\frac{s}{2}}, 0_\perp\right)\,. \end{aligned} \tag{5.10}$$

As usual, it is convenient to work in light-cone coordinates (B.29). For small $\bar{\varepsilon}$, the cross section (5.7) has corrections in $\ln(1/\bar{\varepsilon})$, analogous to the thrust as discussed in Sec. 2.5, which we will organize in the following.

5.2 Factorization of the Cross Section

5.2.1 Leading Regions Near the Two-Jet Limit

As for the thrust, we identify "leading regions" in the momentum integrals of cut diagrams, which can give rise to logarithmic enhancements of the cross section associated with lines approaching the mass shell. Within these regions, the lines of a cut diagram fall into the following subdiagrams:

- A hard-scattering, or "short-distance" subdiagram H, where all components of line momenta are far off-shell, by order Q.
- Jet subdiagrams, J_1 and J_2, where energies are fixed and momenta are collinear to the outgoing primary partons and the jet directions that emerge from the hard scattering. (For $\bar{\varepsilon} = 0$, the sum of all energies in each jet is one-half the total energy.)
- A soft subdiagram, S connecting the jet functions J_1 and J_2, in which the components of momenta k are small compared to Q in all components.

An arbitrary final state N is the union of substates associated with these subdiagrams:

$$N = N_s \oplus N_{J_1} \oplus N_{J_2} \,. \tag{5.11}$$

As a result, the event shape $\bar{f}$ can also be written as a sum of contributions from the soft and jet subdiagrams:

$$\bar{f}(N, a) \;\; = \;\; \bar{f}^N(N_s, a) + \bar{f}^N_{\hat{\Omega}_1}(N_{J_1}, a) + \bar{f}^N_{\hat{\Omega}_1}(N_{J_2}, a) \,. \tag{5.12}$$

The superscript N reminds us that the contributions of final-state particles associated with the soft and jet functions depend implicitly on the full final state, through the determination of the jet axes, as discussed in the previous section.

When we sum over all diagrams that have a fixed final state, the contributions from these leading regions may be factorized into a set of functions, each of which corresponds to one of the generic hard, soft and jet subdiagrams, as discussed in Chapter 2. The cross section becomes a convolution in $\bar{\varepsilon}$, with the sums over states linked by the delta function which fixes $\hat{n}_1$, and by momentum conservation,

$$\begin{aligned}\frac{d\bar{\sigma}^{\rm incl}(\bar{\varepsilon},s,a)}{d\bar{\varepsilon}\,d\hat{n}_1} &= \frac{d\sigma_0}{d\hat{n}_1}\,H(s,\hat{n}_1)\sum_{N_s,N_{J_c}}\int d\bar{\varepsilon}_s\,\mathcal{S}(N_s)\,\delta(\bar{\varepsilon}_s-\bar{f}^N(N_s,a))\\ &\quad\times\prod_{c=1}^{2}\int d\bar{\varepsilon}_{J_c}\,\mathcal{J}_c(N_{J_c})\,\delta(\bar{\varepsilon}_{J_c}-\bar{f}^N_{\bar{\Omega}_c}(N_{J_c},a))\\ &\quad\times(2\pi)^4\,\delta^4(p_I-p(N_{J_2})-p(N_{J_1})-p(N_s))\\ &\quad\times\delta^2(\hat{n}_1-\hat{n}(N))\;\delta(\bar{\varepsilon}-\bar{\varepsilon}_{J_1}-\bar{\varepsilon}_{J_2}-\bar{\varepsilon}_s)\\ &= \frac{d\sigma_0}{d\hat{n}_1}\,\delta(\bar{\varepsilon})+\mathcal{O}(\alpha_s)\,. \end{aligned}\tag{5.13}$$

Here $d\sigma_0/d\hat{n}_1$ is the Born cross section for the production of a single particle (quark or antiquark) in direction $\hat{n}_1$, while the short-distance function $H(s,\hat{n}_1)=1+\mathcal{O}(\alpha_s)$, which describes corrections to the hard scattering, is an expansion in α_s with finite coefficients. The functions $\mathcal{J}_c(N_{J_c})$, $\mathcal{S}(N_s)$ describe the internal dynamics of the jets and wide-angle soft radiation, respectively. We will specify these functions below. We have suppressed their dependence on a factorization scale.

So far, we have specified our sums over states in Eq. (5.13) only when all lines in N_s are soft, and all lines in N_{J_c} have momenta that are collinear, or nearly collinear to p_{J_c}. As $\bar{\varepsilon}$ vanishes, these are the only final-state momenta that are kinematically possible. Were we to restrict ourselves to these configurations only, however, it would not be straightforward to make the individual sums over N_s and N_{J_c} infrared safe. Thus, it is necessary to include soft partons in N_s that are emitted near the jet directions, and soft partons in the N_{J_c} at wide angles. We will show below how to define the functions $\mathcal{J}_c(N_{J_c})$, $\mathcal{S}(N_s)$ so that they generate factoring, infrared safe functions that avoid double counting. We know on the basis of the arguments in Chapter 2 that corrections to the factorization of soft from jet functions are suppressed by powers of the weight function $\bar{\varepsilon}$.

5.2.2 The Factorization in Convolution Form

Although formally factorized, the jet and soft functions in Eq. (5.13) are still linked in a potentially complicated way through their dependence on the jet axes. Our strategy is to simplify this complex dependence to a simple convolution in contributions to $\bar{\varepsilon}$, accurate to leading power in $\bar{\varepsilon}$.

First, we note that the cross section of Eq. (5.13) is singular for vanishing $\bar{\varepsilon}$, but is a smooth function of s and $\hat{n}_1$. We may therefore make any approxi-

mation that changes s and/or $\hat{n}_1$ by an amount that vanishes as a power of $\bar{\varepsilon}$ in the leading regions.

Correspondingly, the amplitudes for jet c are singular in $\bar{\varepsilon}_{J_c}$, but depend smoothly on the jet energy and direction, while the soft function is singular in $\bar{\varepsilon}_s$, but depends smoothly on the jet directions. As a result, at a fixed value of $\bar{\varepsilon}$ we may approximate the jet directions and energies by their values at $\bar{\varepsilon} = 0$ in the soft and jet functions.

Finally, we may make any approximation that affects the value of $\bar{\varepsilon}_{J_c}$ by amounts that vanish faster than linearly for $\bar{\varepsilon} \to 0$. It is at this stage that we will require that $a < 1$, which we will justify in the next subsection.

Furthermore, we assume that a is not large in absolute value. The event shape at fixed angle decreases exponentially with a, and higher-order corrections can be proportional to a. We therefore require that $|\ln \bar{\varepsilon}| \gg |a|$.

With these observations in mind, we enumerate the replacements and approximations by which we reduce Eq. (5.13), while retaining leading-power accuracy.

1. To simplify the definitions of the jets in Eq. (5.13), we make the replacements $\bar{f}^N_{\bar{\Omega}_c}(N_{J_c}, a) \to \bar{f}_c(N_{J_c}, a)$ with

$$\bar{f}_c(N_{J_c}, a) \equiv \frac{1}{\sqrt{s}} \sum_{\text{all } \hat{n}_i \in N_{J_c}} k^a_{i,\perp}\, \omega_i^{1-a}\, (1 - \hat{n}_i \cdot \hat{n}_c)^{1-a} \,. \tag{5.14}$$

   The jet weight function $\bar{f}_c(N_{J_c}, a)$ now depends only on particles associated with N_{J_c}. The contribution to $\bar{f}_c(N_{J_c}, a)$ from particles within region $\bar{\Omega}_c$, is exactly the same here as in the weight (5.2), but we now include particles in all other directions. In this way, the independent sums over final states of the jet amplitudes will be naturally infrared safe. The value of $\bar{f}_c(N_{J_c}, a)$ differs from the value of $\bar{f}^N_{\bar{\Omega}_c}(N_{J_c}, a)$, however, due to radiation outside $\bar{\Omega}_c$, as indicated by the new subscript. This radiation is hence at wide angles to the jet axis. In the elastic limit (5.8), it is also constrained to be soft. Double counting in contributions to the total event shape, $\bar{f}(N, a)$, will be avoided by an appropriate definition of the soft function below. The sums over states are still not yet fully independent, however, because the jet directions $\hat{n}_c$ still depend on the full final state N.

2. Next, we turn our attention to the condition that fixes the jet direction $\hat{n}_1$. Up to corrections in the orientation of $\hat{n}_1$ that vanish as powers of $\bar{\varepsilon}$, we may neglect the dependence of $\hat{n}_1$ on N_s and N_{J_2}:

$$\delta(\hat{n}_1 - \hat{n}(N)) \to \delta(\hat{n}_1 - \hat{n}(N_{J_1}))\,. \tag{5.15}$$

In Section 5.2.3, we show that this replacement also leaves the value of $\bar{\varepsilon}$ unchanged, up to corrections that vanish as $\bar{\varepsilon}^{2-a}$. Thus, for $a < 1$, (5.15) is acceptable to leading power. For $a < 1$, we can therefore identify the direction of jet 1 with $\hat{n}_1$. These approximations simplify Eq. (5.13) by eliminating the implicit dependence of the jet and soft weights on the full final state. We may now treat $\hat{n}_1$ as an independent vector.

3. In the leading regions, particles that make up each final-state jet are associated with states N_{J_c}, while N_s consists of soft particles only. In the momentum conservation delta function, we can neglect the four-momenta of lines in N_s, whose energies all vanish as $\bar{\varepsilon} \to 0$:

$$\delta^4(p_I - p(N_{J_2}) - p(N_{J_1}) - p(N_s)) \to \delta^4(p_I - p_{J_2} - p_{J_1}). \tag{5.16}$$

4. Because the cross section is a smooth function of the jet energies and directions, we may also neglect the masses of the jets within the momentum conservation delta function, as in Eq. (5.10). In this approximation, we derive in the c.m.,

$$\begin{aligned}
\delta^4(p_I - p_{J_2} - p_{J_1}) \;&\to\; \delta(\sqrt{s} - \omega(N_{J_1}) - \omega(N_{J_2}))\,\delta(|\vec{p}_{J_1}| - |\vec{p}_{J_2}|) \\
&\qquad \times \frac{1}{|\vec{p}_{J_1}|^2}\,\delta^2(\hat{n}_1 + \hat{n}_2) \\
&\to\; \frac{2}{s}\,\delta\left(\frac{\sqrt{s}}{2} - \omega(N_{J_1})\right)\,\delta\left(\frac{\sqrt{s}}{2} - \omega(N_{J_2})\right) \\
&\qquad \times \delta^2(\hat{n}_1 + \hat{n}_2)\,.
\end{aligned} \tag{5.17}$$

Our jets are now back-to-back:

$$\hat{n}_2 \to -\hat{n}_1\,. \tag{5.18}$$

Implementing these replacements and approximations for $a < 1$, we rewrite the cross section Eq. (5.13) as

$$\begin{aligned}
\frac{d\bar{\sigma}^{\rm incl}(\bar{\varepsilon}, s, a)}{d\bar{\varepsilon}\,d\hat{n}_1} \;&=\; \frac{d\sigma_0}{d\hat{n}_1}\,H(s, \hat{n}_1, \mu)\,\int d\bar{\varepsilon}_s\,\bar{S}(\bar{\varepsilon}_s, a, \mu) \\
&\qquad \times \prod_{c=1}^{2} \int d\bar{\varepsilon}_{J_c}\,\bar{J}_c(\bar{\varepsilon}_{J_c}, a, \mu)\,\delta(\bar{\varepsilon} - \bar{\varepsilon}_{J_1} - \bar{\varepsilon}_{J_2} - \bar{\varepsilon}_s)\,,
\end{aligned} \tag{5.19}$$

with (as above) $H = 1 + \mathcal{O}(\alpha_s)$. Referring to the notation of Eqs. (5.13) and (5.14), the functions $\bar{S}$ and $\bar{J}_c$ are:

$$\bar{S}(\bar{\varepsilon}_s, a, \mu) \;=\; \sum_{N_s} \mathcal{S}(N_s, \mu)\,\delta(\bar{\varepsilon}_s - \bar{f}(N_s, a)) \tag{5.20}$$

$$\bar{J}_c(\bar{\varepsilon}_{J_c}, a, \mu) = \frac{2}{s}(2\pi)^6 \sum_{N_{J_c}} \mathcal{J}_c(N_{J_c}, \mu)\, \delta(\bar{\varepsilon}_{J_c} - \bar{f}_c(N_{J_c}, a)) \times \delta\left(\frac{\sqrt{s}}{2} - \omega(N_{J_c})\right) \delta^2(\hat{n}_1 \pm \hat{n}(N_{J_c})), \tag{5.21}$$

with the plus sign in the angular delta function for jet 2, and the minus for jet 1. The weight functions for the jets are given by Eq. (5.14) and induce dependence on the parameter a. We have introduced the factorization scale μ, which we set equal to the renormalization scale. The factorized cross section (5.19) is of the same form as the thrust cross section, Eq. (2.83), only the weights differ, with $\bar{\varepsilon}(a = 0) \equiv \tau$. Eq. (5.19) is therefore also illustrated by Fig. 2.8.

We note that we must construct the soft functions $\bar{S}(N_s, \mu)$ to cancel the contributions of final-state particles from each of the $\bar{J}_c(N_{J_c}, \mu)$ to $\bar{\varepsilon}$ from soft radiation outside their respective regions $\bar{\Omega}_c$. Similarly, the jet amplitudes must be constructed to include collinear enhancements only in their respective jet directions. Explicit constructions that satisfy these requirements will be specified in the following subsections.

To disentangle the convolution in (5.19), we take Laplace moments with respect to $\bar{\varepsilon}$, according to Eq. (2.88):

$$\frac{d\sigma^{\text{incl}}(\nu, s, a)}{d\hat{n}_1} = \int_0^\infty d\bar{\varepsilon}\, e^{-\nu\,\bar{\varepsilon}}\, \frac{d\bar{\sigma}(\bar{\varepsilon}, a)}{d\bar{\varepsilon}\, d\hat{n}_1} = \frac{d\sigma_0}{d\hat{n}_1}\, H(s, \hat{n}_1, \mu)\, S(\nu, a, \mu) \prod_{c=1}^{2} J_c(\nu, a, \mu). \tag{5.22}$$

Here and below unbarred quantities are the transforms in $\bar{\varepsilon}$, and barred quantities denote untransformed functions.

$$S(\nu, a, \mu) = \int_0^\infty d\bar{\varepsilon}_s\, e^{-\nu\,\bar{\varepsilon}_s} \bar{S}(\bar{\varepsilon}_s, a, \mu), \tag{5.23}$$

and similarly for the jet functions.

Before giving explicit constructions for the hard, jet, and soft functions in Eq. (5.19), we justify the neglect of recoil effects above for $a < 1$.

5.2.3 Recoil Effects

We return to the justification of the technical step represented by Eq. (5.15). According to this approximation, we may compute the jet functions

by identifying axes that depend only upon particles in the final states N_{J_c} associated with those functions, rather than the full final state N. Intuitively, this is a reasonable estimate, given that the jet axis should be determined by a set of energetic, nearly collinear particles. When we make this replacement, however, the contributions to the event shape from energetic particles near the jet axis may change. This change is neglected in going from the original factorization, Eq. (5.13), to the factorization in convolution form, Eq. (5.19), which is the starting point for the resummation techniques that we employ in this paper. The weight functions $\bar{f}^N(N_i, a)$ in Eq. (5.13) are defined relative to the unit vector $\hat{n}_1$ corresponding to $a = 0$, the thrust-like event shape. The factorization of Eq. (5.13) applies to any $a < 2$, but as indicated by the superscript, individual contributions to $\bar{f}^N(N_i, a)$ on the right-hand side continue to depend on the full final state N, through the identification of the jet axis.

To derive the factorization of Eq. (5.19) in a simple convolution form, we must be able to treat the thrust axis, $\hat{n}_1$, as a fixed vector for each of the states N_s, N_{J_c}. This is possible if we can neglect the effects of recoil from soft, wide-angle radiation on the direction of the axis. Specifically, we must be able to make the replacement

$$\bar{f}^N_{\bar{\Omega}_c}(N_{J_c}, a) \to \bar{f}_c(N_{J_c}, a)\,, \tag{5.24}$$

where $\bar{f}_c(N_{J_c}, a)$ is the event shape variable for jet c, in which the axis $\hat{n}_c$ is specified by state N_{J_c} *only*. Of course, this replacement changes the value of the weight, $\bar{\varepsilon}$, $\bar{f}^N_{\bar{\Omega}_c}(N_{J_c}, a) \neq \bar{f}_c(N_{J_c}, a)$. As we now show, the error induced by this replacement is suppressed by a power of $\bar{\varepsilon}$ so long as $a < 1$. In general, the error is nonnegligible for $a \geq 1$. The importance of recoil for jet broadening, at $a = 1$, was pointed out in [143]. We now discuss how the neglect of such radiation affects the jet axis (always determined from $a = 0$) and hence the value of the event shape for arbitrary $a < 2$.

The jet axis is found by minimizing $\bar{f}(a = 0)$ in each state. The largest influence on the axis $\hat{n}_c$ for jet c is, of course, the set of fast, collinear particles within the state N_{J_c} associated with the jet function in Eq. (5.13). Soft, wide-angle radiation, however, does affect the precise direction of the axis. This is what we mean by 'recoil'.

Let us denote by ω_s the energy of the soft wide-angle radiation that is neglected in the factorization (5.19). Neglecting this soft radiation in the determination of the jet axis will result in an axis $\hat{n}_1(N_{J_c})$, which differs from the axis $\hat{n}_1(N)$ determined from the complete final state (N) by an angle $\Delta_s\phi$:

$$\measuredangle(\hat{n}_1(N), \hat{n}_1(N_{J_c})) \equiv \Delta_s\phi \sim \frac{\omega_s}{Q}\,. \tag{5.25}$$

At the same time, the soft, wide-angle radiation also contributes to the total event shape $\bar{f}(N,a) \sim (1/Q)k_\perp^a (k^-)^{1-a}$ at the level of

$$\bar{\varepsilon}_s \sim \frac{\omega_s}{Q}\,, \tag{5.26}$$

because for such wide-angle radiation, we may take $k_s^- \sim k_{s,\perp} \sim \omega_s$. In summary, the neglect of wide-angle soft radiation rotates the jet axis by an angle that is of the order of the contribution of the same soft radiation to the event shape.

In the factorization (5.19), the contribution of each final-state particle is taken into account, just as in Eq. (5.13). The question we must answer is how the rotation of the jet axis affects these contributions, and hence the value of the event shape.

For a wide-angle particle, the rotation of the jet axis by an angle of order $\Delta_s\phi$ in Eq. (5.25) leads to a negligible change in its contributions to the event shape, because its angle to the axis is a number of order unity, and the jet axis is rotated only by an angle of order $\bar{\varepsilon}_s$. Contributions from soft radiation are therefore stable under the approximation (5.15). The only source of large corrections is then associated with energetic jet radiation, because these particles are nearly collinear to the jet axis.

It is easy to see from the form of the shape function in terms of angles, Eq. (5.4), that for any value of parameter a, a particle of energy ω_i at a small angle θ_i to the jet axis $\hat{n}_1(N)$ contributes to the event shape at the level

$$\bar{\varepsilon}_i \sim \frac{\omega_i}{Q}{\theta_i}^{2-a}\,. \tag{5.27}$$

The rotation of the jet axis by the angle $\Delta_s\phi$ due to neglect of soft radiation may be as large as, or larger than, θ_i. Assuming the latter, we find a shift in the $\bar{\varepsilon}_i$ of order

$$\delta\bar{\varepsilon}_i \equiv \bar{\varepsilon}_i\left(\hat{n}_1(N)\right) - \bar{\varepsilon}_i\left(\hat{n}_1(N_{J_c})\right) \sim \frac{\omega_i}{Q}\,\left(\Delta_s\phi\right)^{2-a} \sim \frac{\omega_i}{Q}\,\left(\frac{\omega_s}{Q}\right)^{2-a} \sim \frac{\omega_i}{Q}\,{\bar{\varepsilon}_s}^{2-a}\,. \tag{5.28}$$

The change in $\bar{\varepsilon}_i$ is thus suppressed by at least a factor ${\bar{\varepsilon}_s}^{1-a}$ compared to $\bar{\varepsilon}_s$, which is the contribution of the wide-angle soft radiation to the event shape. The contributions of nearly-collinear, energetic radiation to the event shape thus change significantly under the replacement (5.15), but so long as $a < 1$, these contributions are power-suppressed in the value of the event shape, both before and after the approximation that leads to a rotation of the axis. For this reason, when $a < 1$ (and only when $a < 1$), the value of the event shape

is stable whether or not we include soft radiation in the determination of the jet axes, up to corrections that are suppressed by a power of the event shape. In this case, the transition from Eq. (5.13) to Eq. (5.19) is justified.

5.2.4 The Short-Distance Function

As we have seen in Sec. 2.4.2, in Feynman gauge the subdiagrams of Fig. 2.8 that contribute to H in Eq. (5.19) at leading power in $\bar{\varepsilon}$ are connected to each of the two jet subdiagrams by a single on-shell quark line, along with a possible set of on-shell, collinear gluon lines that carry scalar polarizations. The hard subdiagram is not connected directly to the soft subdiagram in any leading region.

The couplings of the scalar-polarized gluons that connect the jets with short-distance subdiagrams may be simplified with the help of the Ward identities Fig. 2.2. At each order of perturbation theory, the coupling of scalar-polarized gluons from either jet to the short-distance function is equivalent to their coupling to a path-ordered exponential of the gauge field, oriented in any direction that is not collinear to the jet. Corrections are infrared safe, and can be absorbed into the short-distance function. Let $h(p_{J_c}, \hat{n}_1, \mathcal{A})$ represent the set of all short-distance contributions to diagrams that couple any number of scalar-polarized gluons to the jets, in the amplitude for the production of any final state. The argument $\mathcal{A}$ stands for the fields that create the scalar-polarized gluons linking the short-distance function to the jets. On a diagram-by-diagram basis, h depends on the momentum of each of the scalar-polarized gluons. After the sum over all diagrams, however, we can make the replacement:

$$h(p_{J_c}, \hat{n}_1, \mathcal{A}^{(\mathrm{q},\bar{\mathrm{q}})}) \to \Phi^{(\bar{\mathrm{q}})}_{\xi_2}(0, -\infty; 0)\, h_2(p_{J_c}, \hat{n}_1, \xi_c)\, \Phi^{(\mathrm{q})}_{\xi_1}(0, -\infty; 0)\,, \tag{5.29}$$

where h_2 is a short-distance function that depends only on the total momenta p_{J_1} and p_{J_2}. It also depends on vectors ξ_c that characterize the path-ordered exponentials $\Phi(0, -\infty; 0)$:

$$\Phi^{(\mathrm{f})}_{\xi_c}(0, -\infty; 0) = P e^{-ig_s \int_{-\infty}^{0} d\lambda\, \xi_c \cdot \mathcal{A}^{(\mathrm{f})}(\lambda \xi_c)}\,, \tag{5.30}$$

where the superscript (f) indicates that the vector potential takes values in representation f, in our case the representation of a quark or antiquark. These operators will be associated with gauge-invariant definitions of the jet functions below. To avoid spurious collinear singularities, we choose the vectors ξ_c, $c = 1, 2$, off the light cone. In the full cross section (5.22) the ξ_c-dependence cancels, of course.

The dimensionless short-distance function $H = |h_2|^2$ in Eq. (5.19) depends on $\sqrt{s}$ and $p_{J_c} \cdot \xi_c$, but not on any variable that vanishes with $\bar{\varepsilon}$:

$$H(p_{J_c}, \xi_c, \hat{n}_1, \mu) = H\left(\frac{\sqrt{s}}{\mu}, \frac{p_{J_c} \cdot \hat{\xi}_c}{\mu}, \hat{n}_1, \alpha_s(\mu)\right) , \tag{5.31}$$

where

$$\hat{\xi}_c \equiv \xi_c / \sqrt{|\xi_c^2|} \, . \tag{5.32}$$

Here we have observed that each diagram is independent of the overall scale of the eikonal vector ξ_c^μ.

5.2.5 The Jet Functions

The jet functions and the soft functions in Eq. (5.19) can be defined in terms of specific matrix elements, which absorb the relevant contributions to leading regions in the cross section, and which are infrared safe. Their perturbative expansions specify the functions $\mathcal{S}$ and $\mathcal{J}_c$ of Eq. (5.21). We begin with our definition of the jet functions.

The jet functions, which absorb enhancements collinear to the two outgoing particles produced in the primary hard scattering, can be defined in terms of matrix elements in a manner reminiscent of parton distribution or decay functions [65]. To be specific, we consider the quark jet function:

$$\begin{aligned} \bar{J}'^{\mu}_c(\bar{\varepsilon}_{J_c}, a, \mu) \;=\; & \frac{2}{s} \frac{(2\pi)^6}{\mathcal{N}_C} \sum_{N_{J_c}} \mathrm{Tr}\left[\gamma^\mu \left\langle 0 \left| \Phi^{(\mathrm{q})\,\dagger}_{\xi_c}(0, -\infty; 0) q(0) \right| N_{J_c} \right\rangle \right. \\ & \left. \times \left\langle N_{J_c} \left| \bar{q}(0) \Phi^{(\mathrm{q})}_{\xi_c}(0, -\infty; 0) \right| 0 \right\rangle \right] \\ & \times \delta(\bar{\varepsilon}_{J_c} - \bar{f}_c(N_{J_c}, a)) \, \delta\left(\frac{\sqrt{s}}{2} - \omega(N_{J_c})\right) \, \delta^2(\hat{n}_c - \hat{n}(N_{J_c})) \, , \end{aligned} \tag{5.33}$$

where $\mathcal{N}_C$ is the number of colors, and where $\hat{n}_c$ denotes the direction of the momentum of jet c, Eq. (5.21), with $\hat{n}_2 = -\hat{n}_1$. q is the quark field, $\Phi^{(\mathrm{q})}_{\xi_c}(0, -\infty; 0)$ a path-ordered exponential in the notation of (5.30), and the trace is taken over color and Dirac indices. We have chosen the normalization so that the jet functions $\bar{J}'^{\mu}$ in (5.33) are dimensionless and begin at lowest order with

$$\bar{J}'^{\mu\,(0)}_c(\bar{\varepsilon}_{J_c}, a, \mu) = \beta_c^\mu \, \delta(\bar{\varepsilon}_{J_c}) \, , \tag{5.34}$$

with β_c^μ the lightlike velocities corresponding to the jet momenta in Eq. (5.10):

$$\beta_1^\mu = \delta_{\mu +} \; , \quad \beta_2^\mu = \delta_{\mu -} \, . \tag{5.35}$$

The scalar jet functions of Eq. (5.21) are now obtained by projecting out the component of $J_c'^{\mu}$ in the jet direction:

$$\bar{J}_c(\bar{\varepsilon}_{J_c}, a, \mu) = \bar{\beta}_c \cdot \bar{J'}_c(\bar{\varepsilon}_{J_c}, a, \mu) = \delta(\bar{\varepsilon}_{J_c}) + \mathcal{O}(\alpha_s)\,, \tag{5.36}$$

where $\bar{\beta}_1 = \beta_2$, $\bar{\beta}_2 = \beta_1$ are the lightlike vectors in the directions opposite to β_1 and β_2, respectively. By construction, the $\bar{J}_c$ are linear in $\bar{\beta}_c$.

To resum the jet functions in the variables $\bar{\varepsilon}_{J_c}$, it is convenient to re-express the weight functions (5.14) in combinations of light-cone momentum components that are invariant under boosts in the x_3 direction,

$$\begin{aligned} \bar{f}_1\,(N_{J_1}, a) &= \frac{1}{s^{1-a/2}} \sum_{\hat{n}_i \in N_{J_1}} k_{i,\perp}^a \left(2p_{J_1}^+ k_i^-\right)^{1-a}, \\ \bar{f}_2\,(N_{J_2}, a) &= \frac{1}{s^{1-a/2}} \sum_{\hat{n}_i \in N_{J_2}} k_{i,\perp}^a \left(2p_{J_2}^- k_i^+\right)^{1-a}. \end{aligned} \tag{5.37}$$

Here we have used the relation $\sqrt{s}/2 = \omega_{J_c}$, valid for both jets in the c.m. At the same time, we make the identification,

$$\frac{1}{s}\delta\left(\frac{\sqrt{s}}{2} - \omega(N_{J_c})\right) \delta^2(\hat{n}_c - \hat{n}(N_{J_c})) = \frac{1}{4}\,\delta^3\left(\vec{p}_{J_c} - \vec{p}(N_{J_c})\right), \tag{5.38}$$

which again holds in the c.m. frame. The spatial components of each p_{J_c} are thus fixed. Given that we are at small $\bar{\varepsilon}_{J_c}$, the jet functions may be thought of as functions of the light-like jet momenta $p_{J_c}^{\mu}$ of Eq. (5.10) and of $\bar{\varepsilon}_{J_c}$. Because the vector jet function is constructed to be dimensionless, $\bar{J'}_c^{\mu}$ in Eq. (5.33) is proportional to β_c rather than p_{J_c}. Otherwise, it is free of explicit β_c-dependence.

The jet functions can now be written in terms of boost-invariant arguments, homogeneous of degree zero in ξ_c:

$$\begin{aligned} \bar{J}_c\left(\bar{\varepsilon}_{J_c}, a, \mu\right) &= \bar{\beta}_{c\,\mu} \Bigg[\beta_c^{\mu}\, \bar{J}_c^{(1)}\left(\frac{p_{J_c}\cdot\hat{\xi}_c}{\mu}, \bar{\varepsilon}_{J_c}\frac{\sqrt{s}}{\mu}\left(\frac{\sqrt{s}}{2p_{J_c}\cdot\hat{\xi}_c}\right)^{1-a}, a, \alpha_s(\mu)\right) \\ &\quad + \frac{2\,\xi_c^{\mu}\;\beta_c\cdot\xi_c}{|\xi_c|^2}\,\bar{J}_c^{(2)}\left(\frac{p_{J_c}\cdot\hat{\xi}_c}{\mu}, \bar{\varepsilon}_{J_c}\frac{\sqrt{s}}{\mu}\left(\frac{\sqrt{s}}{2p_{J_c}\cdot\hat{\xi}_c}\right)^{1-a}, a, \alpha_s(\mu)\right)\Bigg], \end{aligned} \tag{5.39}$$

where $\bar{J}^{(1)}$ and $\bar{J}^{(2)}$ are independent functions, and where we have suppressed possible dependence on $\hat{\xi}_{c,\perp}$. For jet c, the weight $\bar{\varepsilon}_{J_c}$ is fixed by $\delta(\bar{\varepsilon}_{J_c} - \bar{f}_c(N_{J_c}, a))$, where on the right-hand side of the expression for the weight

(5.37), the sum over each particle's momentum involves the overall factor $(2p^{\pm}_{J_c}/\sqrt{s})^{1-a}$. After integration over final states at fixed $\bar{\varepsilon}_{J_c}$, the jet can thus depend on the vector $p^{\mu}_{J_c}$. At the same time, it is easy to see from the definition of the weight that $p^{\mu}_{J_c}$ can only appear in the combination $(1/\bar{\varepsilon}_{J_c}\sqrt{s})^{1/(1-a)}\,(2p^{\mu}_{J_c}/\sqrt{s})$. This vector can combine with ξ_c to form an invariant, and all ξ_c-dependence comes about in this way.

Expression (5.39) can be further simplified by noting that

$$2\,\bar{\beta}_c\cdot\xi_c\;\beta_c\cdot\xi_c=\xi_c^2+\xi_{c,\perp}^2\;. \tag{5.40}$$

Choosing $\xi_{c,\perp}=0$, we find a single combination,

$$\bar{J}_c\left(\bar{\varepsilon}_{J_c},a,\mu\right)=\bar{J}_c\left(\frac{p_{J_c}\cdot\hat{\xi}_c}{\mu},\bar{\varepsilon}_{J_c}\,\frac{\sqrt{s}}{\mu}\,\left(\zeta_c\right)^{1-a},a,\alpha_s(\mu)\right)\,, \tag{5.41}$$

where, in the notation of Eq. (5.39), $\bar{J}_c=\bar{J}_c^{(1)}+\bar{J}_c^{(2)}$, and we have defined

$$\zeta_c\equiv\frac{\sqrt{s}}{2p_{J_c}\cdot\hat{\xi}_c}\,. \tag{5.42}$$

In these terms, the Laplace moments of the jet function inherit dependence on the moment variable ν through

$$\begin{aligned}J_c\left(\nu,a,\mu\right)&=\int_0^{\infty}d\bar{\varepsilon}_{J_c}\,\mathrm{e}^{-\nu\bar{\varepsilon}_{J_c}}\,\bar{J}_c\left(\bar{\varepsilon}_{J_c},a,\mu\right)\\&\equiv J_c\left(\frac{p_{J_c}\cdot\hat{\xi}_c}{\mu},\frac{\sqrt{s}}{\mu\nu}\,\left(\zeta_c\right)^{1-a},a,\alpha_s(\mu)\right),\end{aligned} \tag{5.43}$$

where the unbarred and barred quantities denote transformed and untransformed functions, respectively. The soft function will be defined below in a manner that avoids double counting in the cross section.

5.2.6 The Soft Function

Given the definitions for the jet functions in the previous subsection, and the factorization (5.19), we may in principle calculate the soft function S order by order in perturbation theory. We can derive a more explicit definition of the soft function, however, by relating it to an eikonal analog of Eq. (5.19).

As reviewed in Refs. [2, 9] and Sec. 2.2, soft radiation at wide angles from the jets decouples from the collinear lines within the jet. As a result, to compute amplitudes for wide-angle radiation, the jets may be replaced by nonabelian phases, or Wilson lines. We therefore construct a dimensionless

quantity, $\sigma^{(\mathrm{eik})}$, in which gluons are radiated by path-ordered exponentials Φ, which mimic the color flow of outgoing quarks,

$$\Phi^{(\mathrm{f})}_{\beta_c}(\infty,0;x) = P e^{-ig_s\int_0^\infty d\lambda\beta_c\cdot\mathcal{A}^{(\mathrm{f})}(\lambda\beta_c+x)}, \tag{5.44}$$

with β_c a light-like velocity in either of the jet directions. For the two-jet cross section at measured $\bar{\varepsilon}_{\mathrm{eik}}$, we define

$$\begin{aligned}\bar{\sigma}^{(\mathrm{eik})}\left(\bar{\varepsilon}_{\mathrm{eik}},a,\mu\right) \equiv{}& \frac{1}{\mathcal{N}_C}\sum_{N_{\mathrm{eik}}}\left\langle 0\left|\Phi^{(\bar{\mathrm{q}})\dagger}_{\beta_2}(\infty,0;0)\Phi^{(\mathrm{q})\dagger}_{\beta_1}(\infty,0;0)\right|N_{\mathrm{eik}}\right\rangle \\ &\times\left\langle N_{\mathrm{eik}}\left|\Phi^{(\mathrm{q})}_{\beta_1}(\infty,0;0)\Phi^{(\bar{\mathrm{q}})}_{\beta_2}(\infty,0;0)\right|0\right\rangle\ \delta\left(\bar{\varepsilon}_{\mathrm{eik}}-\bar{f}(N_{\mathrm{eik}},a)\right) \\ ={}& \delta(\bar{\varepsilon}_{\mathrm{eik}})+\mathcal{O}(\alpha_s)\,.\end{aligned} \tag{5.45}$$

The sum is over all final states N_{eik} in the eikonal cross section. The renormalization scale in this cross section, which will also serve as a factorization scale, is denoted μ. Here the event shape function $\bar{\varepsilon}_{\mathrm{eik}}$ is defined by $\bar{f}(N_{\mathrm{eik}},a)$ as in Eqs. (5.2) and (5.3), distinguishing between the hemispheres around the jets. As usual, $\mathcal{N}_C$ is the number of colors, and a trace over color is understood.

The eikonal cross section (5.45) models the soft radiation away from the jets, including the radiation into Ω, accurately. It also contains enhancements for configurations collinear to the jets, which, however, are already taken into account by the partonic jet functions in (5.19). Indeed, (5.45) does not reproduce the partonic cross section accurately for collinear radiation. It is also easy to verify at lowest order that even at fixed $\bar{\varepsilon}_{\mathrm{eik}}$ the eikonal cross section (5.45) is ultraviolet divergent in dimensional regularization, unless we also impose a cutoff on the energy of real gluon emission collinear to β_1 or β_2.

The construction of the soft function S from $\bar{\sigma}^{(\mathrm{eik})}$ is nevertheless possible because the eikonal cross section (5.45) factorizes in the same manner as the cross section itself, into eikonal jet functions and a soft function, as in Eq. (2.73). The essential point [81, 147] is that the soft function in the factorized eikonal cross section is the same as in the original cross section (5.19). The eikonal jets organize all collinear enhancements in (5.45), including the spurious ultraviolet divergences. These eikonal jet functions are defined analogously to their partonic counterparts, Eq. (5.33), but now with ordered exponentials replacing the quark fields,

$$\begin{aligned}\bar{J}^{(\mathrm{eik})}_c\left(\bar{\varepsilon}_c,a,\mu\right) \equiv{}& \frac{1}{\mathcal{N}_C}\sum_{N_c^{(\mathrm{eik})}}\left\langle 0\left|\Phi^{(\mathrm{f}_c)\dagger}_{\xi_c}(0,-\infty;0)\Phi^{(\mathrm{f}_c)\dagger}_{\beta_c}(\infty,0;0)\right|N_c^{(\mathrm{eik})}\right\rangle \\ &\left\langle N_c^{(\mathrm{eik})}\left|\Phi^{(\mathrm{f}_c)}_{\beta_c}(\infty,0;0)\Phi^{(\mathrm{f}_c)}_{\xi_c}(0,-\infty;0)\right|0\right\rangle\ \delta\left(\bar{\varepsilon}_c-\bar{f}_c(N_c^{(\mathrm{eik})},a)\right) \\ ={}& \delta(\bar{\varepsilon}_c)+\mathcal{O}(\alpha_s)\,,\end{aligned} \tag{5.46}$$

where f_c is a quark or antiquark, and where the trace over color is understood. The weight functions are given as above, by Eq. (5.14), with the sum over particles in all directions.

In terms of the eikonal jets, the eikonal cross section (5.45) factorizes as

$$\begin{aligned}\bar{\sigma}^{(\mathrm{eik})}\left(\bar{\varepsilon}_{\mathrm{eik}}, a, \mu\right) \;\equiv\; & \int d\bar{\varepsilon}_s\, \bar{S}\left(\bar{\varepsilon}_s, a, \mu\right) \prod_{c=1}^{2} \int d\bar{\varepsilon}_c\, \bar{J}_c^{(\mathrm{eik})}\left(\bar{\varepsilon}_c, a, \mu\right) \\ & \times \delta\left(\bar{\varepsilon}_{\mathrm{eik}} - \bar{\varepsilon}_s - \bar{\varepsilon}_1 - \bar{\varepsilon}_2\right), \end{aligned} \tag{5.47}$$

where we pick the factorization scale equal to the renormalization scale μ. As for the full cross section, the convolution in (5.47) is simplified by a Laplace transformation (5.43) with respect to $\bar{\varepsilon}_{\mathrm{eik}}$, which allows us to solve for the soft function as

$$S\left(\nu, a, \mu\right) = \frac{\sigma^{(\mathrm{eik})}\left(\nu, a, \mu\right)}{\prod_{c=1}^{2} J_c^{(\mathrm{eik})}\left(\nu, a, \mu\right)} = 1 + \mathcal{O}(\alpha_s)\,. \tag{5.48}$$

In this ratio, collinear logarithms in ν and the unphysical ultraviolet divergences and their associated cutoff dependence cancel between the eikonal cross section and the eikonal jets, leaving a soft function that is entirely free of collinear enhancements. The soft function retains ν-dependence through soft emission. In addition, because soft radiation within the eikonal jets can be factored from its collinear radiation, just as in the partonic jets, all logarithms in ν associated with wide-angle radiation are identical between the partonic and eikonal jets, and factor from logarithmic corrections associated with collinear radiation in both cases. As a result, the inverse eikonal jet functions cancel contributions from the wide-angle soft radiation of the partonic jets in the transformed cross section (5.22).

We note that the directions of the non-lightlike eikonals Φ_{ξ_c} in Eq. (5.46) can be inferred from the requirement that the soft function only approximates soft radiation. This can be seen as follows [148]: At the one-loop level in the frame (5.35) the integrand of the eikonal cross section (5.45) is proportional to

$$I_{\sigma^{(\mathrm{eik})}} \sim \frac{1}{k^2 + i\epsilon} \frac{1}{-k^- + i\epsilon} \frac{1}{k^+ + i\epsilon}. \tag{5.49}$$

This expression is only a good approximation if all components are comparably soft. To avoid collinear overcounting we subtract

$$\begin{aligned} I_{\sigma^{(\mathrm{eik})}} - \sum_c I_{J_c^{(\mathrm{eik})}} \;\sim\; & \frac{1}{k^2 + i\epsilon} \left[\frac{1}{-k^- + i\epsilon} \frac{1}{k^+ + i\epsilon} \right. \\ & \left. - \frac{1}{-k^- + i\epsilon} \frac{\xi_1^-}{\xi_1^+ k^- + \xi_1^- k^+ + i\epsilon} - \frac{\xi_2^+}{-\xi_2^+ k^- - \xi_2^- k^+ + i\epsilon} \frac{1}{k^+ + i\epsilon} \right]. \end{aligned}$$

(5.50)

In order that Eq. (5.50) only reproduces the soft region, and in order to avoid spurious Glauber/Coulomb pinches, we have to require that

$$\begin{aligned} \left|\xi_1^+\right| \gg \left|\xi_1^-\right|, \qquad & \left|\xi_2^-\right| \gg \left|\xi_2^+\right|, \\ \xi_1^+ < 0, \qquad & \xi_2^- < 0. \end{aligned} \tag{5.51}$$

In other words, the $\hat{\xi}_c$ are not light-like, and pointing into the past, $\Phi_{\xi_c}^{(\mathrm{f}_c)}(0, -\infty; 0)$.

As in the case of the partonic jets, Eq. (5.43), we need to identify the variable through which ν appears in the soft function. We note that dependence on the velocity vectors β_c and the factorization vectors ξ_c must be scale invariant in each, since they arise only from eikonal lines and vertices. The eikonal jet functions cannot depend explicitly on the scale-less, lightlike eikonal velocities β_c, and $\sigma^{(\mathrm{eik})}$ is independent of the ξ_c. Dependence on the factorization vectors ξ_c enters only through the weight functions, (5.37) for the eikonal jets, in a manner analogous to the case of the partonic jets. This results in a dependence on $(\zeta_c)^{1-a}$, as above, with ζ_c defined in Eq. (5.42). In summary, we may characterize the arguments of the soft function in transform space as

$$S\left(\nu, a, \mu\right) = S\left(\frac{\sqrt{s}}{\mu\nu}\,\left(\zeta_c\right)^{1-a}, a, \alpha_s(\mu)\right). \tag{5.52}$$

5.3 Resummation

We may summarize the results of the previous section by rewriting the transform of the factorized cross section (5.22) in terms of the hard, jet and soft functions identified above, which depend on the kinematic variables and the moment ν according to Eqs. (5.31), (5.43) and (5.52) respectively,

$$\begin{aligned} \frac{d\sigma^{\mathrm{incl}}\left(\nu, s, a\right)}{d\hat{n}_1} \;=\; & \frac{d\sigma_0}{d\hat{n}_1}\, H\left(\frac{\sqrt{s}}{\mu}, \frac{p_{J_c}\cdot\hat{\xi}_c}{\mu}, \hat{n}_1, \alpha_s(\mu)\right) \\ & \times \prod_{c=1}^{2} J_c\left(\frac{p_{J_c}\cdot\hat{\xi}_c}{\mu}, \frac{\sqrt{s}}{\mu\nu}\left(\zeta_c\right)^{1-a}, a, \alpha_s(\mu)\right) S\left(\frac{\sqrt{s}}{\mu\nu}\left(\zeta_c\right)^{1-a}, a, \alpha_s(\mu)\right). \end{aligned} \tag{5.53}$$

For $a = 0$ this coincides with the expression for the thrust in moment space, Eq. (2.89) with slightly changed notation. The natural scale for the strong

coupling in the short-distance function H is $\sqrt{s}/2$. Setting $\mu = \sqrt{s}/2$, however, introduces large logarithms of ν in both the soft and jet functions.

The purpose of this section is to control these logarithms by the identification and solution of renormalization group and evolution equations, as in Sec. 2.5. The cross section (5.22) is independent of the factorization scale, and of the choice of the eikonal directions, $\hat{\xi}_c$, leading to equations analogous to (2.93) and (2.94). The resummation of single logarithms is straightforward. Following Sec. 2.5.1, we obtain analogously

$$\begin{aligned}\frac{d\sigma^{\rm incl}\left(\nu, s, a\right)}{d\hat{n}_1} &= \frac{d\sigma_0}{d\hat{n}_1}\, H\left(\frac{\sqrt{s}}{\mu}, \frac{p_{J_c}\cdot\hat{\xi}_c}{\mu}, \hat{n}_1, \alpha_s(\mu)\right) \\ &\times S\left((\zeta_c)^{1-a}, a, \alpha_s\left(\frac{\sqrt{s}}{\nu}\right)\right) \exp\left\{-\int\limits_{\sqrt{s}/\nu}^{\mu}\frac{d\lambda}{\lambda}\,\gamma_s\left(\alpha_s(\lambda)\right)\right\} \qquad (5.54) \\ &\times J_c\left(\frac{p_{J_c}\cdot\hat{\xi}_c}{\tilde{\mu}_0}, \frac{\sqrt{s}}{\tilde{\mu}_0\nu}\,(\zeta_c)^{1-a}, a, \alpha_s(\tilde{\mu}_0)\right) \exp\left\{-\int\limits_{\tilde{\mu}_0}^{\mu}\frac{d\lambda}{\lambda}\gamma_{J_c}\left(\alpha_s(\lambda)\right)\right\},\end{aligned}$$

where we have left the scale in the jet functions $\tilde{\mu_0}$ free for the moment.

5.3.1 Evolution

The remaining unorganized "large" logarithms in (5.54), are in the jet functions, which we will resum by using the consistency equation (2.94). Analogous to the thrust in Sec. 2.5.2 we obtain the equation satisfied by the jet functions [59, 72],

$$\begin{aligned}&\frac{\partial}{\partial\ln\left(p_{J_c}\cdot\hat{\xi}_c\right)}\ln\; J_c\left(\frac{p_{J_c}\cdot\hat{\xi}_c}{\mu}, \frac{\sqrt{s}}{\mu\nu}\,(\zeta_c)^{1-a}, a, \alpha_s(\mu)\right) \\ &\qquad = K_c\left(\frac{\sqrt{s}}{\mu\,\nu}(\zeta_c)^{1-a}, a, \alpha_s(\mu)\right) + G_c\left(\frac{p_{J_c}\cdot\hat{\xi}_c}{\mu}, \alpha_s(\mu)\right) \qquad (5.55)\end{aligned}$$

The functions K_c and G_c compensate the ξ_c-dependence of the soft and hard functions, respectively, which determines the kinematic variables upon which they may depend. In particular, notice the combination of ν- and ξ_c-dependence required by the arguments of the jet function, Eq. (5.43).

As in Section 2.5.2 $K_c + G_c$ are renormalized additively, and satisfy [59]

$$\mu\frac{d}{d\mu}\; K_c\left(\frac{\sqrt{s}}{\mu\,\nu}\,(\zeta_c)^{1-a}, a, \alpha_s(\mu)\right) = -\gamma_{K_c}\left(\alpha_s(\mu)\right),$$

$$\mu\frac{d}{d\mu}G_c\left(\frac{p_{J_c}\cdot\hat{\xi}_c}{\mu},\alpha_s(\mu)\right) \;=\; \gamma_{K_c}\left(\alpha_s(\mu)\right)\,. \tag{5.56}$$

Since G_c and hence γ_{K_c}, may be computed from virtual diagrams, they do not depend on a, and γ_{K_c} is the universal Sudakov anomalous dimension, computed in Chapter 4 [12, 45, 59, 73].

With the help of these evolution equations, the terms K_c and G_c in Eq. (5.55) can be reexpressed as [75]

$$\begin{aligned}
&K_c\left(\frac{\sqrt{s}}{\mu\,\nu}\left(\zeta_c\right)^{1-a},a,\alpha_s(\mu)\right)+G_c\left(\frac{p_{J_c}\cdot\hat{\xi}_c}{\mu},\alpha_s(\mu)\right)\\
&\quad=K_c\left(\frac{1}{c_1},a,\alpha_s\left(c_1\,\frac{\sqrt{s}}{\nu}\left(\zeta_c\right)^{1-a}\right)\right)+G_c\left(\frac{1}{c_2},\alpha_s\left(c_2\,p_{J_c}\cdot\hat{\xi}_c\right)\right)\\
&\qquad\qquad-\int\limits_{c_1\sqrt{s}\left(\zeta_c\right)^{1-a}/\nu}^{c_2\,p_{J_c}\cdot\hat{\xi}_c}\frac{d\lambda'}{\lambda'}\gamma_{K_c}\left(\alpha_s\left(\lambda'\right)\right)\\
&\quad=-B_c'\left(c_1,c_2,a,\alpha_s\left(c_2\,p_{J_c}\cdot\hat{\xi}_c\right)\right)-2\int\limits_{c_1\sqrt{s}\left(\zeta_c\right)^{1-a}/\nu}^{c_2\,p_{J_c}\cdot\hat{\xi}_c}\frac{d\lambda'}{\lambda'}A_c'\left(c_1,a,\alpha_s\left(\lambda'\right)\right)\,,
\end{aligned} \tag{5.57}$$

where in the second equality we have shifted the argument of the running coupling in K_c, and have introduced the notation

$$\begin{aligned}
B_c'\left(c_1,c_2,a,\alpha_s\left(\mu\right)\right) &\equiv -K_c\left(\frac{1}{c_1},a,\alpha_s\left(\mu\right)\right)-G_c\left(\frac{1}{c_2},\alpha_s\left(\mu\right)\right),\\
2A_c'\left(c_1,a,\alpha_s\left(\mu\right)\right) &\equiv \gamma_{K_c}\left(\alpha_s(\mu)\right)+\beta(g(\mu))\frac{\partial}{\partial g(\mu)}K_c\left(\frac{1}{c_1},a,\alpha_s(\mu)\right).
\end{aligned} \tag{5.58}$$

The primes on the functions A_c' and B_c' are to distinguish these anomalous dimensions from their somewhat more familiar versions given below. As noted above, A_c' is related to A calculated in the previous chapter.

The solution to Eq. (5.55) with $\mu = \tilde{\mu}_0$ is

$$J_c\left(\frac{p_{J_c}\cdot\hat{\xi}_c}{\tilde{\mu}_0}, \frac{\sqrt{s}}{\tilde{\mu}_0\nu}\,(\zeta_c)^{1-a}, a, \alpha_s(\tilde{\mu}_0)\right) = J_c\left(\frac{\sqrt{s}}{2\,\zeta_0\,\tilde{\mu}_0}, \frac{\sqrt{s}}{\tilde{\mu}_0\nu}\,(\zeta_0)^{1-a}, a, \alpha_s(\tilde{\mu}_0)\right)$$
$$\times \exp\left\{-\int\limits_{\frac{\sqrt{s}}{2\zeta_0}}^{p_{J_c}\cdot\hat{\xi}_c}\frac{d\lambda}{\lambda}\Big[B_c'\left(c_1, c_2, a, \alpha_s\left(c_2\lambda\right)\right)\right.$$
$$\left. + 2\int\limits_{c_1\frac{s^{1-a/2}}{\nu(2\,\lambda)^{1-a}}}^{c_2\,\lambda}\frac{d\lambda'}{\lambda'}A_c'\left(c_1, a, \alpha_s\left(\lambda'\right)\right)\Big]\right\}, \tag{5.59}$$

where we evolve from $\sqrt{s}/(2\,\zeta_0)$ to $p_{J_c}\cdot\hat{\xi}_c = \sqrt{s}/(2\,\zeta_c)$ (see Eq. (5.42)) with

$$\zeta_0 = \left(\frac{\nu}{2}\right)^{1/(2-a)}. \tag{5.60}$$

After combining Eqs. (5.54) and (5.59), the choice $\tilde{\mu}_0 = \sqrt{s}/(2\zeta_0) = \frac{\sqrt{s}}{\nu}(\zeta_0)^{1-a}$ allows us to control all large logarithms in the jet functions:

$$J_c\left(\frac{p_{J_c}\cdot\hat{\xi}_c}{\mu}, \frac{\sqrt{s}}{\mu\nu}\,(\zeta_c)^{1-a}, a, \alpha_s(\mu)\right) = J_c\left(1, 1, a, \alpha_s\left(\frac{\sqrt{s}}{2\,\zeta_0}\right)\right)$$
$$\times \exp\left\{-\int\limits_{\sqrt{s}/(2\zeta_0)}^{\mu}\frac{d\lambda}{\lambda}\gamma_{J_c}\left(\alpha_s(\lambda)\right)\right\}$$
$$\times \exp\left\{-\int\limits_{\frac{\sqrt{s}}{2\,\zeta_0}}^{p_{J_c}\cdot\hat{\xi}_c}\frac{d\lambda}{\lambda}\Big[B_c'\left(c_1, c_2, a, \alpha_s\left(c_2\lambda\right)\right)\right.$$
$$\left. + 2\int\limits_{c_1\frac{s^{1-a/2}}{\nu(2\,\lambda)^{1-a}}}^{c_2\,\lambda}\frac{d\lambda'}{\lambda'}A_c'\left(c_1, a, \alpha_s\left(\lambda'\right)\right)\Big]\right\}. \tag{5.61}$$

As observed above, we treat a as a fixed parameter, with $|a|$ small compared to $\ln\nu$.

5.3.2 The Resummed Event Shape

Putting everything together, and setting $\mu = \sqrt{s}/2$, we arrive at

$$\begin{aligned}
\frac{d\sigma^{\text{incl}}(\nu, s, a)}{d\hat{n}_1} &= \frac{d\sigma_0}{d\hat{n}_1}\, H\left(\frac{2p_{J_c}\cdot\hat{\xi}_c}{\sqrt{s}}, \hat{n}_1, \alpha_s(\sqrt{s}/2)\right) \\
&\quad \times S\left((\zeta_c)^{1-a}, a, \alpha_s\left(\frac{\sqrt{s}}{\nu}\right)\right) \exp\left\{-\int_{\sqrt{s}/\nu}^{\sqrt{s}/2}\frac{d\lambda}{\lambda}\gamma_s\left(\alpha_s(\lambda)\right)\right\} \\
&\quad \times \prod_{c=1}^{2} J_c\left(1, 1, a, \alpha_s\left(\frac{\sqrt{s}}{2\,\zeta_0}\right)\right) \exp\left\{-\int_{\sqrt{s}/(2\,\zeta_0)}^{\sqrt{s}/2}\frac{d\lambda}{\lambda}\gamma_{J_c}\left(\alpha_s(\lambda)\right)\right\} \\
&\quad \times \exp\left\{-\int_{\frac{\sqrt{s}}{2\,\zeta_0}}^{p_{J_c}\cdot\hat{\xi}_c}\frac{d\lambda}{\lambda}\left[B_c'\left(c_1, c_2, a, \alpha_s\left(c_2\lambda\right)\right)\right.\right. \\
&\qquad \left.\left. + \;2\int_{c_1\frac{s^{1-a/2}}{\nu(2\,\lambda)^{1-a}}}^{c_2\,\lambda}\frac{d\lambda'}{\lambda'}A_c'\left(c_1, a, \alpha_s\left(\lambda'\right)\right)\right]\right\}.
\end{aligned} \tag{5.62}$$

ν appears in up to two logarithms per loop, characteristic of conventional Sudakov resummation. We work to next-to-leading logarithm in ν, by which we mean the level $\alpha_s^k \ln^k \nu$ in the exponent. As usual, this requires one loop in B_c' and γ_{J_c}, and two loops in the Sudakov anomalous dimension A_c', Eq. (5.58). These functions are straightforward to calculate from their definitions given in the previous sections.

5.4 Results at NLL in Transform Space

In this section, we describe the low-order calculations and results that provide explicit expressions for the resummed event shape distributions at next-to-leading logarithm in ν (NLL). We go on to verify that the cross section is independent on the choice of the eikonal vectors ξ_c, and relate the case $a = 0$ at NLL to the known expressions for the thrust derived with a coherent branching formalism.

Below we employ the standard notation,

$$\gamma(\alpha_s) = \sum_{n=0}^{\infty} \gamma^{(n)} \left(\frac{\alpha_s}{\pi}\right)^n \tag{5.63}$$

for any expansion in α_s.

5.4.1 Analytical Results at NLL

The Soft Function

The soft function is normalized to $S^{(0)} = 1$ as can be seen from (5.48).

The one-loop soft anomalous dimension is readily calculated in Feynman gauge from the combination of virtual diagrams in $\sigma^{(\mathrm{eik})}$, Eq. (5.45), and $J^{(\mathrm{eik})}$, Eq. (5.46), in Eq. (5.48). The calculation and the result are equivalent to those of Ref. [147], where the soft function was formulated in axial gauge,

$$\gamma_s^{(1)} = -2\, C_F \left[\sum_{c=1}^{2} \ln\left(\beta_c \cdot \hat{\xi}_c\right) - \ln\left(\frac{\beta_1 \cdot \beta_2}{2}\right) - 1\right] . \tag{5.64}$$

The first, ξ_c-dependent logarithmic term is associated with the eikonal jets, while the second is a finite remainder from the combination of $\sigma^{(\mathrm{eik})}$ and $J^{(\mathrm{eik})}$ in (5.48). Whenever $\xi_{c,\perp} = 0$, the logarithmic terms cancel identically, leaving only the final term, which comes from the $\hat{\xi}_c$ eikonal self-energy diagrams in the eikonal jet functions.

The Jet Functions

Recall from Eq. (5.36) that the lowest-order jet function is given by $J_c^{(0)} = 1$.

The anomalous dimensions of the jet functions are found to be

$$\gamma_{J_c}^{(1)} = -\frac{3}{2}\, C_F \,, \tag{5.65}$$

the same for each of the jets. The jet anomalous dimensions are process-independent, but of course flavor-dependent. The same anomalous dimensions for final-state quark jets appear in three- and higher-jet cross sections.

The K-G-Decomposition

The anomalous dimension for the K-G-decomposition is, as noted above, the Sudakov anomalous dimension (see Eqs. (4.13) and (4.14)),

$$\gamma_{K_c}^{(1)} = 2C_F, \tag{5.66}$$

$$\gamma_{K_c}^{(2)} = 2C_F K \equiv C_F \left[C_A \left(\frac{67}{18} - \frac{\pi^2}{6} \right) - \frac{10}{9} T_F N_f \right], , \tag{5.67}$$

also independent of the jet-direction.

K_c and G_c, the functions that describe the evolution of the jet functions in Eq. (5.55), are given at one loop by

$$K_c^{(1)} \left(\frac{s^{1-a/2}}{\mu\nu} \left(2p_{J_c} \cdot \hat{\xi}_c \right)^{a-1}, a \right) = -C_F \ln \left(e^{2\gamma_E - (1-a)} \frac{\mu^2 \nu^2}{s^{2-a}} \left(2p_{J_c} \cdot \hat{\xi}_c \right)^{2(1-a)} \right), \tag{5.68}$$

$$G_c^{(1)} \left(\frac{p_{J_c} \cdot \hat{\xi}_c}{\mu} \right) = -C_F \ln \left(e^{-1} \frac{\left(2\, p_{J_c} \cdot \hat{\xi}_c \right)^2}{\mu^2} \right). \tag{5.69}$$

Evolving them to the values of μ with which they appear in the functions A_c' and B_c', Eq. (5.58), they become

$$K_c^{(1)} \left(\frac{1}{c_1}, a \right) = -C_F \ln \left(e^{2\gamma_E - (1-a)} c_1^2 \right), \tag{5.70}$$

$$G_c^{(1)} \left(\frac{1}{c_2} \right) = -C_F \ln \left(e^{-1} \frac{4}{c_2^2} \right). \tag{5.71}$$

Recall that G_c is computed from virtual diagrams only, and thus does not depend on the weight function. It therefore agrees with the result found in [59]. The soft-gluon contribution, K_c, which involves real gluon diagrams, does depend on the cross section being resummed.

With the definitions (5.58) of A_c' and B_c' we obtain

$$A_c'^{(1)} = C_F, \tag{5.72}$$

$$A_c'^{(2)}(c_1, a) = \frac{1}{2} C_F \left[K + \frac{\beta_0}{2} \ln \left(e^{2\gamma_E - 1 + a} c_1^2 \right) \right], \tag{5.73}$$

$$B_c'^{(1)}(c_1, c_2, a) = 2C_F \ln \left(e^{\gamma_E - 1 + a/2} \frac{2\, c_1}{c_2} \right). \tag{5.74}$$

Here β_0 is the one-loop coefficient (A.3) of the QCD beta-function.

The Hard Scattering, and the Born Cross Section

At NLL only the lowest-order hard scattering function contributes, which is normalized to

$$H^{(0)}(\alpha_s(\sqrt{s}/2)) = 1\,. \tag{5.75}$$

At this order the hard function is independent of the eikonal vectors ξ_c, although it acquires ξ_c-dependence at higher order through the factorization described in Sec. 5.2.4. For completeness, we also give the electromagnetic Born cross section $\frac{d\sigma_0}{d\hat{n}_1}$, at fixed polar and azimuthal angle:

$$\frac{d\sigma_0}{d\hat{n}_1} = \mathcal{N}_C \left(\sum_{\rm f} Q_{\rm f}^2\right) \frac{\alpha_{\rm em}^2}{4s} \left(1+\cos^2\theta\right), \tag{5.76}$$

where θ is the c.m. polar angle of $\hat{n}_1$, $e\,Q_{\rm f}$ is the charge of quark flavor f, and $\alpha_{\rm em} = e^2/(4\pi)$ is the fine structure constant.

5.4.2 Independence of the Vectors ξ_c

It is instructive to verify how dependence on the eikonal vectors ξ_c cancels in the exponents of the resummed cross section (5.62) at the accuracy at which we work, single and double logarithms of ν. In these exponents, ξ_c-dependence enters only through the combinations $(\beta_c \cdot \hat{\xi}_c)$ and $(p_{J_c} \cdot \hat{\xi}_c)$.

Let us introduce the following notation for the exponents in Eq. (5.62), to which we will return below:

$$E_1 \equiv -\int_{\sqrt{s}/\nu}^{\sqrt{s}/2} \frac{d\lambda}{\lambda} \gamma_s\left(\alpha_s(\lambda)\right) - \sum_{c=1}^{2} \int_{\sqrt{s}/(2\,\zeta_0)}^{\sqrt{s}/2} \frac{d\lambda}{\lambda} \gamma_{J_c}\left(\alpha_s(\lambda)\right), \tag{5.77}$$

$$E_2 \equiv -\sum_{c=1}^{2} \int_{\sqrt{s}/(2\,\zeta_0)}^{p_{J_c}\cdot\hat{\xi}_c} \frac{d\lambda}{\lambda} \Bigg[B_c'\left(c_1, c_2, a, \alpha_s\left(c_2\lambda\right)\right) + 2 \int_{c_1 \frac{s^{1-a/2}}{\nu(2\,\lambda)^{1-a}}}^{c_2\,\lambda} \frac{d\lambda'}{\lambda'} A_c'\left(c_1, a, \alpha_s\left(\lambda'\right)\right) \Bigg]. \tag{5.78}$$

At NLL, explicit ξ_c dependence is found only in γ_s, Eq. (5.64), for E_1, and in the upper limit of the λ integral of E_2. We then find that

$$\frac{\partial}{\partial \ln \beta_c \cdot \hat{\xi}_c}\left(E_1 + E_2\right) = 2C_F \int_{\sqrt{s}/\nu}^{\sqrt{s}/2} \frac{d\lambda}{\lambda} \frac{\alpha_s(\lambda)}{\pi} - 2C_F \int_{c_1 \frac{s^{1-a/2}}{\nu(2p_{J_c}\cdot\hat{\xi}_c)^{1-a}}}^{c_2\,p_{J_c}\cdot\hat{\xi}_c} \frac{d\lambda'}{\lambda'} \frac{\alpha_s(\lambda')}{\pi} + \text{NNLL}\,. \tag{5.79}$$

Here the second term stems entirely from $A'^{(1)}$, Eq. (5.72). The remaining contributions are of NNLL order, that is, proportional to $\alpha_s^k(\sqrt{s})\ln^{k-1}\left(\nu\,\beta_c\cdot\hat{\xi}_c\right)$, as may be verified by expanding the running couplings. Thus, as required by the factorization procedure, the relevant ξ_c-dependence cancels between the resummed soft and jet functions, which give rise to the first and second integrals, respectively, in Eq. (5.79).

As a result, we can choose

$$p_{J_c}\cdot\hat{\xi}_c=\frac{\sqrt{s}}{2}\,. \tag{5.80}$$

5.4.3 The Inclusive Event Shape at NLL in Transform Space

We can simplify the differential event shape, Eq. (5.62), by absorbing the soft anomalous dimension γ_s into the remaining terms. We will find a form that can be compared directly to the classic NLL resummation for the thrust ($a=0$). This is done by rewriting the integral over the soft anomalous dimension as

$$\begin{aligned}
\int_{\sqrt{s}/\nu}^{\sqrt{s}/2}\frac{d\lambda}{\lambda}\,\gamma_s\left(\alpha_s(\lambda)\right) &= \int_{\sqrt{s}/\left[2(\nu/2)^{1/(2-a)}\right]}^{\sqrt{s}/2}\frac{d\lambda}{\lambda}\,\gamma_s\left(\alpha_s(\lambda)\right)\\
&\quad+\int_{\sqrt{s}/\nu}^{\sqrt{s}/\left[2(\nu/2)^{1/(2-a)}\right]}\frac{d\lambda}{\lambda}\,\gamma_s\left(\alpha_s(\lambda)\right)\\
&= \int_{\sqrt{s}/\left[2(\nu/2)^{1/(2-a)}\right]}^{\sqrt{s}/2}\frac{d\lambda}{\lambda}\,\gamma_s\left(\alpha_s(\lambda)\right)\\
&\quad+(1-a)\int_{\sqrt{s}/\left[2(\nu/2)^{1/(2-a)}\right]}^{\sqrt{s}/2}\frac{d\lambda}{\lambda}\,\gamma_s\left(\alpha_s\left(\frac{s^{1-a/2}}{\nu(2\lambda)^{1-a}}\right)\right)\\
&= (2-a)\int_{\sqrt{s}/\left[2(\nu/2)^{1/(2-a)}\right]}^{\sqrt{s}/2}\frac{d\lambda}{\lambda}\,\gamma_s\left(\alpha_s(\lambda)\right)\\
&\quad-(1-a)\int_{\sqrt{s}/\left[2(\nu/2)^{1/(2-a)}\right]}^{\sqrt{s}/2}\frac{d\lambda}{\lambda}\\
&\qquad\times\int_{s^{1-a/2}/[\nu(2\lambda)^{1-a}]}^{\lambda}\frac{d\lambda'}{\lambda'}\beta(g(\lambda'))\,\frac{\partial}{\partial g}\,\gamma_s\left(\alpha_s(\lambda')\right)\,.
\end{aligned} \tag{5.81}$$

In the first equality we split the λ integral so that the limits of the first term match those of the B_c' integral of Eq. (5.62). In the second equality we have

changed variables in the second term according to

$$\lambda \to \left(\frac{s^{1-\frac{a}{2}}}{2^{1-a}\nu\lambda} \right)^{\frac{1}{1-a}} , \tag{5.82}$$

so that the limits of the second integral also match. In the third equality of Eq. (5.81), we have reexpressed the running coupling at the old scale λ in terms of the new scale. This is a generalization of the procedure of Ref. [149], applied originally to the threshold-resummed Drell-Yan cross section [150, 151].

Using Eq. (5.81), and identifying $p_{J_c} \cdot \hat{\xi}_c$ with $\sqrt{s}/2$ (Eq. (5.80)) in the inclusive event shape distribution, Eq. (5.62), we can rewrite this distribution at NLL as

$$\begin{aligned} \frac{d\sigma^{\rm incl}(\nu, s, a)}{d\hat{n}_1} &= \frac{d\sigma_0}{d\hat{n}_1} \\ &\times \prod_{c=1}^{2} \exp\left\{ - \int_{\sqrt{s}/\left[2(\nu/2)^{1/(2-a)}\right]}^{\sqrt{s}/2} \frac{d\lambda}{\lambda} \Bigg[B_c(c_1, c_2, a, \alpha_s(\lambda)) \right. \\ &\left. + 2 \int_{c_1 \frac{s^{1-a/2}}{\nu(2\lambda)^{1-a}}}^{c_2 \lambda} \frac{d\lambda'}{\lambda'} A_c(c_1, a, \alpha_s(\lambda')) \Bigg] \right\} , \end{aligned} \tag{5.83}$$

where we have rearranged the contribution of γ_s as:

$$\begin{aligned} A_c(c_1, a, \alpha_s(\mu)) &\equiv A'_c(c_1, a, \alpha_s(\mu)) - \frac{1}{4}(1-a)\,\beta(g(\mu))\,\frac{\partial}{\partial g}\,\gamma_s(\alpha_s(\mu)) , \\ B_c(c_1, c_2, a, \alpha_s(\mu)) &\equiv \gamma_{J_c}(\alpha_s(\mu)) + \left(1 - \frac{a}{2}\right)\gamma_s(\alpha_s(\mu)) \\ &\quad + B'_c(c_1, c_2, a, \alpha_s(\mu)) . \end{aligned} \tag{5.84}$$

Next, we replace the lower limit of the λ'-integral by an explicit θ-function. Then we exchange orders of integration, and change variables in the term containing A from the dimensionful variable λ to the dimensionless combination

$$u = \frac{2\lambda\lambda'}{s} . \tag{5.85}$$

We find

$$\frac{d\sigma^{\rm incl}\left(\nu,s,a\right)}{d\hat{n}_1} = \frac{d\sigma_0}{d\hat{n}_1}\prod_{c=1}^{2}\exp\left\{-\int\limits_{\sqrt{s}/\left[2(\nu/2)^{1/(2-a)}\right]}^{\sqrt{s}/2}\frac{d\lambda}{\lambda}B_c\left(c_1,c_2,a,\alpha_s\left(\lambda\right)\right)\right\}$$
$$\times\prod_{c=1}^{2}\exp\left\{-2\int_0^{\sqrt{s}}\frac{d\lambda'}{\lambda'}\int_{\lambda'^2/s}^{\lambda'/\sqrt{s}}\frac{du}{u}\,\theta\left(c_1^{-1}\nu\,\frac{\lambda'^a u^{1-a}}{s^{a/2}}-1\right)\,A_c\left(c_1,a,\alpha_s\left(\lambda'\right)\right)\right\}. \tag{5.86}$$

Here, the θ-function vanishes for small λ', and the remaining effects of replacing the lower boundary of the λ' integral by 0 are next-to-next-to-leading logarithmic.

A further change of variables allows us to write the NLL resummed event shapes in a form familiar from the NLL resummed thrust. In the first line of Eq. (5.86), we replace $\lambda^2 \to us/4$. In the second line we relabel $\lambda' \to \sqrt{q^2}$, and exchange orders of integration. Finally, choosing as in Eq. (3.34)

$$\begin{aligned} c_1 &= e^{-\gamma_E}, \\ c_2 &= 2, \end{aligned}$$

we find at NLL

$$\frac{d\sigma^{\rm incl}\left(\nu,s,a\right)}{d\hat{n}_1} = \frac{d\sigma_0}{d\hat{n}_1}\prod_{c=1}^{2}\exp\left\{\int_0^1\frac{du}{u}\left[\int_{u^2 s}^{us}\frac{dq^2}{q^2}A_c\left(\alpha_s(q^2)\right)\left(e^{-u^{1-a}\nu\left(q^2/s\right)^{a/2}}-1\right)\right.\right.$$
$$\left.\left.+\frac{1}{2}B_c\left(\alpha_s(us/4)\right)\left(e^{-u(\nu/2)^{2/(2-a)}e^{-\gamma_E}}-1\right)\right]\right\}, \tag{5.87}$$

and reproduce the well-known coefficients

$$A_c^{(1)} = C_F, \tag{5.88}$$
$$A_c^{(2)} = \frac{1}{2}C_F K, \tag{5.89}$$
$$B_c^{(1)} = -\frac{3}{2}\,C_F, \tag{5.90}$$

independent of a. In Eq. (5.87), we have made use of the relation (3.30). With these choices, we reproduce the NLL resummed thrust cross section [30, 142] when $a = 0$. This also follows directly from eikonal exponentiation, as shown in Section 3.4.2.

The choices of the c_i in Eq. (3.34) cancel all purely soft NLL components (γ_s and K_c). The remaining double logarithms stem from simultaneously soft and collinear radiation, and single logarithms arise from collinear configurations only. At NLL, the cross section is determined by the anomalous dimension A_c, which is the coefficient of the singular $1/[1-x]_+$ term in the nonsinglet evolution kernel computed in Chapter 4 [12, 68, 95], and the quark anomalous dimension. All radiation in dijet events thus appears to be emitted coherently by the two jets [30, 142]. This, however, is not necessarily true beyond next-to-leading logarithmic accuracy for dijets, and is certainly not the case for multijet events [147].

Explicit Expressions

It is straightforward to perform the integrals in Eq. (5.87), using the running coupling in terms of the coupling α evaluated at the hard scale $\sqrt{s}/2$ (compare to (A.6) and (A.7)):

$$\alpha \equiv \alpha_s\left(\frac{\sqrt{s}}{2}\right) \tag{5.91}$$

$$\alpha_s(\mu) = \frac{\alpha}{1+\frac{\beta_0}{2\pi}\alpha\ln\frac{2\mu}{\sqrt{s}}}\left[1-\frac{\beta_1}{4\pi\beta_0}\frac{\alpha}{1+\frac{\beta_0}{2\pi}\alpha\ln\frac{2\mu}{\sqrt{s}}}\ln\left(1+\frac{\beta_0}{2\pi}\alpha\ln\frac{2\mu}{\sqrt{s}}\right)+\ldots\right]. \tag{5.92}$$

The term with β_1 is only necessary for the integral containing $A_c^{(1)}$. In the following we drop the subscript c and multiply the exponent by 2, since both jets give equal contributions.

We find

$$\frac{1}{\frac{d\sigma_0}{d\hat{n}_1}}\frac{d\tilde{\sigma}(\nu,s,a)}{d\hat{n}_1} = \exp\left\{2\ln(\nu)\,g_1\left(\frac{\beta_0}{2\pi}\frac{\alpha}{2-a}\ln\nu,a\right)\right. \\ \left.+2\,g_2\left(\frac{\beta_0}{2\pi}\frac{\alpha}{2-a}\ln\nu,a\right)+\mathcal{O}\left(\alpha_s^n\ln^{n-1}\nu\right)\right\}, \tag{5.93}$$

where the functions g_1 and g_2 that resum leading and next-to-leading logarithms, respectively, are given by

$$g_1(x,a) = -\frac{4}{\beta_0}\frac{1}{1-a}\frac{1}{x}A^{(1)}\left[\left(\frac{1}{2-a}-x\right)\ln(1-(2-a)x)\right. \\ \left.-(1-x)\ln(1-x)\right], \tag{5.94}$$

$$
\begin{aligned}
g_2(x,a) &= \frac{2}{\beta_0}B^{(1)}\ln(1-x) \\
&\quad -\frac{8}{\beta_0^2}\frac{1}{1-a}A^{(2)}\left[(2-a)\ln(1-x)-\ln(1-(2-a)x)\right] \\
&\quad -\frac{4}{\beta_0}\gamma_E\frac{1}{1-a}A^{(1)}\left[\ln(1-x)-\ln(1-(2-a)x)\right] \\
&\quad +\frac{4}{\beta_0}\ln 2\frac{1}{1-a}\,A^{(1)}\left[(2-a)\ln(1-x)-\ln(1-(2-a)x)\right] \\
&\quad -\frac{\beta_1}{\beta_0^3}\frac{1}{1-a}A^{(1)}\left[2\ln(1-(2-a)x)-2(2-a)\ln(1-x)\right. \\
&\qquad\qquad \left.+\ \ln^2(1-(2-a)x)-(2-a)\ln^2(1-x)\right].
\end{aligned}
\tag{5.95}
$$

The factors of 2 in (5.93) are due to the fact that the two jets give equal contributions. Eq. (5.93) reduces for $a=0$ to the form found in [30], up to the term proportional to $\ln 2$ in g_2 which is due to the fact that we use the hard scale $\sqrt{s}/2$ instead of $\sqrt{s}$ in [30]. The cross section at an arbitrary scale μ is easily found from (5.93) at NLL:

$$
\begin{aligned}
\frac{1}{\frac{d\sigma_0}{d\hat{n}_1}}\frac{d\tilde{\sigma}\left(\nu,s,a\right)}{d\hat{n}_1} &\equiv \left[\,\mathcal{J}(\nu,s,a)\right]^2 \\
&= \exp\left\{2\,\ln(\nu)\,g_1\left(\frac{\beta_0}{2\pi}\frac{\alpha_s(\mu)}{2-a}\ln\nu,a\right)\right. \\
&\quad +2\left(\frac{\beta_0}{2\pi}\right)^2\frac{\alpha_s^2(\mu)}{2-a}\ln^2\nu\,\ln\left(\frac{2\mu}{\sqrt{s}}\right)g_1'\left(\frac{\beta_0}{2\pi}\frac{\alpha_s(\mu)}{2-a}\ln\nu,a\right) \\
&\quad \left.+2\,g_2\left(\frac{\beta_0}{2\pi}\frac{\alpha_s(\mu)}{2-a}\ln\nu,a\right)+\mathcal{O}\left(\alpha_s^n\ln^{n-1}\nu\right)\right\},
\end{aligned}
\tag{5.96}
$$

where

$$
\begin{aligned}
g_1'\left(x,a\right) &= \frac{\partial}{\partial x}g_1(x,a) \\
&= -\frac{4}{\beta_0}\frac{1}{1-a}\frac{1}{x^2}A^{(1)}\left[\ln(1-x)-\frac{1}{2-a}\ln(1-(2-a)x)\right]
\end{aligned}
\tag{5.97}
$$

Setting $\mu=\sqrt{s}$ as in [30] cancels the term proportional to $\ln 2$ in Eq. (5.95), and we reproduce for $a=0$ the form of [30].

5.5 Inverse Transform

To perform the inversion we follow the method of [30], which is well suited for resummed formulae without soft contributions, like (5.87). We also note that there are a variety of other techniques for inverting Laplace transforms, see for example [152, 153], which differ in their treatment of ambiguities in the transform due to the asymptotic nature of the perturbative series. These ambiguities manifest themselves in the transformed cross section (5.87) as singularities when reaching the Landau pole in the running coupling. In this study we bypass these issues by expanding in terms of a fixed coupling, as in (5.93). Nevertheless, we have to keep in mind that our result still contains these ambiguities, which manifest themselves as power corrections. We return to this issue below, in Sec. 5.7.

First, we consider the integrated cross section

$$\frac{d\sigma(\bar{\varepsilon},s,a)}{d\hat{n}_1} \;=\; \frac{d\sigma_0}{d\hat{n}_1}\,\frac{1}{2\pi i}\int_C \frac{d\nu}{\nu} e^{\nu\bar{\varepsilon}}\left[\mathcal{J}(\nu,s,a)\right]^2, \tag{5.98}$$

with $\mathcal{J}$ given in terms of g_1, g_2, and g_1' in Eq. (5.96). The contour lies in the complex plane to the right of all singularities of the integrand. Here we have dropped the subscript c because the two jets give equal contributions.

We can now perform a Taylor expansion of the exponent with respect to $\ln\nu$ around $\ln\nu = \ln 1/\bar{\varepsilon}$, because the functions g_1 and g_2 vary more slowly with ν than $\nu\bar{\varepsilon}$. At NLL accuracy we can neglect all derivatives of order two and higher in the Taylor expansion of the exponent. Performing the integral is then straightforward, using

$$\frac{1}{2\pi i}\int_C du e^{u-(1-\gamma)\ln u} = \frac{1}{\Gamma(1-\gamma)}. \tag{5.99}$$

We find

$$\frac{1}{\frac{d\sigma_0}{d\hat{n}_1}}\frac{d\sigma(\bar{\varepsilon},s,a)}{d\hat{n}_1} \;= \frac{\exp\left\{2\ln\frac{1}{\bar{\varepsilon}}\,g_1(x,a) + 2g_2(x,a) + 2(2-a)x^2\ln\left(\frac{2\mu}{\sqrt{s}}\right)g_1'(x,a)\right\}}{\Gamma\Big[1-2g_1(x,a)-2xg_1'(x,a)\Big]}, \tag{5.100}$$

where

$$x \equiv \frac{\alpha_s(\mu)}{\pi}\frac{\beta_0}{2\,(2-a)}\ln\frac{1}{\bar{\varepsilon}}, \tag{5.101}$$

and the functions $g_i, i = 1, 2$ are given in Eqs. (5.94), (5.95), and (5.97).

The differential cross section (5.7) is easily obtained from Eq. (5.100),

$$\frac{1}{\frac{d\sigma_0}{d\hat{n}_1}} \frac{d\sigma(\bar{\varepsilon}, s, a)}{d\bar{\varepsilon}\, d\hat{n}_1} = \frac{1}{\bar{\varepsilon}} \frac{d}{d \ln \bar{\varepsilon}} \frac{d\sigma(\bar{\varepsilon}, s, a)}{d\hat{n}_1}. \tag{5.102}$$

5.5.1 Double and Leading Logarithmic Approximation

The double logarithmic approximation (DL) which sums only terms proportional to $\alpha_s^n \ln^{2n-1} \bar{\varepsilon}$ in the differential cross section stems entirely from the first order in α_s in g_1 in the numerator. We find a DL contribution *independent of* a

$$\frac{\bar{\varepsilon}}{\frac{d\sigma_0}{d\hat{n}_1}} \frac{d\sigma(\bar{\varepsilon}, s, a)}{d\bar{\varepsilon}\, d\hat{n}_1} = -2A^{(1)} \frac{\alpha_s}{\pi} \ln \bar{\varepsilon}\, e^{-A^{(1)} \frac{\alpha_s}{\pi} \ln^2 \bar{\varepsilon}}. \tag{5.103}$$

Since the DL approximation turns out to be a-independent, this result is equal to the DL approximation for the thrust cross section [154, 155].

The leading logarithmic contribution (LL) is given by

$$\frac{\bar{\varepsilon}}{\frac{d\sigma_0}{d\hat{n}_1}} \frac{d\sigma(\bar{\varepsilon}, s, a)}{d\bar{\varepsilon}\, d\hat{n}_1} = 2 \left(g_1(x) + x g_1'(x)\right) e^{-2 g_1(x) \ln \bar{\varepsilon}}, \tag{5.104}$$

where x is defined in (5.101).

The full result at NLL order can be obtained by inserting (5.100) into (5.102).

5.6 Numerical Results

5.6.1 Matching with Fixed Order Calculations

Analytical fixed order expressions for the thrust exist only up to $\mathcal{O}(\alpha_s)$ [136], for matching at NLL it is necessary, however, to know the fixed order contributions up to $\mathcal{O}(\alpha_s^2)$. These can be calculated numerically, not only for the thrust, using, for example, the program EVENT2 [156].

In the following we will use direct matching, that is, the cross section is computed as

$$\frac{d\sigma\left(\bar{\varepsilon}, s, a\right)}{d\bar{\varepsilon}\, d\hat{n}_1} = \frac{d\sigma_{\text{resum}}\left(\bar{\varepsilon}, s, a\right)}{d\bar{\varepsilon}\, d\hat{n}_1} - \frac{d\sigma_{\text{resum}}^{\text{exp, (2)}}\left(\bar{\varepsilon}, s, a\right)}{d\bar{\varepsilon}\, d\hat{n}_1} + \frac{d\sigma_{\text{fixed}}^{(2)}\left(\bar{\varepsilon}, s, a\right)}{d\bar{\varepsilon}\, d\hat{n}_1}, \tag{5.105}$$

where the subscript resum denotes our resummed cross section, the second term on the right, $d\sigma_{\text{resum}}^{\text{exp, (2)}}$ is the resummed cross section expanded up to

order α_s^2, and $d\sigma^{(2)}_{\text{fixed}}$ is the fixed order cross section calculated with EVENT2 up to order α_s^2. Other matching schemes are possible, they differ from the above formula at order α_s^3 and NNLL.

Determination of the Thrust Axis

The implementation of our generalized weight (5.3) with (5.2) is straightforward, since the weight is defined with respect to the thrust axis, and since the method of event generation in EVENT2 is Lorentz-invariant. The default frame of the program is the partonic center-of-mass frame, which is also convenient for our purposes.

At order $\mathcal{O}(\alpha_s^2)$, up to only four partons contribute to the final state. For two- or three-parton final states, the thrust axis is given simply by the direction of the parton that carries the biggest energy fraction. For four- or higher parton final states, it is best to rewrite Eq. (2.79) as [157]

$$T = \max_{\epsilon_i = \pm 1} \frac{|\sum_i \epsilon_i \vec{p}_i|}{\sum_j |\vec{p}_j|}. \tag{5.106}$$

This may be interpreted as applying Eq. (2.79) to an event with $2n$ particles, half of which carry the momenta in the original directions $\vec{p}_i$ and the other half in the directions $-\vec{p}_i$, which automatically balances the momentum. Eq. (5.106) then follows from [158]

$$\sum_{i \in C_+} \vec{p}_i \cdot \hat{n} = \left| \sum_{i \in C_+} \vec{p}_i \right| \cos\theta_{(\text{tot})n}, \tag{5.107}$$

where C_+ is the class of momenta for which $\vec{p}_i \cdot \hat{n} > 0$ with $\vec{p}_i$ in the doubled set of momenta, and $\theta_{(\text{tot})n}$ is the angle between the sum over all momenta in C_+, $\sum_{i \in C_+} \vec{p}_i \equiv \vec{p}_{\text{tot}}$, and vector $\hat{n}$. Maximizing this expression gives (5.106), where $\theta_{(\text{tot})n} = 0$. Geometrically, this can be interpreted as the task of finding the three-dimensional polygon built out of all participating momenta with the largest diameter. The direction of the largest diameter corresponds to the thrust axis. The momenta comprise a polygon due to momentum conservation $\sum_i \vec{p}_i = 0$, and different orderings of the vectors result in different polygons, possibly with crossing of lines. To find the thrust axis via Eq. (5.106) requires a test of 2^{n-1} possibilities (The factor 2^{-1} comes from the fact that T is unchanged when all $\epsilon_i \to (-\epsilon_i)$.). This is quite feasible and fast for four partons in the final state, the maximal number needed at NLO.

5.6.2 Matched Results at NLL

Here we show some representative results for the matched resummed cross sections for various values of the parameter a. The NLL resummed cross section is found from Eq. (5.100) which is valid up to power corrections for values of $\bar{\varepsilon}$ away from the end-point region $\beta_0/(2\pi)\alpha_s \ln \bar{\varepsilon} < 1$, or $\bar{\varepsilon} > \Lambda_{\rm QCD}/\sqrt{s}$. For $\bar{\varepsilon} \sim \Lambda_{\rm QCD}/\sqrt{s}$ non-perturbative corrections become dominant. We therefore cut off the small values of $\bar{\varepsilon}$ from our plots.

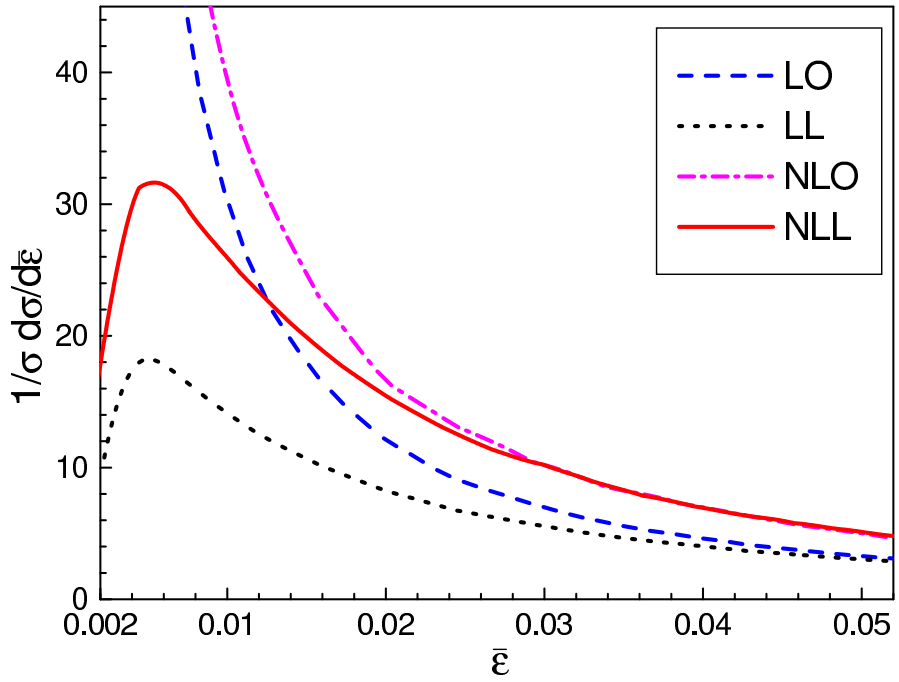

Figure 5.3: Comparison of fixed order and resummed cross sections for $a = -0.5$ at c.m. energy $\sqrt{s} = 91$ GeV as a function of $\bar{\varepsilon}$. Shown are the leading order (LO), matched leading logarithmic (LL), next-to-leading order (NLO) and matched next-to-leading logarithmic (NLL) results.

In Fig. 5.3 we compare the cross sections evaluated at fixed order via EVENT2 [156] with our resummed results matched according to Eq. (5.105). Shown are the differential cross sections $\frac{1}{\sigma}\frac{d\sigma}{d\bar{\varepsilon}}$, normalized by the total cross section, as a function of $\bar{\varepsilon}$ at a center-of-mass energy of $\sqrt{s} = 91$ GeV. As one can see from Fig. 5.3, fixed order calculations are sufficient for not too

small values of $\bar{\varepsilon}$. However, the fixed order results are singular at the phase-space boundary $\bar{\varepsilon} \to 0$, and resummation is necessary for accurate quantitative predictions.

Furthermore, Fig. 5.3 shows that the difference between LL and NLL resummed results is quite sizeable. As mentioned in the introduction to event shapes, Sec. 2.4.1, event shapes are used in precision measurements of the running coupling [159]. Although higher logarithmic corrections are generally expected to be not as sizeable, it may be necessary to include NNLL corrections to reduce the theoretical uncertainty in the determination of α_s. At NNLL accuracy not only the knowledge of the three-loop coefficient $A^{(3)}$ is necessary, whose fermionic part was computed in the previous chapter, but also the full resummed expression (5.62) instead of its simplified version (5.87), valid only up to NLL, has to be used in the computation.

In Fig. 5.4 we plot the matched resummed results at NLL for $a = -1$ and $a = 0$ (the thrust-related shape), normalized as above, $\frac{1}{\sigma}\frac{d\sigma}{d\bar{\varepsilon}}$, as a function of $\bar{\varepsilon}$ for a c.m. energy of $\sqrt{s} = 91$ GeV. For $a = 0$ we reproduce the results of [30]. We compare our predictions, valid at the partonic level, to the corresponding cross sections computed by PYTHIA [160], version 6.215 [161], at the hadronic level, using PYTHIA's implementation of the string fragmentation model [162, 163]. We use the default settings of the program. The string picture seems to model the hadronization process fairly well, as the comparison with some recent data for the thrust shows, displayed also in Fig. 5.4. We note that our definition of the thrust-related shape, Eq. (5.2) at $a = 0$, is only equivalent to $1-T$ at the partonic level, with T defined in terms of three-momenta as in Eq. (2.79). At the partonic level mass-effects are negligible, in contrast to the hadronic level. For the comparison with PYTHIA in Fig. 5.4 we use the definition of our event shape in terms of energies, (5.2), for both the partonic and the hadronic level. Other prescriptions are of course possible [164].

The difference between partonic and hadronic level, in terms of location of the peak and overall shape at small values of $\bar{\varepsilon}$, is due to hadronization and other non-perturbative effects. These, as briefly mentioned in Sec. 1.1.4 and 5.5, manifest themselves as power corrections to the perturbatively calculated cross section. We will give some brief qualitative arguments below, but reserve a more quantitative study for future work.

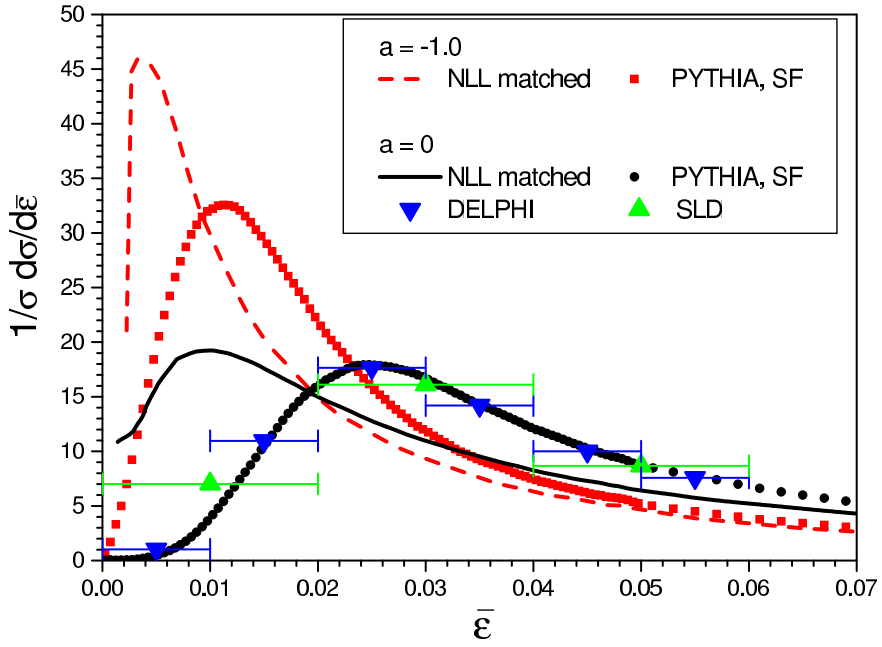

Figure 5.4: Comparison of matched NLL resummed cross sections for $a = -1$ and $a = 0$ to the corresponding cross sections calculated by PYTHIA with string hadronization (SF) at $\sqrt{s} = 91$ GeV. The data for $a = 0$ ($\bar{\varepsilon} = 1 - T$) are taken from [165] (SLD) and [166] (DELPHI).

5.7 Power Corrections

Starting from Eq. (5.87), we can proceed analogously to Sec. 3.4.3 to infer the form of nonperturbative corrections. Changing orders of integration in (5.87), and using Eq. (A.10), we obtain

$$\tilde{\sigma}_a^{(\mathrm{eik})}(\nu) = \exp\left\{2\int_0^{Q^2}\frac{dq^2}{q^2}A\left(\frac{\alpha_s(Q^2)}{1+\frac{\beta_0}{4\pi}\alpha_s(Q^2)\ln\frac{q^2}{Q^2}}\right)\right.$$
$$\left.\times\int_{q^2/Q^2}^{q/Q}\frac{du}{u}\left(e^{-\nu u^{1-a}(q/Q)^a}-1\right)\right\}, \qquad (5.108)$$

where $\sqrt{s} = Q$. Expanding the exponential in the exponent, changing variables as in Eq. (3.39),

$$t_n \equiv n\,t = \frac{n}{2}\alpha_s(Q^2)\ln\frac{Q^2}{q^2}, \tag{5.109}$$

and performing the integral over u results in

$$\tilde{\sigma}_a^{(\mathrm{eik})}(\nu) \;=\; \exp\left\{\frac{2}{1-a}\sum_{n=1}^{\infty}\frac{1}{n^2\,n!}\frac{(-\nu)^n}{\alpha_s(Q^2)}\int\limits_0^{\infty} dt_n\, A\left(\frac{\alpha_s(Q^2)}{1-\frac{\beta_0}{2\pi\,n}t_n}\right)e^{-\frac{t_n}{\alpha_s(Q^2)}} \times\left[1-e^{-\frac{t_n\,(1-a)}{\alpha_s(Q^2)}}\right]\right\}. \tag{5.110}$$

Comparing to the Borel integral, Eq. (1.13), we find an ambiguity proportional to $1/Q$, just as for the thrust. Here, however, corrections are suppressed by non-integer powers, by $\mathcal{O}(1/Q^{1-a})$, due to the lower limit in the integral over u in (5.108).

$$\ln\tilde{\sigma}_a(\nu,Q) = \ln\tilde{\sigma}_{a,\,\mathrm{PT}}(\nu,Q) + \ln\tilde{\sigma}_a^{\mathrm{power}}\left(\frac{\nu}{Q}\right) + \mathcal{O}\left(\frac{\nu}{Q^{2-a}}\right), \tag{5.111}$$

where

$$\ln\tilde{\sigma}_a^{\mathrm{power}}\left(\frac{\nu}{Q}\right) \equiv \frac{1}{1-a}\ln\tilde{f}^{\mathrm{power}}\left(\frac{\nu}{Q}\right). \tag{5.112}$$

Moreover, from Eq. (5.111) with (5.112) we find that shape distributions with two different parameters $a, b < 1$ have leading nonperturbative corrections that are related to each other by [167]

$$\ln\tilde{\sigma}_a^{\mathrm{power}}\left(\frac{\nu}{Q}\right) = \frac{1-b}{1-a}\ln\tilde{\sigma}_b^{\mathrm{power}}\left(\frac{\nu}{Q}\right), \tag{5.113}$$

as was observed by G. Sterman.

As can be seen from Fig. 5.4, these power corrections shift the peak of the cross section as well as change its shape. The leading effect is a shift of the distribution [82, 90, 168]. In general, however, the effect of the leading power corrections is also to change the shape of the distribution [83, 169]. The latter effect is most prominent at small values of the shape, $\bar{\varepsilon} \sim \Lambda_{\mathrm{QCD}}/Q$.

That the leading effect at moderate $\bar{\varepsilon}$ is a shift of the distribution can be seen from the first term in the expansion (5.110), $n = 1$. From the above, the ambiguity due to this term, denoted by the superscript (1), is proportional to

$$\ln\tilde{\sigma}_a^{\mathrm{power}\ (1)} = -\frac{\lambda_1}{1-a}\frac{\nu}{Q}, \tag{5.114}$$

where λ_1 is a nonperturbative, constant parameter (compare to Eqs. (1.6) and (3.36)). Inserting this expression into (5.111), we obtain the cross section in momentum space from (5.98)

$$\frac{d\sigma(\bar{\varepsilon}, s, a)}{d\hat{n}_1} = \frac{d\sigma_0}{d\hat{n}_1} \frac{1}{2\pi i} \int_C \frac{d\nu}{\nu} e^{\nu\left(\bar{\varepsilon} - \frac{1}{1-a}\frac{\lambda_1}{Q}\right)} \left[\mathcal{J}(\nu, s, a)\right]^2 . \tag{5.115}$$

Thus the integrated cross section is shifted to the right by an amount

$$\Delta\bar{\varepsilon}(a, Q) = \frac{1}{1-a}\frac{\lambda_1}{Q}. \tag{5.116}$$

To first approximation this also holds for the differential cross section (5.102) for not too small values of $\bar{\varepsilon}$. As mentioned above, for very small $\bar{\varepsilon} \sim \Lambda_{\mathrm{QCD}}/Q$ not only the first term with $n = 1$ in (5.110) has to be considered. The result is then a change in the overall shape of the distribution [83, 169].

Here we only study the shift of the distribution (5.116), more precisely, the shift of the peak $\Delta\bar{\varepsilon}_p$. From Eq. (5.113) we infer, that the shifts of the peaks for different values of a multiplied by $(1-a)$ are the same when measured at the same scale Q:

$$(1-a)\,\Delta\bar{\varepsilon}_p(a, Q) = (1-b)\,\Delta\bar{\varepsilon}_p(b, Q). \tag{5.117}$$

Fig. 5.5 shows the shifts of the peaks between our NLL resummed predictions and the corresponding hadronic distributions computed with PYTHIA with the string fragmentation model as in Sec. 5.6.2, multiplied by $(1-a)$, at c.m. energy $Q = \sqrt{s} = 91$ GeV. We compare the so-obtained value to the shift of the peak for the thrust ($a = 0$) determined in [170] between resummed predictions and experimental data. The shifts for different values of a obey the relation Eq. (5.117) surprisingly well, although the peaks are at fairly small values of $\bar{\varepsilon}$. This seems to confirm the universality of the power corrections within the class of event shapes under consideration, Eq. (5.113).

5.8 Summary and Outlook

We have introduced a general class of inclusive event shapes in e^+e^- dijet events which reduce to the thrust and the jet broadening distributions as special cases. We have derived analytic expressions in transform space, and have shown the equivalence of our formalism at NLL with the well-known result for the thrust [30, 142]. Separate studies of this class of event shapes at higher orders, more quantitative studies of power corrections, and a comparison to experiment are certainly of interest. We reserve these studies for future work.

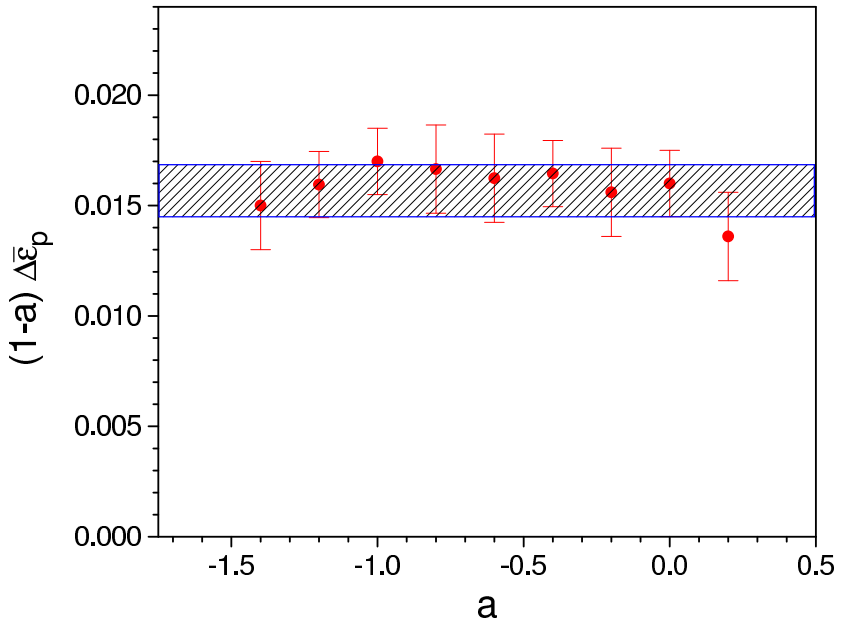

Figure 5.5: Shifts of the peaks $\Delta\bar{\varepsilon}_p(a, Q = \sqrt{s} = 91 \text{ GeV})$ of the distributions $\frac{1}{\sigma}\frac{d\sigma}{d\bar{\varepsilon}}$ between NLL partonic resummed predictions and hadronic cross sections computed with PYTHIA with string fragmentation. The result is multiplied by $(1 - a)$. The blue band is the shift of the peak for the thrust determined in [170] between resummed predictions and experimental data.

Measurements of jet events in general rely on our determination of the energies of jets in the presence of an "underlying event", consisting of particles not directly associated with jet production. An understanding of the underlying event requires good control over perturbative bremsstrahlung associated with the hard scattering itself, so that the two effects may be separated. In the next chapter we will correlate the general class of event shapes discussed above with the measurement of energy flow into restricted parts of phase space. Such correlations between event shapes and energy flow emphasize radiation directly from the partons that undergo the hard scattering. Studies of these shape/flow correlations may therefore help to disentangle the underlying event from the bremsstrahlung of the hard scattering.

Chapter 6

Interjet Energy Flow/Event Shape Correlations

Energy flow [171, 172, 173, 174] into angular regions between energetic jets gives information that is in some ways complementary to what we learn from event shapes. In perturbation theory, the distribution of particles in the final state reflects interference between radiation from different jets [133], and there is ample evidence for perturbative antenna patterns in interjet radiation at both e^+e^- [175, 176, 177, 178, 179] and hadron colliders [180, 181]. Energy flow between jets must also encode the mechanisms that neutralize color in the hadronization process, and the transition of QCD from weak to strong coupling. Knowledge of the interplay between energy and color flows [9, 147] may help identify the underlying event in hadron collisions [182, 183], to distinguish QCD bremsstrahlung from signals of new physics. Nevertheless, the systematic computation of energy flow into interjet regions has turned out to be subtle [184, 185, 186] for reasons that we will review below, and requires a careful construction of the class of jet events.

Here we introduce correlations between event shapes and energy flow, "shape/flow correlations", that are sensitive primarily to radiation from the highest-energy jets. So long as the observed energy is not too small, in a manner to be quantified below, we may control logarithms of the ratio of energy flow to jet energy. This chapter is based on our publications [9, 10, 11].

The energy flow observables that we discuss below are distributions associated with radiation into a chosen interjet angular region, Ω. Within Ω we identify a kinematic quantity $Q_\Omega \equiv \varepsilon Q$, at c.m. energy Q, with $\varepsilon \ll 1$. Q_Ω may be the sum of energies, transverse energies or related observables for the particles emitted into Ω. Let us denote by $\bar{\Omega}$ the complement of Ω. We are interested in the distribution of Q_Ω for events with a fixed number of jets in

$\bar{\Omega}$. This set of events may be represented schematically as

$$A + B \rightarrow \text{ Jets } + X_{\bar{\Omega}} + R_{\Omega}(Q_{\Omega})\,. \tag{6.1}$$

Here $X_{\bar{\Omega}}$ stands for radiation into the regions between Ω and the jet axes, and R_{Ω} for radiation into Ω.

We start by describing the subtleties associated with the computation of interjet energy flow in 6.1, before proposing shape/flow correlations as a means to control secondary effects. After giving a two-loop example, we factorize and resum large logarithmic corrections to the shape/flow correlations in e^+e^- dijet events. In Sections 6.5 and 6.6 we give analytical and numerical results for e^+e^- events at NLL. In Sec. 6.7 we show the application of our formalism to events with hadrons in the initial state. For hadronic events, the nontrivial color flow can be described via matrices in the space of color exchanges. Explicit color decompositions are listed in Appendix C.

6.1 Non-global Logarithms

The subtlety associated with the computation of energy flow concerns the origin of logarithms, and is illustrated by Fig. 6.1. Gluon 1 in Fig. 6.1 is an example of a primary gluon, emitted directly from the hard partons near a jet axis. Phase space integrals for primary emissions contribute single logarithms per loop: $(1/Q_{\Omega})\alpha_s^n \ln^{n-1}(Q/Q_{\Omega}) = (1/\varepsilon Q)\alpha_s^n \ln^{n-1}(1/\varepsilon)$, $n \geq 1$, and these logarithms exponentiate in a straightforward fashion [9]. At fixed Q_{Ω} for Eq. (6.1), however, there is another source of potentially large logarithmic corrections in Q_{Ω}. These are illustrated by gluon 2 in the figure, an example of secondary radiation in Ω, originating a parton emitted by one of the leading jets that define the event into intermediate region $\bar{\Omega}$. As observed by Dasgupta and Salam [184, 185, 186], emissions into Ω from such secondary partons can also result in logarithmic corrections, of the form $(1/Q_{\Omega})\alpha_s^n \ln^{n-1}(\bar{Q}_{\bar{\Omega}}/Q_{\Omega})$, $n \geq 2$, where $\bar{Q}_{\bar{\Omega}}$ is the maximum energy emitted into $\bar{\Omega}$. These logarithms arise from strong ordering in the energies of the primary and secondary radiation because real and virtual enhancements associated with secondary emissions do not cancel each other fully at fixed Q_{Ω}.

If the cross section is fully inclusive outside of Ω, so that no restriction is placed on the radiation into $\bar{\Omega}$, $\bar{Q}_{\bar{\Omega}}$ can approach Q, and the secondary logarithms can become as important as the primary logarithms. Such a cross section, in which only radiation into a fixed portion of phase space (Ω) is specified, was termed "non-global" by Dasgupta and Salam, and the associated logarithms are also called non-global [184, 185, 186, 187, 188, 189, 190, 191].

In effect, a non-global definition of energy flow is not restrictive enough to limit final states to a specific set of jets, and non-global logarithms are produced by jets of intermediate energy, emitted in directions between region Ω and the leading jets. Thus, interjet energy flow does not always originate directly from the leading jets, in the absence of a systematic criterion for suppressing intermediate radiation. Correspondingly, non-global logarithms reflect color flow at all scales, and do not exponentiate in a simple manner. Our aim in this chapter is to formulate a set of observables for interjet radiation in which non-global logarithms are replaced by calculable corrections, and which reflect the flow of color at short distances. By restricting the sizes of event shapes, we will limit radiation in region $\bar{\Omega}$, while retaining the chosen jet structure.

An important observation that we will employ below is that non-global logarithms are not produced by secondary emissions that are very close to a jet direction, because a jet of parallel-moving particles emits soft radiation coherently. By fixing the value of an event shape near the limit of narrow jets, we avoid final states with large energies in $\bar{\Omega}$ away from the jet axes. At the same time, we will identify limits in which non-global logarithms reemerge as leading corrections, and where the methods introduced to study nonglobal effects in Refs. [184, 185, 186, 188, 189, 190, 191] provide important insights.

To formalize these observations, we study below correlated observables for e^+e^- annihilation into two jets. (In Eq. (6.1) A and B denote positron and electron.) In e^+e^- annihilation dijet events, the underlying color flow pattern is simple, which enables us to concentrate on the energy flow within the event. We give an outlook on the application of our formalism to cross sections with hadrons in the initial state, where the color flow is non-trivial [9, 147]. In this chapter, we will correlate the generalized event shape $\bar{f}(a)$, introduced in the previous chapter, with energy flow. To avoid large non-global logarithmic corrections we weigh events by $\exp[-\nu \bar{f}]$, with ν the Laplace transform conjugate variable. The parameter a allows us to dial the amount of energy emitted into the interjet radiation, thus to control non-global logarithmic corrections.

For the restricted set of events with narrow jets, energy flow is proportional to the lowest-order cross section for gluon radiation into the selected region. The resummed cross section, however, remains sensitive to color flow at short distances through anomalous dimensions associated with coherent interjet soft emission. In a sense, our results show that an appropriate selection of jet events automatically suppresses nonglobal logarithms, and confirms the observation of coherence in interjet radiation [133, 180].

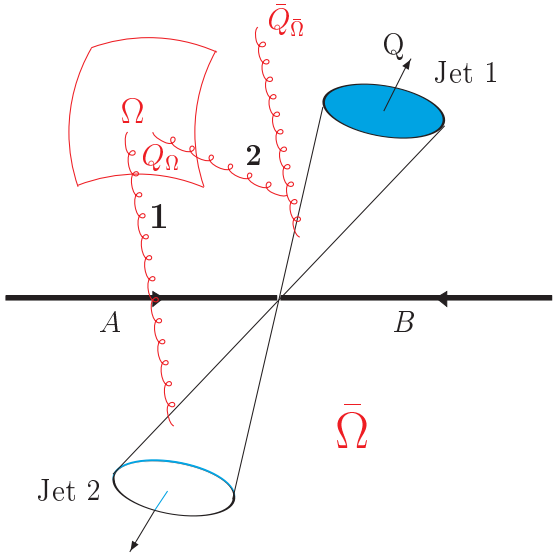

Figure 6.1: Sources of global and non-global logarithms in dijet events. Configuration 1, a primary emission, is the source of global logarithms. Configuration 2 can give non-global logarithms.

6.2 Shape/Flow Correlations in e^+e^- Dijet Events

6.2.1 Shape/Flow Correlations

In the notation of Eq. (6.1), we will study an event shape distribution for the process

$$e^+ + e^- \to J_1(p_{J_1}) + J_2(p_{J_2}) + X_{\bar{\Omega}}\left(\bar{f}\right) + R_\Omega(Q_\Omega)\,, \tag{6.2}$$

at c.m. energy $Q \gg Q_\Omega \gg \Lambda_{\rm QCD}$. Two jets with momenta p_{J_c}, $c = 1, 2$ emit soft radiation (only) at wide angles. Again, Ω is a region between the jets to be specified below, where the total energy or the transverse energy Q_Ω of the soft radiation is measured, and $\bar{\Omega}$ denotes the remaining phase space (see Fig. 6.1). Radiation into $\bar{\Omega}$ is constrained by event shape $\bar{f}$, Eq. (5.3). We refer to cross sections at fixed values (or transforms) of $\bar{f}$ and Q_Ω as shape/flow correlations.

We find the jet axes as described in Section 5.1, minimizing the thrust-related quantity $\bar{f}_{\bar{\Omega}_1}(N, a = 0)$. In contrast to Sec. 5.1, we divide now the phase space into three regions:

- Region Ω, in which we measure, for example, the energy flow,
- Region $\bar{\Omega}_1$, the entire hemisphere centered on $\hat{n}_1$, that is, around jet 1, except its intersection with Ω,
- Region $\bar{\Omega}_2$, the complementary hemisphere, except its intersection with Ω.

We will study the correlations of the set of event shapes $\bar{f}(a)$ with the energy flow into Ω, denoted as

$$f(N) = \frac{1}{\sqrt{s}} \sum_{\hat{n}_i \in \Omega} \omega_i \,. \tag{6.3}$$

The differential cross section for such dijet events at fixed values of $\bar{f}$ and f is given by

$$\begin{aligned} \frac{d\bar{\sigma}(\varepsilon, \bar{\varepsilon}, s, a)}{d\varepsilon \, d\bar{\varepsilon} \, d\hat{n}_1} &= \frac{1}{2s} \sum_N |M(N)|^2 \, (2\pi)^4 \, \delta^4(p_I - p_N) \\ &\quad \times \delta(\varepsilon - f(N)) \, \delta(\bar{\varepsilon} - \bar{f}(N, a)) \, \delta^2(\hat{n}_1 - \hat{n}(N)) \,, \end{aligned} \tag{6.4}$$

to be contrasted with the corresponding inclusive event shape, Eq. (5.7). ε, like $\bar{\varepsilon}$, is required to be much less than unity in the elastic limit:

$$0 < \varepsilon \ll 1. \tag{6.5}$$

We choose our coordinate system in the same way as in the previous chapter, Eq. (5.10).

Here we seek to control corrections in the single-logarithmic variable $\alpha_s(Q) \ln(1/\varepsilon)$, with $\varepsilon = Q_\Omega / Q$. Such a resummation is most relevant when

$$\alpha_s(Q) \ln\left(\frac{1}{\varepsilon}\right) \geq 1 \to \varepsilon \leq \exp\left(\frac{-1}{\alpha_s(Q)}\right) . \tag{6.6}$$

Let us compare these logarithms to non-global effects in shape/flow correlations. At $\nu = 0$ and for $a \to -\infty$, the cross section becomes inclusive outside Ω. As we show below, the non-global logarithms discussed in Refs. [184, 185, 186] appear in shape/flow correlations as logarithms of the form $\alpha_s(Q) \ln(1/(\varepsilon\nu))$, with ν the moment variable conjugate to the event shape.

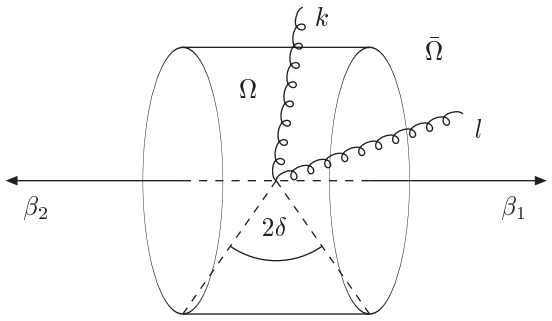

Figure 6.2: A kinematic configuration that gives rise to the non-global logarithms. A soft gluon with momentum k is radiated into the region Ω, and an energetic gluon with momentum l is radiated into $\bar{\Omega}$. Four-vectors β_1 and β_2, define the directions of jet 1 and jet 2, respectively.

To treat these logarithms as subleading for small ε and (relatively) large ν, we require that

$$\alpha_s(Q)\,\ln\left(\frac{1}{\varepsilon\nu}\right) < 1 \rightarrow \varepsilon > \frac{1}{\nu}\,\exp\left(\frac{-1}{\alpha_s(Q)}\right)\,. \tag{6.7}$$

For large ν, there is a substantial range of ε in which both (6.6) and (6.7) can hold. When ν is large, moments of the correlation are dominated precisely by events with strongly two-jet energy flows, which is the natural set of events in which to study the influence of color flow on interjet radiation. (The peak of the thrust cross section is at $(1-T)$ of order one-tenth at LEP energies, corresponding to ν of order ten, so the requirement of large ν is not overly restrictive.) In the next subsection, we show how the logarithms of $(\varepsilon\nu)^{-1}$ emerge in a low order example.

6.2.2 Low Order Example

In this section, we check the general ideas developed above with the concrete example of a two-loop cross section for the process (6.2). This is the lowest order in which a non-global logarithm occurs, as observed in [184, 185, 186]. We normalize this cross section to the Born cross section for inclusive dijet production. A similar analysis for the same geometry has been carried out in [185] and [191].

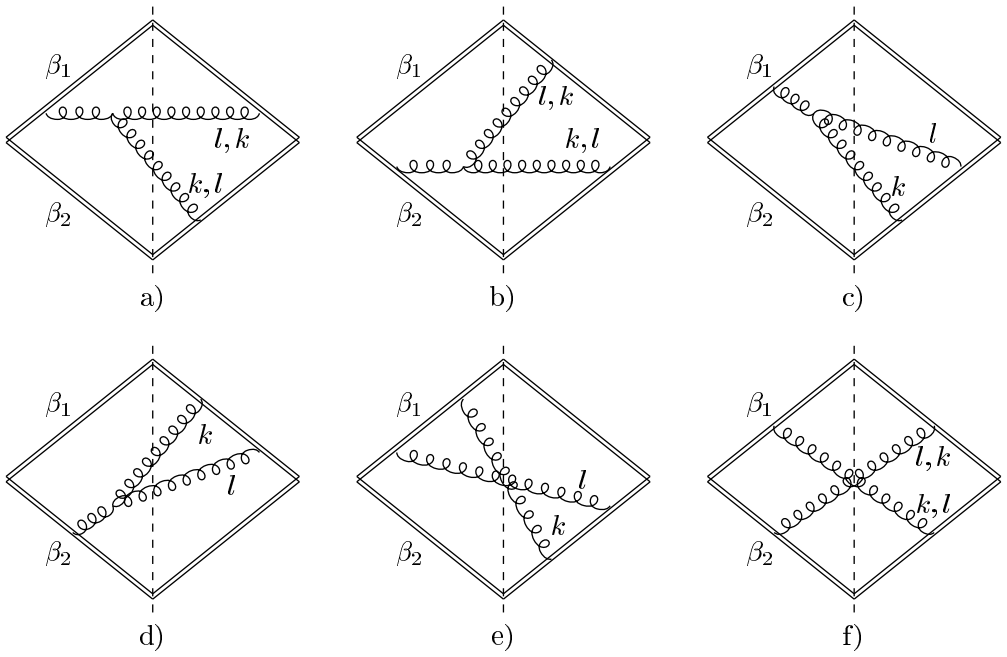

Figure 6.3: The relevant two-loop cut diagrams corresponding to the emission of two real gluons in the final state contributing to the eikonal cross section. The dashed line represents the final state, with contributions to the amplitude to the left, and to the complex conjugate amplitude to the right.

The kinematic configuration we consider is shown in Fig. 6.2. Two fast partons, of velocities $\vec{\beta}_1$ and $\vec{\beta}_2$, are treated in eikonal approximation. In addition, gluons are emitted into the final state. A soft gluon with momentum k is radiated into region Ω and an energetic gluon with momentum l is emitted into the region $\bar{\Omega}$. We consider the cross section at fixed energy, $\omega_k \equiv \varepsilon\sqrt{s}$. As indicated above, non-global logarithms arise from strong ordering of the energies of the gluons, which we choose as $\omega_l \gg \omega_k$. In this region, the gluon l plays the role of a "primary" emission, while k is a "secondary" emission.

For our calculation, we take the angular region Ω to be a "slice" or "ring" in polar angle of width 2δ, or equivalently, (pseudo) rapidity interval $(-\eta, \eta)$, with

$$\Delta\eta = 2\eta = \ln\left(\frac{1+\sin\delta}{1-\sin\delta}\right) , \tag{6.8}$$

The lowest-order diagrams for this process are those shown in Fig. 6.3, including distinguishable diagrams in which the momenta k and l are interchanged.

The diagrams of Fig. 6.3 give rise to color structures C_F^2 and $C_F C_A$, but terms proportional to C_F^2 may be associated with a factorized contribution to the cross section, in which the gluon k is emitted coherently by the combinations of the gluon l and the eikonals. To generate the $C_F C_A$ part, on the other hand, gluon k must "resolve" gluon l from the eikonal lines, giving a result that depends on the angles between $\vec{l}$ and the eikonal directions.

We choose the reference frame such that the momenta of the final state particles are given by:

$$\begin{aligned} \beta_1 &= (1,0,0,1), \\ \beta_2 &= (1,0,0,-1), \\ l &= \omega_l(1, s_l, 0, c_l), \\ k &= \omega_k(1, s_k\cos\phi, s_k\sin\phi, c_k). \end{aligned} \tag{6.9}$$

Here we define $s_{l,k} \equiv \sin\theta_{l,k}$ and $c_{l,k} \equiv \cos\theta_{l,k}$. θ_l is the angle between the vectors $\vec{l}$ and $\vec{\beta_1}$, θ_k is the angle between the vectors $\vec{k}$ and $\vec{\beta_1}$ and ϕ is the azimuthal angle of the gluon with momentum k relative to the plane defined by β_1, β_2 and l. The available phase space in polar angle for the radiated gluons is $\theta_k \in (\pi/2-\delta,\, \pi/2+\delta)$ and $\theta_l \in (0,\, \pi/2-\delta) \cup (\pi/2+\delta,\, \pi)$.

Using the diagrammatic rules for eikonal lines and vertices, as listed in Appendix A.2, we can write down the expressions corresponding to each diagram separately. For example, diagram 6.3 a) gives

$$\begin{aligned} a) + (k \leftrightarrow l) \;=\; & \left[f_{abc}\mathrm{Tr}(\mathrm{T^a T^b T^c})\right]\left(-ig_s^4\,\beta_1^\alpha\beta_2^\beta\beta_1^\gamma\right) V_{\alpha\beta\gamma}(k+l,-k,-l) \\ & \times \frac{1}{\beta_1\cdot(k+l)}\,\frac{1}{2k\cdot l}\,\frac{1}{\beta_1\cdot l}\,\frac{1}{\beta_2\cdot k} \\ + \;\; & (k \leftrightarrow l). \end{aligned} \tag{6.10}$$

$V_{\alpha\beta\gamma}(k+l,-k,-l) = [(2k+l)_\gamma g_{\alpha\beta} + (l-k)_\alpha g_{\beta\gamma} - (2l+k)_\beta g_{\alpha\gamma}]$ is the momentum-dependent part of the three gluon vertex. Using the color identity f_{abc} Tr $(T^a T^b T^c) = iC_F\mathcal{N}_C C_A/2$, and the approximation $\beta_j\cdot l \gg \beta_j\cdot k$ for $j=1,2$, which is valid due to the strong ordering of the final state gluon energies, we arrive at

$$a) + (k \leftrightarrow l) = \frac{1}{4}\,C_F\mathcal{N}_C C_A\,g_s^4\,\frac{\beta_1\cdot\beta_2}{k\cdot l}\left(\frac{1}{\beta_1\cdot k\,\beta_2\cdot l} + \frac{2}{\beta_1\cdot l\,\beta_2\cdot k}\right). \tag{6.11}$$

We proceed in a similar manner for the rest of the diagrams. The results are:

$$b) + (k \leftrightarrow l) \;=\; \frac{1}{4}\,C_F\mathcal{N}_C C_A\,g_s^4\,\frac{\beta_1\cdot\beta_2}{k\cdot l}\left(\frac{2}{\beta_1\cdot k\,\beta_2\cdot l} + \frac{1}{\beta_1\cdot l\,\beta_2\cdot k}\right),$$

$$
\begin{aligned}
c) &= \frac{1}{4}\, C_F \mathcal{N}_C C_A\, g_s^4\, \frac{\beta_1\cdot\beta_2}{k\cdot l}\, \frac{1}{\beta_1\cdot l}\, \frac{1}{\beta_2\cdot k}, \\
d) &= \frac{1}{4}\, C_F \mathcal{N}_C C_A\, g_s^4\, \frac{\beta_1\cdot\beta_2}{k\cdot l}\, \frac{1}{\beta_1\cdot k}\, \frac{1}{\beta_2\cdot l}, \\
e) &= C_F \mathcal{N}_C (C_F - C_A/2)\, g_s^4\, \frac{(\beta_1\cdot\beta_2)^2}{\beta_1\cdot l\, \beta_2\cdot l}\, \frac{1}{\beta_1\cdot k\, \beta_2\cdot k}, \\
f) + (k \leftrightarrow l) &= C_F \mathcal{N}_C (C_F - C_A/2)\, g_s^4\, \frac{(\beta_1\cdot\beta_2)^2}{\beta_1\cdot l\, \beta_2\cdot l}\, \frac{2}{\beta_1\cdot k\, \beta_2\cdot k}. \qquad (6.12)
\end{aligned}
$$

The color factors in the last two equations of (6.12) are obtained from the identity $\mathrm{Tr}(\mathrm{T^a T^b T^a T^b}) = \mathrm{C_F \mathcal{N}_C (C_F - C_A/2)}$. Combining the terms proportional to the color factor $C_F \mathcal{N}_C C_A$, and including the complex conjugate diagrams, we find for the squared amplitude

$$
\begin{aligned}
|M|^2 &= 2\, g_s^4\, C_F \mathcal{N}_C C_A\, \beta_1\cdot\beta_2 \left(\frac{1}{k\cdot l\, \beta_1\cdot k\, \beta_2\cdot l} + \frac{1}{k\cdot l\, \beta_1\cdot l\, \beta_2\cdot k} \right. \\
&\quad \left. - \frac{\beta_1\cdot\beta_2}{\beta_1\cdot l\, \beta_2\cdot l\, \beta_1\cdot k\, \beta_2\cdot k} \right). \qquad (6.13)
\end{aligned}
$$

We take, as indicated above, a Laplace transform with respect to the shape variable, and identify the logarithm in the conjugate variable ν. In the frame (6.9) we find that the logarithmic $C_F C_A$-dependence of Fig. 6.3 may be written as a dimensionless eikonal cross section in terms of one energy and two polar angular integrals as

$$
\begin{aligned}
\frac{d\sigma_{\mathrm{eik}}}{d\,\varepsilon} &= C_F C_A \left(\frac{\alpha_s}{\pi}\right)^2 \frac{1}{\varepsilon} \int_{-\sin\delta}^{\sin\delta} \mathrm{dc_k} \int_{\sin\delta}^{1} \mathrm{dc_l} \int_{\varepsilon\sqrt{\mathrm{s}}}^{\sqrt{\mathrm{s}}} \frac{\mathrm{d}\omega_\mathrm{l}}{\omega_\mathrm{l}}\, \mathrm{e}^{-\nu\,\omega_\mathrm{l}\,(1-\mathrm{c_l})^{1-\mathrm{a}}\,\mathrm{s_l^a/Q}} \\
&\quad \times \left[\frac{1}{c_k + c_l}\, \frac{1}{1+c_k} \left(\frac{1}{1+c_l} + \frac{1}{1-c_k} \right) - \frac{1}{s_k^2}\, \frac{1}{1+c_l} \right]. \qquad (6.14)
\end{aligned}
$$

In this form, the absence of collinear singularities in the $C_F C_A$ term at $\cos\theta_l = +1$ is manifest, independent of ν. Collinear singularities in the l integral completely factorize from the k integral, and are proportional to C_F^2. The logarithmic dependence on ε for $\nu > 1$ is readily found to be

$$
\frac{d\sigma_{\mathrm{eik}}}{d\,\varepsilon} = C_F C_A \left(\frac{\alpha_s}{\pi}\right)^2 \frac{1}{\varepsilon}\, \ln\left(\frac{1}{\varepsilon\nu}\right)\, C(\Delta\eta)\,, \qquad (6.15)
$$

where $C(\Delta\eta)$ is a finite function of the angle δ, or equivalently, of the rapidity width of the region Ω, Eq. (6.8).

$$
C(\delta) = \frac{\pi^2}{6} + \ln\left(\frac{\cot\delta\,(1+\sin\delta)}{4}\right) \ln\left(\frac{1+\sin\delta}{1-\sin\delta}\right) + \mathrm{Li}_2\left(\frac{1-\sin\delta}{2}\right)
$$

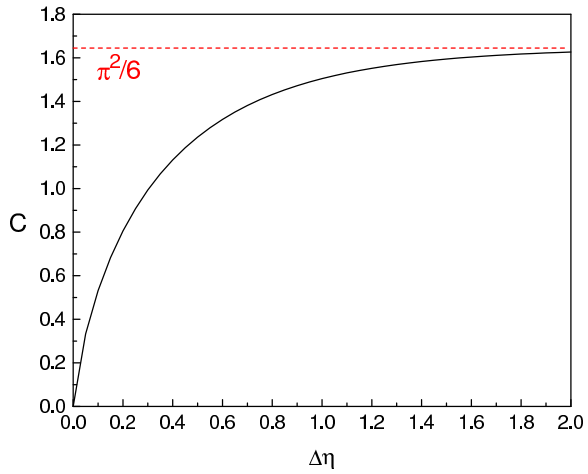

Figure 6.4: $C(\Delta\eta)$, as defined in (6.17), as a function of rapidity width $\Delta\eta$ of the region Ω. The dashed line is its limiting value, $C(\Delta\eta \to \infty) = \pi^2/6$.

$$- \quad \mathrm{Li}_2\left(\frac{1+\sin\delta}{2}\right) - \mathrm{Li}_2\left(-\frac{2\sin\delta}{1-\sin\delta}\right) - \mathrm{Li}_2\left(\frac{1-\sin\delta}{1+\sin\delta}\right). \qquad (6.16)$$

or equivalently,

$$\begin{aligned} C(\Delta\eta) &= \frac{\pi^2}{6} + \Delta\eta\left(\frac{\Delta\eta}{2} - \ln\left(2\sinh(\Delta\eta)\right)\right) + \mathrm{Li}_2\left(\frac{\mathrm{e}^{-\Delta\eta/2}}{2\,\cosh(\Delta\eta/2)}\right) \\ &- \mathrm{Li}_2\left(\frac{\mathrm{e}^{\Delta\eta/2}}{2\,\cosh(\Delta\eta/2)}\right) - \mathrm{Li}_2\left(-2\sinh(\Delta\eta/2)\,\mathrm{e}^{\Delta\eta/2}\right) - \mathrm{Li}_2(\mathrm{e}^{-\Delta\eta}). \end{aligned} \qquad (6.17)$$

The coefficient $C(\Delta\eta)$ as a function of $\Delta\eta$ is shown in Fig. 6.4. Naturally, C is a monotonically increasing function of $\Delta\eta$. For $\Delta\eta \to 0$,

$$C \sim \mathcal{O}(\Delta\eta\,\ln\Delta\eta)\,, \qquad (6.18)$$

and the cross section vanishes, as expected. On the other hand, as the size of region Ω increases, C rapidly saturates and reaches its limiting value [185]

$$\lim_{\Delta\eta\to\infty} C = \frac{\pi^2}{6}\,. \qquad (6.19)$$

We can contrast the result (6.15) to what happens when $\nu = 0$, that is, for an inclusive, non-global cross section. In this case, recalling that $\varepsilon = Q_\Omega/Q$,

we find in place of Eq. (6.15) the non-global logarithm

$$\frac{d\sigma_{\rm eik}}{d\,\varepsilon} = C_F C_A \left(\frac{\alpha_s}{\pi}\right)^2 \frac{1}{\varepsilon} \ln\left(\frac{Q}{Q_\Omega}\right) C(\Delta\eta)\,. \tag{6.20}$$

As anticipated, the effect of the transform is to replace the non-global logarithm in Q/Q_Ω, by a logarithm of $1/(\varepsilon\nu)$. We are now ready to generalize this result, starting from the factorization properties of the cross section near the two-jet limit.

6.3 Factorization of the Cross Section for e^+e^-

As in the previous Chapter, an arbitrary final state N is the union of substates associated with the leading regions:

$$N = N_s \oplus N_{J_1} \oplus N_{J_2}\,. \tag{6.21}$$

Therefore, the event shape $\bar{f}$ can, as above, be written as a sum of contributions from the soft and jet subdiagrams, Eq. (5.12). In contrast, the energy flow weight, $f(N)$, depends only on particles emitted at wide angles, and is hence insensitive to collinear radiation:

$$f(N) = f(N_s)\,. \tag{6.22}$$

Analogous to Eq. (5.19) for the inclusive event shape we can write the cross section in convolution form,

$$\begin{aligned}\frac{d\bar{\sigma}(\varepsilon,\bar{\varepsilon},s,a)}{d\varepsilon\,d\bar{\varepsilon}\,d\hat{n}_1} &= \frac{d\sigma_0}{d\hat{n}_1}\,H(s,\hat{n}_1,\mu)\int d\bar{\varepsilon}_s\,\bar{S}(\varepsilon,\bar{\varepsilon}_s,a,\mu) \\ &\quad\times\prod_{c=1}^{2}\int d\bar{\varepsilon}_{J_c}\,\bar{J}_c(\bar{\varepsilon}_{J_c},a,\mu)\,\delta(\bar{\varepsilon}-\bar{\varepsilon}_{J_1}-\bar{\varepsilon}_{J_2}-\bar{\varepsilon}_s)\,,\end{aligned} \tag{6.23}$$

where we have made the same approximations listed in Sec. 5.2.2. The difference between (5.19) and (6.23) lies in the soft function, which now depends on the energy flow ε.

$$\bar{S}(\varepsilon,\bar{\varepsilon}_s,a,\mu) = \sum_{N_s}\,\mathcal{S}(N_s,\mu)\,\delta(\varepsilon - f(N_s))\,\delta(\bar{\varepsilon}_s - \bar{f}(N_s,a)) \tag{6.24}$$

We will discuss the explicit construction of the new soft function below.

Upon taking the Laplace moments with respect to $\bar{\varepsilon}$, (6.23) becomes a simple product in moment space:

$$\begin{aligned}\frac{d\sigma(\varepsilon,\nu,s,a)}{d\varepsilon\, d\hat{n}_1} &= \int_0^\infty d\bar{\varepsilon}\, e^{-\nu\,\bar{\varepsilon}}\, \frac{d\bar{\sigma}(\varepsilon,\bar{\varepsilon},a)}{d\varepsilon\, d\bar{\varepsilon}\, d\hat{n}_1} \\ &= \frac{d\sigma_0}{d\hat{n}_1}\, H(s,\hat{n}_1,\mu)\, S(\varepsilon,\nu,a,\mu) \prod_{c=1}^{2} J_c(\nu,a,\mu). \qquad (6.25)\end{aligned}$$

Since radiation at wide angles decouples from the jet and the hard scattering functions, these are not affected by measuring the energy flow ε. Their construction is therefore the same as discussed in Sections 5.2.4 and 5.2.5. The construction of the soft function needs to be amended to include dependence on the energy flow.

6.3.1 The Soft Function

Because wide-angle, soft radiation is independent of the internal jet evolution, products of nonabelian phase operators generate the same wide-angle radiation as the full jets. Since Ω is at wide angles from the jets, we can define for the two-jet cross section at measured ε and $\bar{\varepsilon}_{\rm eik}$

$$\begin{aligned}\bar{\sigma}^{(\rm eik)}(\varepsilon,\bar{\varepsilon}_{\rm eik},a,\mu) \equiv \frac{1}{\mathcal{N}_C} &\sum_{N_{\rm eik}} \left\langle 0 \left| \Phi_{\beta_2}^{(\bar{\rm q})\dagger}(\infty,0;0)\Phi_{\beta_1}^{({\rm q})\dagger}(\infty,0;0)\right| N_{\rm eik}\right\rangle \\ &\times \left\langle N_{\rm eik}\left|\Phi_{\beta_1}^{({\rm q})}(\infty,0;0)\Phi_{\beta_2}^{(\bar{\rm q})}(\infty,0;0)\right| 0\right\rangle \\ &\times \delta\left(\varepsilon - f(N_{\rm eik})\right)\delta\left(\bar{\varepsilon}_{\rm eik} - \bar{f}(N_{\rm eik},a)\right) \\ = \;& \delta(\varepsilon)\,\delta(\bar{\varepsilon}_{\rm eik}) + \mathcal{O}(\alpha_s)\,. \qquad (6.26)\end{aligned}$$

The sum is over all final states $N_{\rm eik}$ in the eikonal cross section. μ denotes the renormalization scale which is set equal to the factorization scale. As in the previous chapter, the shape function $\bar{\varepsilon}_{\rm eik}$ is defined by $\bar{f}(N_{\rm eik},a)$ as in Eqs. (5.2) and (5.3), separately for each of the hemispheres around the jets.

In order to avoid double counting of collinear radiation, we subtract eikonal jets as defined in Eq. (5.46). The eikonal cross section (6.26) then factorizes as

$$\begin{aligned}\bar{\sigma}^{(\rm eik)}(\varepsilon,\bar{\varepsilon}_{\rm eik},a,\mu) \;\equiv\; & \int d\bar{\varepsilon}_s\, \bar{S}(\varepsilon,\bar{\varepsilon}_s,a,\mu) \prod_{c=1}^{2} \int d\bar{\varepsilon}_c\, \bar{J}_c^{(\rm eik)}(\bar{\varepsilon}_c,a,\mu) \\ &\times\delta\left(\bar{\varepsilon}_{\rm eik} - \bar{\varepsilon}_s - \bar{\varepsilon}_1 - \bar{\varepsilon}_2\right). \qquad (6.27)\end{aligned}$$

In Laplace transform space (5.43) we can solve for the soft function as

$$S\left(\varepsilon,\nu,a,\mu\right)=\frac{\sigma^{(\mathrm{eik})}\left(\varepsilon,\nu,a,\mu\right)}{\prod_{c=1}^{2}J_{c}^{(\mathrm{eik})}\left(\nu,a,\mu\right)}=\delta(\varepsilon)+\mathcal{O}(\alpha_{s})\,. \tag{6.28}$$

The soft function retains ν-dependence through soft emission, which is also restricted by the weight function ε.

Following the same argumentation as in Sec. 5.2.6 we can deduce the arguments of the soft function in transform space as

$$S\left(\varepsilon,\nu,a,\mu\right)=S\left(\frac{\varepsilon\sqrt{s}}{\mu},\varepsilon\nu,\frac{\sqrt{s}}{\mu\nu}\left(\zeta_{c}\right)^{1-a},a,\alpha_{s}(\mu)\right)\,. \tag{6.29}$$

6.4 Resummation for e^+e^- Shape/Flow Correlations

Summarizing the results so far, we can rewrite Eq. (6.25) in terms of the hard, jet and soft functions identified above, which depend on the kinematic variables and the moment ν according to Eqs. (5.31), (5.43) and (6.29) respectively,

$$\begin{aligned}\frac{d\sigma\left(\varepsilon,\nu,s,a\right)}{d\varepsilon\,d\hat{n}_{1}} &= \frac{d\sigma_{0}}{d\hat{n}_{1}}\,H\left(\frac{\sqrt{s}}{\mu},\frac{p_{J_{c}}\cdot\hat{\xi}_{c}}{\mu},\hat{n}_{1},\alpha_{s}(\mu)\right)\\ &\quad\times\prod_{c=1}^{2}J_{c}\left(\frac{p_{J_{c}}\cdot\hat{\xi}_{c}}{\mu},\frac{\sqrt{s}}{\mu\nu}\left(\zeta_{c}\right)^{1-a},a,\alpha_{s}(\mu)\right)\\ &\quad\times S\left(\frac{\varepsilon\sqrt{s}}{\mu},\varepsilon\nu,\frac{\sqrt{s}}{\mu\nu}\left(\zeta_{c}\right)^{1-a},a,\alpha_{s}(\mu)\right)\,.\end{aligned} \tag{6.30}$$

As above, the natural scale for the coupling in the hard scattering H is $\sqrt{s}/2$. Setting $\mu=\sqrt{s}/2$ in Eq. (6.30) introduces large logarithms of ε in the soft function and large logarithms of ν in the jet and soft functions.

6.4.1 Energy Flow Dependence

To resum large logarithms of ε in the soft function, we use the renormalization group equation

$$\mu\frac{d}{d\mu}\frac{d\sigma\left(\varepsilon,\nu,s,a\right)}{d\varepsilon\,d\hat{n}_{1}}=0 \tag{6.31}$$

which follows from the independence of the physical correlation of the factorization scale. Applying Eq. (6.31) to the factorized correlation (6.30), we derive the following consistency conditions, which are themselves renormalization group equations:

$$\mu\frac{d}{d\mu}\ \ln\ S\left(\frac{\varepsilon\sqrt{s}}{\mu},\varepsilon\nu,\frac{\sqrt{s}}{\mu\nu}(\zeta_c)^{1-a},a,\alpha_s(\mu)\right) \ = \ -\gamma_s\left(\alpha_s(\mu)\right), \tag{6.32}$$

$$\mu\frac{d}{d\mu}\ \ln\ J_c\left(\frac{p_{J_c}\cdot\hat{\xi}_c}{\mu},\frac{\sqrt{s}}{\mu\nu}\left(\zeta_c\right)^{1-a},a,\alpha_s(\mu)\right) \ = \ -\gamma_{J_c}\left(\alpha_s(\mu)\right), \tag{6.33}$$

$$\mu\frac{d}{d\mu}\ \ln\ H\left(\frac{\sqrt{s}}{\mu},\frac{p_{J_c}\cdot\hat{\xi}_c}{\mu},\hat{n}_1,\alpha_s(\mu)\right) \ = \ \gamma_s\left(\alpha_s(\mu)\right)+\sum_{c=1}^{2}\gamma_{J_c}\left(\alpha_s(\mu)\right)\ . \tag{6.34}$$

The anomalous dimensions γ_d, $d=s$, J_c can depend only on variables held in common between at least two of the functions. Because each function is infrared safe, while ultraviolet divergences are present only in virtual diagrams, the anomalous dimensions cannot depend on the parameters ν, ε or a. This leaves as arguments of the γ_d only the coupling $\alpha_s(\mu)$, which we exhibit, and ζ_c, which we suppress for now.

Solving Eqs. (6.32) and (6.33) we find

$$S\left(\frac{\varepsilon\sqrt{s}}{\mu},\varepsilon\nu,\frac{\sqrt{s}}{\mu\nu}\left(\zeta_c\right)^{1-a},a,\alpha_s(\mu)\right) \ = \ S\left(\frac{\varepsilon\sqrt{s}}{\mu_0},\varepsilon\nu,\frac{\sqrt{s}}{\mu_0\nu}\left(\zeta_c\right)^{1-a},a,\alpha_s(\mu_0)\right) \times e^{-\int_{\mu_0}^{\mu}\frac{d\lambda}{\lambda}\gamma_s(\alpha_s(\lambda))}, \tag{6.35}$$

$$J_c\left(\frac{p_{J_c}\cdot\hat{\xi}_c}{\mu},\frac{\sqrt{s}}{\mu\nu}\ \left(\zeta_c\right)^{1-a},a,\alpha_s(\mu)\right) \ = \ J_c\left(\frac{p_{J_c}\cdot\hat{\xi}_c}{\tilde{\mu}_0},\frac{\sqrt{s}}{\tilde{\mu}_0\nu}\ \left(\zeta_c\right)^{1-a},a,\alpha_s(\tilde{\mu}_0)\right) \times e^{-\int_{\tilde{\mu}_0}^{\mu}\frac{d\lambda}{\lambda}\gamma_{J_c}(\alpha_s(\lambda))}, \tag{6.36}$$

for the soft and jet functions. As suggested above, we will eventually pick $\mu\sim\sqrt{s}$ to avoid large logs in H. Using these expressions in Eq. (6.30) we can avoid logarithms of ε or ν in the soft function, by evolving from $\mu_0=\varepsilon\sqrt{s}$ to the factorization scale $\mu\sim\sqrt{s}$. No choice of $\tilde{\mu}_0$, however, controls all logarithms of ν in the jet functions. Leaving $\tilde{\mu}_0$ free, we find for the cross

section (6.30) the intermediate result

$$\begin{aligned}\frac{d\sigma\left(\varepsilon,\nu,s,a\right)}{d\varepsilon\, d\hat{n}_1} &= \frac{d\sigma_0}{d\hat{n}_1}\, H\left(\frac{\sqrt{s}}{\mu}, \frac{p_{J_c}\cdot\hat{\xi}_c}{\mu}, \hat{n}_1, \alpha_s(\mu)\right) \\ &\times S\left(1, \varepsilon\nu, (\zeta_c)^{1-a}, a, \alpha_s(\varepsilon\sqrt{s})\right) \exp\left\{-\int_{\varepsilon\sqrt{s}}^{\mu}\frac{d\lambda}{\lambda}\,\gamma_s\left(\alpha_s(\lambda)\right)\right\} \qquad (6.37) \\ &\times J_c\left(\frac{p_{J_c}\cdot\hat{\xi}_c}{\tilde{\mu}_0}, \frac{\sqrt{s}}{\tilde{\mu}_0\nu}\,(\zeta_c)^{1-a}, a, \alpha_s(\tilde{\mu}_0)\right) \exp\left\{-\int_{\tilde{\mu}_0}^{\mu}\frac{d\lambda}{\lambda}\gamma_{J_c}\left(\alpha_s(\lambda)\right)\right\}.\end{aligned}$$

We have avoided introducing logarithms of ε into the jet functions, which originally only depend on ν, by evolving the soft and the jet functions independently. The choice of $\mu_0 = \varepsilon\sqrt{s}$ or $\sqrt{s}/\nu$ for the soft function is to some extent a matter of convenience, since the two choices differ by logarithms of $\varepsilon\nu$. In general, if we choose $\mu_0 = \sqrt{s}/\nu$, logarithms of $\varepsilon\nu$ will appear multiplied by coefficients that reflect the size of region Ω. An example is Eq. (6.14) above. When Ω has a small angular size, $\mu_0 = \sqrt{s}/\nu$ is generally the more natural choice, since then logarithms in $\varepsilon\nu$ will enter with small weights. In contrast, when Ω grows to cover most angular directions, as in the study of rapidity gaps [192], it is more natural to choose $\mu_0 = \varepsilon\sqrt{s}$.

6.4.2 The Resummed Correlation

The remaining unorganized logarithms reside in the jet functions. Since the definition of the jet functions is unchanged compared to the inclusive event shape of the previous chapter, we can immediately use the conclusions of Section 5.3.1 to resum these logarithms. Using Eq. (5.61) in Eq. (6.37), we obtain after setting $\mu = \sqrt{s}/2$

$$\begin{aligned}\frac{d\sigma\left(\varepsilon,\nu,s,a\right)}{d\varepsilon\, d\hat{n}_1} &= \frac{d\sigma_0}{d\hat{n}_1}\, H\left(\frac{2\,p_{J_c}\cdot\hat{\xi}_c}{\sqrt{s}}, \hat{n}_1, \alpha_s\left(\frac{\sqrt{s}}{2}\right)\right) \\ &\times S\left(1, \varepsilon\nu, (\zeta_c)^{1-a}, a, \alpha_s(\varepsilon\sqrt{s})\right) \exp\left\{-\int_{\varepsilon\sqrt{s}}^{\sqrt{s}/2}\frac{d\lambda}{\lambda}\gamma_s\left(\alpha_s(\lambda)\right)\right\} \\ &\times \prod_{c=1}^{2} J_c\left(1, 1, a, \alpha_s\left(\frac{\sqrt{s}}{2\,\zeta_0}\right)\right) \exp\left\{-\int_{\sqrt{s}/(2\,\zeta_0)}^{\sqrt{s}/2}\frac{d\lambda}{\lambda}\gamma_{J_c}\left(\alpha_s(\lambda)\right)\right\}\end{aligned}$$

$$\times \exp\left\{ - \int\limits_{\sqrt{s}/(2\,\zeta_0)}^{p_{J_c}\cdot\hat{\xi}_c} \frac{d\lambda}{\lambda}\Bigg[B'_c\left(c_1, c_2, a, \alpha_s\left(c_2\lambda\right)\right) + 2 \int\limits_{c_1 \frac{s^{1-a/2}}{\nu(2\,\lambda)^{1-a}}}^{c_2\,\lambda} \frac{d\lambda'}{\lambda'} A'_c\left(c_1, a, \alpha_s\left(\lambda'\right)\right)\Bigg]\right\} . \tag{6.38}$$

Alternatively, we can combine all jet-related exponents in Eq. (6.38) in the correlation. As we have verified in Section 5.4.2, the cross section is independent of the choice of ξ_c. As a result, we can choose $p_{J_c}\cdot\hat{\xi}_c = \frac{\sqrt{s}}{2}$. This choice allows us to combine γ_{J_c} and B'_c in Eq. (6.38),

$$\begin{aligned}
\frac{d\sigma\left(\varepsilon,\nu,s,a\right)}{d\varepsilon\, d\hat{n}_1} \;=\; & \frac{d\sigma_0}{d\hat{n}_1}\, H\left(1,\hat{n}_1,\alpha_s\left(\frac{\sqrt{s}}{2}\right)\right) \\
& \times S\left(1,\varepsilon\nu,1,a,\alpha_s(\varepsilon\sqrt{s})\right) \exp\left\{ - \int\limits_{\varepsilon\sqrt{s}}^{\sqrt{s}/2} \frac{d\lambda}{\lambda}\gamma_s\left(\alpha_s(\lambda)\right)\right\} \prod_{c=1}^{2} J_c\left(1,1,a,\alpha_s\left(\frac{\sqrt{s}}{2\,\zeta_0}\right)\right) \\
& \times \exp\left\{ - \int\limits_{\sqrt{s}/(2\,\zeta_0)}^{\sqrt{s}/2} \frac{d\lambda}{\lambda}\Bigg[\gamma_{J_c}\left(\alpha_s(\lambda)\right) + B'_c\left(c_1, c_2, a, \alpha_s\left(c_2\lambda\right)\right) + 2 \int\limits_{c_1 \frac{s^{1-a/2}}{\nu(2\,\lambda)^{1-a}}}^{c_2\,\lambda} \frac{d\lambda'}{\lambda'} A'_c\left(c_1, a, \alpha_s\left(\lambda'\right)\right)\Bigg]\right\} ,
\end{aligned} \tag{6.39}$$

with ζ_0 given by Eq. (5.60).

In Eqs. (6.38) and (6.39), the energy flow ε appears at the level of one logarithm per loop, in S, in the first exponent. Leading logarithms of ε are therefore resummed by knowledge of $\gamma_s^{(1)}$. At the same time, ν appears in up to two logarithms per loop, as in the inclusive event shape.

Only the soft function S in Eqs. (6.38) and (6.39) contains information on the geometry of Ω. The exponents are partially process-dependent, but geometry-independent. In other words, in Eq. (6.39) the non-global effects are factored from the global event shape, residing only in the soft function and the corresponding anomalous dimension. Dokshitzer and Marchesini [187] have recently obtained the same result, by investigating how parton branching

is affected by correlating the non-global measurement of energy flow with the shape of the jets. Their formalism extends the one presented here to include also non-global effects at leading logarithmic accuracy for ε in the large $\mathcal{N}_C$-limit.

In the next section we will derive explicit expressions for the quantities in (6.39), suitable for resummation to leading logarithm in ε and next-to-leading logarithm in ν.

6.5 Analytical Results for e^+e^- Shape/Flow Correlations

Here we summarize the low-order calculations that provide explicit expressions for the resummed shape/flow correlations and inclusive event shape distributions at next-to-leading logarithm in ν and leading logarithm in ε (we refer to this level collectively as NLL below). Furthermore, we exhibit the expressions for the correlation that we will evaluate numerically in Sec. 6.6.

6.5.1 Results for the Soft Function

As already noted above, the soft function is the only function in the shape/flow correlation that differs from the functions entering the corresponding inclusive event shape because only the soft function depends on the geometry of Ω. Below we give the results for the lowest order soft function for two choices of Ω. The remaining functions in (6.38) are the same as the ones listed in Sec. 5.4.1 for the inclusive event shape.

The soft function is normalized to $S^{(0)}(\varepsilon) = \delta(\varepsilon)$ as can be seen from (6.28). For non-zero ε, $d\sigma/d\varepsilon$ is given at lowest order by

$$S^{(1)}\left(\varepsilon \neq 0, \Omega\right) = C_F \frac{1}{\varepsilon} \int\limits_{\Omega} d\mathrm{PS}_2 \, \frac{1}{2\pi} \frac{\beta_1 \cdot \beta_2}{\beta_1 \cdot \hat{k}\, \beta_2 \cdot \hat{k}}\,, \tag{6.40}$$

where PS_2 denotes the two-dimensional angular phase space to be integrated over region Ω, and $\hat{k} \equiv k/\omega_k$. We emphasize again that the soft function contains the only geometry-dependence of the cross section. Also, $S^{(1)}$ for $\varepsilon \neq 0$ is independent of ν and a.

As an example, consider a cone with opening angle 2δ, centered at angle α from jet 1. In this case, the lowest-order soft function is given by

$$S^{(1)}\left(\varepsilon \neq 0, \alpha, \delta\right) = C_F \frac{1}{\varepsilon} \ln\left(\frac{1-\cos^2\alpha}{\cos^2\alpha - \cos^2\delta}\right). \tag{6.41}$$

Similarly, we may choose Ω as a ring extending angle δ_1 to the right and δ_2 to the left of the plane perpendicular to the jet directions in the center-of-mass. In this case, we obtain

$$S^{(1)}\left(\varepsilon \neq 0, \delta_1, \delta_2\right) = C_F \frac{1}{\varepsilon} \ln\left(\frac{(1+\sin\delta_1)}{(1-\sin\delta_1)}\frac{(1+\sin\delta_2)}{(1-\sin\delta_2)}\right) = C_F \frac{2}{\varepsilon}\,\Delta\eta\,, \quad (6.42)$$

with $\Delta\eta$ the rapidity spanned by the ring. For a ring centered around the center-of-mass ($\delta_1 = \delta_2 = \delta$) the angular integral reduces to the form that we encountered in the example of Sec. 6.2.2, and that we will use in our numerical examples of Sec. 6.6, with $\Delta\eta$ given by Eq. (6.8).

6.5.2 Closed Expressions for the Correlation

Given the explicit results above and in Sec. 5.4.1, the integrals in the exponents of the resummed correlation, Eq. (6.38), may be easily performed in closed form. We give the analytic results for the exponents of Eq. (6.38), as defined in Eqs. (5.77)[1] and (5.78). As in Eq. (5.80), we identify $p_{J_c}\cdot\hat{\xi}_c$ with $\sqrt{s}/2$.

$$e^{E_1(a)} = \left(\frac{\alpha_s(\sqrt{s}/2)}{\alpha_s(\varepsilon\sqrt{s})}\right)^{\frac{4C_F}{\beta_0}} \left(\frac{\alpha_s\left(\frac{\sqrt{s}}{2\,\zeta_0}\right)}{\alpha_s(\sqrt{s}/2)}\right)^{\frac{6C_F}{\beta_0}}, \quad (6.43)$$

$$e^{E_2(a)} = \left(\frac{\alpha_s(c_2\sqrt{s}/2)}{\alpha_s\left(\frac{c_2\sqrt{s}}{2\,\zeta_0}\right)}\right)^{\frac{4C_F}{\beta_0}\kappa_1(a)} \left(\frac{\alpha_s\left(\frac{c_1\sqrt{s}}{2\,\zeta_0}\right)}{\alpha_s\left(\frac{c_1\sqrt{s}}{\nu}\right)}\right)^{\frac{1}{a-1}\frac{4C_F}{\beta_0}\kappa_2(a)} \times \left(\frac{\alpha_s(c_2\sqrt{s}/2)}{\alpha_s\left(\frac{c_1\sqrt{s}}{2\,\zeta_0}\right)}\right)^{\frac{1}{2-a}\frac{8C_F}{\beta_0}\ln(\nu/2)}, \quad (6.44)$$

with

$$\kappa_1(a) = \ln\left(\frac{4}{c_2^2 e}\right) + \frac{4\pi}{\beta_0}\left[\alpha_s\left(\frac{c_2\sqrt{s}}{2\,\zeta_0}\right)\right]^{-1} - \frac{2K}{\beta_0} - \frac{\beta_1}{2\beta_0^2}\ln\left(\left(\frac{\beta_0}{4\pi e}\right)^2 \alpha_s\left(\frac{c_2\sqrt{s}}{2}\right)\alpha_s\left(\frac{c_2\sqrt{s}}{2\,\zeta_0}\right)\right), \quad (6.45)$$

[1]Here we have for the correlation a lower limit of $\varepsilon\sqrt{s}$ instead of $\sqrt{s}/\nu$ in the first term.

$$\kappa_2(a) \;=\; (1-a-2\gamma_E) + \frac{4\pi}{\beta_0}\left[\alpha_s\left(\frac{\sqrt{s}}{\nu}\right)\right]^{-1} - \frac{2K}{\beta_0} \\ -\frac{\beta_1}{2\beta_0^2}\ln\left(\left(\frac{\beta_0}{4\pi e}\right)^2 \alpha_s\left(\frac{c_1\sqrt{s}}{\nu}\right)\alpha_s\left(\frac{c_1\sqrt{s}}{2\,\zeta_0}\right)\right). \tag{6.46}$$

We have used the two-loop running coupling, when appropriate, to derive Eqs. (6.43) - (6.46). The results are expressed in terms of the one-loop running coupling (A.6), and the first two coefficients in the expansion of the QCD beta-function, β_0 and β_1, Eqs. (A.3) and (A.4), respectively.

Combining the expressions for the exponents, Eqs. (6.43) and (6.44), for the Born cross section, Eq. (5.76), and for the soft function, Eq. (6.40), in Eq. (6.38), the complete differential cross section, at LL in ε and at NLL in ν, is given by

$$\frac{d\sigma\,(\varepsilon,\nu,s,a)}{d\varepsilon\,d\hat{n}_1} \;=\; \mathcal{N}_C\left(\sum_{\rm f} Q_{\rm f}^2\right)\frac{\pi\alpha_{\rm em}^2}{2s}\left(1+\cos^2\theta\right)C_F\frac{\alpha_s(\varepsilon\sqrt{s})}{\pi}\frac{1}{\varepsilon} \\ \times \int\limits_{\Omega} d\mathrm{PS}_2\,\frac{1}{2\pi}\frac{\beta_1\cdot\beta_2}{\beta_1\cdot\hat{k}\,\beta_2\cdot\hat{k}}\left(\frac{\alpha_s\left(\frac{\sqrt{s}}{2}\right)}{\alpha_s(\varepsilon\sqrt{s})}\right)^{\frac{4C_F}{\beta_0}}\left(\frac{\alpha_s\left(\frac{\sqrt{s}}{2\,\zeta_0}\right)}{\alpha_s\left(\frac{\sqrt{s}}{2}\right)}\right)^{\frac{6C_F}{\beta_0}} \\ \times \left(\frac{\alpha_s\left(c_2\,\frac{\sqrt{s}}{2}\right)}{\alpha_s\left(\frac{c_2\sqrt{s}}{2\,\zeta_0}\right)}\right)^{\frac{4C_F}{\beta_0}\kappa_1(a)}\left(\frac{\alpha_s\left(\frac{c_1\sqrt{s}}{2\,\zeta_0}\right)}{\alpha_s\left(\frac{c_1\sqrt{s}}{\nu}\right)}\right)^{\frac{1}{a-1}\frac{4C_F}{\beta_0}\kappa_2(a)}\left(\frac{\alpha_s\left(c_2\,\frac{\sqrt{s}}{2}\right)}{\alpha_s\left(\frac{c_1\sqrt{s}}{2\,\zeta_0}\right)}\right)^{\frac{1}{2-a}\frac{8C_F}{\beta_0}\ln\left(\frac{\nu}{2}\right)}. \tag{6.47}$$

These are the expressions that we will numerically evaluate in the next section. We note that this is not the only possible closed form for the resummed correlation at this level of accuracy. When a full next-to-leading order calculation for this set of event shapes is given, the matching procedure of [30, 142] may be more convenient.

6.6 Numerical Results for e^+e^- Shape/Flow Correlations

Here we show some representative examples of numerical results for the correlation, Eq. (6.47). We pick the constants c_i as in Eq. (3.34), unless stated otherwise. The effect of different choices is nonleading, and is numerically small, as we will see below. In the following we choose the region Ω to be a ring between the jets, centered in their center-of-mass, with a width of $\Delta\eta = 2$, or equivalently, opening angle $\delta \approx 50$ degrees (see Eq. (6.8)). The analogous cross section for a cone centered at 90 degrees from the jets (Eq. (6.41)) has a similar behavior. In the following, the center-of-mass energy $Q = \sqrt{s}$ is chosen to be 100 GeV.

Fig. 6.5 shows the dependence of the differential cross section (6.38), multiplied by ε and normalized by the Born cross section, $\frac{\varepsilon d\sigma/(d\varepsilon d\hat{n}_1)}{d\sigma_0/d\hat{n}_1}$, on the measured energy ε and on the parameter a, at fixed ν. In Fig. 6.5 a), we plot $\frac{\varepsilon d\sigma/(d\varepsilon d\hat{n}_1)}{d\sigma_0/d\hat{n}_1}$ for $\nu = 10$, in Fig. 6.5 b) for $\nu = 50$. As ν increases, the radiation into the complementary region $\bar{\Omega}$ is more restricted, as illustrated by the comparison of Figs. 6.5 a) and b). Similarly, as a approaches 1, the cross section falls, because the jets are restricted to be very narrow. On the other hand, as a assumes more and more negative values at fixed ε, the correlations (6.38) approach a constant value. For a large and negative, however, non-global dependence on $\ln \varepsilon$ and $|a|$ will emerge from higher order corrections in the soft function, which we do not include in Eq. (6.47).

In Fig. 6.6 we investigate the sensitivity of the resummed correlation, Eq. (6.47), to our choice of the constants c_i. The effect of these constants is of next-to-next-to-leading logarithmic order in the event shape. We plot the differential cross section $\varepsilon\frac{\varepsilon d\sigma/(d\varepsilon d\hat{n}_1)}{d\sigma_0/d\hat{n}_1}$, at $Q = 100$ GeV, for fixed $\varepsilon = 0.05$ and $\nu = 20$, as a function of a. The effects of changes in the c_i are of the order of a few percent for moderate values of a.

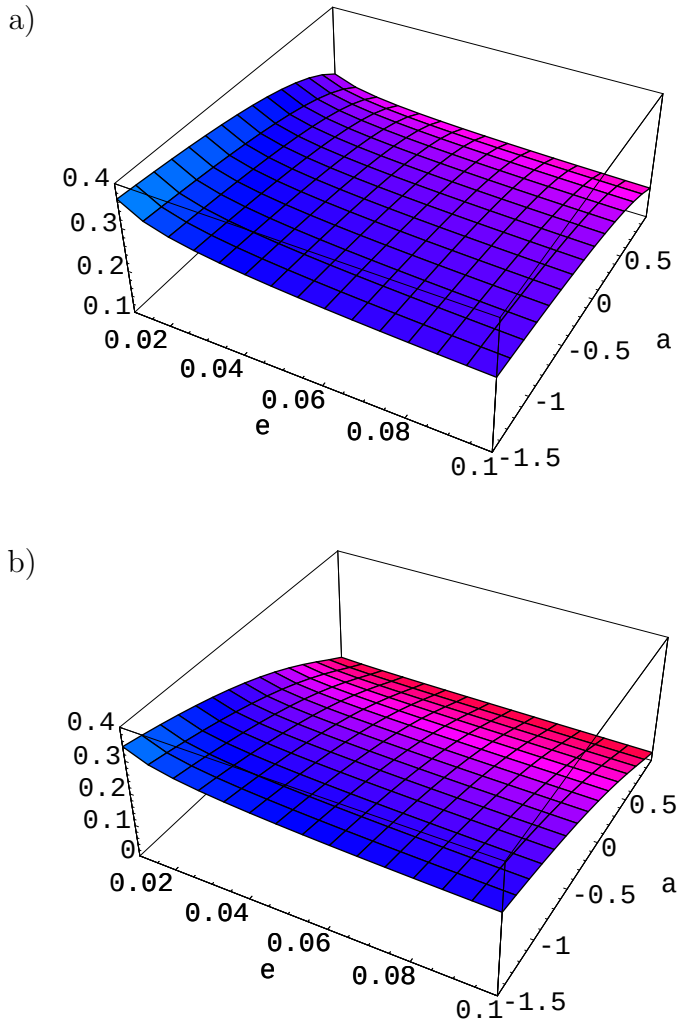

Figure 6.5: Differential cross section $\frac{\varepsilon d\sigma/(d\varepsilon d\hat{n}_1)}{d\sigma_0/d\hat{n}_1}$, normalized by the Born cross section, at $Q = 100$ GeV, as a function of ε and a at fixed ν: a) $\nu = 10$, b) $\nu = 50$. Ω is a ring (slice) centered around the jets, with a width of $\Delta\eta = 2$.

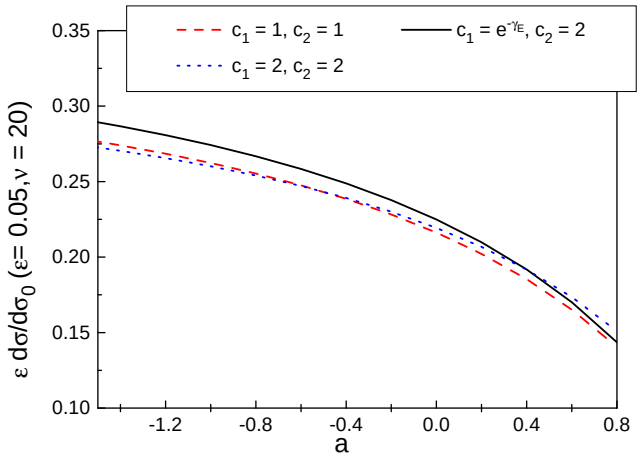

Figure 6.6: Differential cross section $\frac{\varepsilon d\sigma/(d\varepsilon d\hat{n}_1)}{d\sigma_0/d\hat{n}_1}$, normalized by the Born cross section, at $Q = 100$ GeV, as a function of a at fixed $\nu = 20$ and $\varepsilon = 0.05$. Ω is chosen as in Fig. 6.5. Solid line: $c_1 = e^{-\gamma_E}$, $c_2 = 2$, as in Eq. (3.34), dashed line: $c_1 = c_2 = 1$, dotted line: $c_1 = c_2 = 2$.

Finally, we illustrate the sensitivity of these results to the flavor of the primary partons. For this purpose we study the corresponding ratio of the shape/flow correlation to the cross section for gluon jets produced by a hypothetical color singlet source. Fig. 6.7 displays the ratio of the differential cross section $d\sigma^q(\varepsilon, a)/(d\varepsilon d\hat{n}_1)$, Eq. (6.47), normalized by the lowest-order cross section, to the analogous quantity with gluons as primary partons in the outgoing jets, again at $Q = 100$ GeV. This ratio is multiplied by C_A/C_F in the figure to compensate for the difference in the normalizations of the lowest-order soft functions. Gluon jets have wider angular extent, and hence are suppressed relative to quark jets with increasing ν or a, as can be seen by comparing Figs. 6.7 a) and b). Fig. 6.7 a) shows the ratio at $\nu = 10$, and Fig. 6.7 b) at $\nu = 50$. These results suggest sensitivity to the more complex color and flavor flow characteristic of hadronic scattering [9, 147]. We will discuss the extension of the above formalism to correlations with hadronic initial states in the next section.

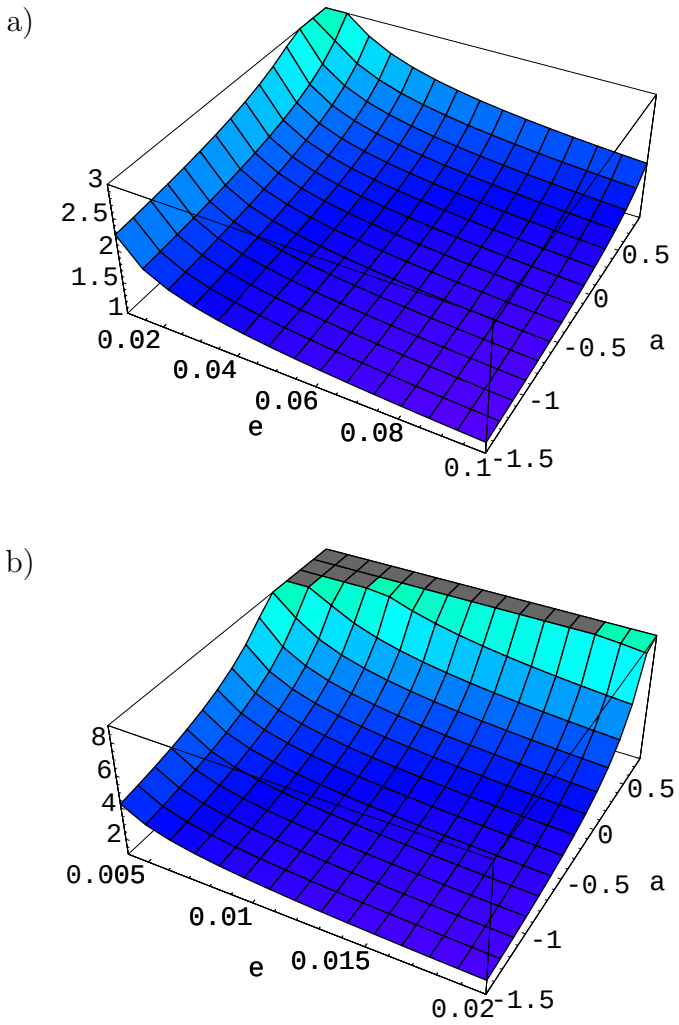

Figure 6.7: Ratios of differential cross sections for quark to gluon jets $\frac{C_A}{C_F}\left(\frac{\varepsilon d\sigma^q/(d\varepsilon d\hat{n}_1)}{d\sigma_0^q/d\hat{n}_1}\right)\left(\frac{\varepsilon d\sigma^g/(d\varepsilon d\hat{n}_1)}{d\sigma_0^g/d\hat{n}_1}\right)^{-1}$ at $Q = 100$ GeV as a function of ε and a at fixed ν: a) $\nu = 10$, b) $\nu = 50$. Ω as in Fig. 6.5, c_1 and c_2 as in Eq. (3.34).

6.7 Extension to Hadronic Cross Sections

The study of interjet radiation in hadronic cross sections may shed light on short-distance color and flavor flow, and on the dynamics of hadronization. Its use in the analysis of jet events in hadronic scattering, to distinguish new physics signals from QCD background, was explored in [180, 193]. The discussion below, which was published in [9], is closely related to the treatment of rapidity gap ("color singlet exchange") events in Refs. [192, 194], for jets at high p_T and large rapidity separations.

In the following we study hadronic events corresponding to Eq. (6.2), that is, the incoming partons are now hadrons:

$$A + B \to J_1(p_{J_1}) + J_2(p_{J_2}) + X_{\bar{\Omega}}\left(\bar{f}\right) + R_\Omega(Q_\Omega)\,, \tag{6.48}$$

We refrain from giving an explicit construction of a shape function $\bar{f}$ suitable for accounting for all incoming (beam) and outgoing jets. Such a construction is certainly possible, although nontrivial due to the more involved kinematics. Below we assume the existence of the shape function $\bar{f}$ and instead concentrate on the study of the interrelation of energy and color flow. We reserve a full study for future work.

6.7.1 Refactorization of the Cross Section

Collinear factorization theorems [1, 2] ensure that we may write the cross section for (6.48) at fixed $\varepsilon = Q_\Omega/Q$ and $\bar{\varepsilon}$ as a sum of convolutions of parton distribution functions ϕ (PDFs) that incorporate long-distance dynamics, with hard-scattering functions, ω, that summarize short-distance dynamics,

$$\begin{aligned}\frac{d\sigma_{AB}}{d\vec{p}_1\, d\varepsilon d\bar{\varepsilon}} \;=\; \sum_{f_A,f_B} \int dx_A\, dx_B\; \phi_{f_A/A}\left(x_A,\mu_F\right) \phi_{f_B/B}\left(x_B,\mu_F\right) \\ \times\, \omega_{f_A f_B}\left(x_A p_A, x_B p_B, \vec{p}_1, \varepsilon, \bar{\varepsilon}, \mu_F, \alpha_s(\mu_F)\right)\,,\end{aligned} \tag{6.49}$$

with factorization scale μ_F. Here the hard scale Q is set by p_T, the transverse momentum of the observed jet. The sum is over parton types, f_A, f_B. Corrections to this relation begin in general with powers of $\Lambda^2_{\rm QCD}/Q^2_\Omega$, due to multiple scattering of partons. Our analysis below, which begins with Eq. (6.49), is thus accurate up to such corrections, and requires that the momenta of the outgoing jets are large compared to the hadronization scale $\sim \Lambda_{\rm QCD}$. We take the renormalization scale equal to the factorization scale.

Soft gluon emission outside the angular extent of the jets decouples from the kinematics of the hard scattering, and from the internal evolution of the

jets [2, 74, 133, 195]. As a result, we may express the partonic cross section in Eq. (6.49) as a sum of terms, each characterized by a definite number of jets produced at the hard scattering. To lowest order in α_s, only two jets are possible. Thus, at leading order, the production of the high-p_T jets is given by the set of Born-level $2 \to 2$ partonic processes, which we label f,

$$\mathrm{f}: \quad f_A + f_B \to f_1 + f_2 \,. \tag{6.50}$$

We distinguish $q\bar{q} \to q\bar{q}$ ($f_1 = q$) from $q\bar{q} \to \bar{q}q$ ($f_1 = \bar{q}$). We may now write the single-jet inclusive cross section at fixed ε and $\bar{\varepsilon}$ as

$$\begin{aligned} \frac{d\sigma_{AB}}{d\eta dp_T d\varepsilon d\bar{\varepsilon}} &= \sum_{\mathrm{f}} \int dx_A dx_B \; \phi_{f_A/A}\left(x_A, \mu_F\right) \phi_{f_B/B}\left(x_B, \mu_F\right) \\ &\qquad \times \delta\left(p_T - \frac{\sqrt{\hat{s}}}{2\cosh\hat{\eta}}\right) \frac{d\hat{\sigma}^{(\mathrm{f})}}{d\hat{\eta} d\varepsilon d\bar{\varepsilon}} \,, \end{aligned} \tag{6.51}$$

with $\hat{\eta} = \eta - (1/2)\ln(x_A/x_B)$ the jet rapidity in the partonic center-of-mass, where η is defined in Eq. (6.8), and $\hat{s} = x_A x_B s$. As above, we neglect the effects of recoil of the observed jet against relatively soft radiation.

The partonic cross section, $d\hat{\sigma}^{(\mathrm{f})}/(d\hat{\eta} d\varepsilon d\bar{\varepsilon})$ can be refactorized analogous to Eq. (6.23), but now we have to take the non-trivial color flow into account. The regions that give leading contributions are as above a hard scattering, soft, and jet functions, two for the outgoing jets, and two jet functions for the beam jets. The latter jets must be defined to avoid double counting due to the parton distribution functions. Such a definition is quite non-trivial. Furthermore, the Glauber/Coulomb region discussed in Sec. 2.2.2 has to be treated with care, since in shape/flow correlations the phase space for radiation is restricted. Nevertheless, with appropriate definitions of the event shape and the jet functions it is possible to avoid contour pinches in the Glauber/Coulomb region, as discussed in [196]. Here we do not attempt to give a full treatment of the beam jets or of the construction of suitable shape functions. Instead, we concentrate on the relation between energy and underlying color flow.

As was observed, for example, in [9, 74, 147, 196], there is no unique way of defining color exchange in a finite amount of time since gluons of any energy, including soft gluons, carry octet color charge. We therefore expect the functions from which we construct the refactorized partonic cross section to be described by matrices in the space of possible color exchanges. This is because as the (re)factorization scale changes, gluons that were included in the hard function become soft and vice versa. Due to intrajet coherence [133], however, the evolution of the jets themselves is independent of the color exchanges. Once a jet is formed, collinear radiation cannot change its color

structure. Therefore, the refactorized partonic shape/flow correlation can be written in moment space as

$$\frac{d\hat{\sigma}^{(\mathrm{f})}(\varepsilon,\nu,p_T,\mu_F)}{d\varepsilon\, d\hat{\eta}} = H_{LI}^{(\mathrm{f})}(p_T,\hat{\eta},\mu,\mu_F)\; S_{IL}^{(\mathrm{f})}(\varepsilon,\nu,\hat{\eta},\mu) \prod_{c=A,B,1,2} J_c^{(\mathrm{f})}(p_T,\hat{\eta},\nu,\mu,\mu_F). \tag{6.52}$$

analogous to the corresponding correlation in e^+e^- events, Eq. (6.25), but now the hard and soft functions, H and S, respectively, are matrices in the space of color flow. Repeated indices in color space, L, I, are summed over. The superscripts (f) label the underlying partonic process, as in (6.50). μ is a refactorization scale, not necessarily equal to the factorization scale in Eq. (6.51). The large scale in the problem is here, from (6.51), the transverse momentum of the observed jet p_T.

In Eq. (6.52), the hard scattering function H_{LI} begins at order α_s^2, while the soft function S_{IL} begins at zeroth order. Compared to the e^+e^- correlation, Eq. (6.25), we have absorbed the lowest order Born cross section into the hard scattering function due to the flavor dependence (6.50). In Appendix C.2 we list the color bases and the hard scattering matrices for all possible partonic subprocesses for proton-antiproton collisions. Let us now turn to the discussion of the soft function.

6.7.2 The Soft Function

As we have seen above, wide-angle soft radiation decouples from jet evolution [44]. Soft radiation away from jet directions is equally well described by radiation from a set of path-ordered exponentials – nonabelian phase operators or Wilson lines – that replace each of the partons involved in the hard scattering (four here),

$$\begin{aligned} \Phi_\beta^{(f)}(\infty,0;x) &= P\exp\left(-ig_s\int_0^\infty d\lambda\; \beta\cdot\mathcal{A}^{(f)}(\lambda\beta+x)\right), \\ \Phi_{\beta'}^{(f')}(0,-\infty;x) &= P\exp\left(-ig_s\int_{-\infty}^0 d\lambda\; \beta'\cdot\mathcal{A}^{(f')}(\lambda\beta'+x)\right), \end{aligned} \tag{6.53}$$

where P denotes path ordering. The first line describes an outgoing, and the second an incoming, parton, whose flavors and four-velocities are f and β, and f' and β', respectively. The vector potentials $\mathcal{A}^{(f)}$ are in the color representation appropriate to flavor f, and similarly for $\mathcal{A}^{(f')}$.

Because wide-angle, soft radiation is independent of the internal jet evolution, products of nonabelian phase operators, linked at the hard scattering

by a tensor in the space of color indices generate the same wide-angle radiation as the full jets. The general form for these operators, exhibiting their color indices, is

$$\begin{aligned}\mathcal{W}^{(\mathrm{f})}_{I\,\{c_i\}}(x) &= \sum_{\{d_i\}} \Phi^{(f_2)}_{\beta_2}(\infty,0;x)_{c_2,d_2}\ \Phi^{(f_1)}_{\beta_1}(\infty,0;x)_{c_1,d_1} \\ &\quad \times \left(c_I^{(\mathrm{f})}\right)_{d_2,d_1;d_A,d_B}\ \Phi^{(f_A)}_{\beta_A}(0,-\infty;x)_{d_A,c_A}\ \Phi^{(f_B)}_{\beta_B}(0,-\infty;x)_{d_B,c_B}\,. \end{aligned} \tag{6.54}$$

The c_I are color tensors in a convenient basis, listed in Appendix C.2. Examples will be given below. The perturbative expansions for these operators are in terms of standard eikonal vertices and propagators, and have been given in detail in Refs. [147, 196]. In these terms, we define an eikonal cross section analogous to Eq. (6.26) $\bar{\sigma}^{(\mathrm{eik})\,(\mathrm{f})}_{IL}$ at measured ε and $\bar{\varepsilon}_{\mathrm{eik}}$ as

$$\begin{aligned}\bar{\sigma}^{(\mathrm{eik})\,(\mathrm{f})}_{IL}\left(\varepsilon,\bar{\varepsilon},\mu,\hat{\eta},\alpha_s(\mu)\right) &= \frac{1}{\mathrm{Tr}\left(c_I^\dagger c_L\right)} \sum_{N_{\mathrm{eik}}} \sum_{\{b_i\}} \langle 0|\,\bar{T}\left[\left(\mathcal{W}^{(\mathrm{f})}_I(0)\right)^\dagger_{\{b_i\}}\right]\,|N_{\mathrm{eik}}\rangle \\ &\quad \times \langle N_{\mathrm{eik}}|\,T\left[\mathcal{W}^{(\mathrm{f})}_L(0)_{\{b_i\}}\right]\,|0\rangle \\ &\quad \times \delta\left(\varepsilon - f(N_{\mathrm{eik}})\right)\ \delta\left(\bar{\varepsilon}_{\mathrm{eik}} - \bar{f}(N_{\mathrm{eik}})\right) \\ &= \mathbf{1}_{IL}\,\delta(\varepsilon)\delta(\bar{\varepsilon}_{\mathrm{eik}}) + \mathcal{O}(\alpha_s). \end{aligned} \tag{6.55}$$

The indices L and I refer to the color exchange at the hard scattering between the partons in reaction f, as built into the definitions of the $\mathcal{W}$'s, Eq. (6.54). The matrix elements in Eq. (6.55) require renormalization, and we may identify the corresponding renormalization scale with the refactorization scale of Eq. (6.52).

The ε-dependence of the matrix $\bar{\sigma}^{(\mathrm{f})}_{IL}$ in Eq. (6.55) is the same as in the full partonic cross section, up to corrections due to differences between the jets and the nonabelian phase operators. The eikonal cross section (6.55) reproduces the wide-angle radiation accurately, however, the approximation fails for collinear radiation. As in the electron-positron case, Eq. (6.27), we have to subtract collinear emission to avoid double counting in the full partonic cross section. Since we have not specified constructions for the beam jets, we do not give explicit constructions of the corresponding eikonal jets. Here we only note that the eikonal jets, like their partonic counterparts, are independent of the color exchange, which is therefore contained fully in the eikonal cross section:

$$S^{(\mathrm{f})}_{IL}\left(\varepsilon,\nu,\hat{\eta},\mu\right) = \frac{\sigma^{(\mathrm{eik}),\,(\mathrm{f})}_{IL}\left(\varepsilon,\nu,\hat{\eta},\mu\right)}{\prod\limits_{c=A,B,1,2} J_c^{(\mathrm{eik})\,(\mathrm{f})}\left(\nu,\hat{\eta},\mu\right)} = \mathbf{1}_{IL}\,\delta(\varepsilon) + \mathcal{O}(\alpha_s)\,. \tag{6.56}$$

Using (6.56) in (6.52) we obtain

$$\frac{d\hat{\sigma}^{(\mathrm{f})}(\varepsilon,\nu,p_T,\mu_F)}{d\varepsilon\, d\hat{\eta}} = H_{LI}^{(\mathrm{f})}(p_T,\hat{\eta},\mu,\mu_F)\; \sigma_{IL}^{(\mathrm{eik})\,(\mathrm{f})}(\varepsilon,\nu,\hat{\eta},\mu) \times \prod_{c=A,B,1,2} \frac{J_c^{(\mathrm{f})}(p_T,\hat{\eta},\nu,\mu,\mu_F)}{J_c^{(\mathrm{eik})\,(\mathrm{f})}(\nu,\hat{\eta},\mu)}. \tag{6.57}$$

We observe that all information about color exchange is contained in the hard scattering and in the eikonal cross section, independent of the details of the partonic and eikonal jets since these are proportional to the identity matrix in color space.

6.7.3 Resummation in Color Space

Without explicitly specifying the definitions of event shape, jet and eikonal jet functions, we can nevertheless proceed in a manner analogous to the e^+e^- case to resum large logarithmic enhancements in ε and partially in ν. Since the jet functions are color diagonal, their solutions to the renormalization group equations are analogous to Eq. (5.59), where the integration limits may be slightly changed, depending on the exact definition of the shape function.

The resummation of large logarithms in the soft function now depends on the color exchange. As above, we demand that the following condition be fulfilled

$$\mu\frac{d}{d\mu}\left[\frac{d\hat{\sigma}^{(\mathrm{f})}}{d\hat{\eta}d\varepsilon}\right] = 0\,. \tag{6.58}$$

This condition applied to the right-hand side of (6.57) leads to a renormalization group equation for the eikonal cross section that encodes all information about the color evolution,

$$\left(\mu\frac{\partial}{\partial\mu} + \beta(g_s)\frac{\partial}{\partial g_s}\right)\sigma_{IL}^{(\mathrm{eik})\,(\mathrm{f})} = -\left(\Gamma_{\mathrm{eik}}^{(\mathrm{f})}(\hat{\eta})\right)_{IJ}^{\dagger}\sigma_{JL}^{(\mathrm{eik})\,(\mathrm{f})} - \sigma_{IJ}^{(\mathrm{eik})\,(\mathrm{f})}\left(\Gamma_{\mathrm{eik}}^{(\mathrm{f})}(\hat{\eta})\right)_{JL}\,, \tag{6.59}$$

with, as usual, $g_s = \sqrt{4\pi\alpha_s}$. Here $\left(\Gamma_{\mathrm{eik}}^{(\mathrm{f})}(\hat{\eta})\right)_{IL}$ may be thought of as an anomalous dimension matrix [147, 196]. This anomalous dimension matrix depends only on the directions of the jets through the directions of the eikonal lines, $\hat{\eta}$, but is geometry-independent otherwise.

To solve Eq. (6.59), we go to a basis for the color matrices $c_I^{(\mathrm{f})}$ that diagonalizes $\Gamma_{\mathrm{eik}}^{(\mathrm{f})}(\hat{\eta})$, through a transformation matrix R,

$$\left(\Gamma_{\mathrm{eik}}^{(\mathrm{f})}(\hat{\eta})\right)_{\gamma\beta} \equiv \lambda_\beta^{(\mathrm{f})}(\hat{\eta})\delta_{\gamma\beta} = R_{\gamma I}^{(\mathrm{f})}\left(\Gamma_{\mathrm{eik}}^{(\mathrm{f})}(\hat{\eta})\right)_{IJ} R^{(\mathrm{f})-1}_{J\beta}, \tag{6.60}$$

where

$$\lambda_\beta^{(\mathrm{f})}(\hat{\eta}) = \sum_{n>0} \left(\frac{\alpha_s}{\pi}\right)^n \lambda_\beta^{(\mathrm{f},\,\mathrm{n})}(\hat{\eta}) \tag{6.61}$$

are the eigenvalues of $\Gamma_{\mathrm{eik}}^{(\mathrm{f})}(\hat{\eta})$. Here and below, Greek indices $\beta,\ \gamma$ indicate that a matrix is evaluated in the basis where the eikonal anomalous dimension has been diagonalized. Thus, for the eikonal and short-distance functions we also write,

$$\begin{aligned} \sigma_{\gamma\beta}^{(\mathrm{eik})\,(\mathrm{f})} &= \left[\left(R^{(\mathrm{f})-1}\right)^\dagger\right]_{\gamma L} \sigma_{LK}^{(\mathrm{eik})\,(\mathrm{f})} \left[R^{(\mathrm{f})-1}\right]_{K\beta} \\ H_{\gamma\beta}^{(\mathrm{f})} &= \left[R^{(\mathrm{f})}\right]_{\gamma K} H_{KL}^{(\mathrm{f})} \left[R^{(\mathrm{f})\dagger}\right]_{L\beta}. \end{aligned} \tag{6.62}$$

The transformation matrix $R^{(\mathrm{f})-1}$ is given by the eigenvectors of the anomalous dimension matrix,

$$\left(R^{(\mathrm{f})\,-1}\right)_{K\beta} \equiv \left(e_\beta^{(\mathrm{f})}\right)_K . \tag{6.63}$$

Analogous to Eq. (6.35) we find the solution to Eq. (6.59), which resums leading logarithms of ε. We introduce a combination of eigenvalues of $\Gamma_{\mathrm{eik}}^{(\mathrm{f})}$, $E_{\gamma\beta}^{(\mathrm{f},\,\mathrm{n})}(\hat{\eta})$, given by

$$E_{\gamma\beta}^{(\mathrm{f},\,\mathrm{n})}(\hat{\eta}) = \lambda_\gamma^{(\mathrm{f},\,\mathrm{n})\star}(\hat{\eta}) + \lambda_\beta^{(\mathrm{f},\,\mathrm{n})}(\hat{\eta}) . \tag{6.64}$$

The soft eikonal function is then

$$\begin{aligned} \sigma_{\gamma\beta}^{(\mathrm{eik})\,(\mathrm{f})}\left(\hat{\eta}, \Omega, \frac{\varepsilon p_T}{\mu}, \varepsilon\nu, \frac{p_T}{\mu\nu}, \alpha_s(\mu)\right) &= \sigma_{\gamma\beta}^{(\mathrm{eik})\,(\mathrm{f})}\left(\hat{\eta}, \Omega, 1, \varepsilon\nu, \alpha_s(\varepsilon p_T)\right) \\ &\quad \times \exp\left\{-\sum_{n>0} E_{\gamma\beta}^{(\mathrm{f},\,\mathrm{n})}(\hat{\eta}) \int_{\varepsilon\, p_T}^{\mu} \frac{d\mu'}{\mu'} \left(\frac{\alpha_s(\mu')}{\pi}\right)^n\right\}, \end{aligned} \tag{6.65}$$

where repeated color indices are summed over. We now set the refactorization scale, μ, equal to the transverse momentum of the observed jet, p_T, and find with Eqs. (6.57) and (6.65), for the partonic cross section,

$$\begin{aligned} \frac{d\hat{\sigma}^{(\mathrm{f})}\left(p_T, \hat{\eta}, \mu_F, \varepsilon, \nu, \alpha_s(\mu_F)\right)}{d\hat{\eta} d\varepsilon} &= \sum_{\beta,\,\gamma} H_{\beta\gamma}^{(\mathrm{f})}\left(p_T, \hat{\eta}, \alpha_s(\mu_F)\right) \\ &\quad \times S_{\gamma\beta}^{(\mathrm{f})}\left(\hat{\eta}, \Omega, 1, \varepsilon\nu, \alpha_s(\varepsilon p_T)\right) \exp\left\{-\sum_{n>0} E_{\gamma\beta}^{(\mathrm{f},\,\mathrm{n})}(\hat{\eta}) \int_{\varepsilon\, p_T}^{\mu} \frac{d\mu'}{\mu'} \left(\frac{\alpha_s(\mu')}{\pi}\right)^n\right\} \end{aligned}$$

$$
\begin{aligned}
&\times \prod_{c=A,B,1,2} J_c^{(\mathrm{f})}(p_T,\hat{\eta},\nu,\mu_F) \\
&= \sum_{\beta,\,\gamma} H_{\beta\gamma}^{(\mathrm{f})}\left(p_T,\hat{\eta},\alpha_s(\mu_F)\right) \\
&\quad \times \sigma_{\gamma\beta}^{(\mathrm{eik})\,(\mathrm{f})}\left(\hat{\eta},\Omega,1,\varepsilon\nu,\alpha_s(\varepsilon p_T)\right) \exp\left\{-\sum_{n>0} E_{\gamma\beta}^{(\mathrm{f},\,\mathrm{n})}(\hat{\eta}) \int_{\varepsilon\, p_T}^{\mu} \frac{d\mu'}{\mu'} \left(\frac{\alpha_s(\mu')}{\pi}\right)^n\right\} \\
&\quad \times \prod_{c=A,B,1,2} \frac{J_c^{(\mathrm{f})}(p_T,\hat{\eta},\nu,\mu_F)}{J_c^{(\mathrm{eik})\,(\mathrm{f})}\left(p_T,\hat{\eta},\nu\right)}. \qquad (6.66)
\end{aligned}
$$

In the second equality we have expressed the soft function in terms of its decomposition into an eikonal function and eikonal jets, Eq. (6.56). As in (6.38) all dependence on ε is factored into the eikonal function and its anomalous dimension, and all geometry dependence is contained in the eikonal matrix, as shown explicitly by the argument Ω.

6.7.4 Renormalization and Color Mixing

We now turn to the calculation of the anomalous dimensions $\Gamma_{\mathrm{eik}}^{(\mathrm{f})}$, introduced in Eq. (6.59) above. The renormalization of multi-eikonal vertices has been discussed in some detail in Ref. [147], and we will follow the method outlined there. In [147], the soft anomalous dimensions $\Gamma_S^{(\mathrm{f})}$ were computed in axial gauge, after dividing an eikonal scattering amplitude by eikonal self-energy functions (eikonal jets). This extra factorization eliminated double poles in dimensional regularization, which are associated with collinear emission by the nonabelian phase operators. In axial gauge, these singularities appear only in self-energy diagrams. In Feynman gauge, the cancellation amounts to dividing out eikonal jet functions, as discussed above. Nevertheless, as already emphasized above, all non-trivial color structure is contained in the eikonal function. The ultraviolet divergences in $\sigma_{IL}^{(\mathrm{eik})\,(\mathrm{f})}$ may be compensated through local counterterms, just as in [147].

We consider the diagrams shown in Fig. 6.8. Figs. 6.8 a) and 6.8 c) are virtual corrections, while 6.8 b) shows the corresponding diagrams for real gluon emission. We compute the counterterms for Fig. 6.8 just as in the previous chapters. From these counterterms, we may simply read off the entries of the anomalous dimension matrix $\Gamma_{\mathrm{eik}}^{(\mathrm{f})}$ in an MS renormalization scheme:

$$
\left(\Gamma_{\mathrm{eik}}^{(\mathrm{f})}(\hat{\eta},\alpha_s(\mu))\right)_{IJ} = -\alpha_s \frac{\partial}{\partial\alpha_s}\left(Z_{\mathrm{eik}\,1}^{(\mathrm{f})}\left(\hat{\eta},\alpha_s(\mu),\varepsilon\right)\right)_{IJ}. \qquad (6.67)
$$

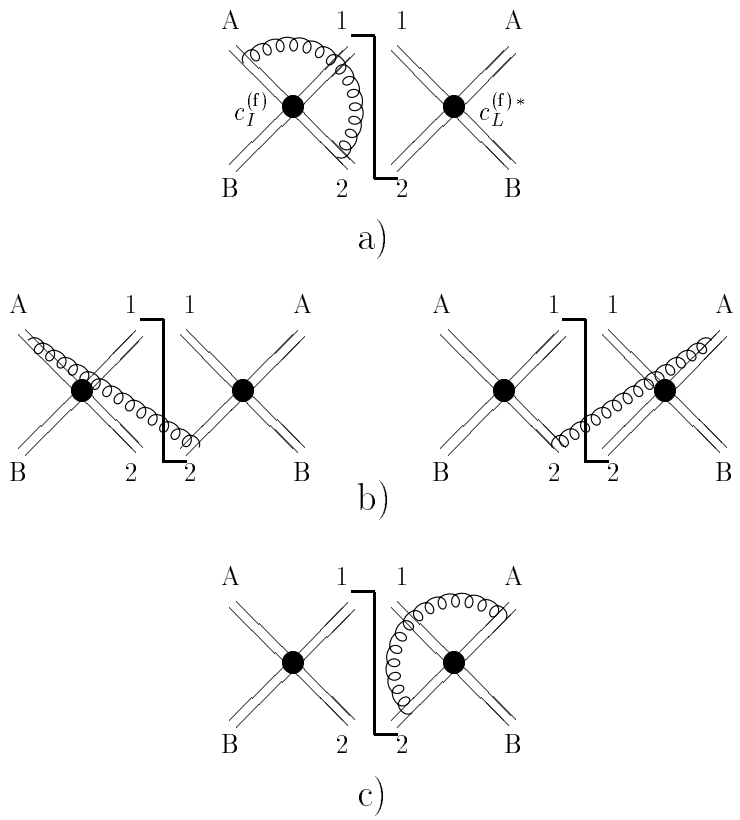

Figure 6.8: Diagrams for the calculation of the anomalous dimension matrix. The double lines represent eikonal propagators, linked by vertices $c_I^{(\mathrm{f})}$ and $c_L^{(\mathrm{f})*}$, in the amplitude and its complex conjugate. The vertical line represents the final state.

Here the subscript 1 denotes the $1/\varepsilon$-pole of the counterterm (compare to Eq. (4.5)). The calculation of the Z's is thus essentially equivalent to the calculation of the anomalous dimensions. To carry out these calculations, however, we must specify a basis of color tensors, c_I. Convenient bases for various $2 \to 2$ scattering processes are listed in Appendix C.1.

Let $Z^{(ij)}$ denote the contribution to the counterterms from all the one-loop graphs in which the gluon connects eikonal lines i and j. In this notation, the calculation of Fig. 6.8 gives us $Z^{(A2)}$. The Z's are constructed to give local counterterms that cancel those ultraviolet divergences that are left over after the real-virtual cancellation has been carried out.

To find the $Z_{IJ}^{(ij)}$'s in the color bases listed in the appendix, we rewrite the

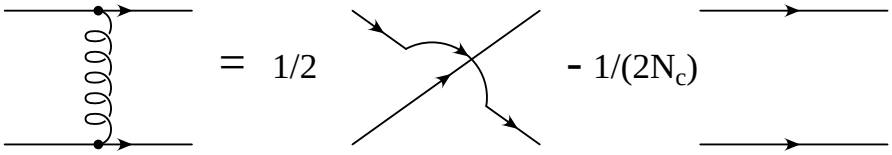

Figure 6.9: Color identity corresponding to Eq. (6.68).

various one-loop virtual diagrams in terms of the original color basis, using the identity shown in Fig. 6.9,

$$T^a_{ij} T^a_{kl} = \frac{1}{2}\left(\delta_{il}\delta_{jk} - \frac{1}{\mathcal{N}_C}\delta_{ij}\delta_{kl}\right) \tag{6.68}$$

for quark processes. For scattering processes involving gluons, many useful identities can be found, for example, in [197]. This procedure results in a 2×2 matrix decomposition for scattering involving only quark and antiquark eikonal lines, describing the mixing under renormalization of their color exchanges. The annihilation of a pair of quark and antiquark eikonals into two gluon eikonal lines gives a 3×3 matrix structure, while for incoming and outgoing gluonic eikonals, we get an 8×8 matrix [147].

For a given $Z^{(ij)}$, the momentum-space integral appears as an overall factor. It is then convenient to introduce the notation

$$\left(Z^{(ij)}_{\text{eik}\,1} - 1\right)_{LI} = \zeta^{(ij)}_{LI}\ \omega^{(ij)}_1\,, \tag{6.69}$$

where the ζ_{LI} are the coefficients that result from the color decomposition of the virtual diagram, and where the $\omega^{(ij)}_1$s include the ultraviolet pole part of the momentum space integral for the eikonal function $\sigma^{(\text{eik})\,(\text{f})}$ and remaining overall constants. Defined in this fashion, the sign of each $\omega^{(ij)}_1$ depends on the flow of flavor in the underlying process (see below). From (6.67) and (6.69) the relation between the ω's and the anomalous dimension matrices is

$$\left(\Gamma^{(\text{f})}_{\text{eik}}\right)_{LI} = -\sum_{\{(ij)\}} {\zeta^{(ij)}}_{LI}\ \omega^{(ij)}_1\ , \tag{6.70}$$

where, as above, the subscript 1 denotes the $1/\varepsilon$ pole.

We note that the color decompositions $\zeta^{(ij)}$ are the same for the eikonal anomalous dimensions and the corresponding first order contributions to the soft function. The difference lies in the momentum parts, which can always

be factored from the color part as in Eq. (6.69).

$$\left(\sigma^{(\mathrm{eik,f})}\right)_{LI} = \sum_{\{(ij)\}} \zeta^{(ij)}{}_{LI}\, \omega^{(ij)}(\Omega)\ , \tag{6.71}$$

analogous to the results for e^+e^- annihilation listed in Section 6.5.1, where now $\omega^{(ij)}$ without subscript denotes the lowest order contribution after cancellation of UV divergences. At lowest order for $\varepsilon \neq 0$, the soft function is independent of the details of the eikonal jets, but depends on the geometry of the region Ω in which the energy flow is measured.

As an example, we give the color decomposition of $\Gamma^{(A2)}$ in $q\bar{q} \to q\bar{q}$, for which we find, using Eq. (6.68),

$$\zeta^{(A2)} = \begin{pmatrix} 0 & \frac{C_F}{2N_C} \\ 1 & -\frac{1}{N_C} \end{pmatrix}\ . \tag{6.72}$$

6.7.5 Results for Lowest Order Momentum Parts

Anomalous Dimensions

The momentum parts of the anomalous dimensions are given by virtual graphs only, because real emissions are restricted over the whole phase space by the weight functions f and $\bar{f}$:

$$\omega_1^{(ij)} = -ig_s^2 \int_{P.P.} \frac{d^nk}{(2\pi)^n} \frac{1}{k^2 + i\epsilon} \frac{\Delta_i\Delta_j\, \beta_i \cdot \beta_j}{(\delta_i\beta_i \cdot k + i\epsilon)\,(\delta_j\beta_j \cdot k + i\epsilon)}. \tag{6.73}$$

P.P. denotes the pole part, and the integral is over all of phase space, independent of the details of the weight functions. In Eq. (6.73), collinear divergences cancel against contributions from eikonal jets. Here $\delta_i = 1(-1)$ for momentum k flowing in the same (opposite) direction as the momentum flow of line i, and $\Delta_i = 1(-1)$ for i a quark (antiquark) line. For example, Fig. 6.8a for $q\bar{q} \to q\bar{q}$ has $i = \mathrm{A}$, $j = 2$, with $\Delta_A = 1$, $\Delta_2 = -1$ and with $\delta_A = \delta_2$.

The factorization of momentum and color parts as in (6.69) is somewhat ambiguous for gluon eikonal lines since here the orientation with which the gluon attaches is important. The sign resulting from the way of attachment can either be factored into the momentum or into the color parts, their product is of course independent of this choice. Below we will attach all gluons in such a way that the momentum parts for processes involving gluons acquire *the same sign* as the momentum parts for the process $q\bar{q} \to q\bar{q}$.

After combining Eq. (6.73) with the eikonal jets, collinear poles cancel. This may not seem obvious from the color decomposition, (6.72), since the

eikonal jets are diagonal in color space. However, the off-diagonal elements are in such combinations that collinear singularities cancel among themselves, without invoking the eikonal jets. The resulting soft anomalous dimension can then be written as

$$\left(\Gamma_S^{(\mathrm{f})}\right)_{LI} = \sum_{\{(ij)\}} \zeta^{(ij)}{}_{LI}\, \Gamma^{(ij)} \,, \tag{6.74}$$

where the $\Gamma^{(ij)}$ are given at lowest order by (compare to (5.64) and [147])

$$\Gamma^{(ij,\,1)} = -\Delta_i \Delta_j \delta_i \delta_j \left[\ln\left(\beta_i \cdot \hat{\xi}_i\right) + \ln\left(\beta_j \cdot \hat{\xi}_j\right) - \ln\left(\frac{\beta_i \cdot \beta_j}{2}\right) - 1 \right], \tag{6.75}$$

where the β_c, $c = A, B, 1, 2$ are lightlike vectors in the directions of the jet momenta p_{J_c}, and the ξ_c are the corresponding non-lightlike eikonal jet momenta, as in the case for e^+e^- annihilation.

Lowest Order Soft Function

On the other hand, the lowest order eikonal function in Eq. (6.66) is given by the integral over the phase space in which the energy flow ε is measured, analogous to the results for e^+e^- annihilation listed in Section 6.5.1. As above, only the eikonal function contributes to the lowest order soft function $S^{(1)}$.

$$\left(S^{(\mathrm{f})}\right)_{LI} = \sum_{\{(ij)\}} \zeta^{(ij)}{}_{LI}\, S^{(ij)} \,. \tag{6.76}$$

The momentum parts of the lowest order soft contributions $S^{(ij,\,1)}$ are thus, analogous to Eq. (6.40) given by

$$S^{(ij,\,1)}(\varepsilon \neq 0, \Omega, \delta_i\beta_i, \delta_j\beta_j, \Delta_i, \Delta_j) = \frac{1}{\varepsilon} \int\limits_{\Omega} d\mathrm{PS}_2\, \frac{1}{2\pi} \frac{\Delta_i \Delta_j\, \beta_i \cdot \beta_j}{\delta_i\beta_i \cdot \hat{k}\, \delta_j\beta_j \cdot \hat{k}} \,, \tag{6.77}$$

where the notation is as in Eq. (6.40).

Color Decompositions

We may summarize the color decompositions of Eqs. (6.74) and (6.76) by introducing the following combinations,

$$\begin{aligned} \alpha^{(\mathrm{f})} &\equiv \phi^{(AB,\mathrm{f})} + \phi^{(12,\,\mathrm{f})}, \\ \beta^{(\mathrm{f})} &\equiv \phi^{(A1,\,\mathrm{f})} + \phi^{(B2,\,\mathrm{f})}, \\ \gamma^{(\mathrm{f})} &\equiv \phi^{(A2,\,\mathrm{f})} + \phi^{(B1,\,\mathrm{f})}, \end{aligned} \tag{6.78}$$

where $\phi^{(ij)}$ denotes either $S^{(ij,1)}$ (Eq. (6.77)) or $\Gamma^{(ij,1)}$ (Eq. (6.75)).

In these terms, both anomalous dimension matrices and lowest order eikonal contributions, in the following collectively denoted by $\mathcal{M}^{(\mathrm{f})}$, for the process $q\bar{q} \to q\bar{q}$ in the basis (C.1) are given by

$$\mathcal{M}^{(q\bar{q}\to q\bar{q})} = \begin{pmatrix} C_F\beta & \frac{C_F}{2\mathcal{N}_C}(\alpha+\gamma) \\ \alpha+\gamma & C_F\alpha - \frac{1}{2\mathcal{N}_C}(\alpha+\beta+2\gamma) \end{pmatrix}. \tag{6.79}$$

The color decompositions of the anomalous dimension matrices and soft functions at lowest order for all other $2 \to 2$ scattering processes are listed in Appendix C.3.

6.7.6 Results for Hadronic Shape/Flow Correlations

From Eq. (6.66) we obtain at LL in the energy flow, ε,

$$\begin{aligned} \frac{d\hat{\sigma}^{(\mathrm{f})}\left(p_T,\hat{\eta},\mu_F,\varepsilon,\nu,\alpha_s(\mu_F)\right)}{d\hat{\eta}d\varepsilon} &= \sum_{\beta,\gamma} H^{(\mathrm{f})}_{\beta\gamma}\left(p_T,\hat{\eta},\alpha_s(\mu_F)\right) \\ &\quad \times S^{(\mathrm{f},1)}_{\gamma\beta}\left(\hat{\eta},\Omega,1,\varepsilon\nu,\alpha_s(\varepsilon p_T)\right)\left(\frac{\alpha_s(p_T)}{\alpha_s(\varepsilon p_T)}\right)^{\frac{2}{\beta_0}E^{(\mathrm{f},1)}_{\gamma\beta}(\hat{\eta})} \\ &\quad \times \prod_{c=A,B,1,2} J^{(\mathrm{f})}_c(p_T,\hat{\eta},\nu,\mu_F). \end{aligned} \tag{6.80}$$

Here, the expression for $S^{(\mathrm{f},1)}$ can be found from (6.76) with (6.77) and the color decompositions listed in Appendix C.3, whereas the eigenvalues are determined from (6.75) and the same color decompositions with (6.74). The resummation of the remaining large logarithms in the jet functions proceeds analogous to the electron-positron case in Sec. 5.3.1, which we will not perform here, since we have not specified the details of the beam jets and the event shape. However, from Eq. (6.80), or in general, from Eq. (6.66) we observe, that also for hadronic processes all information about interjet energy flow is contained in the soft function and its anomalous dimension matrix.

6.8 Summary and Outlook

As was emphasized in [187], most actual experimental measurements involve phase-space restrictions, and are therefore influenced more or less by non-global effects. For example, most detectors do not provide full acceptance over the whole angular region, measurements are restricted over a finite range

of rapidity. It is therefore necessary to provide theoretical predictions that take these non-global effects into account, as in Refs. [184, 185, 186, 187, 188, 189, 190, 191], or alternatively, to study observables that are less sensitive to non-global contributions.

Moreover, as already mentioned in the introductory section to this chapter, the study of energy flow into only part of phase space may shed light on the underlying event, and may help to distinguish multiple scatterings effects, perturbative bremsstrahlung emerging from the primary hard scattering, and possible new physics signals.

Above, we have introduced a set of correlations of interjet energy flow for the general class of event shapes discussed in Chapter 5, and have shown that for these quantities it is possible to control the influence of secondary radiation and non-global logarithms. These correlations are sensitive mainly to radiation emitted directly from the primary hard scattering, through transforms in the weight functions that suppress secondary, or non-global, radiation. We have presented analytic and numerical studies of these shape/flow correlations in e^+e^- dijet events at leading logarithmic order in the flow variable and at next-to-leading-logarithmic order in the event shape. Within our shape/flow correlations the function that encodes the non-global energy flow factorizes from the remaining functions that describe the shape of the event. A similar conclusion was reached in a recent study of such shape/flow correlations (associated distributions) based on coherent parton branching [187].

The application of our formalism to multijet events and to scattering with initial state hadrons is certainly possible, and may shed light on the relationship between color and energy flow in hard scattering processes with non-trivial color exchange. We have illustrated above how non-trivial color flow in events with incoming hadrons is treatable within our formalism. We have shown that, analogous to e^+e^- shape/flow correlations, the information about the energy flow factors from the remainder of the cross section. In the hadronic case, however, this factorization is in terms of matrix multiplication in the space of color exchanges. We have provided complete expressions for hard and soft matrices and soft anomalous dimension matrices for $2 \to 2$ scattering in $p\bar{p}$ collisions. A full treatment of the hadronic case, however, requires an amended definition of the corresponding event shape, which is nontrivial due to the more involved kinematics, and a careful treatment of the incoming jet functions. We postpone the study of these remaining few, but subtle issues. We now summarize the work presented in this thesis.

Chapter 7

Epilogue: Conclusions and Perspectives

In this thesis we have studied soft gluon radiation which arises in (semi-) inclusive cross sections at the edge of phase space. Soft gluons are responsible for large logarithmic corrections that need to be resummed in order to provide reliable quantitative predictions within perturbation theory. We have found that soft gluon radiation at wide angles from the hard scattering decouples, and is well described by emission from path ordered exponentials or eikonal lines that replace the partons involved in the hard scattering.

Cross sections built out of these eikonal lines exponentiate directly by reordering of graphs [76, 77, 78]. This leads to important consequences for physical observables in which soft radiation is not inclusively summed over. The leading logarithmic behavior in such events, which is due to emissions that are simultaneously soft and collinear, is controlled by the anomalous dimension of these eikonal cross sections. The exponentiation of these cross sections has lead us to the development of a simplified method to compute their anomalous dimensions, which we have illustrated with the computation of the fermionic three-loop contribution to the singular coefficients of partonic splitting functions [12].

As noted above, the same anomalous dimensions arise in the resummation of large logarithms in jet events. In the second part of this thesis we have introduced a generalized class of dijet event shapes, and have studied the correlation of these jet shapes with energy flow into the interjet region [10, 11]. Studies of interjet energy flow may help to disentangle the underlying event from soft bremsstrahlung effects and from effects due to new physics (beyond the Standard Model). The study of correlations of energy flow with event shapes is sensitive mainly to emissions directly from the underlying hard scattering and allows us to control the influence of secondary radiation, which, if inclusively summed over, masks the underlying scattering in a highly nontrivial way [184, 185]. We have resummed large logarithms due to soft bremsstrahlung

in the interjet region by solving corresponding evolution equations. The solutions to these evolution equations which follow from factorization contain all large logarithmic corrections in exponentiated form. The leading logarithmic corrections due to soft-collinear emissions can also be obtained by exponentiation of eikonal cross sections on the graphical level, as emphasized above. The remaining exponents are due to only soft or only collinear radiation. At the NLL level, the same result for event shapes and shape/flow correlations can be obtained by studying coherent parton branching [30, 187]. Up to NLL level in dijet events, all radiation appears to be emitted coherently. This, however, is not necessarily true beyond next-to-leading logarithm, and certainly not the case in multi-jet configurations. Nevertheless, our formalism is valid beyond NLL and can in principle be extended to multi-jet events. We have illustrated how it can be applied to events with hadrons in the initial state, for example to $p\bar{p}$ collisions [9].

To summarize, we have attempted to extend the application of perturbative QCD to studies of observables which are sensitive to the radiation into only part of phase space, and we have developed a method which considerably simplifies the computation of the leading effects at higher orders in perturbation theory. These topics are tied together by the mechanisms of soft-gluon factorization which leads to quantities built out solely of eikonal lines. The latter exponentiate directly at the level of Feynman graphs. The possible applications are numerous, for example the quantitative study of power corrections to the cross sections mentioned above, or the complete study of hadronic shape/flow correlations which may shed light on the interplay of color and energy flow. Further studies of these topics will certainly provide more insights into the mechanisms of QCD itself, and facilitate to distinguish QCD effects from signals of new physics in experimental measurements.

To conclude with Aristotle - in this thesis we have attempted to explore some aspects of nature (however, infinitely far from settling questions about principles), starting from QCD which is more knowable to us, and which provides the background to new physics that may be more knowable to nature.

Appendix A

QCD Conventions and Eikonal Feynman Rules

A.1 The Running Coupling

The effective running coupling in QCD

$$\alpha_s = \frac{g_s^2}{4\pi} \tag{A.1}$$

obeys the renormalization group equation

$$\mu \frac{\partial}{\partial \mu} \alpha_s = \beta(\alpha_s) = -\frac{\beta_0}{4\pi}\alpha_s^2 - \frac{\beta_1}{(4\pi)^2}\alpha_s^3 - \dots . \tag{A.2}$$

The expansion of the beta-function is currently known to four loops [198]. In this thesis we only need the one- and two-loop coefficients, given here for SU(N),

$$\beta_0 = \frac{11}{3}C_A - \frac{4}{3}T_F N_f, \tag{A.3}$$

$$\beta_1 = \frac{34}{3}C_A^2 - \frac{20}{3}C_A T_F N_f - 4 C_F T_F N_f. \tag{A.4}$$

C_F, C_A are the Casimirs of the fundamental and the adjoint representation,

$$\begin{aligned} C_F &= \frac{\mathcal{N}_C^2 - 1}{2\,\mathcal{N}_C}, \\ C_A &= \mathcal{N}_C = 3, \end{aligned} \tag{A.5}$$

for SU(3). N_f denotes the number of flavors, and $T_F = 1/2$ is the standard normalization of the generators of the fundamental representation. Beginning with β_2, the coefficients of the expansion of the beta-functions are scheme-dependent at higher orders.

The solution of Eq. (A.2) at one and two loops, respectively, is given by

$$\alpha_s(\mu) = \frac{2\pi}{\beta_0 \ln\left(\frac{\mu}{\Lambda_{\rm QCD}}\right)} + \ldots, \tag{A.6}$$

$$\alpha_s(\mu) = \frac{2\pi}{\beta_0 \ln\left(\frac{\mu}{\Lambda_{\rm QCD}}\right)} \left[1 - \frac{\beta_1}{2\beta_0^2} \frac{\ln\ln\left(\frac{\mu}{\Lambda_{\rm QCD}}\right)^2}{\ln\left(\frac{\mu}{\Lambda_{\rm QCD}}\right)} + \ldots\right]. \tag{A.7}$$

We have introduced the dimensionful scale parameter $\Lambda_{\rm QCD}$ which parameterizes the initial condition to the differential equation (A.2). Conventionally it is determined by the value of α_s at the scale equalling the mass of the Z boson, whose world average is currently determined as [159, 199]

$$\alpha_s(M_Z) = 0.1183 \pm 0.0027. \tag{A.8}$$

$\Lambda_{\rm QCD}$ depends on the number of active flavors, as can be seen from (A.3) and (A.4).

For numerical studies in this thesis we use a value of

$$\Lambda_{\rm QCD} = 161.5 \text{ MeV} \quad \text{for } N_f = 4 \tag{A.9}$$

active flavors, determined by fitting the one-loop term (A.6) to (A.8). Fig. A.1 shows the one-loop coupling with (A.9) as a function of the scale μ (solid black line). For comparison (dashed red line) we plot the coupling at three loops as determined in [199] (the corresponding numerical values can be found in [200]).

At the one-loop level, we can reexpress the coupling given at scale μ in terms of the coupling at scale $\tilde{\mu}$,

$$\alpha_s(\mu) = \frac{\alpha_s(\tilde{\mu})}{1 + \frac{\beta_0}{2\pi}\alpha_s(\tilde{\mu}) \ln\frac{\mu}{\tilde{\mu}}}. \tag{A.10}$$

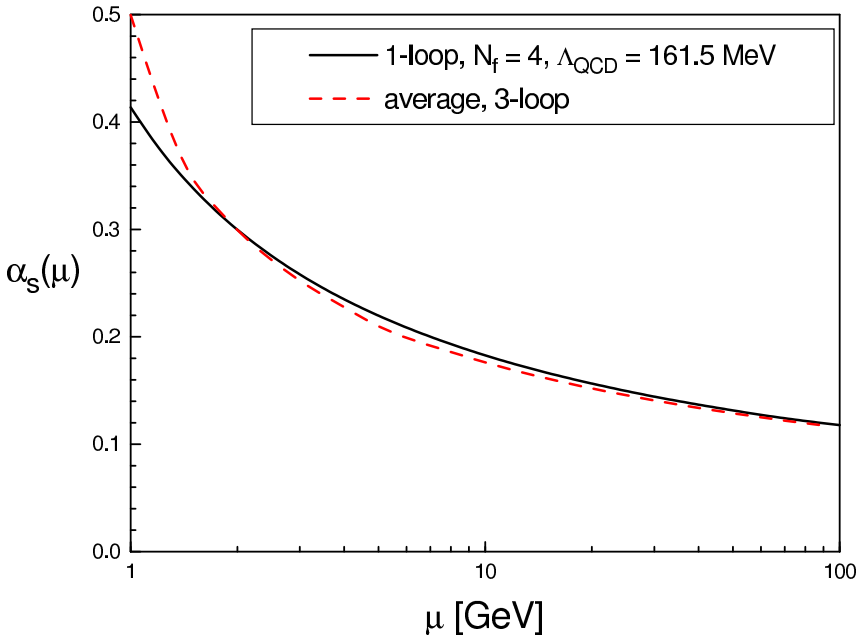

Figure A.1: One-loop (solid line) and three-loop (dashed red line) strong coupling as a function of scale μ (in GeV). The parameters of the one-loop coupling are given in (A.9), the values for the three-loop coupling are taken from [200].

A.2 Eikonal Feynman Rules

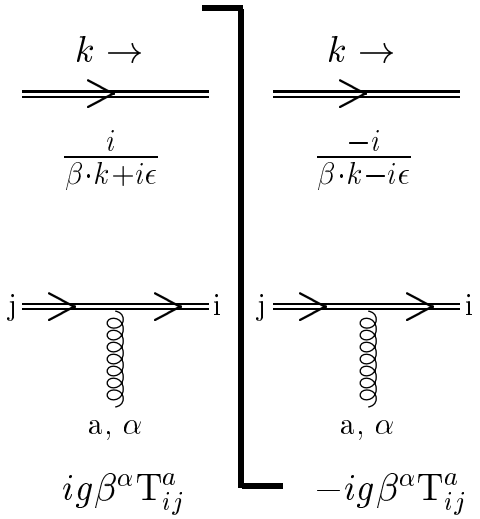

Figure A.2: Feynman rules for eikonal lines in the fundamental representation with velocities β^{μ}, represented by the double lines. The vertical line represents the cut separating the amplitude and its complex conjugate. For an eikonal line in the adjoint representation one has to replace T^{a}_{ij} with if_{ija}.

Appendix B

Multiloop Techniques

In this appendix we collect a few items useful for evaluating multi-loop integrals.

B.1 Feynman Parametrization

Two denominators can be combined by introducing the integral representation:

$$\frac{1}{A}\,\frac{1}{B} = \int\limits_0^1 dx \frac{1}{(xA + (1-x)B)^2}. \tag{B.1}$$

This can be generalized to N factors raised to arbitrary inverse powers $-\eta_i$, $i = 1, \ldots, N$ with the help of integrals over N Feynman parameters x_i:

$$\begin{aligned}\prod_{i=1}^{N} A_i^{-\eta_i} &= \left[\prod_{i=1}^{N} \Gamma(\eta_i)\right]^{-1} \Gamma\left(\sum_{i=1}^{N} \eta_i\right) \int\limits_0^1 dx_1\, x_1^{\eta_1 - 1} \ldots dx_N\, x_N^{\eta_N - 1} \\ &\quad \times \delta\left(1 - \sum_{i=1}^{N} x_i\right) \left(\sum_{i=1}^{N} x_i\, A_i\right)^{-\sum\limits_{i=1}^{N} \eta_i}.\end{aligned} \tag{B.2}$$

B.2 Reduction of Loop Integrals

In the following we will discuss specifically two-loop integrals, but the methods collected below can be generalized to higher orders. Furthermore, we will only discuss the techniques that are needed for the evaluation of the two-loop gluon self-energy, as shown in Table 4.2, graph g)[1]. A more complete

[1]The presented methods apply of course also to the corresponding gluonic part.

overview and a list of further references can be found, for example, in Ref. [121].

We consider two-loop integrals in dimensional regularization of the form

$$I^n\left[\eta_1,\ldots,\eta_N\right] \equiv \int \frac{d^n k}{(2\pi)^n} \int \frac{d^n l}{(2\pi)^n} \frac{\mathcal{N}(k,l)}{A_1^{\eta_1}\ldots A_N^{\eta_N}}, \tag{B.3}$$

where the numerator $\mathcal{N}$ is a function of the loop-momenta $k_i = k, l$, and the external momentum p (or momenta, for graphs with more external legs). The massless propagators are of the form $A_i \sim (k_i \pm f(p,k_i))^2 + i\epsilon$, with $f(p,k_i)$ a function of internal and/or external momenta. The remaining notation is as in Eq. (B.2). In the case of graph g), Table 4.2, the maximal number of different propagators is $n = 5$, for the graphs with denominator structure

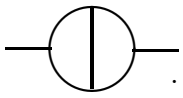

. (B.4)

After applying Feynman parametrization, (B.2), to the scalar version of Eq. (B.3) (we consider the case $\mathcal{N}(k,l) = 1$) we obtain a new, single denominator with the structure

$$\sum_{i=1}^{N} x_i\, A_i = a\, k^2 + b\, l^2 + 2\, c\, k\cdot l + 2\, d\cdot k + 2\, e\cdot l + f, \tag{B.5}$$

where a, b, c are linear combinations of the Feynman parameters x_i, d^μ and e^μ are new vectors that depend on the x_i and the external momentum (more generally, momenta), and f is a scalar, also depending on x_i and the external momentum.

The integral over loop momenta l and k can now be performed via standard techniques, by a change of variables to complete the square:

$$\begin{aligned} k^\mu &\rightarrow K^\mu - \frac{c}{a} L^\mu + \frac{c\, e^\mu - b\, d^\mu}{P}\,, \\ l^\mu &\rightarrow L^\mu + \frac{c\, d^\mu - a\, e^\mu}{P}\,, \end{aligned} \tag{B.6}$$

with

$$P \equiv a\, b - c^2. \tag{B.7}$$

(B.5) becomes

$$a K^2 + \frac{P}{a} L^2 + \frac{Q}{P}, \tag{B.8}$$

where

$$Q \equiv -a\,e^2 - b\,d^2 + 2\,c\,d\cdot e + f(a\,b - c^2). \tag{B.9}$$

With (B.25) we obtain

$$\begin{aligned} I^n\left[\eta_1,\ldots,\eta_N\right] &= -\frac{1}{(4\pi)^n}\left[\prod_{i=1}^{N}\frac{(-1)^{\eta_i}}{\Gamma\left(\eta_i\right)}\int\limits_0^1 dx_i\,x_i^{\eta_i-1}\right]\delta\left(1-\sum_{i=1}^{N}x_i\right) \\ &\quad\times\Gamma\left(\nu-n\right)P^{\nu-3/2n}Q^{n-\nu}, \end{aligned} \tag{B.10}$$

where we have introduced the abbreviation

$$\sum_{i=1}^{N}\eta_i = \nu. \tag{B.11}$$

The integrals over the Feynman parameters in (B.10) can be expressed in terms of Gamma-, Beta- and (generalized) hypergeometric functions (see, for example, [128]). The latter are, however, not always easily expanded into polynomials of ε when working in $n = 4 - 2\varepsilon$ dimensions. In addition, for a higher number of propagators ($N > 5$), it is not easy to find closed expressions. It is advantageous to express all possible integrals in terms of a few, simpler, *Master integrals*.

B.2.1 Integration by Parts

The technique that we use for the calculation of (B.4) to reduce it to Master integrals is termed *integration by parts* (IBP) [14, 201, 202]. IBP allows us to find relations between integrals of the form (B.3) with different powers of η_i, so that we can eventually express all such integrals in terms of those with many $\eta_i = 0$, that is, the corresponding propagators are absent.

IBP identities follow from the fact that the integral over the total derivative with respect to any loop momentum vanishes in dimensional regularization

$$\int\frac{d^nk}{(2\pi)^n}\frac{\partial}{\partial k^\mu}J(k,\,\ldots) = 0, \tag{B.12}$$

where J is a loop integrand, and can be a scalar or a tensor. For two-loop integrals (B.3) these identities can be cast into the form

$$\int\frac{d^nk}{(2\pi)^n}\int\frac{d^nl}{(2\pi)^n}\frac{\partial}{\partial k_i^\mu}\left[\frac{\mathcal{N}^\mu(k_i)}{A_1^{\eta_1}\ldots A_N^{\eta_N}}\right] = 0. \tag{B.13}$$

Applying the derivative to the numerator of (B.3), we obtain

$$\frac{\partial \mathcal{N}^\mu}{\partial k_i^\mu} = n, \tag{B.14}$$

if the numerator depends on k_i and 0 otherwise. Similarly, taking the derivative of one of the terms in the denominator results in

$$\mathcal{N}^\mu \left[\frac{\partial}{\partial k_i^\mu}\frac{1}{A_j^{\eta_i}}\right] = -2\eta_j \frac{\mathcal{N}\cdot A_j}{A_i^{\eta_j+1}}, \tag{B.15}$$

if A_j is k_i-dependent, and 0 otherwise.

The system of equations generated in this manner can then be used to solve for the integrals that have the lowest number of different propagators. We will illustrate this below for (B.4). In (B.15) we have additional numerators of the form

$$2\mathcal{N}\cdot A_j \sim 2\,(k_i+g)\cdot(k_i+h) = (k_i+g)^2 + (k_i+h)^2 - (g-h)^2. \tag{B.16}$$

Reducible numerators can be cancelled against corresponding denominators, and result in simplified integrals. We will deal with *irreducible* numerators in the following.

B.2.2 Numerators

Integrals with irreducible numerators (vectors or tensors) can be dealt with by using the following identities from symmetry considerations

$$\begin{aligned}
\int \frac{d^nk}{(2\pi)^n} k^{\mu_1}\ldots k^{\mu_{2m+1}} f(k^2) &= 0, \quad m \text{ integer},\\
\int \frac{d^nk}{(2\pi)^n} k^\mu k^\nu f(k^2) &= \frac{g^{\mu\nu}}{n}\int \frac{d^nk}{(2\pi)^n} k^2 f(k^2),
\end{aligned} \tag{B.17}$$

and similarly for higher tensors.

Reexpressing numerators involving the momenta k_i in terms of the new variables (B.6) and using Eqs. (B.17), we obtain, for example

$$\begin{aligned}
I^n\left[\eta_1,\ldots,\eta_N\right]\left[k^\mu\right] &\equiv \int \frac{d^nk}{(2\pi)^n}\int \frac{d^nl}{(2\pi)^n}\frac{k^\mu}{A_1^{\eta_1}\ldots A_N^{\eta_N}}\\
&= \int \frac{d^nK}{(2\pi)^n}\int \frac{d^nL}{(2\pi)^n}\frac{c\,e^\mu - b\,d^\mu}{P}\frac{1}{A_1^{\eta_1}\ldots A_N^{\eta_N}}.
\end{aligned} \tag{B.18}$$

In this expression d^μ and e^μ are functions of the external momentum (momenta), independent of the internal loop variables K and L. Comparing this

to Eq. (B.10), we see that factors of x_i can be absorbed into the integrals over Feynman parameters, by increasing the power to which the ith propagator is raised

$$\frac{(-1)^{\eta_i}\, x_i^{\eta_i - 1}}{\Gamma(\eta_i)} x_i = -\eta_i \frac{(-1)^{\eta_i + 1}\, x_i^{\eta_i}}{\Gamma(\eta_i + 1)}, \tag{B.19}$$

whereas the factor $1/P$ can be absorbed by increasing the dimension of the integral

$$P^{\nu - 3/2n} \frac{1}{P} = P^{\nu - 1/2(3n+2)}. \tag{B.20}$$

We can proceed in a similar fashion for more complicated tensors in the numerator. We always obtain integrals that are of the form (B.3), only with increased dimensions and increased powers of numerators η_i.

Example - Reduction of Graph (B.4)

As an example for IBP identities, we express graph (B.4) in terms of simpler Master integrals:

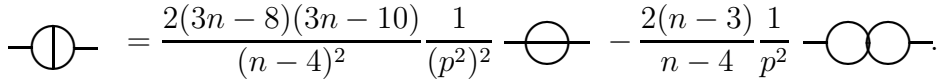

$$= \frac{2(3n-8)(3n-10)}{(n-4)^2} \frac{1}{(p^2)^2}$$

$$- \frac{2(n-3)}{n-4} \frac{1}{p^2}$$

. (B.21)

The expressions for the "sunset" and the "glass" Master integrals are given below.

B.2.3 Collection of a Few Integrals

Here we collect the results for a few standard integrals in Minkowski and Euclidean space, the former can be obtained by performing a Wick rotation to Euclidean space (see, for example, [13]), expressing the n-dimensional Euclidean phase space in terms of polar coordinates

$$\int d^n k_E \to \int d\Omega_{n-1} \int_0^\infty d\kappa \kappa^{n-1} \tag{B.22}$$

and integrating over polar angles:

$$\int d\Omega_m = 2\pi^{m/2} \frac{\Gamma(m/2)}{\Gamma(m)}. \tag{B.23}$$

A general n-dimensional scalar integral in Euclidean space (denoted by the subscript E) is then computed to give

$$\int d^n k_E \left(k_E^2 + M^2\right)^{-s} = \pi^{n/2} \frac{\Gamma(s - n/2)}{\Gamma(s)} \left(M^2\right)^{n/2 - s}. \tag{B.24}$$

The result for its counterpart in Minkowski space is after Wick rotation given by

$$\int d^n k \left(k^2 - M^2 + i\epsilon\right)^{-s} = (-1)^s i\pi^{n/2} \frac{\Gamma(s - n/2)}{\Gamma(s)} \left(M^2\right)^{n/2-s}. \qquad \text{(B.25)}$$

A Few Simple Master Integrals

The calculation of Eq. (B.4), and thus the calculation of graph g) in Table 4.2, is reduced to the calculation of three Master integrals after using the IBP techniques and a bit of algebra to reduce tensor integrals. These loop integrals with two or three propagators are textbook exercises. p denotes the external momentum. They are given in terms of Gamma- and Beta-functions by

$$[\eta_1, \eta_2] \equiv \int \frac{d^n k}{(2\pi)^n} \frac{1}{(k^2)^{\eta_1}} \frac{1}{(k^2 + p^2)^{\eta_2}}$$

$$= \frac{i}{(4\pi)^{n/2}} (-1)^{\eta_1+\eta_2} \frac{\Gamma\left(\eta_1 + \eta_2 - \frac{n}{2}\right)}{\Gamma(\eta_1)\,\Gamma(\eta_2)} B\left(\frac{n}{2} - \eta_1, \frac{n}{2} - \eta_2\right) \left(-p^2\right)^{n/2-\eta_1-\eta_2}, \qquad \text{(B.26)}$$

$$= \frac{i}{(4\pi)^{n/2}} (-1)^{n/2} \Gamma\left(2 - \frac{n}{2}\right) B\left(\frac{n}{2} - 1, \frac{n}{2} - 1\right)$$

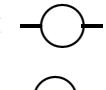
$$\times \left[1, 2 - \frac{n}{2}\right], \qquad \text{(B.27)}$$

$$= \left\{ \right\}^2. \qquad \text{(B.28)}$$

We have listed the sunset and glass graphs for propagators raised to the power 1, that is $\eta_i = 1$.

B.3 Rules for LCOPT

Throughout this thesis our convention for light-cone coordinates is as follows:

$$\begin{aligned} k^+ &= \frac{1}{\sqrt{2}} \left(k^0 + k^3\right), \\ k^- &= \frac{1}{\sqrt{2}} \left(k^0 - k^3\right), \\ k_\perp &= \left(k^1, k^2\right). \end{aligned} \qquad \text{(B.29)}$$

Light-cone ordered perturbation theory is equivalent to the expressions obtained after performing all minus integrals of all loops in a given graph [56, 57, 58]. LCOPT is similar to old-fashioned, or time-ordered, perturbation theory, but ordered along the light-cone, x^+, rather than in x^0. In a LCOPT diagram all internal lines are on-shell, in contrast to a covariant Feynman diagram, which allows us to identify UV divergent loops in eikonal diagrams more easily. This property and the fact that the rules are equivalent to performing all minus integrals make LCOPT especially suited for multi-loop integrals of eikonal diagrams in Feynman gauge. A covariant Feynman diagram is comprised of one or more LCOPT diagrams.

The rules for LCOPT can be summarized as follows:

- We start with forming all possible light-cone orderings of a given covariant diagram.
- Only those configurations are kept which describe possible physical processes once the flow of plus-momenta is specified.
- For every loop we have a factor
$$\frac{dl^+\, d^{2-2\varepsilon} l_\perp}{(2\pi)^{3-2\varepsilon}} \tag{B.30}$$
if we work in $n = 4 - 2\varepsilon$ dimensions.
- For every internal line we have a factor
$$\frac{\theta(l_i^+)}{2l_i^+}, \tag{B.31}$$
corresponding to the flow of plus momentum through the graph.
- Every intermediate virtual state contributes a factor
$$\frac{i}{q^- - \sum_j \frac{l_{j,\perp}^2}{2l_j^+} + i\epsilon}, \tag{B.32}$$
where we sum over all momenta comprising that virtual state, and where q^- is the external minus-momentum of the incoming state(s).
- Every intermediate real state gives a momentum conserving delta-function:
$$2\pi\delta\left(q^- - \sum_j \frac{l_{j,\perp}^2}{2l_j^+}\right), \tag{B.33}$$
where the sum is over all momenta in that real state.

- Since all lines are on-shell, we replace for every Fermion numerator its minus component by its on-shell value:

$$l^- = \frac{l_\perp^2}{2l^+}. \tag{B.34}$$

Appendix C

Color Space Decomposition

Below we list the color bases, and the decompositions of the lowest order hard matrices and soft functions in these bases for various $2 \to 2$ scattering processes relevant for $p\bar{p}$ collisions. We employ various identities from [197] in the calculation of the color decompositions. r_i labels the color of parton i in (6.50). $\mathcal{N}_C$ is the number of colors.

C.1 Color Bases

C.1.1 Basis for $q\bar{q} \to q\bar{q}$

We use the t-channel singlet-octet basis

$$\begin{aligned} c_1 &= \delta_{r_A,r_1}\delta_{r_B,r_2}, \\ c_2 &= -\frac{1}{2\mathcal{N}_C}\delta_{r_A,r_1}\delta_{r_B,r_2} + \frac{1}{2}\delta_{r_A,r_B}\delta_{r_1,r_2}. \end{aligned} \tag{C.1}$$

C.1.2 Basis for $qq \to qq$

The natural t-channel basis for this process is

$$\begin{aligned} c_1 &= \delta_{r_A,r_1}\delta_{r_B,r_2}, \\ c_2 &= -\frac{1}{2\mathcal{N}_C}\delta_{r_A,r_1}\delta_{r_B,r_2} + \frac{1}{2}\delta_{r_A,r_2}\delta_{r_B,r_1}. \end{aligned} \tag{C.2}$$

C.1.3 Basis for $qg \to qg$

Here we use the basis

$$c_1 = \delta_{r_A,r_1}\delta_{r_B,r_2},$$

$$
\begin{aligned}
c_2 &= d_{r_B r_2 c}\,(T_F^c)_{r_1 r_A}\,, \\
c_3 &= i f_{r_B r_2 c}\,(T_F^c)_{r_1 r_A}\,,
\end{aligned}
\tag{C.3}
$$

where c_1 is the t-channel singlet tensor, c_2 and c_3 are the symmetric and antisymmetric octet tensors, respectively.

C.1.4 Basis for $gg \to q\bar{q}$ and $q\bar{q} \to gg$

For these processes it is convenient to use the s-channel color basis

$$
\begin{aligned}
c_1 &= \delta_{r_A, r_B}\delta_{r_1, r_2}, \\
c_2 &= d_{r_A r_B c}\,(T_F^c)_{r_1 r_2}\,, \\
c_3 &= i f_{r_A r_B c}\,(T_F^c)_{r_1 r_2}\,.
\end{aligned}
\tag{C.4}
$$

C.1.5 Bases for $gg \to gg$

The most convenient procedure to calculate the color structure for this process is to start with an overcomplete basis of nine color tensors, then to find a new basis consisting of nine tensors in which the anomalous dimension matrix that we will list below is block diagonal, and finally to reduce the matrix to the minimal basis consisting of eight tensors.

We start with the following set of color tensors

$$
\begin{aligned}
c_1 &= \mathrm{Tr}\,(T_F^{r_A} T_F^{r_B} T_F^{r_2} T_F^{r_1})\,, \\
c_2 &= \mathrm{Tr}\,(T_F^{r_A} T_F^{r_B} T_F^{r_1} T_F^{r_2})\,, \\
c_3 &= \mathrm{Tr}\,(T_F^{r_A} T_F^{r_1} T_F^{r_2} T_F^{r_B})\,, \\
c_4 &= \mathrm{Tr}\,(T_F^{r_A} T_F^{r_1} T_F^{r_B} T_F^{r_2})\,, \\
c_5 &= \mathrm{Tr}\,(T_F^{r_A} T_F^{r_2} T_F^{r_1} T_F^{r_B})\,, \\
c_6 &= \mathrm{Tr}\,(T_F^{r_A} T_F^{r_2} T_F^{r_B} T_F^{r_1})\,, \\
c_7 &= \frac{1}{4}\delta_{r_A, r_1}\delta_{r_B, r_2}, \\
c_8 &= \frac{1}{4}\delta_{r_A, r_B}\delta_{r_1, r_2}, \\
c_9 &= \frac{1}{4}\delta_{r_A, r_2}\delta_{r_B, r_1}.
\end{aligned}
\tag{C.5}
\tag{C.6}
$$

We transform to a new basis of color tensors. This basis can be rewritten in terms of the tensors f and d with the help of the product formula for generators

of $SU(\mathcal{N}_C)$ in the fundamental representation,

$$T_F^i T_F^j = \frac{1}{2\mathcal{N}_C}\delta_{ij}1 + \frac{1}{2}\left(d_{ijk} + if_{ijk}\right)T_F^k. \tag{C.7}$$

After setting $\mathcal{N}_C = 3$, the new basis is given by

$$\begin{aligned}
c_1' &= c_1 - c_3 = \frac{i}{4}\left[f_{r_A r_B c} d_{r_1 r_2 c} - d_{r_A r_B c} f_{r_1 r_2 c}\right], \\
c_2' &= c_2 - c_5 = \frac{i}{4}\left[f_{r_A r_B c} d_{r_1 r_2 c} + d_{r_A r_B c} f_{r_1 r_2 c}\right], \\
c_3' &= c_4 - c_6 = \frac{i}{4}\left[f_{r_A r_1 c} d_{r_B r_2 c} + d_{r_A r_1 c} f_{r_B r_2 c}\right], \\
c_4' &= c_1 + c_3 = \frac{1}{6}\delta_{r_A r_1}\delta_{r_B r_2} + \frac{1}{4}\left[d_{r_A r_1 c} d_{r_B r_2 c} + f_{r_A r_1 c} f_{r_B r_2 c}\right], \\
c_5' &= c_2 + c_5 = \frac{1}{6}\delta_{r_A r_B}\delta_{r_1 r_2} + \frac{1}{4}\left[d_{r_A r_B c} d_{r_1 r_2 c} - f_{r_A r_B c} f_{r_1 r_2 c}\right], \\
c_6' &= c_4 + c_6 = \frac{1}{6}\delta_{r_A r_1}\delta_{r_B r_2} + \frac{1}{4}\left[d_{r_A r_1 c} d_{r_B r_2 c} - f_{r_A r_1 c} f_{r_B r_2 c}\right], \\
c_7' &= c_7, \\
c_8' &= c_8, \\
c_9' &= c_9.
\end{aligned} \tag{C.8}$$

(C.9)

The overcomplete basis (C.8) can be reduced to a basis of 8 $SU(3)$ color tensors. This basis can be partly expressed in terms of t-channel $SU(3)$ projectors for the decomposition into irreducible representations of the direct product $8 \otimes 8$ which corresponds to the color content of a set of two gluons:

$$\left\{c_1', c_2', c_3', P_1, P_{8_S}, P_{8_A}, P_{10\oplus\overline{10}}, P_{27}\right\}, \tag{C.10}$$

where,

$$\begin{aligned}
P_1(r_A, r_B; r_1, r_2) &= \frac{1}{8}\delta_{r_A r_1}\delta_{r_B r_2}, \\
P_{8_S}(r_A, r_B; r_1, r_2) &= \frac{3}{5} d_{r_A r_1 c} d_{r_B r_2 c}, \\
P_{8_A}(r_A, r_B; r_1, r_2) &= \frac{1}{3} f_{r_A r_1 c} f_{r_B r_2 c}, \\
P_{10\oplus\bar{1}0}(r_A, r_B; r_1, r_2) &= \frac{1}{2}\left(\delta_{r_A r_B}\delta_{r_1 r_2} - \delta_{r_A r_2}\delta_{r_B r_1}\right) - \frac{1}{3} f_{r_A r_1 c} f_{r_B r_2 c}, \\
P_{27}(r_A, r_B; r_1, r_2) &= \frac{1}{2}\left(\delta_{r_A r_B}\delta_{r_1 r_2} + \delta_{r_A r_2}\delta_{r_B r_1}\right)
\end{aligned}$$

$$-\frac{1}{8}\delta_{r_A r_1}\delta_{r_B r_2} - \frac{3}{5}d_{r_A r_1 c}d_{r_B r_2 c}. \tag{C.11}$$

C.2 Hard Scattering Matrices

Explicit hard matrices in color space at LO have been given in Ref. [192]. We exhibit them here for the sake of completeness with a trivial change in overall normalization relative to [192].

We will express the hard matrices in terms of the partonic Mandelstam variables

$$\begin{aligned} \hat{s} &= x_A x_B s, \\ \hat{t} &= -p_T^2\left(1+e^{-2\hat{\eta}}\right), \\ \hat{u} &= -(\hat{s}+\hat{t}). \end{aligned} \tag{C.12}$$

We also recall that we have from Eq. (6.51)

$$p_T = \frac{\sqrt{\hat{s}}}{2\cosh\hat{\eta}}. \tag{C.13}$$

C.2.1 Hard Matrices for $q\bar{q} \to q\bar{q}$

In the basis (C.1) the decomposition of the Born level hard scattering for same-flavor $q\bar{q} \to q\bar{q}$ in color space is given by the matrix

$$H^{(1)}\left(\hat{t},\hat{s},\alpha_s(\mu)\right) = \frac{1}{\mathcal{N}_C^2}\frac{\alpha_s^2(\mu)\,\pi}{\hat{s}}\begin{pmatrix} \left(\frac{C_F}{\mathcal{N}_C}\right)^2\chi_1 & \frac{C_F}{\mathcal{N}_C^2}\chi_2 \\ \frac{C_F}{\mathcal{N}_C^2}\chi_2 & \chi_3 \end{pmatrix}, \tag{C.14}$$

where χ_1, χ_2, and χ_3 are defined by

$$\begin{aligned} \chi_1 &= \frac{\hat{t}^2+\hat{u}^2}{\hat{s}^2} \\ \chi_2 &= \mathcal{N}_C\frac{\hat{u}^2}{\hat{s}\hat{t}} - \frac{\hat{t}^2+\hat{u}^2}{\hat{s}^2} \\ \chi_3 &= \frac{\hat{s}^2+\hat{u}^2}{\hat{t}^2} + \frac{1}{\mathcal{N}_C^2}\frac{\hat{t}^2+\hat{u}^2}{\hat{s}^2} - \frac{2}{\mathcal{N}_C}\frac{\hat{u}^2}{\hat{s}\hat{t}}. \end{aligned} \tag{C.15}$$

The unequal-flavor cases, $q\bar{q}' \to q\bar{q}'$ and $q\bar{q} \to q'\bar{q}'$, are found from (C.14) by dropping the s-channel terms for the former, and the t-channel contributions for the latter. The matrix for $q\bar{q} \to \bar{q}q$ can be found from (C.14) via the transformation $\hat{t} \leftrightarrow \hat{u}$.

C.2.2 Hard Matrix for $qq \to qq$

For this process we obtain in the basis Eq. (C.2) a hard matrix which is related to the one for $q\bar{q} \to q\bar{q}$, Eq. (C.14), by the crossing transformation $\hat{s} \leftrightarrow \hat{u}$. So the χ_1, χ_2 and χ_3 are given by

$$\begin{aligned}
\chi_1 &= \frac{\hat{t}^2+\hat{s}^2}{\hat{u}^2} \\
\chi_2 &= \mathcal{N}_C \frac{\hat{s}^2}{\hat{t}\hat{u}} - \frac{\hat{s}^2+\hat{t}^2}{\hat{u}^2} \\
\chi_3 &= \frac{\hat{s}^2+\hat{u}^2}{\hat{t}^2} + \frac{1}{\mathcal{N}_C^2}\frac{\hat{s}^2+\hat{t}^2}{\hat{u}^2} - \frac{2}{\mathcal{N}_C}\frac{\hat{s}^2}{\hat{t}\hat{u}}\,.
\end{aligned} \tag{C.16}$$

As above, for $qq' \to qq'$ only the t-channel terms are kept.

C.2.3 Hard Matrices for $qg \to qg$

In the basis Eq. (C.3) we arrive at a hard matrix of the form

$$H^{(1)}\left(\hat{t},\hat{s},\alpha_s(\mu)\right) = \frac{1}{\mathcal{N}_C(\mathcal{N}_C^2-1)}\,\frac{\alpha_s^2(\mu)\,\pi}{2\hat{s}}\begin{pmatrix} \frac{1}{2\mathcal{N}_C^2}\chi_1 & \frac{1}{2\mathcal{N}_C}\chi_1 & \frac{1}{\mathcal{N}_C}\chi_2 \\ \frac{1}{2\mathcal{N}_C}\chi_1 & \frac{1}{2}\chi_1 & \chi_2 \\ \frac{1}{\mathcal{N}_C}\chi_2 & \chi_2 & \chi_3 \end{pmatrix}, \tag{C.17}$$

with χ_1, χ_2, and χ_3 given by

$$\begin{aligned}
\chi_1 &= -\frac{\hat{s}^2+\hat{u}^2}{\hat{s}\hat{u}} \\
\chi_2 &= 1 - \frac{1}{2}\frac{\hat{t}^2}{\hat{s}\hat{u}} - \frac{\hat{u}^2}{\hat{s}\hat{t}} - \frac{\hat{s}}{\hat{t}} \\
\chi_3 &= 3 - 4\frac{\hat{s}\hat{u}}{\hat{t}^2} - \frac{1}{2}\frac{\hat{t}^2}{\hat{s}\hat{u}}\,.
\end{aligned} \tag{C.18}$$

Again, the matrix for $qg \to gq$ can be found from the above matrix (C.17) by exchanging $\hat{t} \leftrightarrow \hat{u}$.

C.2.4 Hard Matrices for $gg \to q\bar{q}$ and $q\bar{q} \to gg$

In the basis (C.4) we calculated the Born level hard scattering matrix to be

$$H^{(1)}\left(\hat{t},\hat{s},\alpha_s(\mu)\right) = \frac{1}{\bar{N}}\,\frac{\alpha_s^2(\mu)\,\pi}{2\hat{s}}\begin{pmatrix} \frac{1}{2\mathcal{N}_C^2}\chi_1 & \frac{1}{2\mathcal{N}_C}\chi_1 & \frac{1}{\mathcal{N}_C}\chi_2 \\ \frac{1}{2\mathcal{N}_C}\chi_1 & \frac{1}{2}\chi_1 & \chi_2 \\ \frac{1}{\mathcal{N}_C}\chi_2 & \chi_2 & \chi_3 \end{pmatrix}, \tag{C.19}$$

where χ_1, χ_2, and χ_3 are given by

$$\begin{aligned} \chi_1 &= \frac{\hat{t}^2+\hat{u}^2}{\hat{t}\hat{u}} \\ \chi_2 &= 1-\frac{1}{2}\frac{\hat{u}^2-\hat{t}^2}{\hat{t}\hat{u}} \\ \chi_3 &= 6-4\frac{\hat{t}^2}{\hat{s}^2}+\frac{1}{2}\frac{\hat{t}^2+\hat{u}^2}{\hat{t}\hat{u}}\,, \end{aligned} \tag{C.20}$$

and the averaging factor is $\bar{N}=\mathcal{N}_C^2$ for the process $q\bar{q}\to gg$, and $\left(\mathcal{N}_C^2-1\right)^2$ for $gg\to q\bar{q}$. The matrix for $gg\to\bar{q}q$ is once again found by letting $\hat{t}\leftrightarrow\hat{u}$.

C.2.5 Hard Matrix for $gg \to gg$

In the minimal basis consisting of 8 color tensors, (C.10), the hard matrix is found to be block-diagonal

$$H^{(1)}\left(\hat{t},\hat{s},\alpha_s(\mu)\right) = \begin{pmatrix} 0_{3\times3} & 0_{3\times5} \\ 0_{5\times3} & H^{(1)}_{5\times5} \end{pmatrix}, \tag{C.21}$$

with the 5×5 block $H^{(1)}_{5\times5}$

$$H^{(1)}_{5\times5}\left(\hat{t},\hat{s},\alpha_s(\mu)\right) = \frac{1}{16}\,\frac{\alpha_s^2(\mu)\pi}{2\hat{s}}\begin{pmatrix} 9\chi_1 & \frac{9}{2}\chi_1 & \frac{9}{2}\chi_2 & 0 & -3\chi_1 \\ \frac{9}{2}\chi_1 & \frac{9}{4}\chi_1 & \frac{9}{4}\chi_2 & 0 & -\frac{3}{2}\chi_1 \\ \frac{9}{2}\chi_2 & \frac{9}{4}\chi_2 & \chi_3 & 0 & -\frac{3}{2}\chi_2 \\ 0 & 0 & 0 & 0 & 0 \\ -3\chi_1 & -\frac{3}{2}\chi_1 & -\frac{3}{2}\chi_2 & 0 & \chi_1 \end{pmatrix}, \tag{C.22}$$

with χ_1, χ_2, and χ_3 defined by

$$\chi_1 = 1-\frac{\hat{t}\hat{u}}{\hat{s}^2}-\frac{\hat{s}\hat{t}}{\hat{u}^2}+\frac{\hat{t}^2}{\hat{s}\hat{u}}$$

$$\begin{aligned}\chi_2 &= \frac{\hat{s}\hat{t}}{\hat{u}^2} - \frac{\hat{t}\hat{u}}{\hat{s}^2} + \frac{\hat{u}^2}{\hat{s}\hat{t}} - \frac{\hat{s}^2}{\hat{t}\hat{u}} \\ \chi_3 &= \frac{27}{4} - 9\left(\frac{\hat{s}\hat{u}}{\hat{t}^2} + \frac{1}{4}\frac{\hat{t}\hat{u}}{\hat{s}^2} + \frac{1}{4}\frac{\hat{s}\hat{t}}{\hat{u}^2}\right) + \frac{9}{2}\left(\frac{\hat{u}^2}{\hat{s}\hat{t}} + \frac{\hat{s}^2}{\hat{t}\hat{u}} - \frac{1}{2}\frac{\hat{t}^2}{\hat{s}\hat{u}}\right). \quad \text{(C.23)}\end{aligned}$$

For this process we have set explicitly $\mathcal{N}_C = 3$.

C.3 Soft Functions for $2 \to 2$ Scattering

Below we list the anomalous dimension matrices and soft functions at lowest order, Eqs. (6.74) and (6.76), in terms of the combinations (6.78). $\phi^{(ij,\,1)}$ is either $S^{(ij,\,1)}$ (Eq. (6.77)) or $\Gamma^{(ij,\,1)}$ (Eq. (6.75)). Furthermore, we collectively denote anomalous dimension matrices and lowest order eikonal contributions by $\mathcal{M}^{(\mathrm{f})}$,

C.3.1 Soft Matrices for $qq \to qq$

We obtain the color decomposition for $qq \to qq$ in the basis (C.2)

$$\mathcal{M}^{(qq\to qq)} = \begin{pmatrix} C_F\beta^{(qq)} & \frac{C_F}{2\mathcal{N}_C}\left(\alpha^{(qq)} + \gamma^{(qq)}\right) \\ \alpha^{(qq)} + \gamma^{(qq)} & C_F\gamma^{(qq)} - \frac{1}{2\mathcal{N}_C}\left(2\alpha^{(qq)} + \beta^{(qq)} + \gamma^{(qq)}\right) \end{pmatrix}, \quad \text{(C.24)}$$

where we have abbreviated $(qq \to qq)$ by (qq), and where the sign changes compared to $q\bar{q} \to q\bar{q}$ due to the factors of Δ_i are as follows:

$$\begin{aligned}\alpha^{(qq\to qq)} &= -\alpha^{(q\bar{q}\to q\bar{q})} \\ \beta^{(qq\to qq)} &= \beta^{(q\bar{q}\to q\bar{q})} \\ \gamma^{(qq\to qq)} &= -\gamma^{(q\bar{q}\to q\bar{q})}.\end{aligned} \quad \text{(C.25)}$$

C.3.2 Soft Matrix for $qg \to qg$ and $\bar{q}g \to \bar{q}g$

In terms of the $\phi^{(ij,\,1)}$s for $q\bar{q} \to q\bar{q}$, as discussed in Sec. 6.7.5, the anomalous dimension matrix for $qg \to qg$ reads in the basis (C.3)

$$\mathcal{M}^{(qg\to qg)} = \begin{pmatrix} C_F\phi^{(A1,\,1)} + C_A\phi^{(B2,\,1)} & 0 & -\frac{1}{2}(\alpha+\gamma) \\ 0 & \chi & -\frac{\mathcal{N}_C}{4}(\alpha+\gamma) \\ -(\alpha+\gamma) & -\frac{\mathcal{N}_C^2-4}{4\mathcal{N}_C}(\alpha+\gamma) & \chi \end{pmatrix}, \quad \text{(C.26)}$$

where $\chi \equiv \frac{\mathcal{N}_C}{4}(\alpha-\gamma) - \frac{1}{2\mathcal{N}_C}\phi^{(A1,1)} + \frac{\mathcal{N}_C}{2}\phi^{(B2,1)}$. Here and everywhere below we drop the superscripts $(q\bar{q} \to q\bar{q})$.

The matrix for

$$\bar{q}(p_1,r_1) + g(p_2,r_2) \to \bar{q}(p_A,r_A) + g(p_B,r_B)$$

is the same as for

$$q(p_A,r_A) + g(p_B,r_B) \to q(p_1,r_1) + g(p_2,r_2)$$

if we use the same basis and take into account all sign changes due to the eikonal Feynman rules and the relabelling of the color indices.

C.3.3 Soft Matrices for $gg \to q\bar{q}$ and $q\bar{q} \to gg$

In the basis (C.4) the color decomposition for $gg \to q\bar{q}$ is given by

$$\mathcal{M}^{(gg\to q\bar{q})} = \begin{pmatrix} C_F\phi^{(12,1)} + C_A\phi^{(AB,1)} & 0 & \frac{1}{2}(\beta+\gamma) \\ 0 & \xi & \frac{\mathcal{N}_C}{4}(\beta+\gamma) \\ \beta+\gamma & \frac{\mathcal{N}_C^2-4}{4\mathcal{N}_C}(\beta+\gamma) & \xi \end{pmatrix}, \quad \text{(C.27)}$$

where $\xi \equiv \frac{\mathcal{N}_C}{4}(\beta-\gamma) - \frac{1}{2\mathcal{N}_C}\phi^{(12,1)} + \frac{\mathcal{N}_C}{2}\phi^{(AB,1)}$, and the $\phi^{(ij,1)}$ again denote those calculated above for $q\bar{q} \to q\bar{q}$.

The process

$$q(p_2,r_2) + \bar{q}(p_1,r_1) \to g(p_B,r_B) + g(p_A,r_A)$$

is related to the process

$$g(p_A,r_A) + g(p_B,r_B) \to q(p_1,r_2) + \bar{q}(p_2,r_2)$$

by time reversal. After relabelling the color indices appropriately we arrive at the following anomalous dimension matrix where only the diagonal elements are changed compared to the one stated above:

$$\mathcal{M}^{(q\bar{q}\to gg)} = \begin{pmatrix} C_F\phi^{(AB,1)} + C_A\phi^{(12,1)} & 0 & \frac{1}{2}(\beta+\gamma) \\ 0 & \xi' & \frac{\mathcal{N}_C}{4}(\beta+\gamma) \\ \beta+\gamma & \frac{\mathcal{N}_C^2-4}{4\mathcal{N}_C}(\beta+\gamma) & \xi' \end{pmatrix}, \quad \text{(C.28)}$$

where $\xi' \equiv \frac{\mathcal{N}_C}{4}(\beta-\gamma) - \frac{1}{2\mathcal{N}_C}\phi^{(AB,1)} + \frac{\mathcal{N}_C}{2}\phi^{(12,1)}$.

C.3.4 Soft Matrix for $gg \to gg$

The soft matrix for $gg \to gg$ is in the minimal basis (C.10) given by

$$\mathcal{M}^{(gg\to gg)} = \begin{pmatrix} \mathcal{M}_{3\times 3} & 0_{3\times 5} \\ 0_{5\times 3} & \mathcal{M}_{5\times 5} \end{pmatrix}, \tag{C.29}$$

where the matrix $\mathcal{M}_{3\times 3}$ is given by

$$\mathcal{M}_{3\times 3} = \begin{pmatrix} \frac{\mathcal{N}_C}{2}(\alpha+\beta) & 0 & 0 \\ 0 & \frac{\mathcal{N}_C}{2}(\alpha-\gamma) & 0 \\ 0 & 0 & \frac{\mathcal{N}_C}{2}(\beta-\gamma) \end{pmatrix}, \tag{C.30}$$

and $\mathcal{M}_{5\times 5}$ reads

$$\mathcal{M}_{5\times 5} = \begin{pmatrix} 3\beta & 0 & 3(\alpha+\gamma) & 0 & 0 \\ 0 & \frac{3}{4}(\alpha+2\beta-\gamma) & \frac{3}{4}(\alpha+\gamma) & \frac{3}{2}(\alpha+\gamma) & 0 \\ \frac{3}{8}(\alpha+\gamma) & \frac{3}{4}(\alpha+\gamma) & \frac{3}{4}(\alpha+2\beta-\gamma) & 0 & \frac{9}{8}(\alpha+\gamma) \\ 0 & \frac{3}{5}(\alpha+\gamma) & 0 & \frac{3}{2}(\alpha-\gamma) & \frac{9}{10}(\alpha+\gamma) \\ 0 & 0 & \frac{1}{3}(\alpha+\gamma) & \frac{2}{3}(\alpha+\gamma) & 2\alpha-\beta-2\gamma \end{pmatrix}. \tag{C.31}$$

Bibliography

[1] J. C. Collins and D. E. Soper, Ann. Rev. Nucl. Part. Sci. **37**, 383 (1987).

[2] J. C. Collins, D. E. Soper and G. Sterman, in Adv. Ser. Direct. High Energy Phys. **5**, 1 (1988), *Perturbative QCD* (A.H. Mueller, ed.) (World Scientific Publ., 1989).

[3] S. J. Brodsky and G. P. Lepage, in Adv. Ser. Direct. High Energy Phys. **5**, 93 (1988), *Perturbative QCD* (A.H. Mueller, ed.) (World Scientific Publ., 1989).

[4] B. Pire, *Exclusive reactions in QCD*, arXiv:nucl-th/9612009.

[5] N. G. Stefanis, Eur. Phys. J. directC **1**, 7 (1999) [arXiv:hep-ph/9911375].

[6] C. F. Berger, B. Lechner and W. Schweiger, FizikaB **8**, 371 (1999) [arXiv:hep-ph/9901338].

[7] C. F. Berger and W. Schweiger, Phys. Rev. D **61**, 114026 (2000) [arXiv:hep-ph/9910509].

[8] C. F. Berger and W. Schweiger, Eur. Phys. J. **C**, DOI 10.1140/epjc/s2003-01166-8 (2003) [arXiv:hep-ph/0212066].

[9] C. F. Berger, T. Kúcs and G. Sterman, Phys. Rev. D **65**, 094031 (2002) [arXiv:hep-ph/0110004].

[10] C. F. Berger, T. Kúcs and G. Sterman, *Interjet energy flow/event shape correlations*, arXiv:hep-ph/0212343.

[11] C. F. Berger, T. Kúcs and G. Sterman, *Event Shape/Energy Flow Correlations*, to appear in Phys. Rev. **D**, arXiv:hep-ph/0303051.

[12] C. F. Berger, Phys. Rev. D **66**, 116002 (2002) [arXiv:hep-ph/0209107].

[13] G. Sterman, *An Introduction to Quantum Field Theory*, Cambridge University Press, Cambridge, 1993.

[14] G. 't Hooft and M. J. Veltman, Nucl. Phys. B **44**, 189 (1972).

[15] W. A. Bardeen, A. J. Buras, D. W. Duke and T. Muta, Phys. Rev. D **18**, 3998 (1978).

[16] H. D. Politzer, Phys. Rev. Lett. **30** (1973) 1346.

[17] D. J. Gross and F. Wilczek, Phys. Rev. D **8**, 3633 (1973).

[18] *Large Order Behavior Of Perturbation Theory*, eds. J. C. Le Guillou and J. Zinn-Justin, North-Holland, Amsterdam, 1990.

[19] E. Borel, Ann. Sci. Ec. norm. sup. Paris, **16**, 1 (1899).

[20] G. 't Hooft, *Can We Make Sense Out Of 'Quantum Chromodynamics'?*, in *The Whys of Subnuclear Physics*, Proceedings Erice Summer School, ed. A. Zichichi, 1977.

[21] A. I. Vainshtein, *Decaying Systems And Divergence Of The Series Of Perturbation Theory*, Novosibirsk report, 1964, reprinted in *Fun reading for the Arcadyfest* (Minneapolis 2002).

[22] T. Schäfer and E. V. Shuryak, Rev. Mod. Phys. **70**, 323 (1998) [arXiv:hep-ph/9610451].

[23] M. Beneke, Phys. Rept. **317**, 1 (1999) [arXiv:hep-ph/9807443].

[24] M. Beneke and V. M. Braun, *Renormalons and power corrections*, in the Boris Joffe Festschrift *At the Frontier of Particle Physics/Handbook of QCD*, ed. M. Shifman, World Scientific Singapore, 2001, arXiv:hep-ph/0010208.

[25] B. Lautrup, Phys. Lett. B **69**, 109 (1977).

[26] W. Giele *et al.*, *The QCD/SM working group: Summary report*, in *Les Houches 2001, Physics at TeV colliders*, 275, arXiv:hep-ph/0204316.

[27] R. K. Ellis, W. J. Stirling and B. R. Webber, *QCD And Collider Physics*, Cambridge Monogr. Part. Phys. Nucl. Phys. Cosmol. **8**, 1 (1996).

[28] M. Greco and Y. Srivastava, Phys. Rev. D **23**, 2791 (1981) [Erratum-ibid. D **24**, 806 (1981)].

[29] K. Tesima and M. F. Wade, Z. Phys. C **52**, 43 (1991).

[30] S. Catani, L. Trentadue, G. Turnock and B. R. Webber, Nucl. Phys. B **407**, 3 (1993).

[31] G. Sterman, in *QCD and Beyond, Proceedings of the Theoretical Advanced Study Institute in Elementary Particle Physics (TASI 95)*, ed. D. E. Soper, World Scientific, Singapore, 1996 [arXiv:hep-ph/9606312].

[32] F. Bloch and A. Nordsieck, Phys. Rev. **52**, 54 (1937).

[33] D. R. Yennie, S. C. Frautschi and H. Suura, Annals Phys. **13**, 379 (1961).

[34] G. Grammer and D. R. Yennie, Phys. Rev. D **8**, 4332 (1973).

[35] T. Kinoshita, J. Math. Phys. **3**, 650 (1962).

[36] T. D. Lee and M. Nauenberg, Phys. Rev. **133**, B1549 (1964).

[37] T. Muta, *Foundations Of Quantum Chromodynamics. Second Edition*, World Sci. Lect. Notes Phys. **57**, 1 (1998).

[38] G. Sterman, Phys. Rev. D **17**, 2773 (1978).

[39] G. Sterman, Phys. Rev. D **17**, 2789 (1978).

[40] L. D. Landau, Nucl. Phys. **13**, 181 (1959).

[41] J. D. Bjorken, Ph.D. Thesis, Stanford University, 1959.

[42] S. Coleman and R. E. Norton, Nuovo Cim. **38**, 438 (1965).

[43] G. T. Bodwin, S. J. Brodsky and G. P. Lepage, Phys. Rev. Lett. **47**, 1799 (1981).

[44] J. C. Collins and G. Sterman, Nucl. Phys. B **185**, 172 (1981).

[45] A. Sen, Phys. Rev. D **24**, 3281 (1981).

[46] G. 't Hooft, Nucl. Phys. B **33**, 173 (1971).

[47] G. 't Hooft and M. J. Veltman, Nucl. Phys. B **50**, 318 (1972).

[48] C. Becchi, A. Rouet and R. Stora, Commun. Math. Phys. **42**, 127 (1975).

[49] C. Becchi, A. Rouet and R. Stora, Annals Phys. **98**, 287 (1976).

[50] I. V. Tyutin, internal report, 1975.

[51] J. C. Collins, D. E. Soper and G. Sterman, Nucl. Phys. B **261**, 104 (1985).

[52] J. C. Collins, D. E. Soper and G. Sterman, Nucl. Phys. B **308**, 833 (1988).

[53] S. B. Libby and G. Sterman, Phys. Rev. D **18**, 3252 (1978).

[54] G. T. Bodwin, Phys. Rev. D **31**, 2616 (1985) [Erratum-ibid. D **34**, 3932 (1986)].

[55] J. C. Collins, D. E. Soper and G. Sterman, Phys. Lett. B **438**, 184 (1998) [arXiv:hep-ph/9806234].

[56] S. J. Chang and S. K. Ma, Phys. Rev. **180**, 1506 (1969).

[57] J. B. Kogut and D. E. Soper, Phys. Rev. D **1**, 2901 (1970).

[58] S. J. Brodsky, R. Roskies and R. Suaya, Phys. Rev. D **8**, 4574 (1973).

[59] J. C. Collins and D. E. Soper, Nucl. Phys. B **193**, 381 (1981) [Erratum-ibid. B **213**, 545 (1983)].

[60] W. Zimmermann, Commun. Math. Phys. **15**, 208 (1969) [Lect. Notes Phys. **558**, 217 (2000)].

[61] V. N. Gribov and L. N. Lipatov, Yad. Fiz. **15**, 781 (1972) [Sov. J. Nucl. Phys. **15**, 438 (1972)].

[62] L. N. Lipatov, Sov. J. Nucl. Phys. **20**, 94 (1975) [Yad. Fiz. **20**, 181 (1974)].

[63] G. Altarelli and G. Parisi, Nucl. Phys. B **126**, 298 (1977).

[64] Y. L. Dokshitzer, Sov. Phys. JETP **46**, 641 (1977) [Zh. Eksp. Teor. Fiz. **73**, 1216 (1977)].

[65] J. C. Collins and D. E. Soper, Nucl. Phys. B **194**, 445 (1982).

[66] S. J. Brodsky, P. Hoyer, N. Marchal, S. Peigne and F. Sannino, Phys. Rev. D **65**, 114025 (2002) [arXiv:hep-ph/0104291].

[67] X. d. Ji and F. Yuan, Phys. Lett. B **543**, 66 (2002) [arXiv:hep-ph/0206057].

[68] G. P. Korchemsky, Mod. Phys. Lett. A **4**, 1257 (1989).

[69] G. Sterman and S. Weinberg, Phys. Rev. Lett. **39**, 1436 (1977).

[70] E. Farhi, Phys. Rev. Lett. **39**, 1587 (1977).

[71] S. Catani, G. Turnock and B. R. Webber, Phys. Lett. B **295**, 269 (1992).

[72] H. Contopanagos, E. Laenen and G. Sterman, Nucl. Phys. B **484**, 303 (1997) [arXiv:hep-ph/9604313].

[73] G. P. Korchemsky and A. V. Radyushkin, Nucl. Phys. B **283**, 342 (1987).

[74] G. Sterman and M. E. Tejeda-Yeomans, Phys. Lett. B **552**, 48 (2003) [arXiv:hep-ph/0210130].

[75] J. C. Collins, D. E. Soper and G. Sterman, Nucl. Phys. B **250**, 199 (1985).

[76] G. Sterman, in *AIP Conference Proceedings Tallahassee, Perturbative Quantum Chromodynamics*, eds. D. W. Duke, J. F. Owens, New York, 1981.

[77] J. G. Gatheral, Phys. Lett. B **133**, 90 (1983).

[78] J. Frenkel and J. C. Taylor, Nucl. Phys. B **246**, 231 (1984).

[79] M. Levy and J. Sucher, Phys. Rev. **186**, 1656 (1969).

[80] J. Frenkel, J. G. Gatheral and J. C. Taylor, Nucl. Phys. B **233**, 307 (1984).

[81] E. Laenen, G. Sterman and W. Vogelsang, Phys. Rev. D **63**, 114018 (2001) [arXiv:hep-ph/0010080].

[82] G. P. Korchemsky and G. Sterman, Nucl. Phys. B **437**, 415 (1995) [arXiv:hep-ph/9411211].

[83] G. P. Korchemsky and G. Sterman, Nucl. Phys. B **555**, 335 (1999) [arXiv:hep-ph/9902341].

[84] G. Grunberg, Phys. Lett. B **372**, 121 (1996) [arXiv:hep-ph/9512203].

[85] Y. L. Dokshitzer and N. G. Uraltsev, Phys. Lett. B **380**, 141 (1996) [arXiv:hep-ph/9512407].

[86] S. Peris and E. de Rafael, Phys. Lett. B **387**, 603 (1996) [arXiv:hep-ph/9603359].

[87] B. R. Webber, Phys. Lett. B **339**, 148 (1994) [arXiv:hep-ph/9408222].

[88] Y. L. Dokshitzer and B. R. Webber, Phys. Lett. B **352**, 451 (1995) [arXiv:hep-ph/9504219].

[89] R. Akhoury and V. I. Zakharov, Nucl. Phys. B **465**, 295 (1996) [arXiv:hep-ph/9507253].

[90] Y. L. Dokshitzer and B. R. Webber, Phys. Lett. B **404**, 321 (1997) [arXiv:hep-ph/9704298].

[91] E. Gardi and G. Grunberg, JHEP **9911**, 016 (1999) [arXiv:hep-ph/9908458].

[92] G. P. Korchemsky and S. Tafat, JHEP **0010**, 010 (2000) [arXiv:hep-ph/0007005].

[93] E. Gardi and J. Rathsman, Nucl. Phys. B **609**, 123 (2001) [arXiv:hep-ph/0103217].

[94] E. Gardi and J. Rathsman, Nucl. Phys. B **638**, 243 (2002) [arXiv:hep-ph/0201019].

[95] S. Albino and R. D. Ball, Phys. Lett. B **513**, 93 (2001) [arXiv:hep-ph/0011133].

[96] A. Vogt, Phys. Lett. B **497**, 228 (2001) [arXiv:hep-ph/0010146].

[97] D. J. Gross and F. Wilczek, Phys. Rev. D **9**, 980 (1974).

[98] E. G. Floratos, D. A. Ross and C. T. Sachrajda, Nucl. Phys. B **129**, 66 (1977) [Erratum-ibid. B **139**, 545 (1978)].

[99] A. Gonzalez-Arroyo, C. Lopez and F. J. Yndurain, Nucl. Phys. B **153**, 161 (1979).

[100] G. Curci, W. Furmanski and R. Petronzio, Nucl. Phys. B **175**, 27 (1980).

[101] E. G. Floratos, C. Kounnas and R. Lacaze, Nucl. Phys. B **192**, 417 (1981).

[102] J. Kodaira and L. Trentadue, Phys. Lett. B **112**, 66 (1982).

[103] J. A. Gracey, Phys. Lett. B **322**, 141 (1994) [arXiv:hep-ph/9401214].

[104] S. A. Larin, T. van Ritbergen and J. A. Vermaseren, Nucl. Phys. B **427**, 41 (1994).

[105] J. Blümlein and A. Vogt, Phys. Lett. B **370**, 149 (1996) [arXiv:hep-ph/9510410].

[106] S. A. Larin, P. Nogueira, T. van Ritbergen and J. A. Vermaseren, Nucl. Phys. B **492**, 338 (1997) [arXiv:hep-ph/9605317].

[107] A. Rétey and J. A. Vermaseren, Nucl. Phys. B **604**, 281 (2001) [arXiv:hep-ph/0007294].

[108] W. L. van Neerven and A. Vogt, Nucl. Phys. B **603**, 42 (2001) [arXiv:hep-ph/0103123].

[109] W. L. van Neerven and A. Vogt, J. Phys. G **28**, 727 (2002) [arXiv:hep-ph/0107194].

[110] J. A. Vermaseren, S. Moch and A. Vogt, arXiv:hep-ph/0211296.

[111] S. Moch, J. A. Vermaseren and A. Vogt, Nucl. Phys. B **646**, 181 (2002) [arXiv:hep-ph/0209100].

[112] G. P. Korchemsky and G. Marchesini, Nucl. Phys. B **406**, 225 (1993) [arXiv:hep-ph/9210281].

[113] A. M. Polyakov, Nucl. Phys. B **164**, 171 (1980).

[114] I. Y. Arefeva, Phys. Lett. B **93**, 347 (1980).

[115] J. L. Gervais and A. Neveu, Nucl. Phys. B **163**, 189 (1980).

[116] V. S. Dotsenko and S. N. Vergeles, Nucl. Phys. B **169**, 527 (1980).

[117] R. A. Brandt, F. Neri and M. a. Sato, Phys. Rev. D **24**, 879 (1981).

[118] I. A. Korchemskaya and G. P. Korchemsky, Phys. Lett. B **287**, 169 (1992).

[119] N. N. Bogoliubov and O. S. Parasiuk, Acta Math. **97**, 227 (1957).

[120] K. Hepp, Commun. Math. Phys. **2**, 301 (1966).

[121] M. E. Tejeda-Yeomans, *Two-loop QCD corrections for 2 → 2 parton scattering processes*, arXiv:hep-ph/0212315.

[122] S. Wolfram, *The Mathematica Book*, 4th Edition, Cambridge University Press, Cambridge, 1999.

[123] J. A. Vermaseren, *New features of FORM*, arXiv:math-ph/0010025.

[124] E. Braaten and J. P. Leveille, Phys. Rev. D **24**, 1369 (1981).

[125] A. I. Davydychev, P. Osland and O. V. Tarasov, Phys. Rev. D **58**, 036007 (1998) [arXiv:hep-ph/9801380].

[126] L. Lewin, *Polylogarithms and Associated Functions*, North Holland, Amsterdam, 1981.

[127] A. Devoto and D. W. Duke, Riv. Nuovo Cim. **7N6**, 1 (1984).

[128] I. S. Gradshteyn, I. M. Ryzhik, *Table of Integrals, Series, and Products*, 5th Edition, ed. A. Jeffrey, Academic Press, London, 1994.

[129] G. 't Hooft, Nucl. Phys. B **61**, 455 (1973).

[130] S. Bethke, *Jet physics at LEP and world summary of alpha(s)*, arXiv:hep-ex/9812026.

[131] S. Seidel [CDF Collaboration], *Jet physics at the Tevatron*, arXiv:hep-ex/0205013.

[132] O. Gonzalez [H1 Collaboration], *Jet physics at HERA*, arXiv:hep-ex/0211063.

[133] Y. L. Dokshitzer, V. A. Khoze, S. I. Troian and A. H. Mueller, Rev. Mod. Phys. **60**, 373 (1988).

[134] H. Georgi and M. Machacek, Phys. Rev. Lett. **39**, 1237 (1977).

[135] C. L. Basham, L. S. Brown, S. D. Ellis and S. T. Love, Phys. Rev. Lett. **41**, 1585 (1978).

[136] A. De Rujula, J. R. Ellis, E. G. Floratos and M. K. Gaillard, Nucl. Phys. B **138**, 387 (1978).

[137] G. C. Fox and S. Wolfram, Phys. Rev. Lett. **41**, 1581 (1978).

[138] G. Parisi, Phys. Lett. B **74**, 65 (1978).

[139] J. F. Donoghue, F. E. Low and S. Y. Pi, Phys. Rev. D **20**, 2759 (1979).

[140] R. K. Ellis, D. A. Ross and A. E. Terrano, Phys. Rev. Lett. **45**, 1226 (1980).

[141] G. Sterman, Phys. Rev. D **19**, 3135 (1979).

[142] S. Catani, G. Turnock, B. R. Webber and L. Trentadue, Phys. Lett. B **263**, 491 (1991).

[143] Y. L. Dokshitzer, A. Lucenti, G. Marchesini and G. P. Salam, JHEP **9801**, 011 (1998) [arXiv:hep-ph/9801324].

[144] G. P. Korchemsky and G. Sterman, *Universality of infrared renormalons in hadronic cross sections*, arXiv:hep-ph/9505391.

[145] A. V. Belitsky, G. P. Korchemsky and G. Sterman, Phys. Lett. B **515**, 297 (2001) [arXiv:hep-ph/0106308].

[146] A. V. Manohar and M. B. Wise, Phys. Lett. B **344**, 407 (1995) [arXiv:hep-ph/9406392].

[147] N. Kidonakis, G. Oderda and G. Sterman, Nucl. Phys. B **531**, 365 (1998) [arXiv:hep-ph/9803241].

[148] J. C. Collins and F. Hautmann, Phys. Lett. B **472**, 129 (2000) [arXiv:hep-ph/9908467].

[149] S. Catani and L. Trentadue, Nucl. Phys. B **353**, 183 (1991).

[150] G. Sterman, Nucl. Phys. B **281**, 310 (1987).

[151] S. Catani and L. Trentadue, Nucl. Phys. B **327**, 323 (1989).

[152] H. Contopanagos and G. Sterman, Nucl. Phys. B **419**, 77 (1994) [arXiv:hep-ph/9310313].

[153] S. Catani, M. L. Mangano, P. Nason and L. Trentadue, Nucl. Phys. B **478**, 273 (1996) [arXiv:hep-ph/9604351].

[154] P. Binetruy, Phys. Lett. B **91**, 245 (1980).

[155] G. Schierholz, *E+ E- Jets*, in SLAC Summer Inst. (1979), p. 476.

[156] S. Catani and M. H. Seymour, Phys. Lett. B **378**, 287 (1996) [arXiv:hep-ph/9602277].

[157] S. Brandt and H. D. Dahmen, Z. Phys. C **1**, 61 (1979).

[158] S. Brandt, C. Peyrou, R. Sosnowski and A. Wroblewski, Phys. Lett. **12**, 57 (1964).

[159] S. Bethke, *alpha(s) 2002*, arXiv:hep-ex/0211012.

[160] T. Sjostrand, P. Eden, C. Friberg, L. Lonnblad, G. Miu, S. Mrenna and E. Norrbin, Comput. Phys. Commun. **135**, 238 (2001) [arXiv:hep-ph/0010017].

[161] T. Sjostrand, L. Lonnblad and S. Mrenna, *PYTHIA 6.2: Physics and manual*, arXiv:hep-ph/0108264.

[162] B. Andersson, G. Gustafson, G. Ingelman and T. Sjostrand, Phys. Rept. **97**, 31 (1983).

[163] B. Andersson, *The Lund Model*, Cambridge Monogr. Part. Phys. Nucl. Phys. Cosmol. **7**, 1 (1997).

[164] G. P. Salam and D. Wicke, JHEP **0105**, 061 (2001) [arXiv:hep-ph/0102343].

[165] K. Abe *et al.* [SLD Collaboration], Phys. Rev. D **51**, 962 (1995) [arXiv:hep-ex/9501003].

[166] P. Abreu *et al.* [DELPHI Collaboration], Z. Phys. C **73**, 11 (1996).

[167] G. Sterman, *Approaching the final state in perturbative QCD*, arXiv:hep-ph/0301243.

[168] Y. L. Dokshitzer, A. Lucenti, G. Marchesini and G. P. Salam, Nucl. Phys. B **511**, 396 (1998) [Erratum-ibid. B **593**, 729 (2001)] [arXiv:hep-ph/9707532].

[169] G. P. Korchemsky, *Shape functions and power corrections to the event shapes*, arXiv:hep-ph/9806537.

[170] P. A. Movilla Fernandez, S. Bethke, O. Biebel and S. Kluth, Eur. Phys. J. C **22**, 1 (2001) [arXiv:hep-ex/0105059].

[171] N. A. Sveshnikov and F. V. Tkachov, Phys. Lett. B **382**, 403 (1996) [arXiv:hep-ph/9512370].

[172] F. V. Tkachov, Int. J. Mod. Phys. A **12**, 5411 (1997) [arXiv:hep-ph/9601308].

[173] G. P. Korchemsky, G. Oderda and G. Sterman, *Power corrections and nonlocal operators*, arXiv:hep-ph/9708346.

[174] C. F. Berger *et al.*, in *Proc. of the APS/DPF/DPB Summer Study on the Future of Particle Physics (Snowmass 2001)* ed. N. Graf, eConf **C010630**, P512 (2001) [arXiv:hep-ph/0202207].

[175] W. Bartel *et al.* [JADE Collaboration], Phys. Lett. B **101**, 129 (1981).

[176] W. Bartel *et al.* [JADE Collaboration], Z. Phys. C **21**, 37 (1983).

[177] M. Althoff *et al.* [TASSO Collaboration], Z. Phys. C **29**, 29 (1985).

[178] M. Z. Akrawy *et al.* [Opal Collaboration], Phys. Lett. B **261**, 334 (1991).

[179] R. Akers *et al.* [OPAL Collaboration], Z. Phys. C **68**, 531 (1995).

[180] J. R. Ellis, V. A. Khoze and W. J. Stirling, Z. Phys. C **75**, 287 (1997) [arXiv:hep-ph/9608486].

[181] B. Abbott *et al.* [D0 Collaboration], Phys. Lett. B **464**, 145 (1999) [arXiv:hep-ex/9908017].

[182] J. Huston [CDF Collaboration], Int. J. Mod. Phys. A **16S1A**, 219 (2001).

[183] V. Tano, *The underlying event in hadron hadron collisions*, arXiv:hep-ex/0205023.

[184] M. Dasgupta and G. P. Salam, Phys. Lett. B **512**, 323 (2001) [arXiv:hep-ph/0104277].

[185] M. Dasgupta and G. P. Salam, JHEP **0203**, 017 (2002) [arXiv:hep-ph/0203009].

[186] M. Dasgupta and G. P. Salam, JHEP **0208**, 032 (2002) [arXiv:hep-ph/0208073].

[187] Y. L. Dokshitzer and G. Marchesini, *On large angle multiple gluon radiation*, arXiv:hep-ph/0303101.

[188] A. Banfi, G. Marchesini, Y. L. Dokshitzer and G. Zanderighi, JHEP **0007**, 002 (2000) [arXiv:hep-ph/0004027].

[189] S. J. Burby and E. W. Glover, JHEP **0104**, 029 (2001) [arXiv:hep-ph/0101226].

[190] A. Banfi, G. Marchesini and G. Smye, JHEP **0208**, 006 (2002) [arXiv:hep-ph/0206076].

[191] R. B. Appleby and M. H. Seymour, JHEP **0212**, 063 (2002) [arXiv:hep-ph/0211426].

[192] G. Oderda, Phys. Rev. D **61**, 014004 (2000) [arXiv:hep-ph/9903240].

[193] V. A. Khoze and W. J. Stirling, Z. Phys. C **76**, 59 (1997) [arXiv:hep-ph/9612351].

[194] G. Oderda and G. Sterman, Phys. Rev. Lett. **81**, 3591 (1998) [arXiv:hep-ph/9806530].

[195] A. Bassetto, M. Ciafaloni, G. Marchesini and A. H. Mueller, Nucl. Phys. B **207**, 189 (1982).

[196] N. Kidonakis, G. Oderda and G. Sterman, Nucl. Phys. B **525**, 299 (1998) [arXiv:hep-ph/9801268].

[197] A. J. MacFarlane, A. Sudbery and P. H. Weiz, Commun. Math. Phys. **11**, 77 (1968).

[198] T. van Ritbergen, J. A. Vermaseren and S. A. Larin, Phys. Lett. B **400**, 379 (1997) [arXiv:hep-ph/9701390].

[199] K. Hagiwara *et al.* [Particle Data Group Collaboration], Phys. Rev. D **66**, 010001 (2002).

[200] I. Hinchliffe, `http://www-theory.lbl.gov/~ianh/alpha/alpha.html`, 2001.

[201] F. V. Tkachov, Phys. Lett. B **100**, 65 (1981).

[202] K. G. Chetyrkin and F. V. Tkachov, Nucl. Phys. B **192**, 159 (1981).